Histone Deacetylase Inhibition Increases the Radiosensitivity of HPV-Negative Head and Neck Squamous Cell Carcinoma Cells

Thesis submitted in accordance with the requirements of the University of Liverpool for the degree of Doctor in Philosophy by

Jennifer Antrobus

September 2023

ABSTRACT

The majority of head and neck cancers are squamous cell carcinomas (HNSCCs), which develop from the mucosal epithelium lining the head and neck. HNSCC is the seventh most common cancer worldwide, with approximately 1.1 million cases and 500,000 deaths per year. Currently, the main treatments for HNSCC are surgical resection, radiotherapy, and chemotherapy, with the aim of effectively treating the cancer whilst preserving the maximum amount of organ function. Despite the success of radiation-based treatments for HNSCC, radioresistance is a common occurrence. Furthermore, HPV-negative HNSCC has an overall worse prognosis than its HPV-positive counterpart, likely due to the degradation of p53 and Rb proteins in HPV-positive tumours. Importantly, HPV-positive HNSCCs are more radiosensitive than HPV-negative cases, due to the impairments in DNA damage repair and cell cycle regulation. Therefore, it is important that new strategies for sensitising HPV-negative HNSCCs to radiotherapy are identified in order to improve prognosis and survival.

This research began with a screen of 183 FDA-approved drugs to identify novel radiosensitisers of HPV-negative HNSCC. For this, 3D spheroid models were utilised, which provide a more thorough insight into the radiosensitising potential of the drugs, as they are more representative of clinical tumours compared to 2D cell culture techniques. Through this screen, two promising drugs have been identified, both of which inhibit histone deacetylases (HDACs), which are enzymes involved in the regulation of chromatin structure.

In mammalian cells, genomic DNA is packaged with histone proteins and condensed into chromatin. To gain access to the DNA, chromatin remodelling is required, and is carried out through the post-translational modification of histones. Histone acetylation is one of the most well understood modifications and is controlled by histone acetyltransferases (HATs) and HDACs. HDACs have also been shown to have some involvement in the DNA damage response, which is a crucial pathway in the cellular response to radiotherapy. Consequently, HDAC inhibitors have been investigated as potential radiosensitisers *in vitro* and *in vivo* to improve the efficacy or radiotherapy in specific tumour types. In this research, I have demonstrated that the HDAC inhibitor pracinostat and the combined HDAC and EGFR inhibitor CUDC-101 can radiosensitise HNSCC grown as both 2D and 3D models in a cell line-dependent manner. Further investigation confirmed that these inhibitors significantly impair the efficiency of DNA double strand break repair.

Overall, this research has identified CUDC-101 and pracinostat as two novel radiosensitisers of HPV-negative HNSCC *in vitro*. Both inhibitors were shown to work in a cell line-dependent manner, providing a potential opportunity for the future development of a personalised radiosensitisation treatment for selective HNSCC patients.

ACKNOWLEDGEMENTS

First and foremost, I would like to thank Professor Jason Parsons for giving me the opportunity to join his group and carry out this research. I am grateful for all of his support and guidance during my time in the lab.

I would also like to thank all the past and present members of the Parsons Group for making my time in this lab so enjoyable. In particular, I would like to acknowledge Rhianna Hill and Matthew Fok for being the most supportive colleagues I could have asked for, I really wouldn't have been able to do this PhD without all of the advice, support, friendship, laughs and coffee you have provided me, I'm so so grateful for you both – Team Jujube will live on forever! I would also like to thank Dr. Chumin Zhou, Hayley Fowler, Emily Robinson, and Dr. Beth Wilkinson for all their support over the last three years.

I wouldn't be where I am today without my family. Thank you to my parents, Alison and Derek, for supporting and encouraging me my whole life and always believing in me (and for the lifts, the food, and letting me live at home while I did this PhD!). Lucy, Helen and Catherine, my wonderful big sisters – you are all inspiring and amazing and I love you all, thank you for always being there for me. I'd also like to thank my brothers-in-law, Lee, Matthew, and Jon, for their support, and my niece and nephew Emily and Jack for all the cuddles and cheering me up when I needed it.

To my wonderful, wonderful friends: Mags, Kirsty, Autumn, Alice, Alicia, Sarah, Sarah, Yas, and Bronwyn – you are all incredible and I honestly would not have coped without you all in the last few years. Thank you for always being there and believing in me, for reminding me to take breaks and for all the laughs and distractions. You got me through the days where I didn't think I could do this, and hyped me up when I needed it, I will forever be grateful for you all.

Finally, I'd like to dedicate this work to my grandparents. Grandma – thank you for always believing in me and supporting me for my whole life. Grandad Antrobus – the cleverest and funniest man I've ever met, thank you for being an inspiration. Grannie – it's not maths but it is science, and I hope I made you proud. And Grandad Clarke – **I really do think I'm dead good now**.

TABLE OF CONTENTS

LIST OF FIGURES

LIST OF TABLES

LIST OF ABBREVIATIONS

3meA	M3-methyladenine
53BP1	p53-binding protein 1
7meG	N7-methylguanine
8-oxoG	8-oxoguanine
A	Adenine
A-NHEJ	Alternative NHEJ
Acetyl CoA	Acetyl coenzyme A
ACR	ATP-dependent chromatin remodelling complex
AKT	Protein kinase B
ALT	Alternative lengthening of telomeres
AP site	Apurinic/apyrimidic site
APAF-1	Apoptotic protease-activating factor-1
APE1	AP endonuclease 1
APL	Acute promyelocytic leukaemia
APS	Ammonium persulphate
ARP	Actin-related protein
ATP	Adenine triphosphate
Bcl-2	B-cell lymphoma 2
BER	Base excision repair
BLM	Bloom syndrome RecQ-like helicase
bp	Base pairs
BRCA1/2	Breast cancer type 1/2 susceptibility protein
BSA	Bovine serum albumin
C	Cytosine
C-NHEJ	Canonical NHEJ
Caspase	Cysteine-aspartic protease
CDK	Cyclin dependent kinase
CDKI	CDK inhibitor
CDKN2A	Cyclin dependent kinase inhibitor 2A
CHD	Chromodomain helicase DNA-binding
CK2	Casein kinase 2

CML	Chronic myeloid leukaemia
CtIP	Carboxy-terminal binding protein-interacting protein
D-loop	Displacement loop
DDR	DNA damage response
DER	Dose enhancement ratio
DISC	Death-inducing signalling complex
DMAP1	DNMT1-associated protein 1
DMEM	Dulbecco's modified eagle's medium
DMSO	Dimethyl sulfoxide
DNA	Deoxyribonucleic acid
DNA polymerase β	Polβ
DNA-PK	DNA-dependent protein kinase
DNA-PKcs	DNA-dependent protein kinase catalytic subunit
DNMT1	DNA methyltransferase 1
dRP	Deoxyribosephosphate
DSB	Double strand break
DSB	Double-strand break
DSBR	DSB repair
DTT	Dithiothreitol
E6-AP	E6-associated protein
EBV	Epstein-Barr virus
ECM	Extracellular matrix
EDTA	Ethylenediaminetetraacetic acid
EGF	Epidermal growth factor
EGFR	Epidermal growth factor receptor
EMT	Epithelial to mesenchymal transition
ERRα	Oestrogen-related receptor α
ESR1	Oestrogen receptor 1
EXO1	Exonuclease 1
FBS	Fetal bovine serum
FEN-1	Flap endonuclease-1
FGF	Fibroblast growth factor
G	Guanine
GBM	Glioblastoma multiforme

GSK-3	Glycogen synthase kinase 3
HAT	Histone acetyltransferase
HBOC syndrome	Hereditary breast and ovarian cancer syndrome
HDAC	Histone deacetylase
HDACi	HDAC inhibitor
HIF	Hypoxia-inducible factor
HMG1/2	High mobility group 1/2
HMGB3	High-mobility group box 3
hMSH2	Human MutS homolog 2
HnMT	Histone methyltransferase
HNSCC	Head and neck squamous cell carcinoma
HP1	Heterochromatin protein 1
HPV	Human papilloma virus
HR	Homologous recombination
HSA domain	Helicase/SANT-associated domain
HSS domain	HAND-SANT-SLIDE domain
IAP	Inhibitor of apoptosis
IMRT	Intensity modulated radiotherapy
INO80	Inositol-requiring 80
IR	Ionising radiation
ISWI	Imitation switch
LET	Linear energy transfer
LMPA	Low melting point agarose
LOH	Loss of heterozygosity
LP-BER	Long-patch base excision repair
MAPK	Mitogen activated protein kinase
MDM2	Mouse double minute 2 homolog
MDSC	Myeloid-derived suppressor cell
MEF2	Myocyte enhancement factor 2
MEK	MAPK kinase
MEM	Minimal essential medium
MET	Mesenchymal to epithelial transition
MLH1	MutL homolog 1
MMP	Matrix metalloproteinase

MMR	Mismatch repair
MOMP	Mitochondrial outer membrane permeabilisation
MRN complex	MRE11-RAD50-NBS1 complex
mRNA	Messenger RNA
MSH2	MutS homolog 2
MTA1	Metastasis tumour antigen 1
MTH1	2-hydroxy-dATP diphosphatase
NADH	Nicotinamide adenine dinucleotide
NER	Nucleotide excision repair
NF-κB	Nuclear factor kappa-light-chain enhancer of activated B cells
NHEJ	Non-homologous end joining
NK cells	Natural killer cells
NMPA	Normal melting point agarose
NSCLC	Non-small cell lung cancer
NTH1	Human endonuclease III
OGG1	8-oxoG glycosylase
OSCC	Oral squamous cell carcinoma
p53-mut	Mutant p53
p53-WT	Wild-type p53
PAGE	Polyacrylamide gel electrophoresis
PARP	Poly (ADP-ribose) polymerase
PBS	Phosphate buffered saline
PBT	Proton beam therapy
PCNA	Proliferating cell nuclear antigen
PCR1/2	Polycomb repressive complex 1/2
PCV	Packed cell volume
PDGF	Platelet derived growth factor
PDGFR	Platelet-derived growth factor receptor
PI3K	Phosphoinositide 3-kinase
PLK-1	Polo-like kinase-1
PMSF	Phenylmethylsulphonyl fluoride
PNPK	Polynucleotide kinase/phosphatase
Polδ	DNA polymerase δ
Polε	DNA polymerase ε

PPAR	Peroxisome proliferator-activated receptors
PPOL	Potentially malignant lesion
PTM	Post-translational modification
PUA	Phospho-α,β-unsaturated aldehyde
PVDF	Polyvinylidene difluoride
RARA	Retinoic receptor alpha
Rb	Retinoblastoma
RNA	Ribonucleic acid
ROS	Reactive oxygen species
RPA	Replication protein A
SCC	Squamous cell carcinoma
SDS	Sodium dodecyl sulphate
SDSA	Synthesis-dependent strand annealing
SF	Surviving fraction
Sir2	Silent information regulator
siRNA	Short interfering RNA
SMAC	Second mitochondria-derived activator of caspase
SOBP	Spread out Bragg peak
SP-BER	Short-patch base excision repair
SRCAP	SWR1C/p400/Snf2-related CBP activator protein
SSB	Single-strand break
ssDNA	Single-stranded DNA
STAT3	Signal transducer and activator of transcription 3
SWI/SNF	Switch/sucrose non-fermentable
T	Thymine
TAM	Tumour-associated macrophage
TBP	TATA binding protein
TEMED	Tetramethylethylenediamine
TERT	Telomerase reverse transcriptase
TME	Tumour microenvironment
TNF	Tumour necrosis factor
TP53	Tumour protein 53
tRNA	Transfer RNA
TSP-1	Thrombospondin 1

VEGF	Vascular endothelial growth factor
VPA	Valproic acid
XBP1	X-box binding protein 1
XIAP	X-linked inhibitor of apoptosis
XRCC1/4	X-ray cross-complementing protein 1/4

CHAPTER 1: INTRODUCTION

1.1. The Hallmarks of Cancer

Cancer is an extremely complex and heterogeneous group of diseases wherein uncontrolled cell division leads to the development of tumours, which have the potential to metastasise away from the primary site to other parts of the body and can also form secondary tumours. Healthy cells in the body gradually progress from a normal to a neoplastic state, obtaining a number of defining characteristics as they do. These characteristics are known as the hallmarks of cancer, and include the maintenance of proliferative signalling, the ability to avoid tumour suppressors, avoiding apoptosis, enabling replicative immortality, induction of angiogenesis, the ability to invade and metastasise to distant parts of the body, the deregulation of cellular energetics, and finally, the ability to evade immune destruction (1). Instability of the genome and increased levels of inflammation underlie the acquisition of these characteristics.

1.1.1. Maintaining proliferative signalling

Cell proliferation is a fundamental process for the growth of multicellular organisms. Under normal conditions, a variety of proteins within cells control the production of signals that promote growth and determine entry into the cell cycle (figure 1.1). The cell cycle is a progression of events that occurs within cells, leading to cell growth, division, and the production of daughter cells. There are four phases in the eukaryotic cell cycle: G_1, S, G_2, and M. Collectively, G_1, S and G_2 are known as interphase, and M is mitosis. To ensure that cells undergoing division are undamaged – and thus produce healthy and

undamaged daughter cells – checkpoints are present at two points in the cell cycle: between the G_1 and S phases (G_1/S) and between the G_2 and M phases (G_2/M). During the G_1 phase, cell growth occurs and the production of proteins and organelles, such as mitochondria and ribosomes, increases. At the end of G_1, the cell passes through the G_1/S checkpoint, during which it is checked for correct size, nutrients, growth factors, and external conditions. If everything is correct at this stage, the cell will commit to progressing through the rest of the cell cycle. If the cell detects any damage or any other cellular issues, it will undergo cell cycle arrest – known as G_0 phase. The next phase of the cell cycle, S phase, is a period of DNA synthesis. During this period of the cycle, every chromosome is replicated and the amount of DNA present in the cell doubles. Transcription and translation levels in the cell are generally much lower at this stage, however the level of histone production increases with the level of DNA replication. The cell then moves into G_2 phase, in which protein synthesis and rapid cell growth occur, and following this, the cell begins to prepare itself for mitosis. Before entering M phase, the cell must pass through the G_2/M checkpoint, which is largely regulated by the p53 protein. Here, the DNA is checked for damage or incomplete replication. Once any damage has been repaired, the cell progresses to mitosis, during which the cell divides to produce two identical daughter cells.

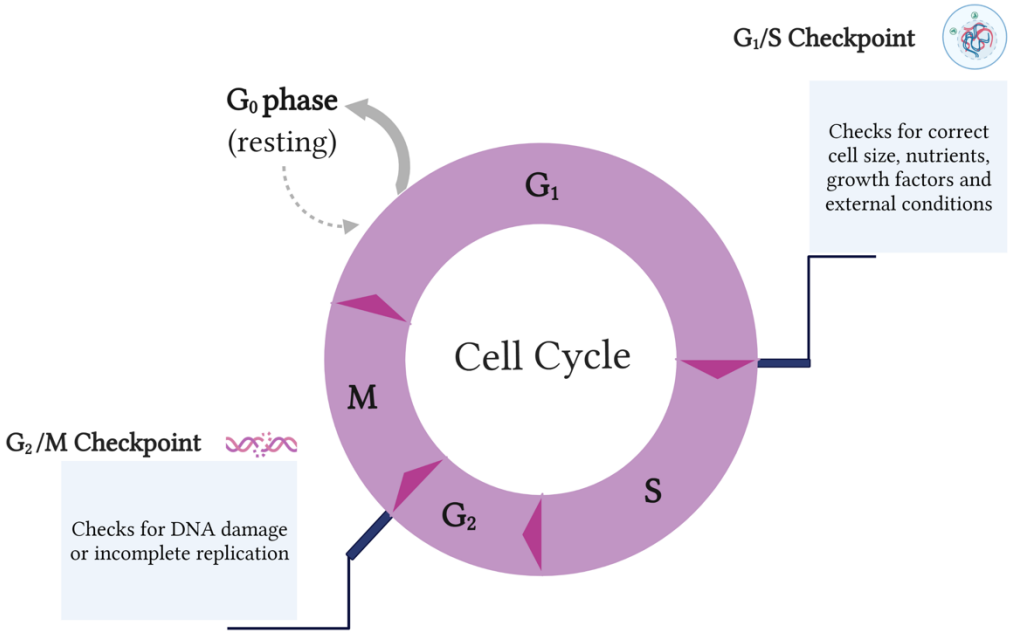

Figure 1.1: The Cell Cycle

The eukaryotic cell cycle consists of 4 phases: G_1, S, G_2, and M. In the G_1 phase, the cell undergoes a period of growth and increases the production of proteins and organelles. Before moving into the S phase, the cell is checked to ensure it is the correct size and possesses the correct nutrients and growth factors at the G_1/S checkpoint. If any issues are detected at this checkpoint, the cell undergoes cell cycle arrest. On the other hand, if everything is correct, the cell can pass into S phase, in which DNA synthesis occurs. The G_2 phase follows, which consists of protein synthesis and rapid cell growth. The cell passes through a final checkpoint, the G_2/M checkpoint, to ensure there is no DNA damage present before entering mitosis.

Normally, the cell cycle is tightly monitored by an array of proteins whose role is to ensure that cell growth and division occurs in the correct manner, and to prevent cells with high levels of DNA damage from passing through the cycle. These proteins include cyclin-dependent kinases (CDKs), polo-like kinase-1 (PLK-1) and aurora kinases.

CDKs are small kinase molecules that rely on the binding of cyclin, a regulatory protein, for their function. The main CDKs involved in the cell cycle are CDK4 and CDK6, which phosphorylate a number of crucial substrates to stimulate progression through the various stages of the cell cycle (2). CDK

protein activity is regulated by interaction with CDK inhibitor proteins (CKIs), which block the binding of CDKs to cyclin, thus inhibiting their activity (3). For example, the *CDKN2A* gene encodes two CKIs, p16 and p14arf. p16 inhibits CDK4/6 activity to block retinoblastoma (Rb) activation (4), and p14arf activates p53 (5) – both of these activities block G_1/S transition and the p16 and p14arf proteins are therefore classed as tumour suppressors. PLK-1 is a serine/threonine protein kinase involved in the transition from the G_2 to the M phase of the cell cycle (6). The main functions of PLK-1 are to reinforce the functional maturation of the centrosome during this transition and to ensure the bipolar spindle is correctly established (7). If PLK-1 does not function correctly, centrosome abnormalities can result in the improper segregation of chromosomes, aneuploidy, and eventually tumourigenesis (8). Aurora kinases are a family of three enzymes, AURKA, AURKB and AURKC, all of which are essential for correct cell cycle progression and cellular proliferation. AURKA induces the separation of duplicated centrosomes and the entrance into mitosis, while AURKB is involved in the condensation of chromosomes and the attachment of the mitotic spindle (9, 10). AURKC differs to AURKA and AURKB, as it is involved in the regulation of meiosis rather than mitosis, and is specifically expressed in oocytes and sperm cells (11).

These proteins are vital for correct regulation of the cell cycle. However, if these proteins are dysfunctional and the cell cycle is not regulated correctly, cells with high levels of damage are allowed to pass through into cell division. This allows damage to accumulate in cells, contributing to the transition from a healthy to a cancerous cell, as well as allowing tumour cells with high levels of damage to continue to pass through the cycle and proliferate (12). Incorrect cell cycle functioning that is seen in cancer cells can result from mutations in genes directly encoding the cell cycle proteins discussed above. For example, the expression level of *CDKN2A* is altered in approximately 58 % of head and

neck squamous cell carcinomas (HNSCCs) (13), and the *PLK1* gene is commonly overexpressed in HNSCCs (14). An overexpression of aurora kinases is associated with aneuploidy and genetic instability (15), and in HNSCCs, increased levels of AURKA have been linked to a decrease in both overall and disease-free survival (16). Mutations can also be found in genes involved in upstream signalling pathways that indirectly impact the activity of cell cycle proteins, such as poly (ADP-ribose) polymerases (PARPs), which are involved in DNA repair (17).

1.1.2. Avoiding tumour suppressors

As well as the ability to maintain proliferative signalling, malignant cells also have the capability to avoid the effects of growth suppressor proteins. There are multiple types of growth suppressor proteins, which all work in different ways, such as DNA damage response proteins, cell cycle control proteins, and inducers of apoptosis (18). These proteins act as negative regulators of cell proliferation, therefore playing a vital role in the prevention of tumourigenesis. If not for the role of growth suppressors, damaged cells could freely proliferate, leading to an accumulation of abnormal cells that could eventually form a malignant tumour. Growth suppressor proteins are therefore more commonly known as 'tumour suppressors', and mutations in the genes encoding these proteins result in a predisposition to a number of different cancer types (19). The Knudson hypothesis, also known as the two-hit hypothesis, suggests that one functional allele is sufficient for the correct functioning of tumour suppressor proteins, and that both alleles must be inactivated in order for the protein to become dysfunctional (20).

Knudson's work led to the identification of the first tumour suppressor gene, *Rb*, through studies of the rare childhood eye tumours of the same name. It

was found that mutations in *Rb* conferred a susceptibility to tumour formation (21), and later studies have shown that Rb has a direct role in cell cycle progression. The Rb protein functions during the G_1 phase of the cell cycle and is particularly important during the G_1/S checkpoint, where it can block entry into the S-phase of the cycle and therefore inhibit cell proliferation (22). Rb belongs to a family of proteins called pocket proteins, which are named for the conserved binding pocket region which the proteins share. There are three pocket proteins: Rb/p105, p107 and Rb2/p130, and an overexpression of each of these proteins has been shown to induce cell cycle arrest (23). The pocket proteins also interact with E2F transcription factors, and this complex can bind to the promoter region of genes required for G_1/S transition, thereby repressing their transcription (24), and they also possess the ability to block G_1/S transition in E2F-independent manners, such as interaction with various CDK proteins. If the *Rb* gene is mutated and the protein becomes dysfunctional, there will be insufficient suppression of the cell cycle, and uncontrolled cell proliferation may occur.

One of the few tumour suppressor genes that does not follow Knudson's two-hit hypothesis is *tumour protein 53 (TP53),* which encodes p53, a crucial protein often described as 'the guardian of the genome'. *TP53* is mutated in approximately 50 % of human cancers (25), making it the most commonly mutated gene across all cancer types. An inherited mutation in a *TP53* allele results in Li-Fraumeni syndrome, a disorder in which individuals are predisposed to a spectrum of early onset cancers, including sarcomas and breast cancer (26). In healthy cells, levels of p53 are fairly low, however cellular stress leads to an increase in protein levels and an amplified ability of p53 to bind to DNA, where it regulates levels of transcription (27, 28). An increase in p53 activity is linked to the activation of genes involved in both cell cycle arrest and DNA repair, and p53 has been shown to function in each of

the various DNA repair pathways (29). p53 has also been shown to function at the G_1/S cell cycle checkpoint, where it specifically inhibits the activation of CDKs upon DNA damage in order to induce cell cycle arrest (30). Therefore, a dysfunctional copy of p53 can lead to the accumulation of DNA damage and no suppression of proliferation in damaged cells, eventually leading to tumourigenesis.

Further well-characterised examples of tumour suppressor genes are the *breast cancer type 1/2 susceptibility protein* (*BRCA1/BRCA2)* genes, which encode proteins of the same names. BRCA1 is an E3 ubiquitin protein ligase that is recruited to sites of DNA double strand breaks (DSBs), where it interacts with the DNA repair protein RAD51 (31). There is also evidence that BRCA1 may have a role in DNA DSB end resection, due to its interactions with the MRE11-RAD50-NBS1 (MRN) complex (32). BRCA2 has a similar role, in that it recruits RAD51 to the site of DSBs to induce the homologous recombination (HR) pathway of DNA repair (33). Due to their functions in the DNA damage response pathways, BRCA1 and BRCA2 are vital tumour suppressor proteins. A mutation in just one allele of either *BRCA1* or *BRCA2* leads to hereditary breast and ovarian cancer (HBOC) syndrome, in which there is a lifetime risk of 50 – 80 % for developing breast cancer, and a 30 – 50 % risk of developing ovarian cancer. HBOC syndrome also results in a predisposition to other cancers such as pancreatic, stomach, laryngeal and fallopian tube cancer (34).

1.1.3. Avoiding apoptosis

Apoptosis is the process of programmed cell death that occurs in multicellular organisms. It has a role in a variety of biological processes, including embryonic development, ageing, and disease. Importantly, apoptosis is crucial for the maintenance of homeostasis in cell population numbers (35). There are

many components in the apoptosis pathway (figure 1.2). Upstream apoptosis regulators can be intrinsic, in that they deal with the intracellular signals being generated, or extrinsic, in that they process extracellular signals (36). In the extrinsic apoptosis pathway, extracellular ligands activate transmembrane receptors such as tumour necrosis factors (TNFs) and Fas receptors (37), which then recruit adaptor proteins. Adaptor proteins bind to initiators procaspase-8 and procaspase-10 to form the death-inducing signalling complex (DISC) (38). The DISC activates cysteine-aspartic protease (caspase)-8, triggering the execution phase of apoptosis (39). On the other hand, the intrinsic apoptosis pathway involves the function of the mitochondria. Stimuli such as DNA damage, growth factor deprivation and cellular calcium deficiency upregulate BH3-only proteins, which are members of the B-cell lymphoma 2 (Bcl-2) family. BH3-only proteins activate BAX and BAK, which then oligomerise and cause mitochondrial outer membrane permeabilisation (MOMP) – this is the point of no return for a cell undergoing apoptosis (40). The permeabilisation of the mitochondrial membrane allows intermembrane proteins, such as cytochrome C and second mitochondria-derived activator of caspase (SMAC), to be released into the cytoplasm. Cytochrome C interacts with apoptotic protease-activating factor-1 (APAF-1), dATP and procaspase-9 to form the apoptosome, which allows the conversion of procaspase-9 into caspase-9. Caspase-9 then activates caspases-3 and -7, which act as executioner proteins (39).

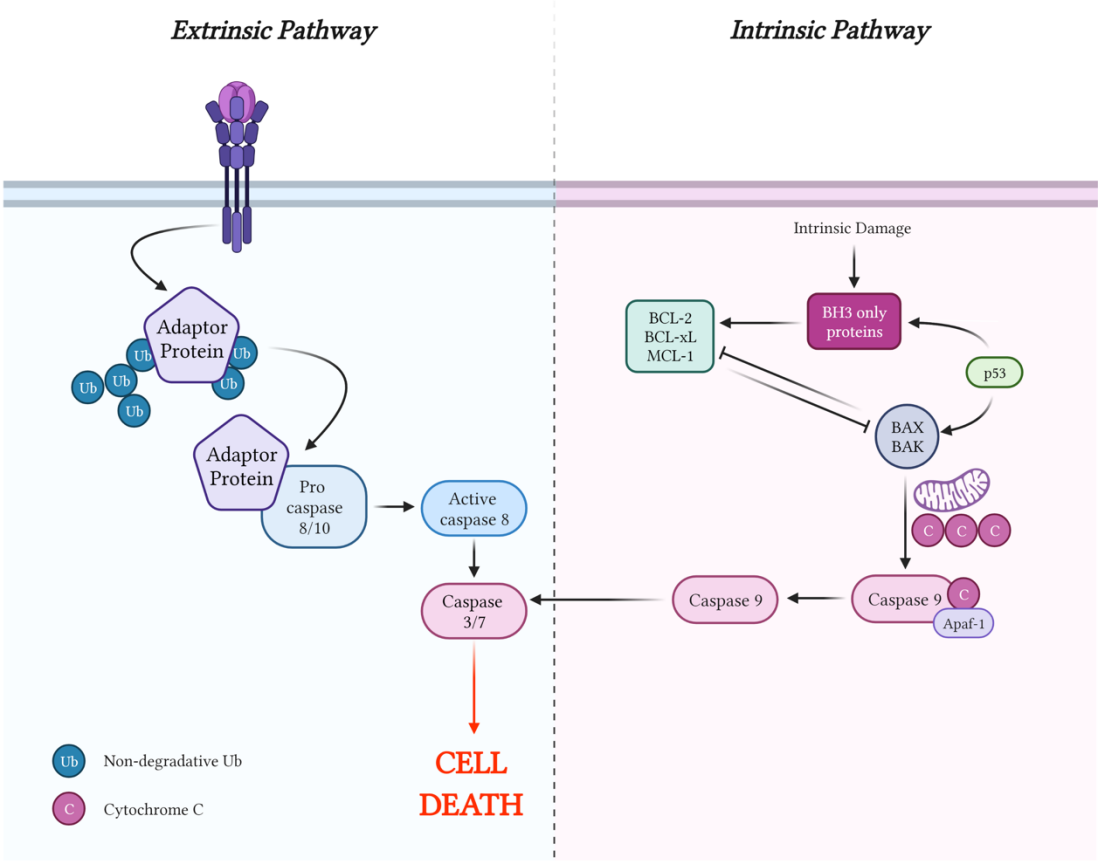

Figure 1.2: The Pathways of Apoptosis

In the extrinsic apoptosis pathway, extracellular ligands activate transmembrane receptors, which then recruit adaptor proteins. Adaptor proteins bind to initiators procaspase-8 and procaspase-10 to form the DISC, which activates caspase-8 and triggers the execution phase of apoptosis. In the intrinsic pathway, there is an upregulation of BH3-only proteins. BH3-only proteins activate BAX and BAK, which cause MOMP, allowing intermembrane proteins, such as cytochrome to be released into the cytoplasm. Cytochrome C interacts with APAF-1, dATP and procaspase-9 to form the apoptosome, which allows the conversion of procaspase-9 into caspase-9. Caspase-9 then activates caspases-3 and -7, which act as executioner proteins.

It is well understood that apoptosis is a natural barrier to cancer development (41). In order to maintain the correct amounts of cell survival and apoptosis, there needs to be a careful balance of pro- and anti-apoptotic signalling within the cell (36). There are a multitude of proteins involved in maintaining this balance, and mutations in any of them can result in the formation of tumours. For example, the Bcl-2 family of proteins regulate cell death by controlling the activity of BAX and BAK, proteins that have a role in the intrinsic apoptosis pathway (36). An increase in Bcl-2 levels can disrupt the balance of BAX and

BAK activity in the cell, ultimately reducing levels of apoptosis and contributing to tumour growth (42). As discussed above, caspases are some of the most important proteins in the apoptosis pathways, as they are actively involved in inducing cell death in the final stages of apoptosis. A deficiency of caspase enzymes has been shown to be a causative agent for a wide variety of tumour types, including breast, colon, tongue and prostate cancers (43). Caspase-8 is the most commonly mutated member of the caspase family in cancers. In the wild-type setting, caspase-8 triggers the execution phase in the intrinsic apoptosis pathway (44), therefore a dysfunctional copy of this protein will result in deficiencies in apoptosis, aiding tumour development. Another group of proteins involved in maintaining the correct level of apoptosis are inhibitor of apoptosis (IAP) proteins, which are endogenous inhibitors of cell death. They block the activation of caspases to prevent the initiation of pro-apoptotic pathways in normal cells (45). IAPs display aberrant expression in a variety of human cancers as a result of genetic alterations or the loss of upstream inhibitors, and an increased level of IAP proteins has been associated with tumour progression and treatment failure (46). Survivin is a member of the IAP family and displays high levels of expression in many human cancers (47), although interestingly, survivin does not appear to be present in normal adult cells (48). 80 % of oral squamous cell carcinomas (OSCCs) display significantly high levels of survivin expression, as do 50 % of oral pre-malignant lesions, suggesting that elevated expression of survivin may be linked to the early stages of tumourigenesis (49). Nuclear factor kappa-light-chain-enhancer of activated B cells (NF-κB) is a protein complex involved in multiple cellular processes, including the regulation of cell survival. One of the functions of NF-κB is to stimulate the expression of anti-apoptosis genes, including caspase inhibitors and IAPs (50), therefore overexpression of these proteins leads to cell proliferation and tumour growth (51). Many human cancers are thought to utilise elevated levels of NF-κB signalling to avoid

apoptosis and maintain proliferation, for example, the activity of NF-κB is enhanced in approximately 41 % of nasopharyngeal cancers (52).

1.1.4. Enabling replicative immortality

One of the most defining features of tumour cells is their unlimited replicative abilities. Normal, healthy cells have a defined number of replicative cycles they can pass through before undergoing senescence – a process in which the cells enter a non-proliferative state, but do not die – or apoptosis. This is known as the Hayflick limit (53). Helping to maintain this replicative limit are the telomeres, nucleoprotein complexes that cap the end of linear chromosomes. Telomeric DNA consists of 5 – 12 kb of hexanucleotide repeats – 5′-TTAGGG-3′ – with a single-strand overhang. The DNA is bound by a protein complex called shelterin, which has 6 subunits: TRF1, TRF2, POT1, TIN2, TPP1 and Rap1. Shelterin prevents the telomere end from being incorrectly recognised as a DNA DSB and being processed by DNA damage repair proteins. If not for the shelterin complex, telomere ends would be joined together via non-homologous end joining (NHEJ), thus shelterin has a vital role in maintaining genome integrity (54). With every cell division, the telomeres of somatic cells shorten by 60 – 120 base pairs (55), and once the telomeres have reached a critical length, the cell will enter telomere-induced crisis, which is characterised by replicative senescence and chromosome end-to-end fusions, alongside extensive apoptosis (56). Telomere shortening and the resulting apoptosis therefore prevents accumulation of cells with genomic instability and is consequently a crucial anti-cancer mechanism.

Cancer cells have the ability to bypass the Hayflick limit by activating telomere maintenance mechanisms. Between 85 – 90 % of cancers utilize telomerase, a reverse transcriptase enzyme, to prevent telomere shortening (57). Telomerase

adds new telomeric repeats onto the end of the chromosome via its telomerase reverse transcriptase (TERT) component, and telomerase RNA, which provides the template for DNA synthesis (58). It is active in embryonic and stem cells, but virtually undetectable in healthy adult somatic cells (59). In contrast, telomerase is reactivated in approximately 85 % of human cancers via a variety of mechanisms including promoter mutations and genetic amplification (60). Those cancers that do not re-activate telomerase instead use a process known as alternative lengthening of telomeres (ALT). ALT utilises the HR process normally used for DNA repair to maintain telomere length (61).

1.1.5. Induction of angiogenesis

Tumours, like healthy tissues, require a supply of nutrients and oxygen, and a method of metabolic waste removal. To meet these requirements, tumours develop their own blood supply by triggering numerous angiogenic switches. The development of vasculature in the human body takes place during embryogenesis, where new endothelial cells are produced, and they form tubes. This process is known as vasculogenesis, while angiogenesis is the sprouting of new blood vessels from existing ones (1). Normally, the vasculature remains fairly inactive after morphogenesis, except during processes such as wound healing. However, tumours appear to maintain angiogenic signalling and thus constantly generate new blood vessels to sustain tumourigenesis (62). Tumours that do not have a blood supply are unable to develop beyond a certain point, however by expressing high levels of signalling proteins that are involved in angiogenesis, such as vascular endothelial growth factor (VEGF) and thrombospondin 1 (TSP-1), the tumour can proliferate and metastasise.

VEGF is a crucial mediator of angiogenesis during embryonic development, and also plays a role in maintaining the homeostasis of endothelial cells in adults (1). An upregulation of VEGF, which can be caused by hypoxic conditions or mutations in oncogenes, increases pro-angiogenic signalling in the cell and thus contributes to tumour growth (63, 64). On the other hand, TSP-1 acts in the opposite way to VEGF and suppresses pro-angiogenic signalling to maintain balance in the cell. Incorrect TSP-1 expression, therefore, can promote angiogenesis to encourage tumour growth (65). The triggering of the angiogenic switch has been shown to be an early event in tumour development, suggesting that this is a key characteristic of tumours (66). However once angiogenesis has been initiated, tumours display wide variations in the extent to which they are vascularized (67).

1.1.6. Invasion and metastasis

One of the defining characteristics of a high pathological grade tumour is its ability to invade local tissues and metastasise to distant parts of the body (figure 1.3), and the majority of cancer-related deaths are caused by invasion and metastasis. There are five key steps in cancer cell metastasis: invasion, intravasation, circulation, extravasation, and colonisation.

It has been shown that as cancer cells develop the ability to spread, they undergo changes in morphology and cell-cell adhesion (1). There are many proteins involved in maintaining correct cell-cell adhesion, such as matrix metalloproteinases (MMPs). MMPs are zinc-dependent endoproteinases that can modulate cell-cell adhesion in tissues, and therefore incorrect MMP expression may lead to tumour metastasis (68). One of the most important cell-cell adhesion molecules is E-cadherin, which displays aberrant expression in many cancers. Studies have confirmed E-cadherin's role as a tumour

suppressor, as re-introducing the protein in cancer cells lacking E-cadherin leads to the inhibition of tumour progression and invasion (69), and the loss of E-cadherin has been linked to more advanced tumours and worse prognosis in cancer patients (70). E-cadherin is also a key player in the process of epithelial to mesenchymal transition (EMT), in which immotile epithelial cells are transformed into motile mesenchymal cells, allowing for cell migration. EMT is critical during embryonic development, but has also been heavily implicated in promoting the invasion and metastasis of cancers (71). The transition from epithelial to mesenchymal states is controlled by a wide range of growth factors and signalling pathways, and appears to proceed in a step-wise fashion in contrast to being a binary switch as previously believed (72-74). There are a variety of triggers for EMT in cancer cells, including metabolic stressors, hypoxia, and the diversity of the microenvironment (75, 76). Single cells disseminate from the tumour during EMT and transition from epithelial to mesenchymal cells. These single cells are then free to invade the blood vessels, thus allowing them to spread throughout the body. This movement of cancer cells into the vasculature is known as intravasation. Most cancer cells travel through the blood vessels as single cells; however, others may move as clusters, and these clusters are more likely to form secondary tumours in a new location (77). Extravasation is the movement of the cancer cells out of the blood vessels to a new site. During this process, the cancer cells enter small capillaries and become trapped, leading to the cells exiting the vessels and entering new tissues (78). Interestingly, the process of EMT is reversible (mesenchymal to epithelial transition (MET)), and metastasising cancer cells are thought to employ this process once they have reached a new location in the body in order to start developing secondary tumours (79), completing the final stage of the metastasis cascade: colonisation.

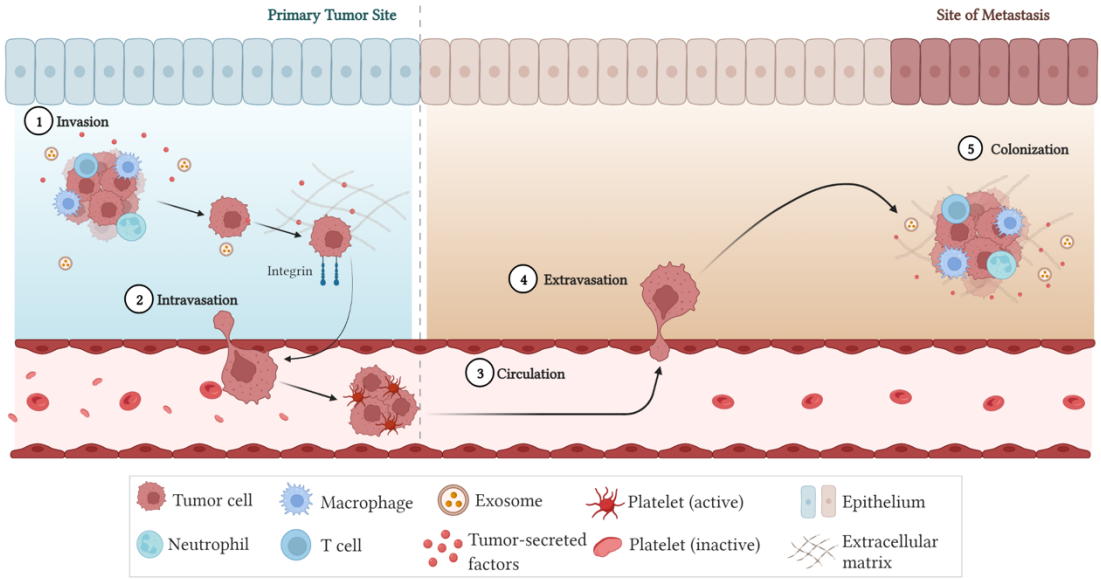

Figure 1.3: The Metastasis Cascade

There are 5 key steps to the metastasis cascade. It begins with invasion, where cancer cells undergo EMT, and this is followed by intravasation, the movement of cancer cells into the vasculature. Next, the cancer cells enter small capillaries and become trapped, leading to the cells exiting the vessels and entering new tissues – this is extravasation. Metastasising cancer cells are thought to reverse EMT when they have reached a new location and start developing secondary tumours (colonisation).

1.1.7. Deregulating cellular energetics

In healthy cells, energy metabolism starts with anaerobic glycolysis – a process by which glucose is converted into pyruvate, producing adenosine triphosphate (ATP) and reduced nicotinamide adenine dinucleotide (NADH) as by-products. Pyruvates are oxidised to form acetyl coenzyme A (acetyl CoA), which is then involved in the aerobic stage of the metabolism cascade. The Krebs cycle is the next step of the process, in which acetyl CoA is further oxidised and undergoes a series of reactions to produce energy-rich ATP. Carbon dioxide and water are produced as waste products during this aerobic process. The final stage of energy metabolism, the electron transport chain, produces large amounts of ATP via the movement of high-energy electrons.

In anaerobic conditions, healthy cells cannot move past the glycolysis stage of metabolism, and less ATP is produced.

Abnormal energy metabolism in cancer cells has been recognised since the 1930s, and in the 1950s it was first described that, even in the presence of oxygen, cancer cells reprogram their metabolism and energy production to undergo 'aerobic glycolysis', also known as the Warburg effect (80). This is a form of specialised fermentation, in which the pyruvate produced during glycolysis is converted into lactate rather than being oxidised into acetyl CoA. This does not generate as much ATP as normal aerobic respiration; however, it does allow cancer cells to increase the production of molecules such as nucleotides, amino acids, and lipids, which are required for the production of new cells (81). In essence, the Warburg effect favours proliferation over ATP production. Cancer cells compensate for the decrease in ATP production by increasing the transport of glucose into the cytoplasm via the upregulation of transporters such as GLUT1 and GLUT3 (82). The expression levels of the genes encoding these transporters, as well as other genes involved in energy metabolism, can be activated by the hypoxia-inducible factor (HIF) transcription factors (83). HIF expression is induced in hypoxic conditions, like those in the interior of many tumours, and thus the internal environment of the tumours is crucial to the reprogramming of their energy metabolism.

1.1.8. Avoiding immune destruction

The immune system is made up of a variety of different cell types, including B cells, T cells, natural killer (NK) cells, and phages, that work to protect the body from infections and illnesses, including cancer. The immune system is responsible for removing many developing tumours, and therefore any tumours that do develop have managed to evade the surveillance of the

immune system (1). This idea is further supported by the fact that individuals with a dysfunctional immune system have a higher incidence of a variety of cancer types (84). There are two mechanisms employed by cancer cells to avoid immune surveillance: avoiding recognition by the immune system, and initiating immunosuppressive conditions in the tumour microenvironment (TME) (85).

In order to avoid detection by the immune system, cancer cells decrease the expression of tumour-specific antigens on the surface of the cell, thus preventing T-cells from recognising them as harmful and destroying them. The genetic mutations that cause the decrease in antigen expression are relatively common, for instance the loss of heterozygosity (LOH) in genes encoding human leukocyte antigens is seen in approximately 40 % of non-small cell lung cancers and has been associated with immune therapy resistance in both colorectal, melanoma, and lung cancer patients (86-88). Furthermore, studies have shown that cancer cells develop ways to avoid recognition and attack by NK cells. NK cells work by swiftly removing any malignant cells they detect in the body in response to specific ligands which are present on target cells, and are therefore a crucial part of the immune response to cancer development (89). Dysfunctional NK activity is associated with a worse prognosis and may be linked to cancer metastasis, highlighting how important these cells are (90, 91). *In vitro* experiments have shown that breast and lung cancer cell lines downregulate the activators of NK cells on their surface, thus preventing detection (92). The TME consists of a number of key components, such as the proteoglycans, tumour-associated fibroblasts and hyaluronic acid of the extracellular matrix (ECM), tumour parenchyma cells, blood and lymph vessels, mesenchymal cells, tumour infiltrating immune cells, and various enzymes, chemokines and cytokines (93, 94). Both the

immune and non-immune components of the TME have critical functions in cancer progression and tumour control.

Research has shown that tumour-infiltrating immune cells, such as myeloid-derived suppressor cells (MDSCs), cytotoxic lymphocytes, and tumour-associated macrophages (TAMs) can influence tumour development and act as determining factors in prognosis. For example, MDSCs and TAMs have been demonstrated to enhance tumour progression (95, 96), and cytotoxic lymphocytes have been positively correlated with prognosis in several cancer types, including hepatocellular carcinoma and colorectal cancer (97, 98). Moreover, chemokines and cytokines can also influence anti-tumour immune responses (99, 100). Tumour-associated fibroblasts provide growth factors for the cancer cells, and are critical for the formation of the ECM (101). Other non-immune cell lineages in the TME, such as mesenchymal stem cells, have the potential to differentiate into other types of cells required for tumour development and angiogenesis, as well as forming new carcinoma cells (102). The various components of the TME are understood to be vital determining factors in the development, progression, and prevention of tumours, and the status of the TME has been linked to cancer prognosis and outcome (94).

1.2. Head and Neck Squamous Cell Carcinoma

Cancer is one of the leading causes of mortality worldwide, and in 2020, nearly 10 million deaths were attributed to a form of the disease (103). Head and Neck Squamous Cell Carcinoma (HNSCC) is the sixth most common cancer worldwide, with approximately 1.1 million cases and 500,000 deaths per year, according to data from 2021 (104). The incidence of HNSCC appears to be rising – there has been an average increase of 24 % in the last decade, potentially as a result of increasing incidences of HPV-infection (105). The

survival rates of HNSCC are extremely varied, with 10-year survival ranging from 19 – 59 %, and 5-year survival ranging from 28 – 67 % (105).

1.2.1. Head and Neck Squamous Cell Carcinoma Development

Head and neck cancers are a group of cancers that arise in regions including the oral cavity, nasal cavity, pharynx, larynx, salivary glands, and sinuses (figure 1.4). The majority of head and neck cancers are squamous cell carcinomas (SCCs) and develop from the mucosal epithelium lining the head and neck.

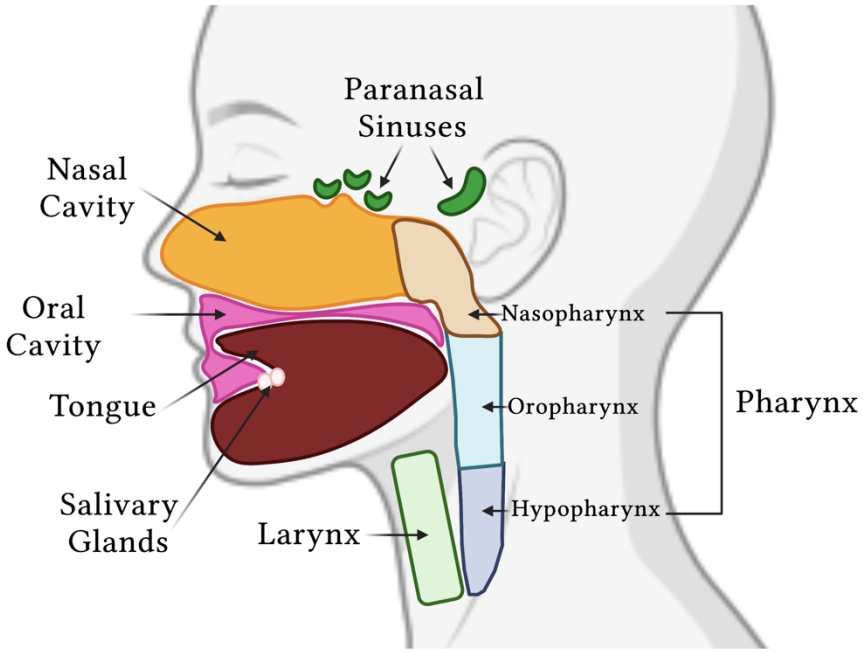

Figure 1.4: Head and Neck Cancer Regions

HNSCCs develop from the mucosal epithelium lining in a variety of regions in the head and neck, including the oral cavity, nasal cavity, pharynx, larynx, salivary glands, and sinuses.

HNSCC is an extremely heterogenous and complex disease involving a wide variety of risk factors. The main risk factors are tobacco consumption, alcohol

consumption, and infection with viruses such as Epstein-Barr virus (EBV) and human papilloma virus (HPV), notably HPV types 16 and 18. Alcohol and tobacco consumption appear to synergise with one another, promoting the carcinogenic effects (106), and heavy smokers or drinkers have a 35-fold increase in their risk of developing HNSCC (107). Smoking and alcohol intake both cause DNA damage in cells, contributing to the overall genomic instability that underlines the hallmarks of cancer. In geographical terms, smoking and alcohol consumption are the most widely occurring risk factors, whereas other risk factors are much more localised to certain populations. For example, chewing of areca nut products such as betel quid is associated with high rates of oral cavity cancer in India, Taiwan, and some provinces of China (108). Interestingly, the incidence of HNSCC is 21 % higher in the North West of England compared to the national average (109). Moreover, there is a higher prevalence of HPV in males, thus making them more at risk of developing HNSCC (110, 111). A small proportion of HNSCCs develop from pre-existing lesions such as leukoplakia (white lesions) or erythroplakia (red lesions) – these are known as potentially malignant lesions (PPOLs). For the most part, however, HNSCCs develop *de novo* from normal mucosa (112). HNSCC develops in a stepwise manner from normal mucosa to an invasive carcinoma, and there are several key genetic alterations associated with each step of the progression.

The transition from normal mucosa to hyperplasia is associated with the LOH of chromosome 9p21, a region which includes the gene *cyclin dependent kinase inhibitor 2A* (*CDKN2A*) and its alternate reading frame product *ARF*, both of which act as tumour suppressors (113). The next stage of progression is the transformation from hyperplasia to dysplasia. This is characterised by the LOH of chromosomes 3p21, which harbours cancer-related genes such as transcriptional regulators of *TERT* (114), and 17p13, which is the locus of the

TP53 tumour suppressor (113). LOH of chromosomes 11q17, 13q21 and 14q32 marks the transition from dysplasia to carcinoma *in situ*, and results in the amplification of the *CCND1* gene, which encodes the cell cycle protein cyclin D1 (113). Currently, it is unclear as to whether it is simply the occurrence of these genetic alterations that contribute to HNSCC development, or whether this specific chronological sequence of events is required. According to data from The Cancer Genome Atlas, the most frequently altered genes in HNSCC are *CDKN2A* (22 % of samples) and *TP53* (72 % of samples) (115). HPV has the capability to induce carcinogenesis as it carries 2 oncogenes within its genome – E6 and E7 – which promote tumour formation in infected cells (116).

1.2.2. p53 Mutations in Head and Neck Squamous Cell Carcinoma

Mutations of the *TP53* gene are amongst the most common mutations in HNSCCs. More specifically, tumours originating from the larynx and hypopharynx have the highest *TP53* mutation rate (117). The majority of *TP53* mutations in HNSCCs are missense mutations, and are thought to occur early during carcinogenesis, as research has shown that *TP53* mutations are often found in premalignant lesions (115, 118). The p53 protein has a key role in the cellular response to stress and is activated through phosphorylation or acetylation immediately following detection of genotoxic stress. This leads to the transcription of a huge variety of downstream genes involved in cell cycle arrest, metabolism, senescence and apoptosis, and the overall impact prevents the proliferation of cells with DNA damage (119). Most *TP53* mutations arise in the DNA-binding domain, and loss-of-function p53 mutants have a complete lack of transcriptional function, thus preventing the transcription of downstream proteins. Loss of p53 function therefore results in deficits in cell cycle control and apoptosis, and research has highlighted the role of p53 in the regulation of cell metabolism (120). Interestingly, gain-of-function *TP53*

mutations can also occur, which enhance tumourigenic and metastatic potential of cells as well as increasing resistance to chemotherapy agents (120). Gain-of-function p53 mutants have been demonstrated to exert control over genome stability, EMT, angiogenesis, metabolism, and inflammation – the hallmarks of cancer (121-123).

1.2.3. HPV-Positive Head and Neck Squamous Cell Carcinoma

HPV is a small DNA virus that infects basal cells of stratified epithelium tissue (124). It has a genome of approximately 8 kilobases, encoding 8 proteins essential for viral infection and replication. There are 6 early genes in the HPV genome, *E1, E2, E4, E5, E6* and *E7*, which are transcribed during the early stages of the replication cycle (125). There are also 2 late genes present in HPV, *L1* and *L2*, which encode the viral capsid proteins. Genes *E1* – *E5* have regulatory functions, such as DNA replication, transcription control and cellular proliferation (125). The *E6* and *E7* genes encode proteins that modify the cell cycle and have the ability to inactivate p53 and Rb respectively in normal cells (126) (figure 1.5). The E6 protein has a role in sustaining proliferative signalling and impairing the DNA damage response in cells via the degradation of the p53 protein. E6 forms a complex with E6-associated protein (E6-AP), a ubiquitylation enzyme. This complex ubiquitylates p53, thus marking it for degradation (127). p53 has important roles in maintaining genomic integrity, and its degradation results in a loss of control of the cell cycle and uncontrolled cell growth, as well as increased genome instability (128). The E7 protein, on the other hand, affects the activity of the Rb tumour suppressor protein. Rb normally represses the expression of enzymes involved in DNA replication via the binding of E2F transcription factors (129). The E7 protein disrupts Rb function by binding to essential regions called the 'pocket domains' on the protein (130). Binding of E7 to the pocket domains prevents

interactions between Rb and E2F transcription factors, thus removing any control over cell growth (131). This leads to uncontrolled proliferation of cells with DNA damage, therefore contributing to the development of cancers (132). Studies suggest that those who are infected with HPV-16 are 14 times more likely to develop HNSCC, predominantly in the oropharynx, than those who are not (133). Data from 2017 suggests that 30.8 % of oropharyngeal SCCs can be attributed to HPV infection, and the vast majority of these patients (~86 %) are male (134). HPV-positive HNSCC is a distinct biological entity and has a better overall prognosis than its HPV-negative counterpart as a result of the loss of Rb/p53 functions causing increased sensitivity to treatment modalities.

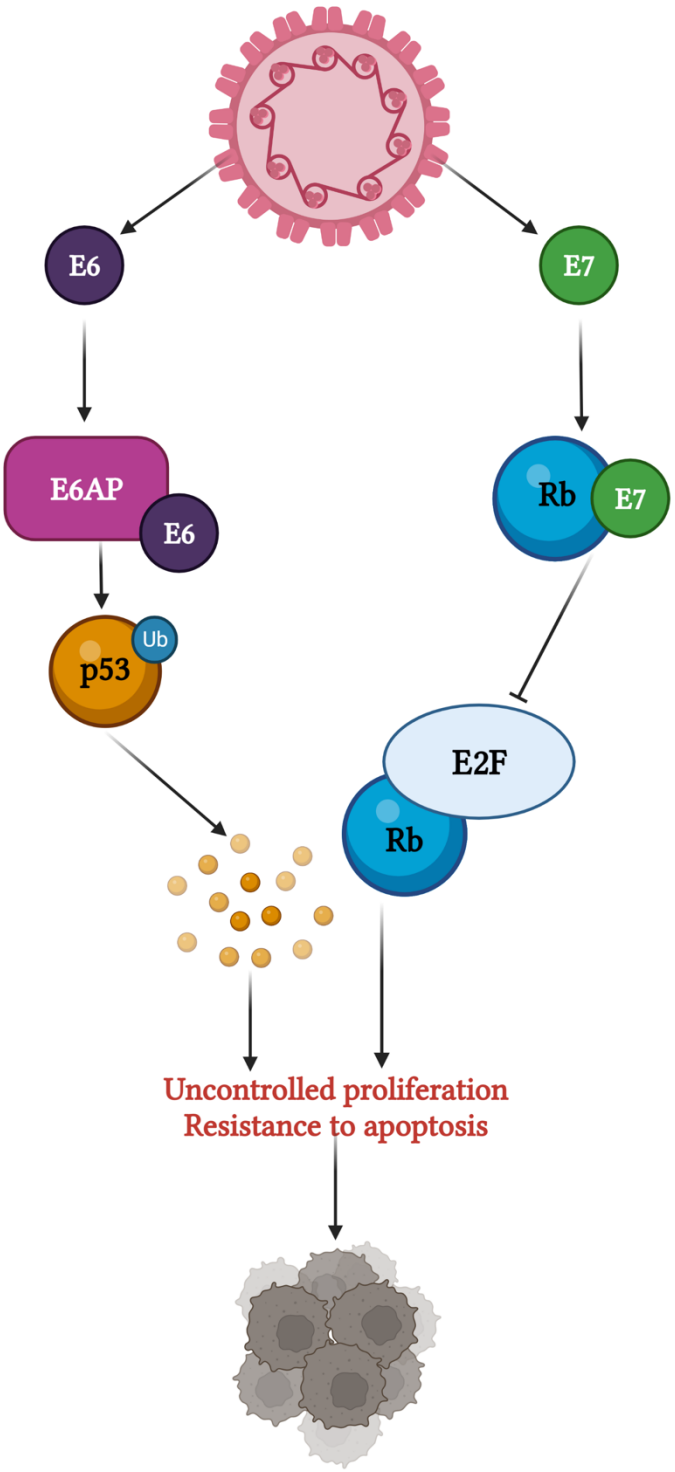

Figure 1.5: How HPV Causes Cancer

The HPV genes E6 and E7 encode tumour-promoting proteins. E6 forms a complex with E6AP, and this complex ubiquitylates p53, marking it for degradation. p53 degradation results in a loss of control of the cycle and uncontrolled cell growth. Meanwhile, the E7 protein disrupts Rb function by binding to essential pocket domains. This prevents interactions between Rb and E2F transcription factors, thus removing any control over cell growth. This leads to uncontrolled proliferation of cells with DNA damage, therefore contributing to the development of cancer.

1.2.4. Current HNSCC Treatments

Currently, the main treatments for HNSCC are surgical resection, radiotherapy, and chemotherapy, with the aim of effectively treating the cancer whilst preserving the maximum amount of organ function. Small cancers with no spread to the lymph nodes (or restricted spread to a single node) can be effectively treated with a single type of therapy – most commonly either surgery or radiation. These cases have high survival rates, with a progression-free survival rate of over 80 % according to 2018 data (135). Cancers in the oral cavity are often treated through surgical resection, while cancers of the larynx or pharynx are generally treated with radiation. More advanced tumours are treated with a combination of the three therapies - surgical resection followed by chemotherapy and radiotherapy together (chemoradiation). This reduces the chance of recurrence and increases survival rates, however, it is also shown to enhance the late toxicities of radiation, such as chronic dysphagia (difficulty swallowing), and may increase the risk of non-cancer-related mortality (136, 137).

The standard chemotherapy treatment for HNSCC is cisplatin, a platinum-based drug that generates DNA damage. Cisplatin interacts with nucleophilic N7-sites of purine bases, forming DNA-protein and DNA-DNA crosslinks (138). The majority of cisplatin-induced damage is in the form of intrastrand DNA adducts, which induces apoptosis in cancer cells. The DNA adducts are recognised by DNA damage recognition proteins, such as human MutS homolog 2 (hMSH2), which is part of the mismatch repair (MMR) pathway, non-histone chromosomal high-mobility group 1 and group 2 (HMG1/2) proteins, and TATA binding protein (TBP) (139, 140). The activation of DNA damage response proteins leads to the stimulation of several downstream pathways and processes, for example, the activation of cell cycle checkpoints.

After treatment with cisplatin, cells have been shown to arrest during S-phase, and then inhibit Cdc2-cyclin A/B kinases to induce G_2/M cell cycle arrest (141). Cisplatin treatment also results in the activation of the Bax apoptosis protein and the stimulation of the ATR checkpoint kinase, which activates p53 via phosphorylation, thus initiating the apoptosis cascade (140, 142).

Radiotherapy is used as both a curative and a palliative treatment for HNSCC patients. Intensity modulated radiotherapy (IMRT), in which the radiation beam is shaped to accurately fit the tumour and reduce the dose of radiation to healthy tissue, is most commonly used (143). In recent years, there has been an increase in the use of particle ion therapy, such as proton beam therapy (PBT) to treat certain cancers. PBT is more targeted than conventional radiotherapy as it has a low entrance dose, which increases along the radiation track before peaking at a well-defined region known as the Bragg peak. After peaking, the energy rapidly drops at the distal fall-off (144). This allows the radiation dose to be targeted to specific tumour regions while minimising energy deposition to surrounding healthy tissues. Moreover, combining proton beams with differing initial energies produces a so-called spread-out Bragg peak (SOBP), enabling the targeting of proton irradiation to a larger tumour volume.

1.3. Radiotherapy and the DNA Damage Response

1.3.1. Radiotherapy

During radiotherapy, patients are exposed to ionising radiation (IR), which deposits energy in cells as it passes through the tissues in the body. This damages the DNA in any cells subjected to the IR, including both cancerous

and healthy cells (145). On average, 1 Gy IR induces 1000 single-strand breaks (SSBs), 30 double-strand breaks (DSBs), 850 pyrimidine lesions and 450 purine lesions per cell, the most toxic of which are DSBs (146-148). In healthy cells, DNA damage response (DDR) pathways are activated to repair this IR-induced damage. However, cancer cells have defects in these pathways, and therefore the majority of tumour types are less efficient at repairing the damage caused by IR in comparison to healthy cells, resulting in cancer cell death (149). There are some exceptions, for example, glioblastoma cells tend to have upregulated DDR pathways, allowing the efficient repair of damage and the avoidance of cell death (150). Conventional low-linear energy transfer (LET) radiation causes the majority of damage indirectly through the generation of reactive oxygen species (ROS) upon interaction with water molecules in the cells (145). Cellular sensitivity to radiation is therefore dependent on the extent of DNA damage generated within the cell, and how able the cell is to repair this damage (151).

1.3.2. Radioresistance in HNSCC

Despite the success of radiation-based treatments for HNSCC, radioresistance is a common occurrence. In radioresistant cases of HNSCC, there is either: a lack of response, a partial response, or recurrence after an initial response (152). Approximately 25 % of all HNSCC patients exhibit local relapses after treatment, and this failure of radiotherapy means that patients must undergo surgical salvage, which highly impacts their quality of life (153). Radioresistant cancer cells have a variety of characteristics that contribute to this phenotype, such as an enhancement of DDR proteins. The major pathway for DSB repair is NHEJ, and an overexpression of major NHEJ proteins including Ku80, ATM and TRIP13 has been associated with radioresistance of HNSCC *in vitro* (154-158). Moreover, there has been some suggestion that the p53 status of the

tumour cells can contribute to radiosensitivity, as p53 contributes to the regulation of the DDR and cell survival following exposure to radiation. HNSCC cases that display higher levels of therapy resistance and locoregional recurrence often carry mutations in the *TP53* gene (*p53-mut*). As a result, these cells cannot efficiently repair the radiation-induced damage, nor can they undergo cell death. Thus, these cells proliferate in their damaged state and contribute to the overall tumour radioresistance (159). Mutations in the *TP53* gene could also explain the relative radiosensitivity of HPV-positive HNSCCs in comparison to their HPV-negative counterparts. 75 – 85 % of HPV-negative HNSCCs carry *TP53* mutations (*p53-mut*), while most HPV-positive tumours have wild-type p53 (*p53-WT*) (160). However, more research is required to fully elucidate the associations between HPV status, *TP53* mutations, and radioresistance. Another possible explanation for tumour radioresistance is overexpression of the epidermal growth factor receptor (EGFR), as an increase in levels of EGFR in tumours has been linked to locoregional failure following radiotherapy (161). This could be due to the regulation of DSB repair, as EGFR can form complexes with the DNA-dependent protein kinase (DNA-Pk), or could be a result of altered signalling through pathways controlled by EGFR, such as phosphoinositide 3-kinase (PI3K) and Ras pathways (162-164). Finally, tumour hypoxia has been shown to contribute to radioresistance. Hypoxia develops due to an imbalance between the supply and demand for oxygen in the cancer cells, and in the low oxygen conditions in the hypoxic tumour core there are reduced levels of DNA damage induced by IR (165-168).

Due to the significant reduction in patient survival and quality of life caused by radioresistant tumours, it is crucial that research aims to identify novel methods of increasing tumour radiosensitivity and thus improve patient outcomes.

1.3.3. DNA

DNA is the hereditary material found in almost every cell in every organism and is necessary for life. The three-dimensional structure of DNA was discovered in 1953, and consists of two complementary polynucleotide chains in a double helical structure held together by hydrogen bonds (169). The DNA polymer is comprised of repeating monomer units called nucleotides (figure 1.6a), formed from a deoxyribose sugar, a phosphate group, and one of four nitrogenous bases: adenine (A), guanine (G), thymine (T) and cytosine (C) (figure 1.6b). These bases pair along the double helix structure in a specific manner – A always pairs with T, and G with C (170). The order in which the bases are arranged along the sugar-phosphate backbone is crucial, as it forms the genetic code.

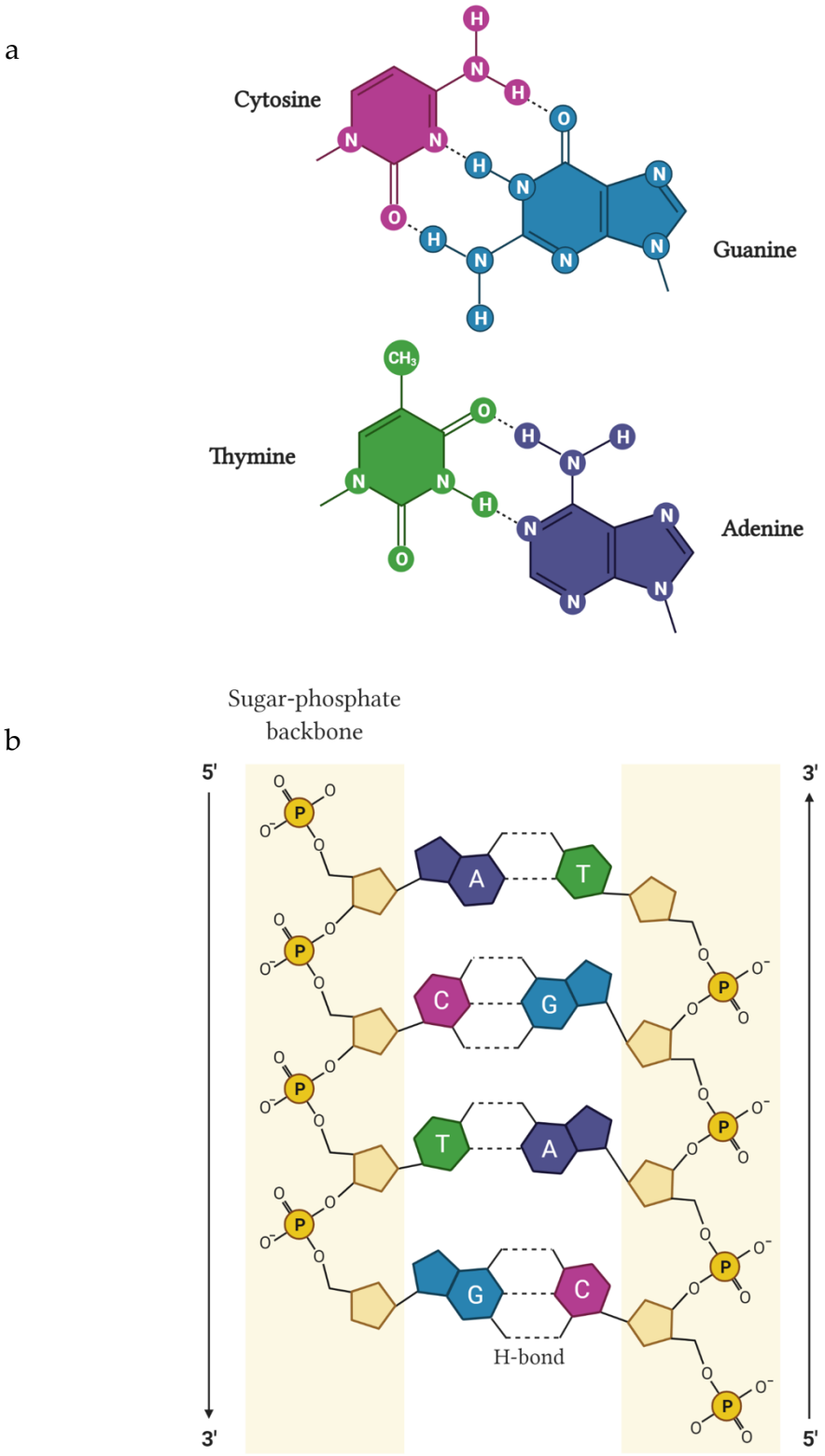

Figure 1.6: The Structure of DNA

a) The DNA double helix is comprised of repeating monomer units called nucleotides, formed from a deoxyribose sugar, a phosphate group, and one of four nitrogenous bases: adenine (A), guanine (G), thymine (T) and cytosine (C). b) These bases pair along the double helix structure in a specific manner – A always pairs with T, and G with C. The order in which the bases are arranged along the sugar-phosphate backbone is crucial, as it forms the genetic code.

Within the 6.4 billion base pairs of the diploid human genome, there are functional, coding units called genes, as well as long stretches of non-coding regions of DNA. Genes are transcribed by an enzyme called RNA polymerase to produce a strand of messenger RNA (mRNA). The mRNA is complementary to the DNA strand from which it was transcribed in all aspects but one – the base uracil replaces thymine in RNA. This mRNA strand is then translated into a protein by transfer RNA (tRNA) molecules. The sequence of bases on the mRNA are read in triplets – known as codons – and each triplet codes for a single amino acid. The amino acids are joined by peptide bonds, and the polypeptide eventually folds into a three-dimensional protein. The sequence of amino acids – and thus the initial DNA sequence of the gene – is crucial for the correct function of proteins, and therefore maintaining genomic integrity is vital to the survival and functioning of cells.

1.3.4. DNA Damage

DNA, like all other biological molecules, is susceptible to damage. The double helical structure of DNA provides a degree of protection; however, the DNA is consistently exposed to damaging agents, both endogenous and exogenous. Endogenous damage is caused by the interaction of DNA with water and ROS, resulting in damage such as oxidation and hydrolysis. On the other hand, exogenous damage results from environmental, physical, or chemical sources, including IR (171). If DNA damage is not repaired correctly and efficiently, the accumulation of genomic instability can have catastrophic consequences at the cellular level, leading to apoptosis, as well as contributing to the development of human diseases, including cancers (172).

Endogenous DNA Damage

Endogenous damage accounts for the majority of DNA damage within a cell. The simplest form of endogenous DNA damage is hydrolysis. The N-glycosidic bond in DNA, which connects the base and sugar components, is particularly vulnerable to hydrolysis, which results in a separation of the base from the phosphodiester backbone, forming an apurinic/apyrimidic (AP) site (173). The purine bases (A and G) have a loss rate 20 times faster than the pyrimidine bases (T and C), and therefore these reactions are often referred to as depurination reactions (174). During replication, DNA polymerases preferentially incorporate adenine opposite the AP site, which results in frameshift mutations or base-pair substitutions, and thus AP sites are highly mutagenic (175). As well as AP sites, hydrolysis can also cause hydrolytic deamination of bases containing an NH_2 group. This most often occurs in cytosine, which forms the base uracil following deamination – this occurs at a rate of 100 – 500 deamination events per cell per day (176). Hydrolytic deamination causes mutagenic nucleotide sequence changes that are commonly found in cancer-associated genes.

Another form of endogenous DNA damage is oxidation. Oxidative DNA damage is caused by ROS, which are inevitably produced during normal physiological processes in the cell such as metabolism and respiration. Exogenous sources of DNA damage, such as IR, can also produce ROS (145). There are different types of ROS, including hydroxyl radicals, hydrogen peroxide, and superoxide anions, amongst many more (173). ROS can cause a variety of different DNA lesions at a rate of ~10,000 lesions per cell per day (177). Guanine is the most susceptible to ROS of the four DNA bases due to its low redox potential, and is the most commonly modified (178). Hydroxyl radicals hydroxylate guanine at the C8 position to produce 8-oxoguanine (8-

oxoG) (179). 8-oxoG can be erroneously paired with adenine by DNA polymerases during replication, causing GC to TA transversion mutations, which are highly mutagenic and can contribute to the formation of cancers (180, 181).

Exogenous DNA Damage

Exogenous DNA damage is caused by environmental sources, both physical and chemical in nature, such as radiation and alkylating agents. Alkylating agents are found in diesel pollutants and tobacco smoke, among other sources, and are also used as chemotherapeutic agents for cancer treatment (182-184). The alkylation of DNA can be as simple as the addition of a single methyl group to a nucleotide base (185), and can also can cause secondary DNA damage through AP sites, DNA strand breaks, and interstrand crosslinks (182). The most commonly methylated base is N7-methylguanine (7meG) (184), which accounts for 75 % of all methylated bases and occurs at a rate of 4000 residues per day (186). 7meG does not alter the coding specificity of the base, however the N-glycosidic bond connecting 7meG to the DNA backbone is easily destabilised, creating cytotoxic AP sites (185). Another common alkylation is N3-methyladenine (3meA), which is extremely cytotoxic. The methyl group enters the minor groove of the DNA helix, which blocks DNA polymerases and halts replication (187, 188).

As mentioned in section 1.3.1, IR is another source of DNA damage, and can arise from exogenous sources such as cosmic radiation. IR passes through the cell in high-energy tracks, depositing energy and ionising any atoms it interacts with via the stripping of electrons. Ionisation leads to direct induction of DNA damage, as well as the production of chemical modifications and the breaking of covalent bonds (146, 189). IR also generates damage indirectly

through the radiolysis of water and the generation of ROS, thus causing oxidative DNA lesions (190). A variety of different radiation-induced DNA lesions have been identified, including oxidative base lesions, AP sites, DNA strand or DNA-protein crosslinking, sugar modifications, SSBs and DSBs (146, 189).

DSBs are the most cytotoxic lesion induced by IR. They are formed when breaks in the DNA phosphodiester backbone occur on opposing strands within 1-20 base pairs of one another, separating the two strands – this makes damage repair significantly more difficult compared to other types of DNA damage (191). If unrepaired, DSBs result in apoptosis, and if repaired incorrectly they are highly mutagenic and can contribute to the development of cancers (192). SSBs are generated when a complete nucleotide is lost from the DNA strand, leaving a gap in the phosphodiester backbone and damage at the 5′ and/or 3′ ends of the break (193). SSBs are the most common form of DNA damage, accounting for approximately 75 % of all lesions (194), and if left unrepaired can cause DNA replication fork stalling – a process which can result in the formation of DSBs (195, 196). SSBs also contribute to mutagenesis and genomic instability in cancer formation.

1.3.5. The DNA Damage Response

Maintaining genomic stability is crucial for survival, as it conserves correct cellular function and allows for the successful replication of DNA and the passing of genetic information to progeny. As discussed in section 1.3.4, DNA is constantly exposed to endogenous and exogenous sources of damage which disrupts the stability of the genome, and the accumulation of DNA damage is well recognised as a causative agent of cancer (197). In order to minimise the build-up of damage, cells possess an intricate network of DDR pathways,

which involve multiple signalling and effector systems that function alongside DNA damage sensors and cell cycle checkpoints. The choice of repair pathway depends on several factors, including the cell cycle stage and the type and amount of damage that has occurred. DDR pathways aim to repair the DNA damage, but if repair is not possible, cell cycle arrest, senescence, replication regulation, or apoptosis will be induced (172, 197). There are over 450 genes involved in the DDR (198), and the pathways are regulated by a vast set of post-translational modifications (PTMs), such as acetylation, phosphorylation, methylation and ubiquitination, which have key functions in controlling chromatin structure, transcription, protein degradation, signal transduction, and enzyme activity (199, 200). There are four major pathways in the DDR: DSB repair, nucleotide excision repair (NER), MMR, and base excision repair (BER). DSB and BER are the main pathways utilised to repair radiation-induced DNA DSBs and SSBs respectively.

Double Strand Break Repair

DSBs are the most cytotoxic form of DNA damage, and incorrect repair can have catastrophic consequences in the cell, such as genomic rearrangements and cell death. The genomic rearrangements that may develop from DSBs can also contribute to the development and progression of cancers (192, 201). However, it is also important to note that the generation of DSBs is a key step during meiosis, where it contributes to genetic diversity in offspring (202), and for increasing the diversity of antigen receptors and immunoglobins in immune cells via the process of V(D)J recombination (203). In situations where DBSs are not beneficial for the cell, two pathways are utilised for their repair: NHEJ and HR.

1.3.5.1.1. Non-Homologous End Joining

NHEJ (figure 1.7) is the predominant pathway for the repair of DSBs and occurs throughout all stages of the cell cycle. As NHEJ repairs DNA irrespective of homology, it is an error-prone process that has been linked to genomic aberrations (204, 205). There are two sub-pathways of NHEJ: canonical NHEJ (C-NHEJ) and alternative NHEJ (A-NHEJ).

The first stage of NHEJ is DSB recognition. In C-NHEJ, the Ku70/80 heterodimer binds to the DSB and forms a ring structure at the break site to protect the broken ends and act as a scaffold for the recruitment of DNA-dependent protein kinase catalytic subunit (DNA-PKcs), establishing the DNA-PK holoenzyme (206, 207). DNA-PKcs, once activated, acts as an important regulatory kinase in the NHEJ pathway (208), and is crucial for the recruitment and activation of end-processing factors such as Artemis. Artemis removes the 5′ and 3′ DNA overhangs from the break in an endonucleolytic manner, allowing the X-ray cross-complementing protein 4 (XRCC4)-DNA ligase IV complex to ligate the DNA ends (209, 210). Other end-processing factors may be recruited before the ends can be ligated, for example, polynucleotide kinase/phosphatase (PNKP) and the MRN complex (211, 212). If necessary, nucleotide addition occurs via Pol X family members Pol μ and Pol λ (213, 214). A-NHEJ, on the other hand, utilises poly (ADP-ribose) polymerase 1 (PARP1) as a scaffold for proteins such as the MRN complex, PNPK and Artemis (212), and XRCC1 in complex with DNA ligase IIIα performs the final ligation step of the process (215).

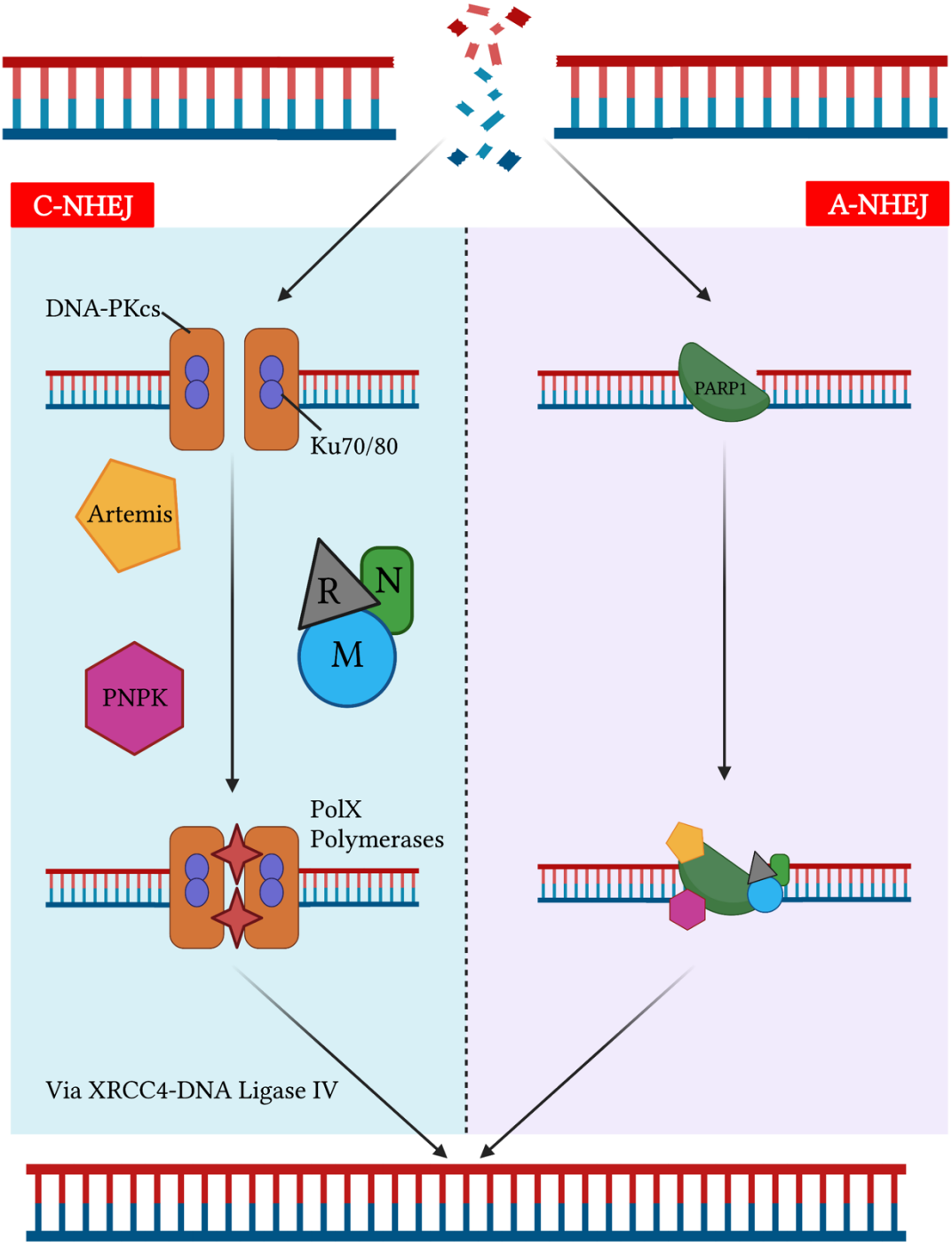

Figure 1.7: The Non-Homologous End Joining Pathways

In C-NHEJ, the Ku70/80 heterodimer binds to the DSB and recruits DNA-PKcs, which is vital for the recruitment and activation of end-processing factors such as Artemis. Artemis removes the 5′ and 3′ DNA overhangs from the break, which allows the XRCC4-DNA ligase IV complex to ligate the DNA. Other end-processing factors may be recruited before the ends can be ligated, such as PNKP and the MRN complex. If necessary, nucleotide addition occurs via Pol X family members. A-NHEJ, on the other hand, utilises PARP1 as a scaffold for proteins such as the MRN complex, PNPK and Artemis, and an XRCC1-DNA ligase IIIα complex performs the final ligation step.

1.3.5.1.2. Homologous Recombination

In contrast to NHEJ, HR (figure 1.8) is an error-free process as it employs homologous sister chromatids as a template for DSB repair (216). This requirement restricts HR to the S and G_2 phases of the cell cycle, however results in a repair process with high levels of precision (217).

There are a number of different sub-pathways of HR, however they share the same essential features of the process, beginning with the recruitment of the MRN complex to the break site, which results in the formation of 3′ single-stranded regions of DNA (218). The MRE11 subunit of the MRN complex is chiefly responsible for DNA end resection, in combination with carboxy-terminal binding protein-interacting protein (CtIP), however exonuclease 1 (EXO1) and Bloom syndrome RecQ-like helicase (BLM) are also involved (219, 220). Replication protein A (RPA) then coats the single-stranded DNA (ssDNA) overhang to protect the DNA from self-annealing, preventing the formation of secondary structures (219). RAD51 then replaces RPA, forming nucleoprotein filaments, which induces a search for homology in the sister chromatid, template pairing, and finally, strand invasion (221). These initial stages of HR are regulated by BRCA1, BRCA2, RAD52 and RAD54, proteins which are all crucial to the repair process (221-223). Strand invasion results in the formation of a displacement loop (D-loop) due to interaction between the invading strand and the sister chromatid. The ssDNA within the D-loop is then used as a primer for DNA synthesis, catalysed by DNA polymerase I and using the homologous strand as a template (206). The final stages of HR occur through synthesis-dependent strand annealing (SDSA) or DSB repair (DSBR). In the SDSA pathway, the invading strand separates from the undamaged template strand, anneals to the end of the DNA break, and DNA synthesis and ligation occurs to generate non-crossover intact DNA (224, 225). DSBR, on the

other hand, pairs both of the 3'-ssDNA overhangs with the template DNA, forming double Holliday junctions. Following cleavage and ligation, crossover or non-crossover DNA is formed, repairing the break (224, 226).

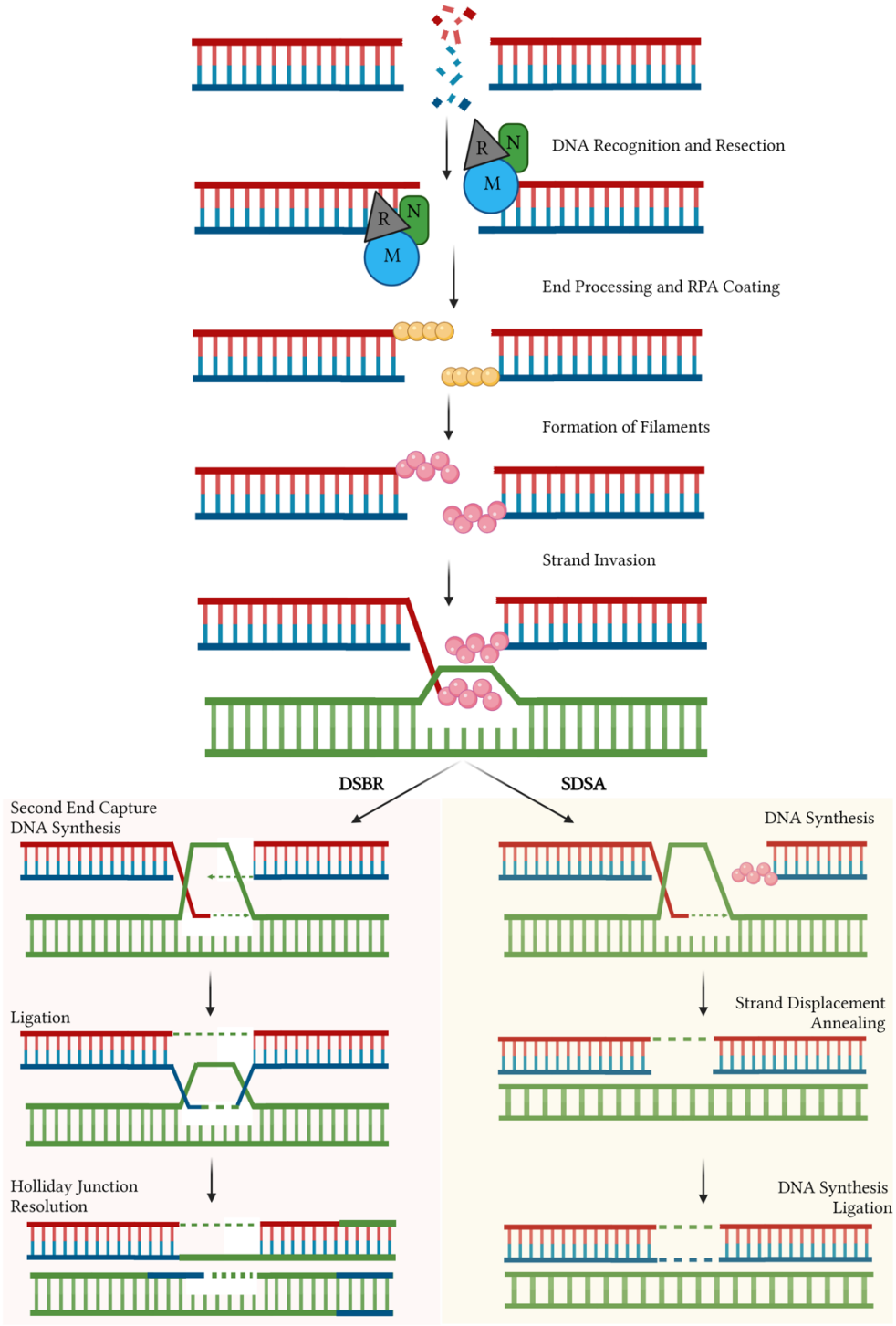

Figure 1.8: The Homologous Recombination Pathways

HR begins with the recruitment of MRN to the break site, which results in the formation of 3′ ssDNA. RPA coats the ssDNA overhang to prevent the formation of secondary structures, and RAD51 replaces RPA, forming nucleoprotein filaments. This induces a search for homology in the sister chromatid, template pairing, and strand invasion, forming a D-loop. The final stages of HR occur through either SDSA or DSBR. In the SDSA pathway, the invading strand separates from the undamaged template strand, anneals to the end of the DNA break, and DNA synthesis and ligation occurs to generate non-crossover intact DNA. In DSBR, both 3′-ssDNA overhangs are paired with the template DNA, forming double Holliday junctions. Following cleavage and ligation, crossover or non-crossover DNA is formed, repairing the break.

Base Excision Repair

BER is the predominant mechanism used for the repair of IR-induced SSBs and is a highly conserved pathway with homologous proteins functioning in bacteria, yeast, and animals (227). The vast majority of radiation-induced DNA lesions are SSBs, with 1 Gy of X-rays generating ~1000 SSBs per cell in contrast to only 20 – 40 DSBs per cell (147). If unrepaired, accumulated SSBs contribute to genomic instability and have been associated with the onset of cancer. The BER pathway is divided in to four distinct stages – DNA base damage excision, AP site incision, DNA end processing, and DNA ligation – and there are two sub-pathways: short-patch BER (SP-BER) and long-patch BER (LP-BER).

SP-BER (figure 1.9) is the principle BER sub-pathway, repairing approximately 80 % of all damaged bases (228). SP-BER is initiated by the detection and removal of the DNA lesion by a damage-specific DNA glycosylase. There are 11 different DNA glycosylases in humans, which can be divided in to two categories: monofunctional glycosylases and bifunctional glycosylases. The monofunctional glycosylases can only catalyse the hydrolytic cleavage of the N-glycosidic bond between the deoxyribose sugar and the nitrogenous base (229). Excision of the damaged base by a monofunctional glycosylase forms an AP site, leading to the recruitment of AP endonuclease 1 (APE1) and PARP1. APE1 hydrolyses the DNA backbone at the AP site, generating a SSB with 5′-deoxyribosephosphate (dRP) and 3′-hydroxyl ends (230, 231), while PARP1 adds poly-ADP-ribose polymers onto repair proteins such as DNA polymerase β (Polβ) and XRCC1, increasing the efficiency of their recruitment to damage sites (232). Polβ removes the dRP, generating a 5′-phosphate., whilst simultaneously inserting the correct nucleotide. On the other hand, bifunctional glycosylases human endonuclease III (NTH1) and 8-oxoG glycosylase (OGG1) possess AP-lyase activity as well as their glycosylase

activity, allowing them to cut the phosphodiester backbone on the 3′ side of the damaged base (β-elimination), creating a 3′-phospho-α,β-unsaturated aldehyde (PUA) and a 5′-phosphate (233). APE1 removes the PUA, leaving a 3′-hydroxyl end (234). Thus, in both cases, a single nucleotide gap is generated with 3′-hydroxyl and 5′-phosphate ends. Polβ then fills the gap with the correct nucleotide, and a complex of DNA ligase IIIα and XRCC1 is recruited to seal the nick (228, 234).

LP-BER (figure 1.9) is only used when a 5′ blocking lesion is generated through the oxidation or reduction of the an AP site that is resistant to Polβ dRP-lyase activity (235). In this pathway, the excision of the damaged base and end processing occur as in SP-BER with a monofunctional glycosylase. However, in LP-BER, after Polβ inserts the new nucleotide into the gap there is a switch to one of the DNA replication polymerases δ or ε (Polδ/Polε). In a process called strand displacement, Polδ or Polε then synthesises 2 – 12 nucleotides from the 3′ end of the DNA repair site, which displaces a 5′-flap structure (181, 236). The flap structure is removed by a complex consisting of flap endonuclease-1 (FEN-1) and proliferating cell nuclear antigen (PCNA), and a PCNA/DNA ligase I complex then seals the nick (228, 234).

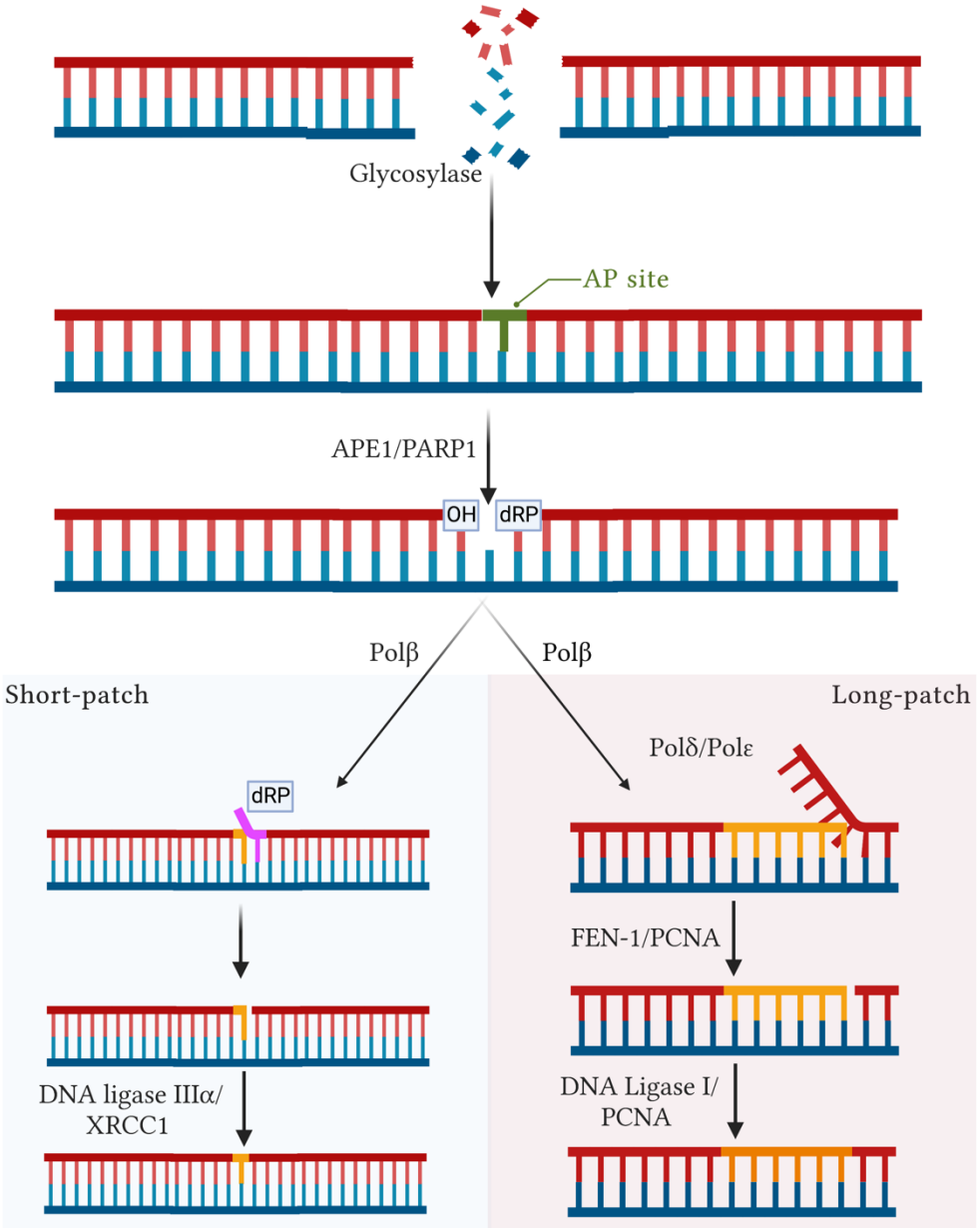

Figure 1.9: The Base Excision Repair Pathways

BER is initiated by the detection and removal of the lesion by a DNA glycosylase. Excision of the damaged base by a monofunctional glycosylase forms an AP site, leading to the recruitment of APE1 and PARP1. APE1 hydrolyses the DNA backbone at the AP site, generating a SSB with 5′-dRP and 3′-hydroxyl ends, and PARP1 generates PAR polymers on repair proteins to increase the efficiency of their recruitment. DNA Polβ removes the dRP, generating a 5′-phosphate. In SP-BER, bifunctional glycosylases cut the phosphodiester backbone on the 3′ side of the damaged base PUA and a 5′-phosphate. APE1 removes the PUA, leaving a 3′-hydroxyl end. Polβ then fills the gap with the correct nucleotide, and a complex of DNA ligase IIIα and XRCC1 is recruited to seal the nick. In LP-BER, after Polβ inserts the new nucleotide into the gap there is a switch to one of the DNA replication polymerases δ or ε. In a process called strand displacement, Polδ or Polε synthesises 2-12 nucleotides from the 3′ end of the DNA repair site, which displaces a 5′-flap structure. The flap structure is removed by a complex consisting of FEN-1 and PCNA, and a PCNA/DNA ligase I complex seals the nick.

1.4. Chromatin

1.4.1. Chromatin Organisation

Within eukaryotic cells, the majority of DNA is located inside the nucleus, which is 6 μm in diameter. However, the DNA on all 46 human chromosomes would span approximately 2 meters in length if laid out end-to-end. Consequently, to ensure the DNA fits into the nucleus, it must be folded into a highly condensed structure. This structure is known as chromatin, and is organised chiefly by histones, but also by non-histone chromosomal proteins, which bind to the DNA and provide structure to the chromosomes. As well as allowing the DNA to fit into the nucleus, the compaction of DNA into chromatin also acts as a protective measure against DNA damage, helps to control gene expression, and adds strength to the DNA structure during cell division.

Nucleosomes are the basic units of chromatin (figure 1.10). They are formed from ~145 – 147 base pairs (bp) of DNA wrapped ~1.65 times around a histone octamer consisting of two copies each of the core histone proteins H2A, H2B, H3 and H4 (237). The formation of these nucleosome units is initiated by the wrapping of recently synthesised DNA around a H3-H4 tetramer, and the subsequent addition of two H2A-H2B dimers (237). The structure is stabilised through interaction between positively charged amino acid residues on the histone octamer and the minor groove of the DNA phosphate backbone, giving rise to 14 weak DNA-histone bonds (238). Nucleosomes are joined together by short (~15 – 20 bp) segments of linker DNA, which is associated with the linker histones H1 and H5, to form the so-called 'beads-on-a-string' nucleosome array structure (239). This then folds into a higher-order structure

of a 30-nanometre chromatin fibre (240), which undergoes supercoiling during cell division to form the metaphase chromosomes seen during mitosis and meiosis (241). Tightly packed chromatin is known as heterochromatin and is associated with the transcriptional silencing of genes. Conversely, euchromatin is a loosely packed, relaxed region, and due to easy access by transcription factors, is associated with transcriptional activity.

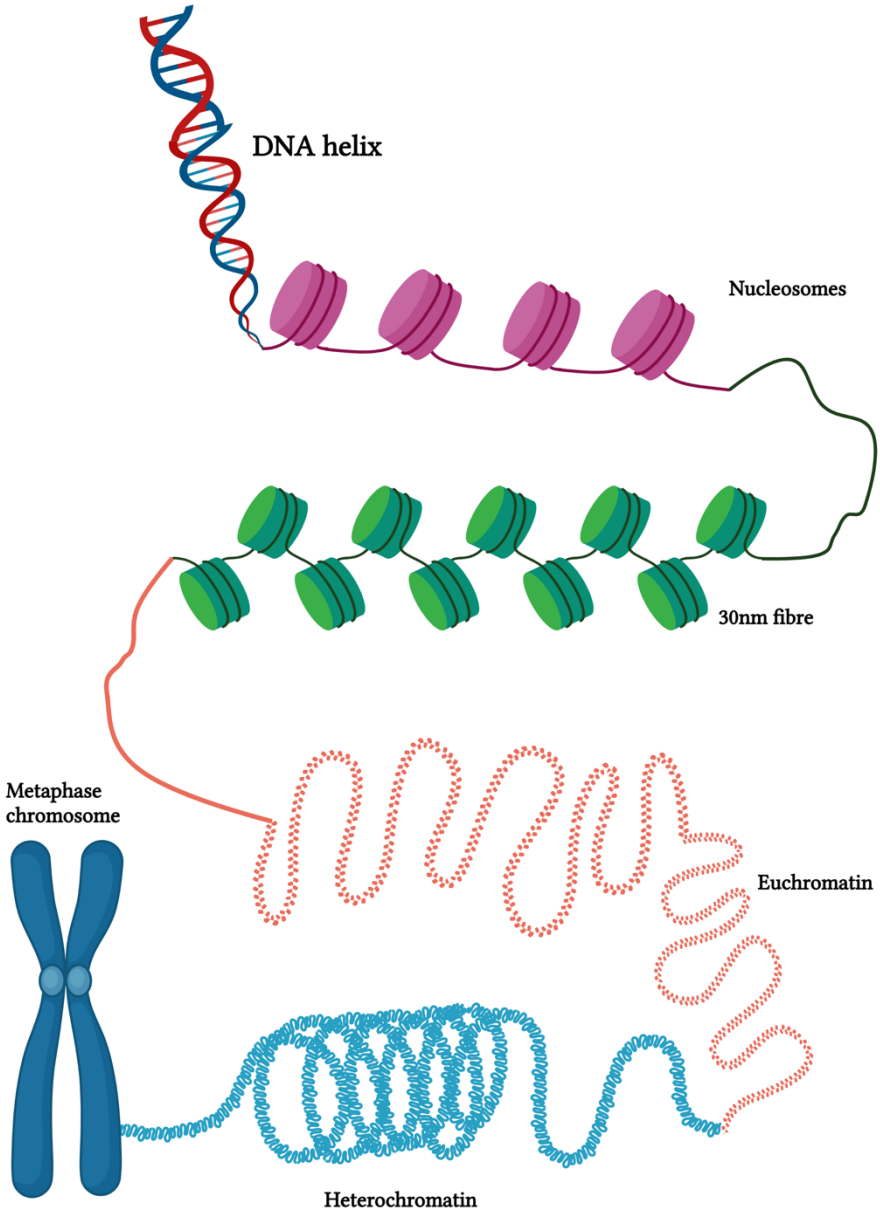

Figure 1.10: The Structure of Chromatin

The basic units of chromatin are formed from ~145 – 147 bp of DNA wrapped ~1.65 times around a histone octamer, forming a nucleosome. Nucleosomes are joined together by short segments of linker DNA to form the 'beads-on-a-string' nucleosome array structure, which folds into a 30-nanometre chromatin fibre. The fibre undergoes supercoiling during cell division and can exist as either tightly packed heterochromatin or loosely packed euchromatin.

The N-terminal tails of histones protrude from the nucleosome structure. This allows for the addition and removal of histone PTMs such as phosphorylation, acetylation, methylation, ubiquitylation, SUMOlyation and PARylation, which can regulate and remodel the chromatin structure (242, 243). PTMs work alone, but also through the recruitment of ATP-dependent chromatin remodelling complexes, to influence the structure of chromatin (244). Local changes in chromatin structure allow the cell to perform DNA-dependent processes, including regulating gene expression through transcription and stimulating DNA damage repair.

Nucleosome Structure

The crystal structure of the nucleosome was ascertained in 1997, and clearly shows ~146 bp of DNA wrapped in a left-handed superhelix ~1.65 times around a histone octamer (237). The histone octamer consists of two copies each of the core canonical histones H2A, H2B, H3, and H4 (245), which are positively charged and composed of three α-helices divided by two loops (α1-L1- α2-L2- α3). This motif is crucial for the nucleosome structure, as it allows the histone proteins to form heterodimers. Each domain in the motif pairs with a complementary histone fold to form a handshake motif (237, 245, 246). H2A pairs to H2B, and H3 pairs to H4. The core histone octamer therefore contains four heterodimers: 2 H2A/H2B, and 2 H3/H4. The α2 and α3 helices in histone H3 allow for the two H3/H4 heterodimers to interact with one another via a four-helix bundle, forming $(H3/H4)_2$ tetramers. The H2A/H2B heterodimers bind to the $(H3/H4)_2$ tetramers via H4 and H2B histone folds, forming the ordered histone octamer (247). The octamer binds the majority of nucleosomal DNA, approximately 121 bp in total. A variety of electrostatic interactions,

hydrogen bonds and protein interactions are employed to stabilise the nucleosome structure (237, 238).

Nucleosome Array Structure

While the majority of nucleosomal DNA wraps around the histone octamer, ~15 – 20 bp acts as so-called 'linker DNA'. These short sections of DNA associate with the linker histones H1 and H5 to join the nucleosomes together and form arrays with a 'beads-on-a-string'-like structure. These arrays are compacted further to form the secondary structure of chromatin: 30 nm chromatin fibres. This was first noted in 1980 (248), however the structure is yet to be resolved. Currently, there are two possible models for the structure of the chromatin fibres. The one-start solenoid model suggests that the nucleosomes are joined along a superhelical path (240, 249, 250), while the two-start zig zag model states that two rows of nucleosomes are connected by straight linker DNA, either in a longitudinal or radial arrangement (251-253).

Higher Order Chromatin Structures

The proposed model for higher order structures of chromatin is largely based on studies of extracted metaphase chromosomes. These chromosomes consist of a scaffold in the characteristic shape of a metaphase chromosome, surrounded by a ring of DNA. The DNA ring contains many loops of 30 – 90 kilobases, each of which are anchored to the scaffold (254). This radial-loop model, however, cannot be extrapolated to other higher order structures, including interphase chromosomes (255). Other models have therefore been suggested, including a molten globe or polymer melt physical arrangement of irregularly folded, compacted nucleosome arrays (256-258). This model does

not explain the rod-like structures observed in chromatin during metaphase, and it is likely that there are a variety of chromatin organising proteins, including polycomb repressive complex 1/2 (PCR1/2) and heterochromatin protein 1 (HP1), that are involved in managing the final levels of higher order organisation (259).

1.4.2. Histone Variants

Histone variants can be substituted for the core canonical histones in order to provide the octamer with different functions. The histone with the highest number of variants is histone H2A, of which H2A.X and H2A.Z are the most well characterised. Histone H2A.X is phosphorylated and functions in several cellular processes, for example: the DNA damage response (γH2AX), chromatin remodelling processes, and inactivation of X-chromosomes. Meanwhile, histone H2A.Z is involved in transcription, DNA repair and recruitment of RNA Polymerase II (260). γH2AX is commonly used as a marker for DNA damage, as the phosphorylation of this histone variant by ATM and ATR acts as a recruiter for key DNA repair proteins (261).

1.4.3. Regulation of Chromatin Structure

It is crucial for cellular function that chromatin has a dynamic structure. During processes such as transcription or DNA replication and repair, the DNA must be accessible to a variety of proteins, and thus the chromatin must change from a heterochromatic configuration to a euchromatic one. The regulation of chromatin structure is controlled by either ATP-dependent chromatin remodelling complexes (ACRs) or through post-translational modification of histones.

Chromatin Remodelling Complexes

There are several multi-subunit chromatin remodelling complexes that function in mammalian cells. These complexes utilise the energy generated from the hydrolysis of ATP to alter the structure of nucleosome arrays and thus regulating the accessibility of DNA (262). There are four main subfamilies of ACRs: imitation switch (ISWI), chromodomain helicase DNA-binding (CHD), inositol-requiring 80 (INO80), and switch/sucrose non-fermentable (SWI/SNF) (263). These families work in different ways to remodel chromatin; however, they all share a number of features. Each ACR has a single catalytic subunit containing an ATPase domain, which is split into two RecA-like lobes (DExx and HELICc). They also display a greater affinity for the nucleosome in comparison to naked DNA, and carry domains to regulate the ATPase domain and to allow interaction with other proteins – these can be chromatin proteins, chaperone proteins, or transcription factors (264).

ISWI chromatin remodellers have an ATPase domain with a carboxy-terminal HAND-SANT-SLIDE (HSS) domain, and two RecA-like lobes (265). The HSS domain binds to linker DNA and the unmodified tail of histone H3 (266, 267) This subfamily of ACRs alter the accessibility of chromatin through the assembly and spacing of nucleosomes, however a select number of ISWI ACRs carry additional subunits that actively promote gene transcription (264, 268). CHD chromatin remodellers have a similar ATPase domain to the ISWI family, however the CHD ATPase carries two unique chromodomains (269). Furthermore, the C-terminus of CHD proteins contains a NegC domain adjacent to a DNA-binding domain, which, in contrast to the ISWI family, contains only the SANT and SLIDE domains (270, 271). CHDs have an array of functions, and are involved in nucleosome spacing (272), exposing

promoter regions of DNA to transcription factors (273), and editing chromatin through the incorporation of the histone variant H3.3, which is essential for replication-independent chromatin assembly (274). The INO80 subfamily of ACRs contains an ATPase domain with a prominent insertion between two RecA-like lobes, which binds an individual heterohexameric ring of the helicase-related ruvB-like proteins Rvb1 and Rvb2, one actin-related protein (ARP) and one member of the YL-1 protein family (264). Moreover, the N-terminus of INO80 ACRs contains a helicase/SANT-associated (HSA) domain, which functions to nucleate actin and ARPs (275). INO80 family members can alter nucleosome spacing and chromatin access, however their main function is in editing. For example, H2A-H2B dimers can be replaced with histone variants by the SWR1C/p400/Snf2-related CBP activator protein (SRCAP) complex, and INO80C has been shown to catalyse the replacement of H2A.Z-H2B variant dimers with canonical H2A-H2B dimers (276, 277). In SWI/SNF ACRs, the RecA-like lobes of the ATPase domain flank a small, highly conserved insertion – a HSA domain (278, 279). This family of chromatin remodellers slide and eject nucleosomes from DNA, which facilitates chromatin access, and they are thus highly associated with gene activation and repression (244).

Post-Translational Modifications

Pioneering research carried out in the 1960s identified that histone subunits can carry PTMs (242). There are a number of tail protrusions in the nucleosome; a total of eight N-terminal tails – one from each histone protein – and two C-terminal tails from histone H2A are found in the structure. The main function of these tails is to provide sites for PTMs, as well as allowing for interaction with other nucleosomes (243, 247). Due to their ability to alter chromatin structure, PTMs have a critical influence upon transcription, and

also have an impact on DNA replication and repair (280). There are a number of different types of PTM, the most common including histone methylation, phosphorylation, and acetylation.

Histone methylation generally occurs on lysine and arginine sidechains on histones H3 and H4, and either inhibits or stimulates the recruitment of histone-binding proteins to impact gene expression (281). Methylation is controlled by histone methyltransferases (HnMTs) and histone demethylases, and the most commonly methylated residues are K4, K9 and K27 on H3, and K20 on H4 (282). These residues can be mono-, di-, or tri-methylated, and the impact of histone methylation on gene expression is dependent upon both the residue and the degree of methylation. For example, H3K4, H3K36 and H3K79 modifications are associated with transcriptional activation, whereas H3K9, H3K27 and H4K20 modifications have been linked to transcriptional repression (283).

Phosphorylation of serine, threonine and tyrosine residues is controlled by kinase proteins, which add phosphate groups onto the amino acids, and phosphatases, which remove them. The phosphorylation of histones adds a negative charge to the octamer, reducing the strength of its interaction with positively charged DNA and changing the overall chromatin structure (280). Histone phosphorylation therefore impacts several cellular processes, and perhaps most important is its role in the DNA damage response. In mammals, phosphorylation of S139 on the histone variant H2AX (γH2AX) is a crucial marker of DNA damage, acting to ensure DSBs are recognised by the repair machinery (284).

Histone acetylation is one of the most well understood histone PTMs. This type of modification is controlled by histone acetyltransferases (HATs) and

histone deacetylases (HDACs) and has important roles in gene expression. The addition of acetyl groups to the N-terminal tails of the histones neutralises the positive charge of the octamer, leading to less interaction with the DNA – similar to histone phosphorylation (285). This makes the chromatin more accessible to transcription machinery, allowing for gene expression. Gene expression can be switched off by the activity of HDACs, which remove the acetyl groups and restore the strong interaction between the histone and DNA. Histone acetylation and deacetylation has been implicated in both the HR and NHEJ DNA DSB repair pathways (286, 287).

1.5. Histone Deacetylases

There are 18 HDAC enzymes in humans, which are organised into classes based on function and sequence homology (figure 1.11). Classes I, II and IV are made up of the 'classical' Zn^{2+}-dependent HDACs, and class III contains NAD^{+}-dependent sirtuins (288). A Zn^{2+}-dependent catalytic HDAC domain is present in all class I, II and IV HDACs, and some individual enzymes contain extra functional domains. Class II HDACs contain unique domains for nuclear localisation and export signals, which allow for movement between the cytoplasm and nucleus (289), as well as a binding domain specific to the myocyte enhancement factor 2 (MEF2) transcription factor (290). Furthermore, HDAC6 contains a zinc finger binding domain, while HDAC10 contains a leucine-rich region. Sirtuins, the class III HDACs, are structurally distinct from classes I, II and IV. They are homologous to the yeast silent information regulator 2 (Sir2) protein (291), and are ubiquitously expressed in humans (292). HDACs have been linked to all 8 hallmarks of cancer (figure 1.12) and have therefore been linked to the development of multiple tumour types (table 1.1).

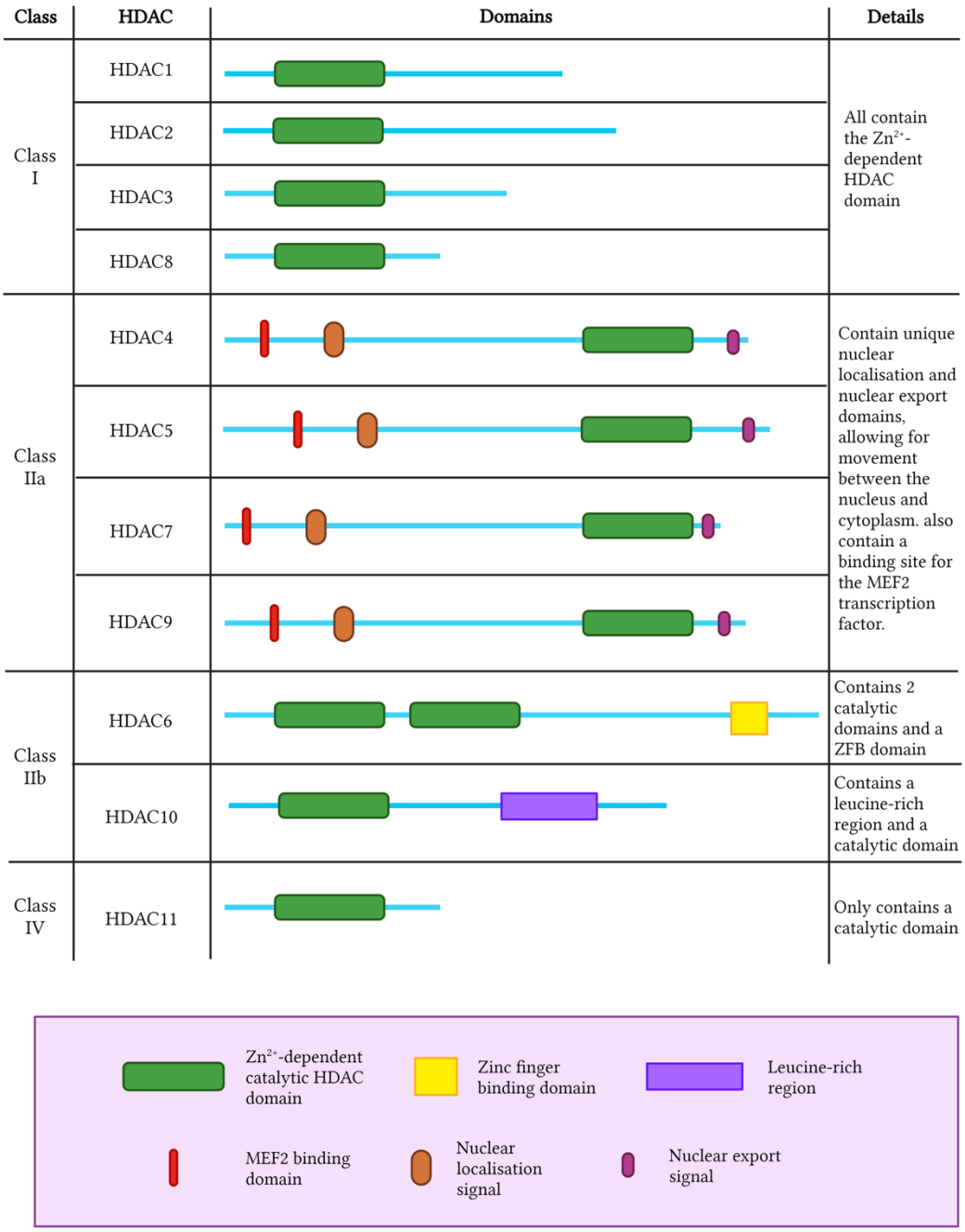

Figure 1.11: The Classes of HDACs

In humans there are 18 HDAC enzymes, which are organised into classes based on function and sequence homology. Classes I, II and IV are made up of the 'classical' Zn^{2+}-dependent HDACs, which all carry a Zn^{2+}-dependent catalytic HDAC domain. Class II HDACs also contain unique domains for nuclear localisation and export signals, which allow for movement between the cytoplasm and nucleus, plus a binding domain specific to MEF2. HDAC6 contains a zinc finger binding domain, while HDAC10 contains a leucine-rich region.

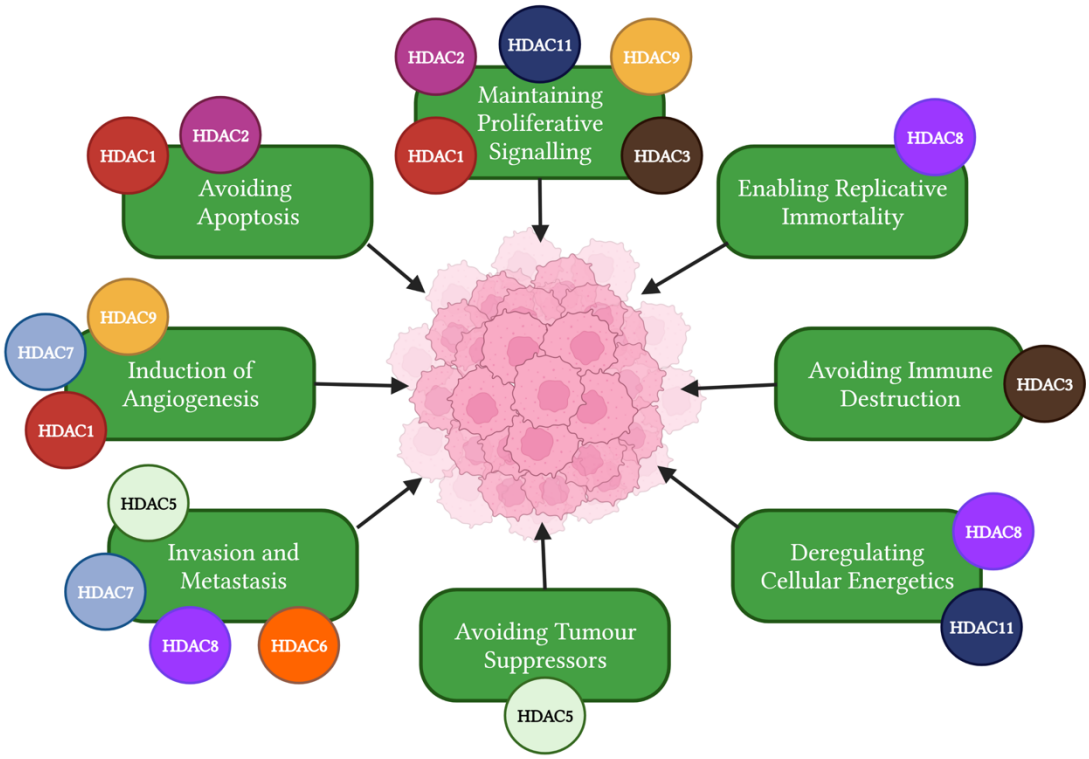

Figure 1.12: HDACs and the Hallmarks of Cancer

The involvement of various HDACs with the 8 hallmarks of cancer.

Table 1.1 Cellular targets and tumour associations of HDACs

Class	HDAC	Cellular targets	Tumour Association	Reference
I	HDAC1	CoREST transcriptional complex, BRG1-RB1-HDAC1 complex, SP1/3 transcription factors, NF-κB, HIF-1α	Gastric, pancreatic, colorectal, prostate, hepatocellular, lung, breast	(293-306)
	HDAC2	CoREST transcriptional complex, DNMT/DMAP1, MTA1, p53	Cervical, gastric, breast, prostate	(295, 299, 301, 307-311)
	HDAC3	BCL6, XBP1, AKT1, N-CoR	Acute promyelocytic leukaemia, hepatocellular, colorectal, breast	(312-318)
	HDAC8	Telomerase, ERRα	Neuroblastoma, breast	(319-322)
II	HDAC4	HIF-1α, CDK	Oesophageal, glioma, gastric, colorectal	(323-328)
	HDAC5	MEF2C, MTA1, ESR1, Rb, RARA	Hepatocellular, colorectal, breast, lung	(329-336)
	HDAC6	ESR1, HIF-1α, Aggresome	**OSCC**, ovarian, breast	(323, 329, 337-340)
	HDAC7	RARA, FOXP3, Stat3	**Nasopharyngeal**, lung, breast, gastric	(330, 341-345)
	HDAC9	MEF2, C-Jun, Aldehyde Dehydrogenase 1A3	**OSCC**, lung, hepatocellular, breast	(346-351)
	HDAC10	PTPN22, AKT, DNA Repair	Lung, colorectal, ovarian	(352-357)
IV	HDAC11	p53, Cell Cycle Progression, Glycolysis	Pituitary, neuroblastoma, hepatocellular	(358-360)

The various cellular targets of each HDAC, plus the tumour types they have been associated with. HDACs specifically associated with HNSCC are **highlighted**. Taken from our review (361).

1.5.1. Class I HDACs

Class I HDACs (HDAC1, HDAC2, HDAC3 and HDAC8) are localised to the nucleus, and function as a catalytic subunit in protein complexes that are heavily involved in transcriptional repression (362).

HDAC1

HDAC1 is part of the CoREST complex along with HDAC2. This complex ensures that neuronal genes are transcriptionally silenced in non-neuronal tissues (295). HDAC1 is also a component of the BRG1-RB1-HDAC1 complex, which is a negative regulator of transcription in resting neurons (298), and also regulates the function of the SP1 and SP3 transcription factors (293, 296). Furthermore, HDAC1 and HDAC2 have been shown to inhibit the transcription of NF-κB (294), and knocking out HDAC1 and HDAC2 simultaneously is sufficient to induce apoptosis (363). HDAC1 overexpression has been suggested as a prognostic marker for gastric cancer, and it has been suggested that there is an upregulation of HDAC1 in ~60 % of gastric cancer cases (299, 300). Furthermore, an increased level of HDAC1 has been observed in both colorectal and prostate cancer (299, 303). In pancreatic cancer, it has been suggested that HDAC1 regulates the expression of the HIF-1α transcription factor, which promotes angiogenesis and tumour survival in hypoxic conditions, and an increase in both HDAC1 and HIF-1α expression has been associated with poor prognosis in pancreatic cancer patients (297). Higher levels of HDAC1 expression have been associated with invasion, advanced stage disease and poor survival in hepatocellular carcinoma (304), and a meta-analysis of patients with lung cancer showed that the expression of HDAC1 is linked to poor overall survival (305). Conversely, increased HDAC1 expression in breast cancer was linked to improved survival and

decreased tumour sizes (306). Together, these data show there is a strong link between HDAC1 expression and the development of specific cancers.

HDAC2

HDAC2 forms a complex with DNA methyltransferase 1 (DNMT1) and the DNMT1-associated protein 1 (DMAP1) to deacetylate histones following DNA replication during the cell cycle (309), and is also involved in metastasis tumour antigen 1 (MTA1)-mediated transcriptional co-repression of genes including *BRCA1, ESR1, TFF1* and *CDKN1A*, which all encode key cancer-associated proteins (307). Moreover, HDAC2 increases the DNA binding of p53, leading to decreased proliferation and senescence induction (308). HDAC2 is upregulated in the dysplasia transition region of cervical cancers and has a higher expression level during the polyp stage of carcinogenesis (310), and in a retrospective study of gastric cancer patients, HDAC2 upregulation was linked to a decrease in 3-year survival (299). In breast cancer, an increased level of HDAC2 expression is correlated with HER2 upregulation (311), and the upregulation of HDAC1/2 has been correlated with increased differentiation and proliferation in prostate cancer (301).

HDAC3

HDAC3 is thought to be involved in the functioning of the BCL6 transcriptional repressor via H3K27 deacetylation on gene enhancer elements, allowing B cells to undergo rapid changes in response to various cellular signals (314). Also, HDAC3 has been shown to interact with X-box binding protein 1 (XBP1) to reduce oxidative stress in endothelial cells via increased protein kinase B (AKT) phosphorylation (313). In acute promyelocytic

leukaemia (APL), HDAC3 has been associated with leukemogenesis via transcriptional repression in a complex with N-CoR (312), and in hepatocellular carcinoma, a reduction of HDAC3 has been directly correlated with H3K9 hyperacetylation, leading to a decline in DNA damage control and the transcription of tumour-related genes (315). Furthermore, HDAC3 has been associated with proliferation and differentiation in colorectal cancer cells, in which it has been suggested that decreased levels of HDAC3 can reduce proliferation (316, 317). In a study of 145 breast cancer patient samples, HDAC3 expression was negatively correlated with the expression of oestrogen and progesterone receptors, and positively correlated with overexpression of EGFR. High HDAC3 expression was also linked to poor overall survival (318). In another study of breast cancer, HDAC3 increased the expression of high-mobility group box 3 (HMGB3) and promoted the immune escape of cancer cells (364).

HDAC8

HDAC8 has been associated with the regulation of telomerase activity and with tumour cell survival (319, 365). Furthermore, HDAC8 has been shown to modify the transcriptional activity of oestrogen-related receptor α (ERRα), which is involved in glycolysis and oxidative phosphorylation (320). In neuroblastoma, an expression study of HDAC1-11 revealed that HDAC8 expression alone was associated with tumour development. HDAC8 was also correlated with advanced disease and metastasis, as well as decreased rates of overall survival (321). Furthermore, HDAC8 expression has been shown to be increased in breast cancer, and associated with dissemination and EMT of breast cancer cells (322).

1.5.2. Class II HDACs

Class II HDACs are divided into two classes. Class IIa HDACs (HDAC4, HDAC5, HDAC7 and HDAC9) are expressed in the nucleus and cytoplasm, and have been shown to have critical functions in regulating the expression of MEF2, a key protein in embryonic development (366, 367). On the other hand, the class IIb HDACs (HDAC6 and HDAC10) have minimal enzymatic activity, and are reliant on a multiprotein complex containing HDAC3 and a transcriptional corepressor, N-CoR/SMRT to carry out their deacetylase function (368). Class II HDACs are expressed in the skeletal, heart, and smooth muscle, as well as brain tissues, and therefore appear to be tissue-specific (369).

Class IIa HDACs

1.5.2.1.1. HDAC4

HDAC4 and HDAC6 have been demonstrated to function in the regulation of HIF-1α transcription, and are therefore implicated in tumour angiogenesis (323). HIF-1α undergoes acetylation at lysines 532 and 674, leading to its degradation or transcriptional activity, respectively (370, 371). It appears therefore that HDAC4 is actively involved in the hypoxic response, and further evidence demonstrates that knockdown of HDAC4 results in an increase in the response and adaptation of cancer cells to hypoxia, as well as altering HIF-1-mediated transcription of genes involved in glycolysis and chemoresistance (372). In oesophageal SCCs, HDAC4 overexpression has been correlated with higher tumour grade, advanced clinical stage and poor survival, and has also been shown to promote proliferation via the upregulation of CDKs (373). The role of HDAC4 in cancer cell proliferation has

also been shown in glioblastoma, gastric cancer, and colorectal cancer, where it promotes growth through p21 repression (326-328).

1.5.2.1.2. HDAC5

HDAC5 actively represses the transcription of MEF2C, which is involved in muscle maturation and vascular development (331), and has also been implicated in MTA1-mediated epigenetic regulation of the *oestrogen receptor 1* (*ESR1*) gene, which is involved in cellular proliferation and differentiation (329). Moreover, HDAC5 has been demonstrated to act as a co-repressor of retinoic receptor alpha (RARA), which is involved in a variety of processes such as cell growth (330). Studies have further established that HDAC5 interferes with the function of the *Rb* tumour suppressor gene (332), and can promote migration of colon cancer cells (374). An increased expression of HDAC5 has been seen in multiple cancer types, including hepatocellular carcinoma, colorectal, breast, and lung cancer, and is associated with proliferation, invasion, and apoptosis inhibition in cancer cells (333-336).

1.5.2.1.3. HDAC7

Silencing of HDAC7 leads to an alteration in morphology, migration and capillary forming abilities of endothelial cells *in vitro*, and the enzyme has therefore been implicated in angiogenesis (375). Similarly to HDAC5, HDAC7 also acts as a corepressor of RARA, preventing its binding to DNA (330), and is thought to be involved in transcriptional repression via complex formation with the FOXP3 regulator protein, which is involved in controlling the activity of regulatory T cells (342). It has been shown that an upregulation of HDAC7 in nasopharyngeal carcinoma, lung cancer and breast cancer is associated with

higher levels of proliferation and disease progression (341, 343, 344). Furthermore, in lung cancers, HDAC7 has been shown to deacetylate and inhibit Stat3 expression, enhancing tumourigenesis (341), and has been linked to poor prognosis and metastasis in gastric cancer (345).

1.5.2.1.4. HDAC9

Similarly to other HDACs, HDAC9 has been suggested to be involved in angiogenesis (351). HDAC9 recruits HDAC1/3 to alter MEF2-dependent transcription, which inhibits skeletal muscle myogenesis and may be involved in heart development (346). Moreover, HDAC9 is thought to repress c-Jun kinase activation, thus inhibiting downstream signalling through the MAPK pathway (348). In OSCC, higher expression levels of HDAC9 are associated with increases in cell growth and cell cycle progression (350), while on the other hand, a different study observed a decreased level of HDAC9 in lung cancer cells in comparison to healthy cells (349). The expression levels of HDAC9 have also been positively correlated with the number of dedifferentiation markers in a database of hepatocellular carcinoma patients, and has been associated with the expression of *aldehyde dehydrogenase 1A3*, a gene commonly mutated in hepatocellular carcinoma (347).

Class IIb HDACs

1.5.2.1.5. HDAC6

Similar to HDAC5, HDAC6 is involved in the MTA1-mediated regulation of ESR1 expression (329). HDAC6 also has a crucial role in the degradation of misfolded proteins. If misfolded proteins are too abundant to be degraded via

the chaperone refolding system, HDAC6 mediates their transport to a cytoplasmic juxtanuclear structure called the aggresome (337). Moreover, HDAC6 has been implicated in cancer cell metastasis (376), and in OSCC, a higher level of HDAC6 has been linked to a higher primary tumour stage (340). Expression of HDAC6 was shown to be increased in both high-grade and low-grade ovarian cancer samples in comparison to benign lesions and healthy ovarian cells (338). Intriguingly, on the other hand, mRNA levels of HDAC6 have been shown to be higher in breast cancer patients with small, low histologic grade, hormone positive tumours. In the same study, HDAC6 levels were positively correlated with disease-free survival and a better response to endocrine therapy (339).

1.5.2.1.6. HDAC10

It has been reported that HDAC10 is involved DNA damage repair through associations with DSB formation and the expression of *MLH1* and *MSH2/6*, which are genes involved in the MMR DNA damage repair pathway (352, 353). Furthermore, HDAC10 may promote angiogenesis via the modulation of PTPN22/ERK signalling (354). Research has also suggested that HDAC10 regulates AKT signalling to alter cellular proliferation (355). HDAC10 has been shown to have increased expression in lung and colorectal cancer (353, 355), and deletions of HDAC10 were linked to a sensitivity to platinum therapy in ovarian cancer (356).

1.5.3. Class IV HDACs

The only class IV HDAC is HDAC11, which is expressed mainly in the nucleus, and is generally localised to the brain, heart, skeletal muscle and

kidney tissues (377). In pituitary tumours, HDAC11 is negatively correlated with levels of p53 (360), and research has shown that there is a role for HDAC11 in the cell cycle progression of neuroblastoma cells (359). A study in hepatocellular carcinoma suggested that HDAC11 can also regulate cellular metabolic processes, such as glycolysis (358).

1.5.4. Non-Histone Targets of HDACs

A large number of non-histone proteins can also undergo PTMs, with approximately 2000 proteins in the human proteome having been identified as having acetylated residues (378-380). Thus, HDACs have also been associated with the deacetylation of lysine residues on non-histone proteins, including α-tubulin and heat shock protein 90 (HSP90). Interestingly, deacetylation of both of these proteins is controlled by HDAC6. α-tubulin acetylation levels are associated with the stability of microtubules (381), and HDAC6 inhibition has been shown to decrease microtubule stability, which results in an enhancement of cell motility (382). Furthermore, there is evidence that α-tubulin acetylation and HDAC6 activity are also linked to neuronal polarity and cell morphology (383). HSP90 is a molecular chaperone protein and is key for the correct assembly and structural maturation of other proteins. This function has been shown to be regulated by acetylation, and hyperacetylation of HSP90, which is caused by lack of HDAC6 activity, results in a loss of the chaperone function and can have catastrophic downstream consequences through the accumulation of misfolded proteins (384). One such example is the stability of HIF-1α, which is a key regulator of the cellular response to hypoxia.

1.5.5. HDACs in the Cellular DNA Damage Response

Levels of histone acetylation have been associated with the regulation of the cellular DDR. After the induction of IR-induced DNA damage, chromatin structure is altered to allow the access of DNA repair factors to the DNA, followed by the restoration of chromatin structure to its original state. Therefore, HDACs have been implicated in the maintenance of dynamic acetylation equilibrium of DDR proteins (385), and this is supported by data from studies of HDAC inhibitors (HDACis). For example, one study demonstrated that the pan-HDACi, vorinostat, reduced the activation of ATM after DSB induction in a dose- and time-dependent manner (386).

Class I HDACs in the DDR

HDAC1 and HDAC2 have been associated with the control of several central DDR proteins, including ATM, ATR and BRCA1. Research has also shown that HDAC1 and HDAC2 rapidly localise to sites of IR-induced DNA damage, and then gradually dissociate. At the damage sites, HDAC1/2 regulate the acetylation of H3K56, which decreases after DNA damage. This process is also sensitive to class I/II HDACis (387). It has also been noted that the short interfering RNA (siRNA)-mediated depletion of HDAC1/2 resulted in hypersensitivity to IR and phleomycin, increased the DNA damage-induced phosphorylation of CHK1/2 and p53, and increased levels of γH2AX. Based on these results, it has been suggested that HDAC1/2 impair DSB repair. Supporting this, it has been shown that HDAC1/2-depleted cells have major defects in the NHEJ pathway, specifically the persistence of Ku70 and Artemis at DNA damage sites (387).

HDAC3 function has also been shown to be key for the efficient repair of DSBs. HDAC3 inactivation in mouse embryonic fibroblasts lead to higher sensitivity to doxorubicin, a topoisomerase II inhibitor, and to cisplatin (388). These results suggest that a lack of HDAC3 leads to inefficient DNA repair. Furthermore, this study also suggested that the loss of HDAC3 impedes the DDR by targeting the chromatin structure, as HDAC3 is not recruited to DNA damage sites, and the localisation of other DDR proteins, such as RAD51, BRCA1, and MRE11, is not impacted by the loss of HDAC3 (389). A decrease in global heterochromatin levels *in vivo* and a 5 – 8-fold increase in the number of chromosomal breaks and gaps in metaphase chromosomes have both been observed after HDAC3 inhibition, and thus, HDAC3 is thought to be crucial for maintaining genome stability and contributes to efficient DNA repair.

Class II HDACs in the DDR

HDAC4 has been shown to interact with p53-binding protein 1 (53BP1) during DSB repair (390), and localises to nuclear foci after IR treatment in a dose-dependent manner. These HDAC4 foci were observed to have similar kinetics to 53BP1 foci, and further investigation showed that HDAC4 and 53BP1 colocalise to sites of DSBs. Moreover, decreased levels of 53BP1 were seen after silencing HDAC4, and vice versa, suggesting that HDAC4 and 53BP1 may maintain the stability of each other. Silencing of either HDAC4 or 53BP1 decreases 53BP1 foci following DNA damage, further supporting the notion that HDAC4 is involved in the repair of DSBs.

HDAC6 has also been shown to play a regulatory role in the DDR via its interactions with MutL homolog 1 (MLH1) and MutS protein homolog 2 (MSH2), two key DNA MMR proteins. It has been shown that HDAC6 deacetylates MLH1 on lysines 33, 241, 361 and 377, blocking the formation of

the MutLα-MutSα complex, and inhibiting the MMR pathway (391). HDAC6 also has been reported to reduce the stability of the MSH2 via its deacetylation (392). This evidence highlights a significant role for HDAC6 in the regulation of DNA MMR.

HDAC9 and HDAC10 are also thought to be involved in the DDR, specifically in the HR pathway, as one study demonstrated that using siRNA to reduce levels of HDAC9/10 led to significantly less activity of HR, and sensitised cells to mitomycin C (393). However, the mechanism by which HDAC9 and HDAC10 influence HR is currently unclear.

1.5.6. HDAC Inhibitors and Radiosensitivity

Due to their role in the cellular DDR, several HDACis have been investigated for their impact on the radiosensitivity of specific tumour models (table 1.2). It is worth noting that, to date, there has been very little research into the effects of HDACi on the radiosensitivity of HNSCC. In fact, only one inhibitor, resminostat, has been shown to radiosensitise HNSCC cells (394).

Table 1.2: HDAC inhibitors and their impacts on tumour cell radiosensitivity

Inhibitor	Target	Radiosensitivity impact	Reference
Valproic Acid	Class I	Effectively radiosensitised colorectal cancer, oesophageal cancer and thyroid cancer cells to photons, and hepatocellular carcinoma cells to PBT	(395-398)
Vorinostat	Non-Selective	Increased sensitivity of melanoma, lung cancer, breast cancer, and colorectal cancer cells to photons	(399-401)
CUDC-101	HDAC1-10, EGFR, HER2	Radiosensitised pancreatic cancer, breast cancer, and glioblastoma cells to photons	(402, 403)
Panobinostat	Non-Selective	Sensitised bladder cancer, hepatocellular carcinoma, prostate cancer cells to photons, and hepatocellular carcinoma cells to PBT	(404-406)
Romidepsin	Class I	Increases the sensitivity of bladder cancer, rhabdomyosarcoma, and retinoblastoma cells to photons	(407-409)
Mocetinostat	Class I	Radiosensitised bladder cancer cells to photons	(405)
Belinostat	Non-Selective	Sensitises rhabdomyosarcoma, cervical cancer, and colorectal cancer cell lines to photons	(410, 411)
Resminostat	Non-Selective	Sensitises HNSCC cells to photons	(394)

A summary of the increased radiosensitivity of tumour cell lines after treatment with various HDAC inhibitors. Taken from our review (361).

Valproic acid (VPA)

A large number of studies have focused on valproic acid (VPA), a branched-chain saturated fatty acid which inhibits class I HDACs and has been shown to induce radiosensitisation in multiple cancer types. In colorectal cancer cells (LS174T and HCT116), treatment with 500 μM VPA for 16 hours pre-irradiation resulted in p53-dependent radiosensitisation (395). Moreover, the same study demonstrated that, in the LS174T and HCT116/p53$^{+/+}$ cell lines, VPA treatment significantly increased the sub-G_1 population of cells, which is

indicative of apoptosis. However, this was not observed in the HCT116/p53$^{-/-}$ cells, thus demonstrating the key role of p53 in radiation-induced cell killing. Further analysis showed that γH2AX levels were increased from 2 – 24 h with the combination treatment in the p53-positive cell lines, which indicates that treatment with VPA elevates levels of IR-induced DSBs. VPA was also studied *in vivo* using nude mice with HCT116-derived xenograft tumours treated with VPA (6 x 300mg/kg) and IR (10 Gy), either alone or in combination. This revealed that the combination of VPA with IR decreased the growth of p53-containing xenografts but not of those that were p53-negative. These data are similar to another study conducted in oesophageal SCC cells (TE9, TE10, TE11 and TE14), where VPA treatment (500 μM for 24 h) increased cellular radiosensitivity (2 – 6 Gy X-rays) (397) associated with increased γH2AX levels 2 h post-IR (6 Gy), and interestingly decreased the expression levels of RAD51. Analysis of annexin V staining demonstrated that the combination treatment resulted in an increase in both early and late apoptotic cells. More recently, studies in thyroid cancer cells showed that treatment with VPA (1 mM for 24 h) increased cellular sensitivity to IR (1 – 8 Gy), although the relative effect was mild in TPC-1 cells (dose enhancement ratio (DER) = 1.1) compared to WRO cells (DER = 1.3) (396). In the same study, normal thyroid epithelial cells (Nthy-ori 3-1) also displayed apparent increases in radiosensitivity (DER = 1.3). The combination of VPA with IR did not have a significant impact on cell cycle distribution of cancer cells compared to the irradiation alone, although there was some evidence of increases in cell death after pre-treatment with VPA before irradiation (3 Gy; at 24 h and 48 h in WRO and TPC-1, respectively). The combination treatment did significantly increase γH2AX foci numbers, and similar to the study in OSCC cells described above, led to decreases in RAD51 protein levels post-IR.

Vorinostat

Vorinostat (MK0683; suberoylanilide hydroxamic acid (SAHA)), similar to VPA, is a non-selective HDACi. It is a synthetic hydroxamic acid derivative and has been shown to increase radiosensitivity of several cancer types both *in vitro* and *in vivo*. In melanoma cell lines (A375 and MeWo), pre-treatment with vorinostat (2.5 μM for 24 h) led to increases in radiosensitivity (DER = 1.4 (A375) and 1.3 (MeWo)), and the same effect was observed in non-small cell lung cancer cells (A549; DER = 1.7) after irradiation with γ-rays (2 – 6 Gy) (400). The combined treatment of vorinostat (2.5 – 10 μM) and radiation (5 Gy) in A375 cells resulted in higher levels of apoptosis compared to vorinostat as a single agent, and this appeared to be linked to a reduction in levels of Ku70, Ku86 and RAD50 proteins. However, no quantitative analysis was performed to support the significance of this data. Furthermore, analysis of γH2AX demonstrated that there were increased DSB levels and persistence 30 min – 24 h post-treatment with vorinostat (2.5 μM) plus γ-irradiation (5 Gy) in comparison to irradiation alone, implying that the combined treatment leads to an altered DDR which is responsible for the enhanced radiosensitisation. In a study of breast tumour brain metastasis cells (MDA-MB-231-BR), treatment with vorinostat (0.5 μM for 16 h) led to an enhanced radiosensitisation (DER = 1.3), and this was also observed in breast adenocarcinoma (T47D; DER = 1.2) and in ovarian adenocarcinoma (NCI/ADR-RES; DER = 1.5) cells (399). In the MDA-MB-231-BR cells, further experimentation demonstrated that vorinostat (1 μM) in combination with X-rays (2 Gy) resulted in a significant increase in γH2AX foci in comparison to IR alone, signifying defects in the repair of DSBs. This increase in γH2AX foci was also linked to a significant increase in mitotic catastrophe in the cells at 72 h post-IR. Finally, mice bearing MDA-MB-231-BR xenografts exhibited a significant delay in tumour growth when treated with

vorinostat (50 mg/kg) before irradiation (3 Gy) in comparison to either treatment alone. The impact of vorinostat in radiosensitising colorectal cancer cells (HCT116, HT29, KM20L2 and SW620) under conditions of both normoxia and hypoxia has also been studied. All cell lines displayed significant radiosensitisation after treatment with vorinostat (1 – 2 μM for 18 h) and a single dose of X-rays (5 Gy) in 1 % hypoxia (401). Similar observations were seen in normoxic conditions. Subsequent *in vivo* experiments using SW620- and HCT116-derived xenografts demonstrated that there was an increased delay of tumour growth after vorinostat plus irradiation (daily injection of 100 mg/kg for four days prior to irradiation) compared to the treatments alone. Furthermore, the addition of capecitabine (359 mg/kg) led to optimal tumour growth delay.

CUDC-101

CUDC-101 is a small-molecule multi-targeting inhibitor of HDAC1-10, EGFR and HER2. Treatment with CUDC-101 (0.5 μM for 24 h) and 5 Gy X-rays in pancreatic cancer cells (MIA PaCa-2, Su.86.86 and T3M-4) significantly reduced cell survival in comparison to either CUDC-101 or radiation alone (402). The radiosensitising ability of CUDC-101 was also demonstrated in 3D spheroid models of Su.86.86 and T3M-4 cells treated with either 0.25 or 0.5 μM CUDC-101 and 5 Gy X-rays. Further experimentation into the mechanisms of radiosensitisation showed that all three cell lines treated with CUDC-101 (3 μM for 24 h) and X-rays (5 Gy) had reduced PARP-1 levels, however, there was no change in γH2AX foci. The combined inhibitor plus radiation treatment (0.5 or 3 μM CUDC-101 with 5 Gy X-rays) did enhance the levels of sub-G_1 cells, indicating an increase in cells in apoptosis. This was further supported by a reduction in levels of survivin and x-linked inhibitor of apoptosis (XIAP). Taken together, these results indicate that, at least in pancreatic cells, CUDC-

101 acts as a radiosensitiser *in vitro*, and this study also demonstrated that CUDC-101 was a more effective radiosensitiser than vorinostat. There is also evidence from a scientific conference report that treatment with CUDC-101 (either 0.5 μM or 1 μM) enhances radiosensitivity in glioblastoma and breast cancer cell lines (U251 and MDA-MB-231, respectively; DER = 1.42), and this effect may be associated with a delay in the repair of DSBs and an increase in mitotic catastrophe (403).

Panobinostat

Panobinostat (LBH-589; Farydak) is a cinnamic hydroxamic acid analogue and another non-selective HDACi. In prostate cancer cell lines (PC-3 and LNCaP), panobinostat treatment (2.5 – 15 μM for 24 h, dependent on the cell line) combined with photon irradiation (2 – 8 Gy) significantly decreased cell survival (DER = 1.3 and 1.8). This enhanced radiosensitivity was not observed in normal prostate epithelial cells (RWPE-1). The combination treatment increased the number of cells in subG$_1$ phase (2 – 72 h post-irradiation with 2 Gy), indicating an increase in apoptosis. Alongside this, decreased activation of CHK1 and CHK2 was also observed, which suggests a lack of cell cycle checkpoint activation. Furthermore, the combination of panobinostat and radiation (at 24 and 72 h post-IR) resulted in higher levels of γH2AX compared to the radiation alone, plus a reduction in BRCA1, BRCA2 and RAD51 foci, suggesting a deficiency in HR repair of DSBs. Interestingly, the levels of Ku70 and Ku86 were also reduced following combination treatment, implying that NHEJ activity may also be affected (406). In a more recent study of bladder cancer-derived xenografts (RT112-derived), treatment with panobinostat (10 mg/kg for 6 h) enhanced the response of the cells to X-ray irradiation (5 x 4 Gy) (405). When delivered intravenously, panobinostat preferentially accumulated in the xenografts compared to the plasma, suggesting possible tumour-cell

specificity. This study was then expanded *in vitro* to investigate the specificity of the HDAC. In the bladder cancer cell lines (RT112, CAL29 and T24), panobinostat (50 nM for 24 h) decreased gene expression and protein levels of HDAC2 and HDAC7, and variable decreases and increases in other HDACs were observed in a cell-line dependent manner. Supporting research showed that an siRNA knockdown of HDAC1 and HDAC2 enhanced the radiosensitivity of RT112 cells, suggesting these are the potentially important targets for panobinostat.

Romidepsin

The class I-specific HDACi romidepsin (FK288; FR901228; Istodax) is a bicyclic depsipeptide antibiotic, and several studies have revealed its potential as a radiosensitiser. Firstly, a study using bladder cancer cell lines (RT112, MBT2 and HT1376) demonstrated that romidepsin (0.4 – 2.5 nM for 24 h, dependent on the cell line) effectively radiosensitised the cells to γ-rays (2 – 6 Gy). Subsequently, romidepsin (4 mg/kg) with γ-radiation (6 Gy) as a combined treatment was investigated in a RT112-derived xenograft model, and this demonstrated that the combination significantly reduced tumour growth compared to the monotherapies alone. This study also provided limited evidence in RT112 cells that romidepsin increases γH2AX levels immediately and 4 h post-IR compared to exposure to radiation only. Furthermore, NHEJ and HR repair pathways appeared to be less efficient after treatment with romidepsin, which indicates that the observed radiosensitisation effect may be due to effects on DSB repair (407). Furthermore, a study of rhabdomyosarcoma cells (RH30 and RD) revealed that pre-treatment with romidepsin (0.6 – 1.4 nM for 24 h, depending on the cell line) was sufficient to radiosensitise RH30 cells to 4 Gy X-rays, but interestingly did not radiosensitise RD cells. Consistent with this observation, it was also noted that romidepsin treatment increased

γH2AX expression following exposure to IR in RH30 cells only, and in *in vivo* experiments, 1.2 mg/kg romidepsin treatment combined with radiotherapy)5 x 2 Gy) significantly reduced tumour growth in RH30 xenografts, while having no impact on RD-derived xenografts. From this study, it appears that romidepsin has a cell line-dependent radiosensitisation effect (408). Moreover, 2 – 8 nM romidepsin synergistically enhanced IR-induced apoptosis following 2 – 10 Gy X-rays in retinoblastoma cells (Y79 and WERI-Rb1), as well as increasing γH2AX and acetylated/phosphorylated p53 levels (409).

Mocetinostat

A single study involving the benzamide class I HDACi mocetinostat (MGCD0103) (0.75 – 1.5 μM for 24 h, dependent on the cell line) has shown that treatment with the inhibitor reduced the survival rate of bladder cancer cells (RT112 and T24) when given in conjunction with X-ray irradiation (2 – 8 Gy) (405). Direct comparative analysis was not performed in this study; however, it was suggested that mocetinostat had an enhanced radiosensitisation effect compared to the HDACi panobinostat. Mechanistic studies revealed that similar to panobinostat, mocetinostat decreased levels of HDAC2, but also in the MRE11 exonuclease, which indicates that radiosensitisation could be due to impaired DSB repair.

Belinostat

Belinostat (PXD101) is a hydroxamic acid-type non-selective HDACi and similar to mocetinostat, there is only a single report describing this as a radiosensitiser. This study focused on rhabdomyosarcoma cells (RD and RH3), and showed that belinostat (0.23 or 0.41 μM for 24 h) enhanced the cellular

response following photon radiation (4 Gy) compared to the HDACi or IR alone (410). Further mechanistic studies revealed that combining belinostat with IR increased γH2AX foci 24 h post-IR compared to the radiation alone, although this was only observed in one of the cell lines (RD). Moreover, in both rhabdomyosarcoma cell lines, there was a significant increase in the formation of ROS after the combined treatment compared to either treatment alone, and evidence suggested that this effect was mediated through the suppression of the phosphorylation of DNA-Pk and BRCA1. Further work carried out *in vivo* using RD and RH30-derived xenografts showed that there was a significant tumour growth delay after combined belinostat (40 mg/kg daily for 12 days) and photon irradiation (6 x 2 Gy) compared to either treatment alone. Collectively, this data suggests that belinostat is an apparent effective radiosensitiser of rhabdomyosarcoma *in vitro* and *in vivo*.

Abexinostat

The pan-HDACi abexinostat (PCI-24781; CRA-024781) is hydroxamate-based and has been shown to enhance the radiosensitivity of cervical, colorectal, and non-small cell lung cancer (NSCLC) cell lines. Firstly, cervical cancer (SiHa) and colorectal cancer (WiDr) cells were treated with a combination of abexinostat (0.3 or 3 μM for 20 h before and 4 h post-IR) and X-rays (2 – 8 Gy). This significantly decreased cancer cell survival (DER = 1.5 and 1.2 for SiHa and WiDr, respectively), but interestingly did not appear to impact the response of normal fibroblasts (411). In contrast to other HDACi, it was observed that abexinostat did not affect DSB repair, as demonstrated by γH2AX and comet assay analysis. In the second study, NSCLC (A549 and H460) were treated with abexinostat (0.4 and 0.7 μM in A549, 0.1 and 0.2 μM in H460 treated for 24 h) and γ-radiation (2 – 6 Gy), and a significant radiosensitisation effect was observed (412). This effect was dose-dependent

(DER = 1.3 – 1.7 and 1.2 – 1.9 for A549 and H460, respectively), and interestingly was more pronounced under severely hypoxic conditions (0.1 % oxygen) (DER = 2.3 – 2.4 and 1.7 – 3.2 for A549 and H460, respectively). In H460 cells, treatment with abexinostat alone (0.2 μM for 24 or 48 h) increased cellular apoptosis, although this was not enhanced in combination with IR. In this study, the combined treatment of abexinostat (0.2 μM) and γ-radiation (4 Gy) resulted in delayed DSB repair compared to either treatment alone, as demonstrated via γH2AX and 53BP1 foci formation (24 h post-IR. It was also indicated that the combined treatment resulted in a significant reduction in levels of MRE11, RAD51 and NBS1. Finally, using A549 and H460-derived xenografts, abexinostat (25 mg/kg twice daily) and X-ray irradiation (3 x 2 Gy) significantly increased the delay in tumour growth compared to either treatment alone, and thus there is evidence that abexinostat can function as an effective radiosensitiser for NSCLC both *in vitro* and *in vivo*.

Resminostat

Resminostat is a pan-HDAC inhibitor that has been shown to have anti-tumour effects via impairment of AKT signalling. A 2017 study by Enzenhofer *et al* revealed the impacts of resminostat on HNSCC cell lines FaDu and SCC25. Cells were treated with resminostat (0 – 25 μM) prior to irradiation with 2, 4, 6, or 8 Gy X-rays, and clonogenic assays were performed. Concentrations of 1.25 μM and 2.5 μM resminostat significantly reduced clonogenic survival, and data suggests that this inhibitor works synergistically with irradiation to decrease cell survival (394).

CHAPTER 2: AIMS

HNSCC is the seventh most common cancer worldwide, with rising incidence levels. Risk factors for developing HNSCC include smoking, alcohol intake, and infection with HPV, particularly HPV-16. Radiotherapy is one of the main treatment options for HNSCC and can be used successfully in both curative and palliative settings. It has been well established that patients with HPV-positive disease respond better to radiotherapy due to a defective cell cycle and impairment of the DDR, and thus have a more favourable overall prognosis. However, radioresistance is a common occurrence, particularly in patients with HPV-negative HNSCC, and remains a significant barrier to effective treatment. It is therefore vital to identify alternative combinatorial strategies for increasing the sensitivity of HPV-negative tumours to radiotherapy, which will, in the long term, improve the survival rates and quality of life for patients with HNSCC. I hypothesised that specific inhibitors, identified from an FDA-approved drug library, could be repurposed, and utilised as effective radiosensitisers of relatively radioresistant HPV-negative HNSCC. The specific aims of this research were therefore to:

- Utilise a 3D spheroid growth screen to identify candidate drugs within an FDA-approved drug library that may radiosensitise HPV-negative HNSCC cells.
- Validate the effects of the candidates selected from the screen both in 3D HNSCC spheroid growth and 2D clonogenic survival assays, and to confirm their function as radiosensitisers.
- Uncover the mechanisms behind the radiosensitising potential of these validated drugs in HNSCC cells.

CHAPTER 3: METHODS

3.1. Materials

3.1.1. General Laboratory Reagents

General laboratory reagents were obtained from Sigma-Aldrich (St. Louis, USA), Bio-Rad (Hemel, Hempstead, UK) and Fisher Scientific (Loughborough UK).

3.1.2. Tissue Culture Reagents

Tissue culture reagents were obtained from Sigma-Aldrich (St. Louis, USA) and are listed below:

- Dulbecco's phosphate buffered saline (PBS) - modified, without calcium chloride and magnesium chloride
- 0.25 % Trypsin-EDTA solution – 2.5 g porcine trypsin, 0.2 g EDTA, 4NA/L Hanks' Balanced Salt Solution with phenol red, sterile filtered
- Dulbecco's Modified Eagle's Medium (DMEM) – 25 mM HEPES and sodium bicarbonate, 4500 mg/L glucose, sterile filtered
- Minimal Essential Medium (MEM) – 25 mM HEPES, without L-glutamine, sterile filtered
- Advanced DMEM/F12 (aDMEM/F12) – reduced serum, 110 mg/L sodium pyruvate, sterile filtered

3.1.3. Antibodies

Antibodies were used to detect proteins of interest during immunoblotting. The antibodies used in this research were diluted in Odyssey blocking buffer (LI-COR Biosciences, Cambridge, UK) and 1 x phosphate buffered saline (PBS) 1:1 with 1 % tween-20 (Sigma-Aldrich, St. Louis, Missouri, USA) for immunoblotting, and 2 % BSA solution for immunofluorescence. The primary antibodies used are summarised in table 3.1, and the secondary antibodies summarised in table 3.2.

Table 3.1: List of primary antibodies

Antibody	Reactivity	Dilution	Source	Code
γH2AX	Mouse monoclonal	1:5000	Abcam	ab26350
Acetyl-Histone H3 (K14)	Rabbit polyclonal	1:1000	Cell Signalling	4318
Acetyl-Histone H3 (K18)	Rabbit polyclonal	1:1000	Cell Signalling	9675
Acetyl-Histone H3 (K27)	Rabbit polyclonal	1:1000	Cell Signalling	4353
Acetyl-Histone H3 (K56)	Rabbit polyclonal	1:1000	Cell Signalling	4243
Acetyl-Histone H4 (K5)	Rabbit monoclonal	1:1000	Cell Signalling	8647
Acetyl-Histone H4 (K8)	Rabbit polyclonal	1:1000	Cell Signalling	2594
Histone H4	Rabbit polyclonal	1:1000	Santa Cruz	sc-10810

List of the primary antibodies used during this research. Host organism, reactivity, concentration, dilution, source, and code are displayed. Antibodies were acquired from Abcam (Cambridge, UK), Bethyl Labs (Montgomery, Texas, USA), Cell Signalling (Danvers, Massachusetts, USA), Santa Cruz (California, USA) and Sigma-Aldrich (St. Louis, Missouri, USA).

Table 3.2: List of secondary antibodies

Antibody	Host	Dilution	Source	Code
Alexa Fluor 680 anti-mouse IgG	Goat	1:10,000	Invitrogen	A21057
Alexa Fluor 680 anti-rabbit IgG	Goat	1:10,000	Invitrogen	A21076
IR Dye 800 anti-rabbit IgG	Goat	1:10,000	Li-Cor	926-32211
IR Dye 800 anti-mouse IgG	Goat	1:10,000	Li-Cor	926-32210
Alexa Fluor 555 Anti-Mouse	Goat	1:500	Invitrogen	A32727

List of the secondary antibodies used during this research. Host organism, dilution, source, and code are listed. Secondary antibodies were acquired from LI-COR Biosciences (Cambridge, UK) and Invitrogen (Thermo Fisher Scientific, Loughborough, UK).

3.2. Drug Screening

3.2.1.1. Initial Drug Screen

The drug library used in this research was acquired from SelleckChem (Texas, USA). The full drug library contained 1953 drugs and following a literature search of the various cellular targets of these drugs, I chose 29 targets that were associated with the hallmarks of cancer or had previously been linked to cellular radiosensitivity. This totalled 183 drugs which were used for screening (table 3.3). The screen revealed 17 candidate radiosensitisers, which were further validated in both 2D and 3D models, concluding with 2 confirmed radiosensitisers (figure 3.1). All drugs in the library were provided in powder form (1 mg) and suspended in 100 µL DMSO. For the drug screen and initial validation of candidates, concentrations of 10 µM and 0.3 µM were made, and diluted 1:10 in the spheroid wells to reach final concentrations of 1 µM and 0.03 µM. FaDu cells were chosen for the initial drug screen, as they display relatively higher levels of radioresistance in contrast with other HNSCC cell lines, and previous work in the Parsons group by Dr. Chumin Zhou established that FaDu cells grow extremely well as 3D spheroids, enabling both small and large changes in growth to be monitored through radiation and/or drug treatment (413).

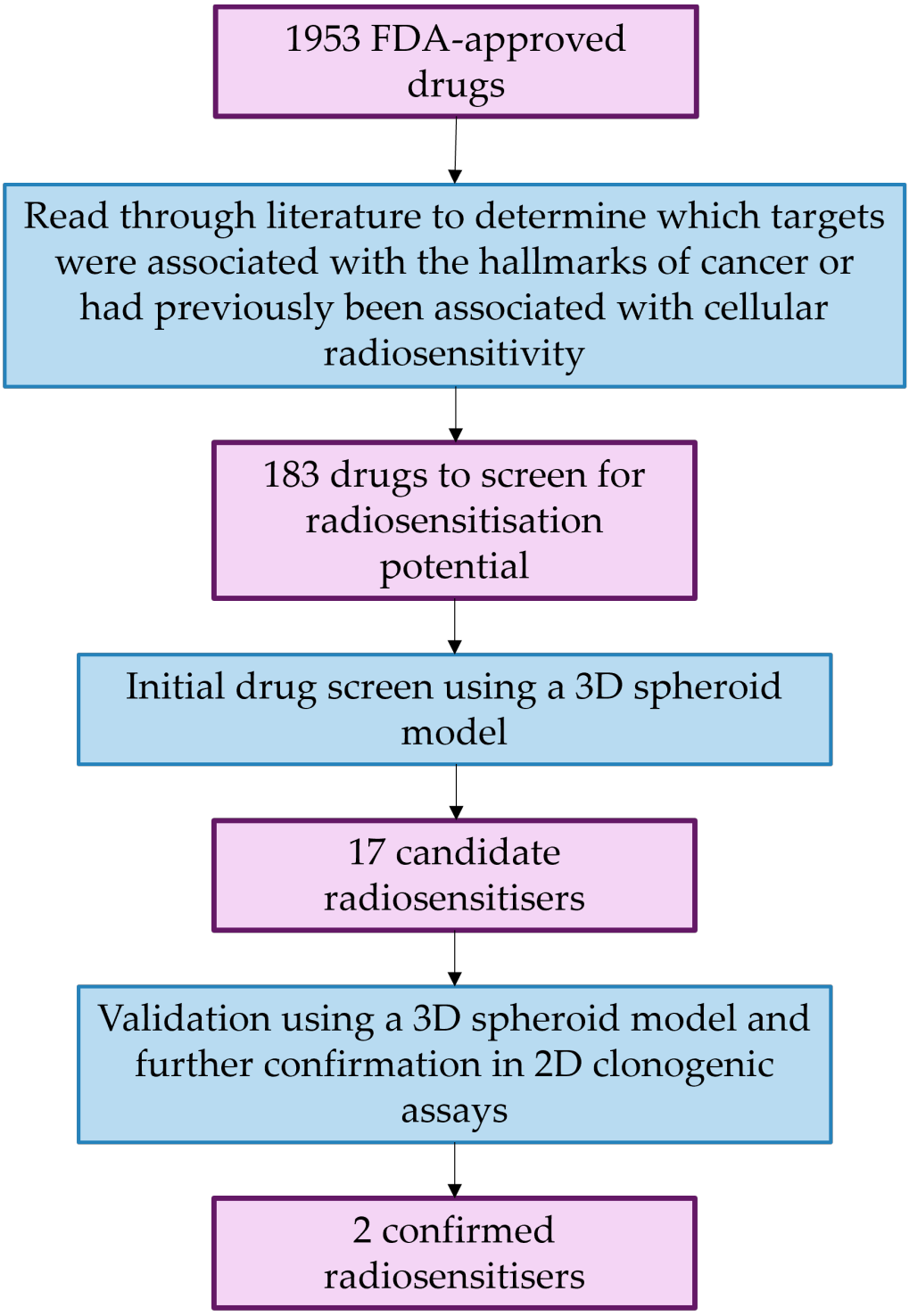

Figure 3.1: Drug screen process

The process of narrowing down drugs in the initial library to be used for screening, the initial screen and validation processes to reveal 2 confirmed radiosensitisers.

Table 3.3: List of drugs used in the initial screen

Code	Product Name	Target
S1117	Triciribine	AKT
S7492	Uprosertib (GSK2141795)	AKT
S7521	Afuresertib (GSK2110183)	AKT
S1048	Tozasertib (VX-680, MK-0457)	Aurora Kinase
S1133	Alisertib (MLN8237)	Aurora Kinase
S1147	Barasertib (AZD1152-HQPA)	Aurora Kinase
S8048	Venetoclax (ABT-199, GDC-0199)	Bcl-2
S2248	Silmitasertib (CX-4945)	Casein Kinase
S7326	Tasisulam	Caspase
S7775	Emricasan	Caspase
S1153	Roscovitine (Seliciclib, CYC202)	CDK
S2768	Dinaciclib (SCH727965)	CDK
S7158	Abemaciclib (LY2835219)	CDK
S7440	Ribociclib (LEE011)	CDK
S1230	Flavopiridol (Alvocidib)	CDK
S1774	Thioguanine	DNA Methyltransferase
S1782	Azacitidine	DNA Methyltransferase
S1200	Decitabine	DNA Methyltransferase
S4294	Procainamide HCl	DNA Methyltransferase, Sodium Channel
S1156	Capecitabine	DNA/RNA Synthesis
S1192	Raltitrexed	DNA/RNA Synthesis
S1199	Cladribine	DNA/RNA Synthesis
S1209	Fluorouracil (5-Fluoracil, 5-FU)	DNA/RNA Synthesis
S1212	Bendamustine HCl	DNA/RNA Synthesis
S1213	Nelarabine	DNA/RNA Synthesis
S1218	Clofarabine	DNA/RNA Synthesis
S1221	Dacarbazine	DNA/RNA Synthesis
S1229	Fludarabine Phosphate	DNA/RNA Synthesis
S1289	Carmofur	DNA/RNA Synthesis
S1299	Floxuridine	DNA/RNA Synthesis
S1300	Tegafur (FT-207, NSC 148958)	DNA/RNA Synthesis
S1302	Ifosfamide	DNA/RNA Synthesis
S1305	Mercaptopurine (6-MP)	DNA/RNA Synthesis
S1840	Lomustine	DNA/RNA Synthesis
S1896	Hydroxyurea	DNA/RNA Synthesis
S4252	Mechlorethamine HCl	DNA/RNA Synthesis
S4288	Chloroambucil	DNA/RNA Synthesis
S4504	6-MP Monohydrate	DNA/RNA Synthesis
S3669	Carmustine	DNA/RNA Synthesis
S5293	Nimustine Hydrochloride	DNA/RNA Synthesis
S5297	Vidarabine monohydrate	DNA/RNA Synthesis
S5582	Cytarabine hydrochloride	DNA/RNA Synthesis
S5552	Amenamevir	DNA/RNA Synthesis
S1760	Rifapentine	DNA/RNA Synthesis

S1764	Rifampin	DNA/RNA Synthesis
S1778	Trifluridine	DNA/RNA Synthesis
S1784	Vidarabine	DNA/RNA Synthesis
S1790	Rifaximin	DNA/RNA Synthesis
S1907	Metronidazole	DNA/RNA Synthesis
S2029	Uridine	DNA/RNA Synthesis
S2794	Sofosbuvir (PSI-7977, GS-7977)	DNA/RNA Synthesis
S3001	Clevudine	DNA/RNA Synthesis
S4227	Fidaxomicin	DNA/RNA Synthesis
S4297	Mupirocin	DNA/RNA Synthesis
S7975	Favipiravir (T-705)	DNA/RNA Synthesis
S8146	Mitomycin C	DNA/RNA Synthesis
S1334	Flupirtine maleate	DNA/RNA Synthesis
S1983	Adenine HCl	DNA/RNA Synthesis
S4035	Vitamin D2	DNA/RNA Synthesis
S5484	Rimantadine Hydrochloride	DNA/RNA Synthesis
S1214	Bleomycin sulphate	DNA/RNA Synthesis
S1237	Temozolomide	DNA/RNA Synthesis, Autophagy
S1949	Menadione	DNA/RNA Synthesis, phosphatase
S1491	Fludarabine	DNA/RNA Synthesis, STAT
S1025	Gefitinib (ZD1839)	EGFR
S1392	Pelitinib (EKB-569)	EGFR
S2727	Dacomitinib (PF299804, PF299)	EGFR
S2755	Varlitinib	EGFR
S2922	Icotinib	EGFR
S7284	Rociletinib (CO-1686, AVL-301)	EGFR
S7297	Osimertinib (AZD9291)	EGFR
S7786	Erlotinib	EGFR
S4667	Lidocaine hydrochloride	EGFR
S5098	Gefitinib hydrochloride	EGFR
S8294	Olmutinib (HM61713, BI 1482694)	EGFR, BTK
S1194	CUDC-101	EGFR, HDAC, HER2
S1028	Lapatinib (GW-572016) Ditosylate	EGFR, HER2
S7810	Afatinib (BIBW2992) Dimaleate	EGFR, HER2
S1011	Afatinib (BIBW2992)	EGFR, HER2
S2111	Lapatinib	EGFR, HER2
S1342	Genistein	EGFR, Topoisomerase
S7854	Ulixertinib (BVD-523, VRT752271)	ERK
S2823	Tideglusib	GSK-3
S1053	Entinostat (MS-275)	HDAC
S1085	Belinostat (PXD101)	HDAC
S1090	Abexinostat (PCI-24781)	HDAC
S1096	Quisinostat (JNJ-26481585) 2HCl	HDAC
S1122	Mocetinostat (MGCD0103)	HDAC
S1515	Pracinostat (SB939)	HDAC
S2693	Resminostat	HDAC
S4125	Sodium Phenylbutyrate	HDAC
S8001	Ricolinostat (ACY-1215)	HDAC
S1703	Divalproex Sodium	HDAC

S3944	Valproic acid	HDAC
S1030	Panobinostat (LBH589)	HDAC
S2216	Mubritinib (TAK 165)	HER2
S7358	Poziotinib (HM781-36B)	HER2, EGFR
S5500	Amodiaquine hydrochloride	HnMT
S7015	Birinapant	IAP
S7205	Idasanutlin (RG-7388)	Mdm2
S1008	Selumetinib (AZD6244)	MEK
S1475	Pimasertib (AS-703026)	MEK
S2673	Trametinib (GSK1120212)	MEK
S7007	Binimetinib (MEK162, ARRY-162, ARRY-438162)	MEK
S8041	Cobimetinib (GDC-0973, RG7420)	MEK
S7505	(S)-crizotinib	MTH1
S1044	Temsirolimus (CCI-779, NSC 683864)	mTOR
S1120	Everolimus (RAD001)	mTOR
S5003	Tacrolimus (FK506)	mTOR
S2658	Omipalisib (GSK2126458, GSK458)	mTOR, PI3K
S7646	Voxtalisib (XL765, SAR245409)	mTOR, PI3K
S5733	Stearic acid	NF-kB
S3137	Sodium salicylate	NF-κB
S4073	Sodium 4-Aminosalicylate	NF-κB
S1848	Curcumin	NF-κB, HDAC, HAT, Nrf2
S1574	Doramapimod (BIRB 796)	p38 MAPK
S7215	Losmapimod (GW856553X)	p38 MAPK
S7799	Pexmetinib (ARRY-614)	p38 MAPK, Tie-2
S1004	Veliparib (ABT-888)	PARP
S1060	Olaparib (AZD2281, Ku-0059436)	PARP
S1087	Iniparib (BSI-201)	PARP
S1098	Rucaparib (AG-014699, PF-01367338) phosphate	PARP
S7625	Niraparib (MK-4827) Tosylate	PARP
S2741	Niraparib (MK-4827)	PARP
S1470	Orantinib (TSU-68, SU6668)	PDGFR
S2730	Crenolanib (CP-868596)	PDGFR
S4736	Trapidil	PDGFR
S2475	Imatinib (STI571)	PDGFR
S7781	Sunitinib	PDGFR, c-Kit, VEGFR
S1040	Sorafenib Tosylate	PDGFR, Raf, VEGFR
S1065	Pictilisib (GDC-0941)	PI3K
S2226	Idelalisib (CAL-101, GS-1101)	PI3K
S2814	Alpelisib (BYL719)	PI3K
S7028	Duvelisib (IPI-145, INK1197)	PI3K
S7645	Pilaralisib (XL147)	PI3K
S1362	Rigosertib (ON-01910)	PLK
S2235	Volasertib (BI 6727)	PLK
S1729	Gemfibrozil	PPAR
S1794	Fenofibrate	PPAR

S2075	Rosiglitazone HCl	PPAR
S4527	Fenofibric acid	PPAR
S2505	Rosiglitazone maleate	PPAR
S2665	Ciprofibrate	PPAR
S4159	Bezafibrate	PPAR
S4207	Clofibric Acid	PPAR
S8432	Troglitazone (CS-045)	PPAR
S2590	Pioglitazone	PPAR
S2556	Rosiglitazone	PPAR
S5487	Cefoperazone sodium	PPARd
S1267	Vemurafenib (PLX4032, RG7204)	Raf
S2807	Dabrafenib (GSK2118436)	Raf
S5069	Dabrafenib Mesylate	Raf
S7108	Encorafenib (LGX818)	Raf
S7397	Sorafenib	Raf
S1130	Sepantronium Bromide (YM155)	Survivin
S4238	Cepharanthine	TNF-alpha
S1567	Pomalidomide	TNF-alpha
S1029	Lenalidomide (CC-5013)	TNF-alpha
S8034	Apremilast (CC-10004)	TNF-alpha, PDE
S1623	Acetylcysteine	TNF-alpha, ROS
S1208	Doxorubicin (Adriamycin) HCl	Topoisomerase
S1223	Epirubicin HCl	Topoisomerase
S1225	Etoposide	Topoisomerase
S1231	Topotecan HCl	Topoisomerase
S1367	Amonafide	Topoisomerase
S1787	Teniposide	Topoisomerase
S3035	Daunorubicin HCl	Topoisomerase
S1222	Dexrazoxane HCl (ICRF-187, ADR-529)	Topoisomerase
S2485	Mitoxantrone 2HCl	Topoisomerase
S2492	Novobiocin Sodium	Topoisomerase
S1340	Gatifloxacin	Topoisomerase
S1465	Moxifloxacin HCl	Topoisomerase
S1756	Enoxacin	Topoisomerase
S2064	Balofloxacin	Topoisomerase
S2328	Nalidixic acid	Topoisomerase
S3181	Flumequine	Topoisomerase
S4119	Pefloxacin Mesylate Dihydrate	Topoisomerase
S4591	Nitroxoline	Topoisomerase
S4604	Levofloxacin hydrate	Topoisomerase
S2217	Irinotecan HCl Trihydrate	Topoisomerase
S1228	Idarubicin HCl	Topoisomerase
S1940	Levofloxacin	Topoisomerase
S5059	Pixantrone Maleate	Topoisomerase

A list of the 183 drugs used in the initial drug screen. Codes, alternate names, and targets are listed. All drugs came from SelleckChem.

3.2.1.2. *Validation and Mechanistic Experiments*

Once the list of drugs had been narrowed down to five candidates, new stocks of these drugs were purchased to take forward for the remainder of the research. These drugs were CUDC-101, pracinostat, mocetinostat, genistein, and lidocaine HCl, and are detailed in table 3.4. These drugs were diluted to 10 mM stock in DMSO and stored as 1 mM aliquots at -80 °C. 1 mM stocks were used periodically and aliquoted at 100 µM, then used at a concentration of 0.5 µM for experiments.

Table 3.4: List of drugs taken forward

Drug Name	**Code**	**Target**
CUDC-101	S1194	EGFR, HER2, HDAC
Pracinostat (SB939)	S1515	HDAC
Mocetinostat (MGCD0103)	S1122	HDAC
Lidocaine HCl	S4667	EGFR
Genistein (NPI 031L)	S1342	EGFR

List of the five inhibitors used during validation and mechanistic experiments. Name, code, and inhibitor target are listed. All inhibitors were acquired from SelleckChem.

3.3. Cell Culture

3.3.1. Cell Line Culture

All cell culture work was carried out in class II hood cabinets with laminar flow, cleaned before and after each use with 70 % ethanol and sterilised with ultra-violet light exposure. A humidified cell culture incubator set to standard conditions of 37 °C, and 5 % CO_2 was used for cell growth and maintenance, and all cells were cultured using tissue culture grade plastics.

FaDu and A253 cells came from ATCC (Teddington, UK), and UM-SCC-6, UM-SCC-12, UM-SCC-17A and UM-SCC-11b cells were provided by Prof. T. Carey, University of Michigan, USA. All cells were cultured as monolayers in either MEM or DMEM supplemented with 10 % fetal bovine serum (FBS), 1 x penicillin-streptomycin, 2 mM L-glutamine and 1 x non-essential amino acids. The identity of the cells was verified in our laboratory by short tandem repeat (STR) profiling. Characteristics of each cell line are summarised in table 3.5.

Table 3.5: Cell lines used in this research

Cell Line	Location	Culture Medium	P53 Status	HPV Status
FaDu	Hypopharynx	MEM	mut	-
A253	Oral Cavity	DMEM	mut	-
UM-SCC-6	Tongue	DMEM	WT	-
UM-SCC-12	Oral Cavity	DMEM	mut	-
UM-SCC-17A	Oral Cavity	DMEM	WT	-
UM-SCC-11b	Oral Cavity	DMEM	mut	-

Cell lines used through this research and their characteristics, including location of origin site, culture medium, p53 status (mut: mutant p53, WT: wild-type p53), HPV status (-; negative).

3.3.2. Thawing Cells

Cells were frozen in cryovials containing 90 % FBS and 10 % dimethyl sulfoxide (DMSO) and kept in liquid nitrogen for long-term storage. Upon removal from nitrogen, they were thawed in a 37 °C water bath for 1 minute. 1 ml of fresh medium was added dropwise to the vial before the cells had completely thawed and gently mixed with the pipette. This suspension was transferred into a 15 ml tube and mixed with 8 ml of media, then centrifuged at 300 x g for 5 minutes. After centrifugation, the supernatant was removed, and the pellet was resuspended in 1 ml of fresh medium. The suspension was

then transferred to a T75 cell culture flask containing 11 ml of medium, which was then kept in the incubator under standard conditions (37 °C, 5 % CO_2) to allow cell growth.

3.3.3. Passaging Cells

Cells growing in T75 flasks eventually become confluent and need to be passaged into new flasks to allow room for growth and sufficient nutrients. When cells in the flask reached 80 % confluency, the media was removed and the cells were washed with 7 ml of PBS, which was also removed. 1 ml of 0.25 % trypsin-EDTA was added, and the flask was incubated for 2 – 10 minutes at 37 °C to allow enzyme activation and cell detachment. After incubation, 9 ml of fresh media was added to neutralise the trypsin, and the solution was mixed with the pipette to generate a cell suspension. A portion of this suspension was added to a new T75 flask, topped up to 12 ml total with fresh media, and placed in the incubator (37 °C, 5 % CO_2) to allow continued growth.

3.3.4. Freezing Cells

After approximately 20 passages, cells need replacing with early passage cells. A supply of these cells was maintained and kept in long-term storage in liquid nitrogen. When cells were initially thawed, they are split into multiple flasks where they were grown to 80 % confluency. The media was removed, and the cells were washed with 7 ml of PBS. As described above, 0.25 % trypsin-EDTA solution was added for 2 – 10 minutes at 37 °C to promote cell detachment, and 9 ml of fresh medium was then added. This cell suspension was transferred to a 15 ml tube and centrifuged at 300 x g for 5 minutes. After removing the supernatant, the cell pellet was resuspended in 1 – 2 ml of

medium with 90 % FBS and 10 % DMSO. This was then transferred into 1 or 2 cryovials, depending on the pellet size. The cryovials were placed into a -80 °C freezer for 24 hours in a CoolCell Freezing Container (Corning, New York, USA) to allow for a slow drop in temperature. After 24 hours, the vials were transferred to liquid nitrogen.

3.4. Cell Irradiation

Cell irradiations were carried out in the laboratory using a CellRad X-ray irradiator (Faxitron Bioptics, Tuscon, USA). A standard rate of 3 Gy/minute, 3 mA, and 100 kV was used and radiation doses (1 – 4 Gy) were given in a time-controlled manner. Plates were positioned in the centre of the irradiation field.

3.5. Clonogenic Survival Assays

Cell survival and proliferation following treatment with drugs and/or irradiation was analysed using colony formation (clonogenic) assays. Following the cell passaging steps as described in section 3.3.3, a 10 µl sample was counted on a haemocytometer under a light microscope. Cell concentration in the suspension was determined and the required volume for a specific number of cells was calculated. For 0 Gy conditions, each cell line was used at a density of 1000/cells per well. Increased seeding densities were used for higher doses of IR to ensure enough cells survived to form colonies (table 3.6).

Table 3.6: Seeding densities for clonogenic assays

Radiation Dose	Seeding Number
0 Gy	1000
1 Gy	2000
2 Gy	4000
4 Gy	8000

Relative seeding numbers for clonogenic assays for each radiation dose. The same seeding density was used for each cell line.

After counting, a stock solution of cells was prepared, and a defined number of single cells (table 3.6) were seeded into 6-well plates (Thermo Fisher, Massachusetts). Plates were then left for 6 hours in the cell culture incubator (37 °C, 5 % CO_2) to allow the cells to attach to the surface. After this time, the medium was removed and fresh medium containing either DMSO or drug treatment was added. The plates were then incubated for 24 hours before being irradiated as described in section 3.4 at increasing doses of 1 – 4 Gy. The treatment media was removed immediately after irradiation and replaced with fresh media. Plates were then incubated for another 6 – 10 days in the cell culture incubator to allow time for the single cells to form colonies (containing 50 cells or more). After this time, the medium was removed from the wells and the plates were washed with PBS. The cells were then fixed and stained with crystal violet (6 % glutaraldehyde and 0.5 % crystal violet) for 30 minutes. After staining, plates were washed with water and left to air dry overnight. Colonies were counted using the GelCount colony counter (Oxford Optronics, Oxford, UK). The relative colony forming units (surviving fraction, SF) is the number of colonies per treatment relative to the number of colonies in the unirradiated control. Plating efficiencies and surviving fractions were calculated for each condition using equations 3.1 and 3.2. The plating efficiency was approximately 20 % for all cell lines used in this research.

Equation 3.1: Plating efficiency for clonogenic assays

$$Plating\ efficiency = \frac{Number\ of\ colonies\ for\ unirradiated\ control}{Seeding\ density\ of\ unirradiated\ control}$$

Equation 3.2: Surviving fraction for clonogenic assays

$$Surviving\ Fraction = \frac{Number\ of\ colonies\ for\ selected\ condition}{Seeding\ Density\ of\ selected\ condition\ x\ average\ plating\ efficiency}$$

3.6. Spheroid Growth Screen and Assays

3D spheroid growth assays were used to analyse the impact of various inhibitors alone or in combination with X-ray irradiation. This technique involves using cells grown as microscopic 3D spheres in suspension as opposed to a monolayer of cells used in routine cell culture. After passaging FaDu cells as described in section 3.3.3, remaining cells were centrifuged in a 15 ml tube at 300 x g for 5 minutes. The supernatant was removed, and the pellet was resuspended in 3 ml of spheroid medium – aDMEM/F12 (Sigma-Aldrich, St Louis, USA) supplemented with 1 % B27, 0.5 % N2, 2 mM L-glutamine, 1 x penicillin-streptomycin, and 5 µg/ml heparin, plus 0.02 % epidermal growth factor (EGF) and 0.01 % fibroblast growth factor (FGF) immediately before use. Cell concentration in the suspension was estimated using a 10 µl sample on a haemocytometer. A stock solution of cells was prepared with the cell suspension and fresh spheroid medium to ensure the correct number of 500 cells per well. The total volume of cell suspension was 90 µl per well. The spheroids were seeded into 96-well ultra-low attachment found bottom plates (Costar, Sigma-Aldrich, St Louis, USA). Only the central wells in the plate were used in order to minimise any variability in the dose of X-rays given to the spheroids, and any empty wells on the plate were filled

with 100 µl PBS to prevent the spheroid wells drying out. The plates were then stored in the cell culture incubator under standard conditions (37 °C, 5 % CO_2) to allow spheroid formation.

24 hours after seeding, the spheroids were treated with inhibitors or DMSO as a control. The inhibitors were prepared as 10x stock solutions and 10 µl was added into the 90 µl already in the well. After 24 hours of inhibitor treatment, individual spheroids were imaged using a light microscope (AMG EVOS, Thermo Fisher Scientific, Massachusetts, USA) and then the plates were irradiated with 1 – 2 Gy X-rays as described in section 3.4. Immediately after irradiation, 50 µl of the medium in the well was removed and replaced with 100 µl of fresh spheroid medium with no inhibitors or DMSO. Plates were then imaged on days 5, 8, 10, 12 and 15 post-seeding, and the images were analysed using ImageJ. Spheroid diameter was measured, converted to a radius (r), and the volume (v) of the spheroid was calculated using equation 3.3. The volume of the spheroids on each day was compared to the volume on day 3 to calculate fold increase in growth using equation 3.4.

Equation 3.3: Volume of a spheroid

$$V = \frac{4}{3}\pi r^3$$

Equation 3.4: Fold increase in spheroid growth

$$Fold\ Increase\ in\ Growth = \frac{Volume\ on\ day\ X}{Volume\ on\ day\ 3}$$

For comparative analysis of spheroid growth under different treatment conditions, the fold increase in growth of the inhibitor-treated spheroids was normalised to the fold increase in growth of the DMSO control spheroids. Inhibitor alone treatments were normalised to DMSO alone, while inhibitor

plus IR spheroids were normalised to DMSO plus IR. The DMSO controls were set to 100 % growth.

3.7. Western Blot

3.7.1. Cell Harvesting

Cells were seeded in 10 cm dishes and incubated at 37 °C, 5 % CO_2 until ~80 % confluent. Cells were then treated with inhibitors for 24 hours, and then either irradiated with 4 Gy X-rays or left unirradiated before adding fresh media. To harvest the cells, the medium was removed, and the cells were washed with ice-cold PBS. 5 ml of fresh ice-cold PBS was added to the dish, and the cells were scraped off the plastic and transferred into a 15 ml tube. This was repeated, and the cells were then centrifuged at 300 x g for 5 minutes at 4 °C to form a pellet. After removing the supernatant, the pellet was resuspended in 1 ml of ice-cold PBS, transferred to a 1.5 ml tube, and centrifuged again at 300 x g for 5 minutes at 4 °C. After centrifugation, the supernatant was removed, and the pellet was stored at -80 °C for at least 1 hour.

3.7.2. Acid Extraction of Histones

To analyse histone acetylation sites in a more effective manner, acid extraction of histones was used as an alternative to using whole cell extracts, as previously used in the Parsons laboratory (414). Following cell harvesting as described in section 3.7.1., the cell pellet was resuspended in 100 µl of hypotonic buffer (10 mM Tris-HCl (pH 8.0), 1 mM KCl and 1.5 mM $MgCl_2$) containing 1 µg/µl each of pepstatin, chymostatin, leupeptin and aprotinin, N-Ethylmaleimide and 100 µM of PMSF. The suspension was then incubated for

30 minutes at 4 °C on a shaker. After incubation, the suspension was centrifuged at 10,000 x g for 10 minutes at 4 °C. The supernatant containing the cytoplasmic fraction was removed and the pellet containing the nuclei was resuspended in 80 µl of 0.4 M sulfuric acid and incubated overnight at 4 °C on a shaker. The next day, samples were centrifuged at 16,000 x g for 10 minutes at 4 °C. The supernatant containing the histones was transferred to a fresh 1.5 ml tube, and trichloroacetic acid was added dropwise whilst inverting the tube to a final concentration of 33 %. The samples were incubated on ice for 30 minutes, then centrifuged again at 16,000 x g for 10 minutes at 4 °C to pellet the histones. The histone pellet was washed with 100 µl ice-cold acetone, centrifuged again at 16,000 x g for 10 minutes at 4 °C, and the wash was repeated. The pellets were then left at room temperature for 10 – 15 minutes to air dry, dissolved in 50 µl of dH_2O, and protein concentration was measured by Nanodrop.

3.7.3. Sodium dodecyl sulphate-polyacrylamide gel electrophoresis (SDS-PAGE)

Sodium dodecyl sulphate-polyacrylamide gel electrophoresis (SDS-PAGE) was used in order to separate proteins in a whole cell extract or purified histones according to their molecular weight. To study proteins with a higher molecular weight, precast gradient gels of 4 – 12 % Tris-Glycine were used (Invitrogen, Thermo Fisher Scientific, Loughborough, UK), while 16 % Tris-Glycine gels were used for lower molecular weight proteins. 16 % gels were prepared by making the separating portion with 377 mM Tris-HCl pH 8.8, 0.1 % SDS, 2 mM ethylenediaminetetraacetic acid (EDTA), 16 % acrylamide/bis solution (30:0.8; Bio-Rad, Hemel, Hempstead, UK), 0.1 % ammonium persulphate (APS), and 0.1 % tetramethylethylenediamine (TEMED), and pouring it into a 1.5 mm gel cassette until it was ¾ full. The solution was

overlaid with 1 ml of 100 % ethanol to ensure a level separating gel without bubbles and left to set. After approximately 30 minutes, the gel was set, and the ethanol was removed. The cassette was washed with dH_2O before the 5 % stacking gel solution – 125 mM Tris-HCl pH 6.8, 0.1 % SDS, 2 mM EDTA, 5 % acrylamide/bis solution (30:0.8; Bio-Rad, Hemel, Hempstead, UK), 0.1 % APS, and 0.1 % TEMED – was poured over the top of the separating gel. A 10- or 15-well comb was inserted into the cassette, and the stacking portion was left to set for approximately 30 minutes.

Purified histones (typically 20 µg) were prepared in SDS-PAGE sample buffer (25 mM Tris-HCl pH 6.8, 2.5 % mercaptoethanol, 1 % SDS, 10 % glycerol, 0.05 mg/ml bromophenol blue, and 1 mM EDTA) and heated for 5 minutes at 95 °C to denature the proteins. The samples were then loaded into the wells on the polyacrylamide gel. Electrophoresis was performed in 1 x Tris-glycine SDS (TGS) running buffer (25 mM Tris-HCl pH 8.3, 192 glycine, and 0.1 % SDS; Fisher Scientific, Loughborough, UK) at 125 V for 2 hours in an SDS-PAGE Mini Gel Tank (Fisher Scientific, Loughborough, UK). In the first well, 1 µl of the Precision Plus Protein All Blue Prestained Protein Standards (10 kDa – 250 kDa; Bio-Rad Laboratories, California, USA) was loaded as a protein marker. Protein levels were analysed following electrophoresis by immunoblotting.

3.7.4. Immunoblotting

Immunoblotting was used to visualise proteins of interest. To do this, the proteins were transferred from the SDS-PAGE gel to an Immobilon polyvinylidene difluoride (PVDF) membrane (Millipore, Watford, UK). The PVDF membrane was activated in 100 % methanol for 15 seconds, washed in dH_2O for 1 minute, then washed in cold transfer buffer (1 x Tris-glycine (TG; 25 mM Tris-HCl pH 8.3, 192 mM glycine; Fisher Scientific, Loughborough,

UK), 20 % methanol) for at least 1 minute. Two pieces of filter paper and two sponges were also soaked in cold transfer buffer for at least 1 minute. One of the sponges was placed in the base of a Mini Blot Module (Fisher Scientific, Loughborough, UK), followed by a piece of filter paper, then the SDS-PAGE gel, which had been removed from the cassette and rinsed in transfer buffer. The PVDF membrane was placed on top of the gel, followed by the second piece of filter paper and the second sponge. The top of the module was then fixed into place and the module was transferred into the Mini Gel Tank. After filling the interior of the module with cold transfer buffer, and the tank with dH2O, the transfer was conducted at 20 V for 1.5 hours.

Once the transfer was complete, the PVDF membrane was washed in PBS for 5 minutes, and then blocked in Odyssey blocking buffer (LI-COR Biosciences, Cambridge, UK) diluted 1:1 in PBS for at least 1 hour at room temperature with rocking at 25 rpm. The blocking buffer was removed, and the membrane was incubated in the primary antibody (Table 3.1), which was diluted in Odyssey blocking buffer (previously diluted 1:1 in 1 x PBS) with 0.1 % Tween 20, overnight at 4 °C with rocking at 25 rpm. The PVDF membrane was then washed three times in 1 x PBS with 0.1 % Tween 20, each wash lasted 5 minutes and was done at room temperature. The PVDF membrane was then incubated with the secondary antibody (Table 3.2) diluted in Odyssey blocking buffer diluted 1:1 in 1 x PBS for 1 hour at room temperature with 25 rpm rocking. After blocking, the membrane was again washed three times in 1 x PBS with 0.1 % Tween 20 as above. Finally, the membrane was scanned and quantified using the LI-COR Odyssey Infrared Imaging System (LI-COR Biosciences, Cambridge, UK).

3.8. Neutral Comet Assay

The neutral comet assay was used to investigate DSB repair kinetics following the induction of IR-induced DNA damage (415). Microscope slides were prepared in advance by coating with 1 ml 1 % normal melting point agarose (NMPA; Fisher Scientific, Loughborough, UK) in dH_2O. FaDu, UM-SCC-12, and UM-SCC-11b cells were seeded in 6 cm dishes at a seeding density of 250,000 cells in 3 ml per dish. The cells were left to attach to the dish for 24 hours, then the media was removed and replaced with fresh media containing either DMSO or 0.5 μM inhibitor. After 24-hour drug treatment, the cells were trypsinised, diluted to 100,000 cells per ml, and 250 μl of cell suspension was seeded into a 24-well plate (Greiner, CELLSTAR® multiwell culture plates, Sigma-Aldrich, St Louis, USA) on ice. DNA damage was induced with 4 Gy X-rays as described in section 3.4, and following this cells were mixed with 800 μl of 1 % low melting point agarose (LMPA; Fisher Scientific, Loughborough, UK) in PBS, and loaded onto a pre-coated microscope slide. The agarose was allowed to set on ice, and slides were placed into a humidified incubator at 37 °C for 0, 2 and 4 hours to permit DNA repair to occur. After the incubation period, the slides were lysed in coplin jars containing cold lysis buffer (2.5 M NaCl, 100 mM EDTA, 10 mM Tris base (pH 10.5), 1 % N-lauroylsarcosine (pH 9.5), 10 % DMSO and 1 % Tween-20) at 4 °C for at least 1 hour. Following this, the slides were washed 3 times for 5 minutes with 1 ml cold electrophoresis buffer (1 x TBE (18 mM Tris-borate, 0.4 mM EDTA, pH 8.3), then placed in a comet assay tank (Appleton Woods Ltc, Birmingham, UK) and the DNA was allowed to unwind for 30 minutes. After this time, electrophoresis was performed at 25 V, 20 mA for 25 minutes. The slides were subsequently washed 3 times for 5 minutes with 1 ml cold PBS, and then left to air dry overnight. The next day, the slides were rehydrated with dH_2O (pH 8) for 30 minutes, stained with 1 ml SYBR Gold (1:20,000 in dH_2O (pH 8); Fisher

Scientific, Loughborough, UK) for 30 minutes, and left to air dry overnight again in a light protected environment. The slides were then imaged using the BX61 Olympus microscope at 10 x magnification (Olympus, Shinjuku, Japan). 10 images were taken per slide containing at least 5 cells per image. The images were then analysed using the Komet 6.0 software (Andor Technology, Belfast) to calculate the percentage tail DNA values.

3.9. Fluorescent Immunostaining

Fluorescent immunostaining was used to visualise γH2AX foci at the sites of IR-induced DSB damage. Round glass coverslips with a diameter of 13 mm (Nunc Thermanox, Fisher Scientific, Loughborough, UK) were sterilised in 100 % ethanol and placed in the bottom of 3.5 cm dishes. FaDu, UM-SCC-12 and UM-SCC-11b cells were seeded into the dishes at a seeding density of 200,000 cells per dish in 2 ml. The cells were left to attach for 24 hours, then the media was removed and replaced with fresh media containing DMSO or 0.5 μM inhibitor. After 24-hour drug treatment, the dishes were irradiated, and the media was replaced. At 0, 1-, 4-, 8- and 24-hours post-irradiation, the media was removed from the dishes and the cells were washed with PBS before fixation with 1 ml 10 % formalin (Sigma-Aldrich, St Louis, USA) for 10 minutes at room temperature. The cells were once again washed with PBS, and single coverslips were removed from the dish and placed into 24-well plates (Greiner, CELLSTAR® multiwell culture plates, Sigma-Aldrich, St Louis, USA). The cells were permeabilised with 500 μl 0.2 % triton (200 μl Triton x-100, 100 ml PBS) for 10 minutes and subsequently washed 3 times with 500 μl 0.1 % Tween (100 μl Tween, 100 ml PBS). The coverslips were then incubated with 500 μl of 2 % BSA solution (500 mg BSA, 25 ml PBS) for 1 hour on a rocker at room temperature to prevent non-specific antibody binding. 200 μl of the

primary antibody (table 3.1) was then added, and the coverslips were incubated overnight at 4 °C on a rocker. The following day, coverslips were washed 3 times with PBS, then incubated with 200 µl of secondary antibody (table 3.2) for 1 hour at room temperature in a light protected environment. The coverslips were then washed in PBS for 10 minutes on a rocker and then left to dry for at least 1 hour, still in a light protected environment. Once dry, the coverslips were mounted on to a microscope slide using Fluoroshield containing DAPI (Sigma-Aldrich, St Louis, USA). A BX61 Olympus microscope (Olympus, Shinjuku, Japan) was used to capture images of the slides. 5 representative images were captured for each coverslip, and 2 coverslips from each condition were imaged. Foci numbers were quantified using ImageJ.

CHAPTER 4: RESULTS I

Comprehensive drug screen to identify candidate radiosensitisers of HPV-negative HNSCC *in vitro*

4.1. Introduction

Radiotherapy is used as a successful treatment for HNSCC patients in both curative and palliative settings, however radioresistance is a common occurrence, particularly in HPV-negative disease. It is therefore imperative to identify novel methods of sensitising HPV-negative HNSCCs to ionising radiation in order to improve prognosis and survival. One such method of radiosensitisation is the combination of targeted drugs with radiation treatment to increase cell death, and for the initial stage of this research I aimed to utilise drug screening to identify novel radiosensitisers of HNSCC cells *in vitro*. From a library of 1954 FDA-approved drugs, I selected 183 to screen (see table 3.3), covering 29 cellular targets. These targets had a wide variety of cellular functions and have been associated with the development and progression of cancer.

A large number of the drugs in the library target cellular components involved in cell growth, cell survival and the regulation of apoptosis, including the Bcl-2 family of proteins, caspases, IAP proteins, NF- κB, peroxisome proliferator-activated receptors (PPARs), TNF-α and platelet-derived growth factor receptor (PDGFR). Previous studies have demonstrated success in pharmacologically targeting these proteins to increase the effectiveness of radiotherapy and induce radiosensitivity in multiple cancer types *in vitro* (416-423). Furthermore, several of the cellular targets are involved in maintaining correct regulation of the cell cycle, including CDKs, topoisomerase enzymes,

glycogen synthase kinase 3 (GSK-3), mouse double minute 2 homolog (MDM2), PLK-1, topoisomerase, and aurora kinases. Inhibitors of a number of these proteins, including some available in the drug library used in this research, have been shown to effectively radiosensitise a variety of cancer types (424-429). Moreover, proteins involved in various cell signalling pathways were also selected for targeting during this screen, including EGFR, AKT, mTOR, and mitogen-activated protein kinase-kinases (MEKs) (430-433). DNA associated proteins have also been selected for this drug screen. For example, drugs targeting DDR-associated proteins such as casein kinase 2 (CK2), 2-hydroxy-dATP diphosphatase (MTH1), and PARPs, were all selected, and have previously been shown to have radiosensitisation potential (434-436). Additionally, I also chose to screen drugs targeting proteins involved in the regulation of chromatin organisation, including DNMTs, HDACs and HnMTs, which have been demonstrated to radiosensitise cancer cells *in vitro* in previous research (412, 437).

4.2. 3D Spheroid Model of HNSCC

The first stages of this research employed a 3D spheroid model of HNSCC. Previous work in our laboratory by Dr. Chumin Zhou successfully established well-characterised spheroid models using multiple HNSCC cell lines (413), and it is understood that spheroids are a more accurate representation of *in vivo* and clinical tumours than 2D models due to their multi-layered composition. Particularly related to drug screening, factors such as oxygen gradients and growth kinetics, as well as drug penetrance, can have a substantial effect on the cellular response to drug treatment *in vitro*, however, cannot be replicated in 2D models. 3D models therefore have a more comparable response to solid tumours (438). FaDu cells were chosen for these

experiments, as they display relatively higher levels of radioresistance in contrast with other HNSCC cell lines, and were previously shown by Dr. Chumin Zhou to grow extremely well as 3D spheroids enabling both small and large changes in growth to be monitored through radiation and/or drug treatment (413).

As an initial starting point, the growth of 3D spheroids of FaDu cells were monitored over a period of 15 days, both in the absence and presence of radiation. As described in section 3.6, FaDu cells were seeded into 96-well plates (500 cells/well) and left overnight to form spheroids. On Day 3 post-seeding, spheroids were treated with 1 Gy X-rays, or left untreated as a control. The spheroids were imaged on days 3, 5, 8, 10, 12 and 15 post-seeding, and the volume and fold increase in growth of the spheroids was calculated. In the absence of any inhibitor treatments or exposure to IR, spheroids grew approximately 80.6-fold over the course of 15 days post-seeding (figure 4.1). The rate of growth was initially slow, with only an average 3.45-fold increase between days 3 and 5. However, the rate of growth then began to increase exponentially, with an average 15.3-fold increase by day 8. By day 10, the spheroids had grown an average of 29.0-fold, 47.1-fold by day 12, and as mentioned above, an average of 80.6-fold by day 15. In comparison, spheroids treated with 1 Gy X-rays on day 3 post-seeding had a growth rate of, on average, 50 % lower than unirradiated with spheroids at each time point (figure 4.1). By 15 days post-seeding, the irradiated spheroids only had an average increase in growth of 47.5-fold.

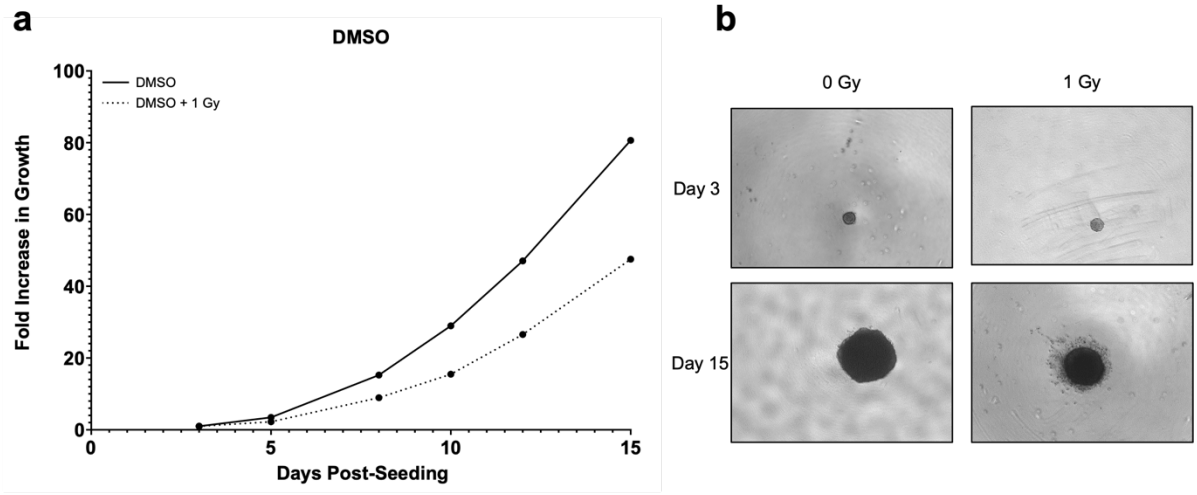

Figure 4.1: FaDu spheroid growth

FaDu cells were seeded at a density of 500 cells/well in ULA plates and left to form spheroids of approximately 200 µm in diameter. On day 3 post-seeding, spheroids were irradiated with 1 Gy X-rays. Images of the spheroids were captured on days 3, 5, 8, 10, 12 and 15 post-seeding, and used to analyse the increase in growth. a) the fold increase in growth of FaDu spheroids alone and after 1 Gy X-ray treatment. b) spheroids on day 3 and 15 post-seeding after either control-only or IR treatment.

4.3. Drug Screen and Identification of Candidate Radiosensitisers

To assess the radiosensitisation potential of the 183 drugs selected, FaDu cells were seeded as described above, at a density of 500 cells per well and left overnight to form spheroids. On day 2, individual spheroids were treated with the drugs (or a DMSO control) at high and low concentrations of 1 µM and 0.03 µM. 24 hours after drug treatment, the spheroids were irradiated with X-rays at 1 Gy, and subsequently imaged on days 3, 5, 8, 10, 12 and 15 post-seeding. Spheroid volume and fold increase in growth was calculated to determine if the drugs displayed a radiosensitisation effect, however only single spheroids were analysed for each treatment, so statistical analysis was not performed at this stage. Percentage growth of treated spheroids compared to the control spheroids was calculated for both drug concentrations, and any drugs reducing growth by 50 % or more compared to DMSO were taken into

consideration to take forward to the next stage of research (figures 4.2, 4.3, 4.4 and 4.5).

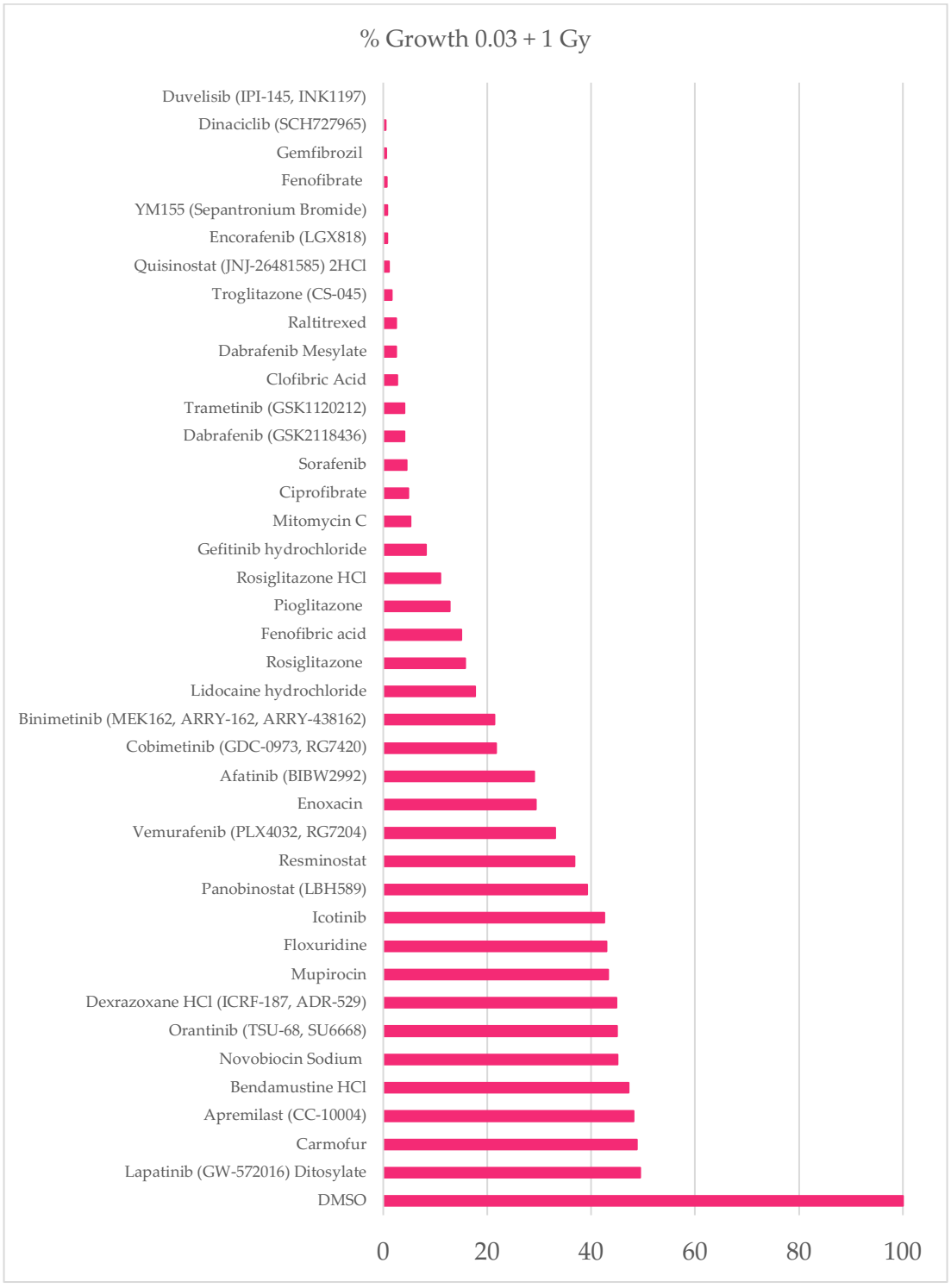

Figure 4.2: Relative percentage growth of spheroids after 0.03 μM inhibitor and X-ray treatment

The fold increase in spheroid growth on day 15 following 0.03 μM inhibitor plus 1 Gy X-rays was compared to DMSO plus 1 Gy X-rays to calculate a relative percentage growth. These graphs demonstrate the inhibitors that caused a reduction in growth of greater than 50 % relative to controls.

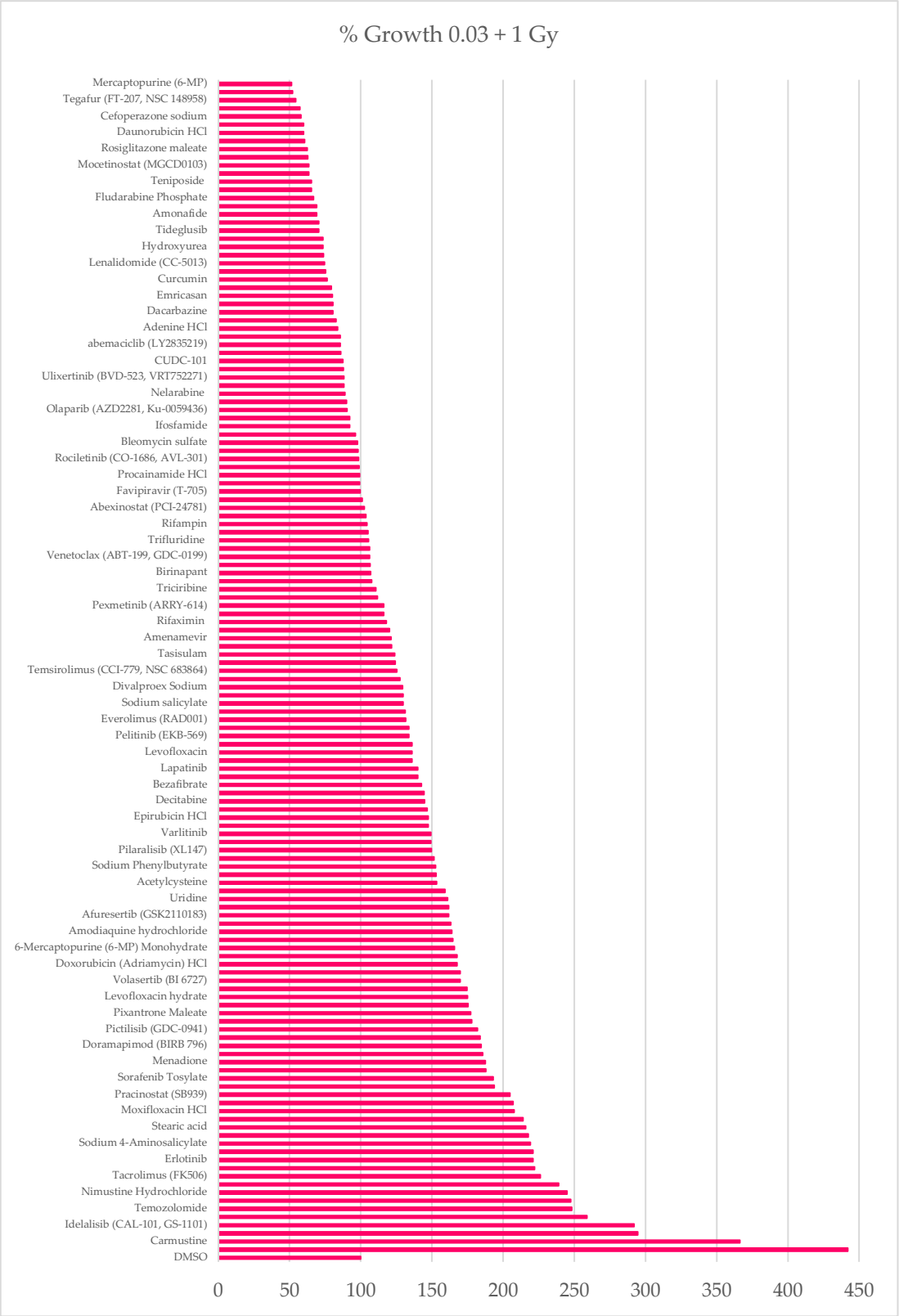

Figure 4.3: Relative percentage growth of spheroids after 0.03 μM inhibitor and X-ray treatment

The fold increase in spheroid growth on day 15 following 0.03 μM inhibitor plus 1 Gy X-rays was compared to DMSO plus 1 Gy X-rays to calculate a relative percentage growth. These graphs demonstrate the inhibitors that caused a reduction in growth of less than 50 % relative to controls.

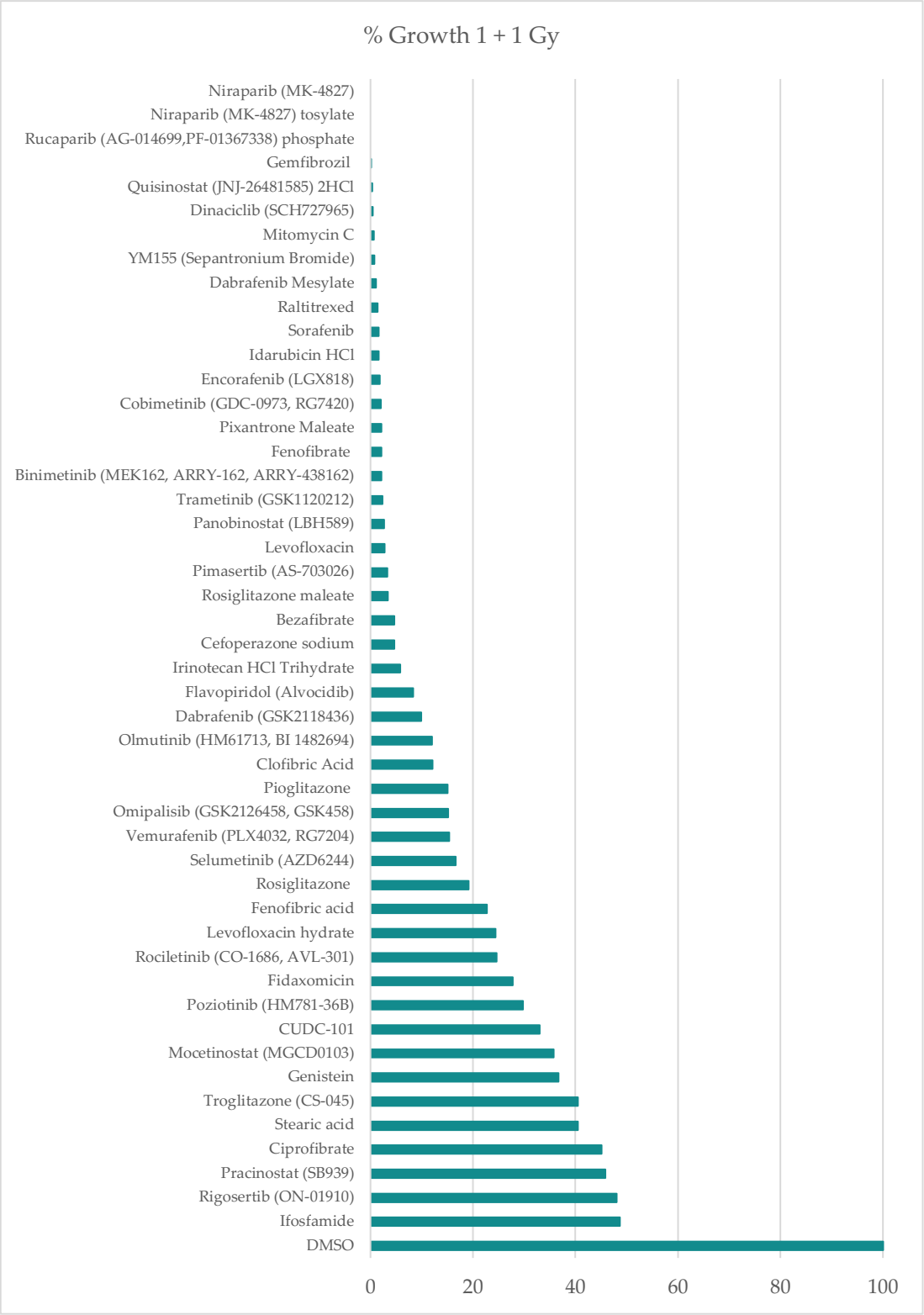

Figure 4.4: Relative percentage growth of spheroids after 1 μM inhibitor and X-ray treatment

The fold increase in spheroid growth on day 15 following 1 μM inhibitor plus 1 Gy X-rays was compared to DMSO plus 1 Gy X-rays to calculate a relative percentage growth. These graphs demonstrate the inhibitors that caused a reduction in growth of greater than 50 % relative to controls.

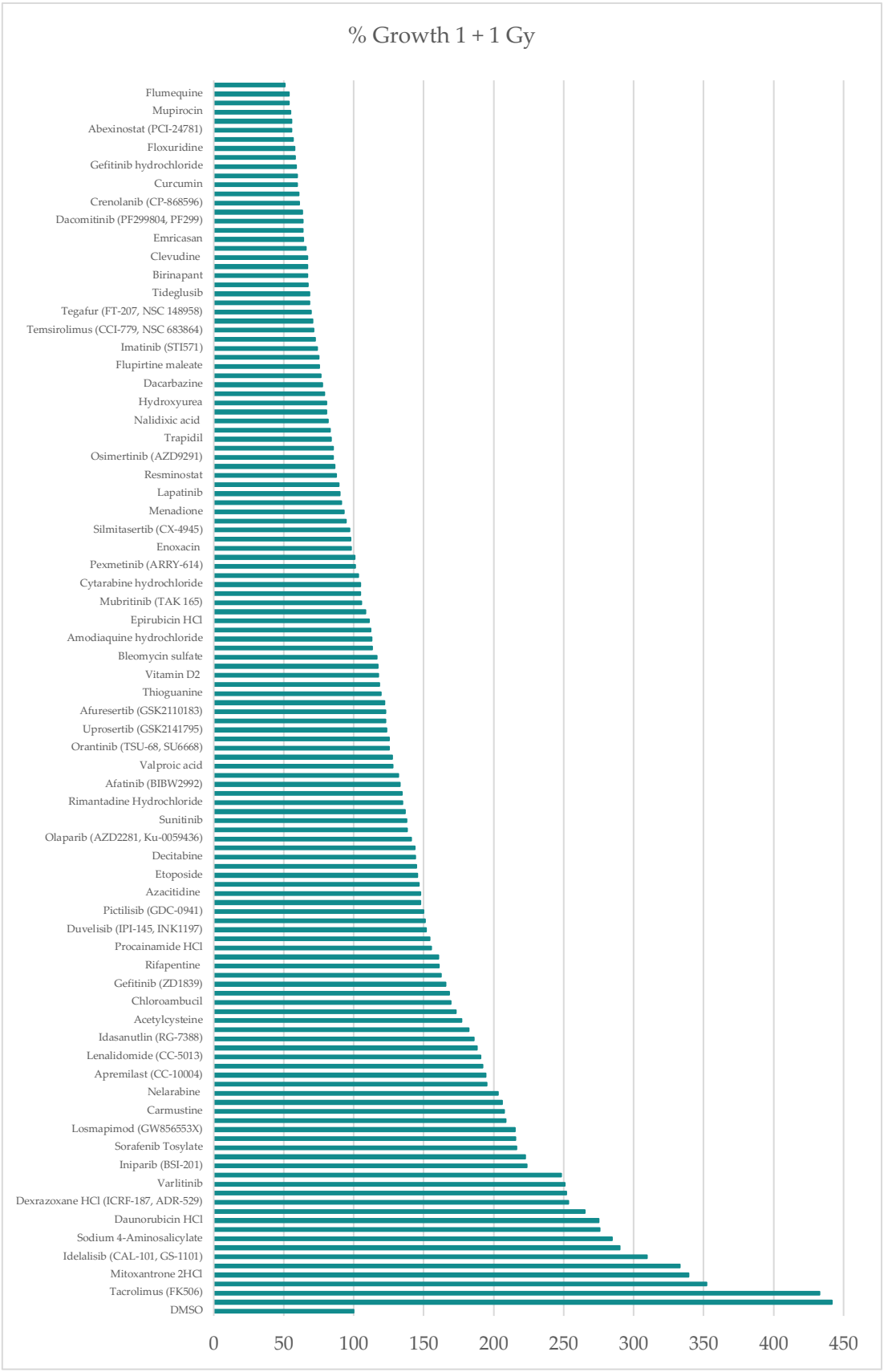

Figure 4.5: Relative percentage growth of spheroids after 1 μM inhibitor and X-ray treatment

The fold increase in spheroid growth on day 15 following 1 μM inhibitor plus 1 Gy X-rays was compared to DMSO plus 1 Gy X-rays to calculate a relative percentage growth. These graphs demonstrate the inhibitors that caused a reduction in growth of less than 50 % relative to controls.

Any drugs that reduced growth by 50 % or more at both 0 Gy and 1 Gy were removed, as the effect was likely to be due to the toxicity of the drug alone rather than a radiosensitisation effect. Using this approach, 17 candidate drugs (table 4.1) were identified as being potential radiosensitisers, the results of which are described in more detail below.

Table 4.1: Radiosensitisation candidates identified in the initial drug screen

Catalog No.	Drug Name	Target	Category
S5733	Stearic Acid	NF-kB	Cell Growth and Survival
S1470	Orantinib (TSU-68, SU6668)	PDGFR	
S8034	Apremilast (CC-10004)	TNF-alpha, PDE	
S1122	Mocetinostat (MGCD0103)	HDAC	Chromatin Organisation
S1515	Pracinostat (SB939)	HDAC	
S2693	Resminostat	HDAC	
S2922	Icotinib	EGFR	Cell Signalling
S7284	Rociletinib (CO-1686, AVL-301)	EGFR	
S4667	Lidocaine Hydrochloride	EGFR	
S1194	CUDC-101	EGFR, HDAC, HER2	
S1011	Afatinib (BIBW2992)	EGFR, HER2	
S1342	Genistein	EGFR, Topoisomerase	Cell Signalling/Cell Cycle Regulation
S1222	Dexrazoxane HCl (ICRF-187, ADR-529)	Topoisomerase	Cell Cycle Regulation
S2492	Novobiocin Sodium	Topoisomerase	
S1756	Enoxacin	Topoisomerase	
S4227	Fidaxomicin	DNA/RNA Synthesis	DNA/RNA Synthesis
S4297	Mupirocin	DNA/RNA Synthesis	

From the 183 drugs tested for radiosensitising ability, 17 were identified as potential radiosensitisers and taken forward for further validation. These covered a variety of cellular targets, plus included drugs from all five categories that were covered in the initial drug screen.

Table 4.2: Percentage growth of candidate drugs

Category	Drug Name	Percentage Growth			
		0.03 μM	0.03 μM + 1 Gy	1 μM	1 μM + 1 Gy
Cell growth and survival	Stearic Acid	106.081866	215.8819824	232.2555	**40.512462**
	Orantinib	70.61649338	**44.93342914**	65.334783	125.32001
	Apremilast	134.0293612	**48.15604618**	136.92029	194.19019
Chromatin organisation	Mocetinostat	98.77182742	63.46417747	299.49182	**35.792426**
	Pracinostat	245.8835247	204.8096028	212.9548	**45.873678**
	Resminostat	246.3650658	**36.75511044**	142.39668	87.559069
Cell signalling	Icotinib	82.91699713	**42.56494135**	125.50851	85.099391
	Rociletinib	86.19368281	98.39491705	72.796624	**24.628714**
	Lidocaine HCl	163.7614235	**17.63874013**	194.40902	63.20108
	CUDC-101	214.6416754	87.22260787	115.45913	**33.022632**
	Afatinib	411.1797484	**29.06320977**	200.16205	132.82327
	Genistein	56.52849158	52.10648951	60.327424	**36.700763**
Cell cycle regulation	Dexrazoxane HCl	268.2817205	**44.83681495**	262.29589	253.3539
	Novobiocin Sodium	192.4491895	**45.13819166**	130.13689	195.09392
	Enoxacin	84.39105103	**29.38024569**	68.038766	97.947437
DNA/RNA synthesis	Fidaxomicin	137.271577	149.1467641	105.46837	**27.791293**
	Mupirocin	116.6723565	**43.32407806**	96.531869	54.689534

Percentage growth was calculated by comparing spheroid volume on day 15 to spheroid volume on day 3. Any drugs causing a percentage growth lower than 50 % only when combined with 1 Gy X-rays (**highlighted**) were identified as potential radiosensitisers.

4.3.1. Cell Growth and Survival Candidates

It is well understood that a balance between cell death and survival is crucial, and that many cancer cells exhibit anti-apoptotic signalling to resist cell death. Thus, it makes sense that drugs impacting the function of vital proteins related to the processes of cell growth, survival and apoptosis could contribute to an increase in cancer cell death and cellular radiosensitisation. Three of the candidate drugs identified in the screen targeted proteins involved in regulating cell growth and survival: the NF-kB inhibitor stearic acid, the PDGFR inhibitor orantinib, and the TNF-alpha inhibitor apremilast.

Stearic acid as a single-agent therapy (at 0.03 μM) did not cause a decrease in spheroid growth, as this was comparable to the DMSO control over the 15 days post-seeding, with only a very minor percentage increase in growth of 106 % on day 15. Meanwhile, 1 μM stearic acid appeared to increase spheroid growth quite significantly at each time point, causing an increased percentage growth of 232 % compared to DMSO controls on day 15. Interestingly, 0.03 μM plus 1 Gy X-rays was observed to slightly promote spheroid growth between days 12 and 15 post-seeding compared to the DMSO + 1 Gy controls, and these spheroids had a percentage growth of 215 % compared to controls on day 15. On the other hand, 1 μM stearic acid combined with 1 Gy X-rays decreased spheroid growth, particularly on days 12 and 15 post-seeding. It is important to note here that, upon observation of the spheroid on day 15, there did not appear to be a marked reduction in growth compared to other conditions. However, the spheroid was larger on day 3 in comparison to those following other treatments, thus the overall growth was reduced and by day 15 this spheroid had a percentage growth of 40 % compared to irradiated controls (figure 4.5).

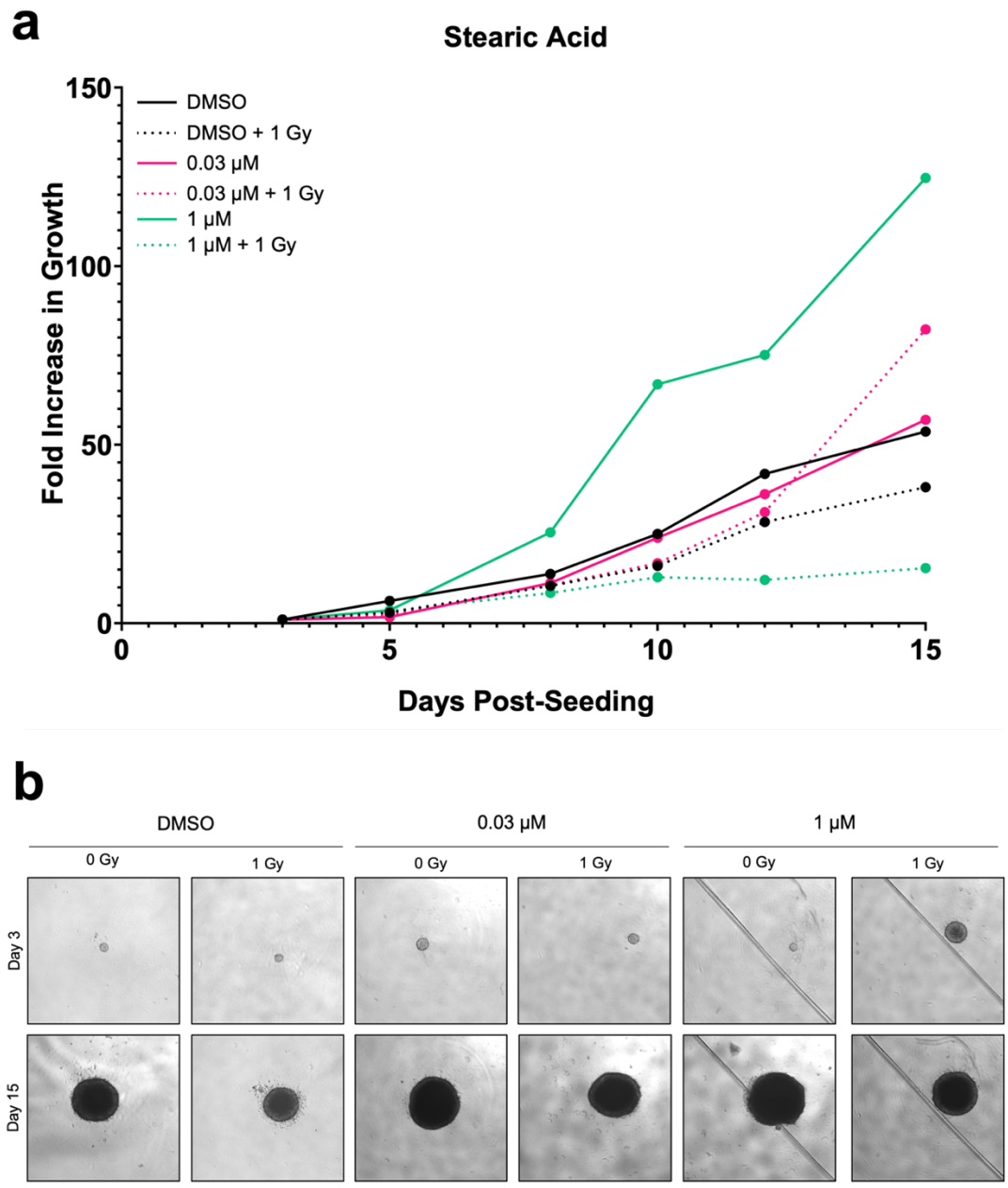

Figure 4.6: Spheroid growth following stearic acid treatment

a) FaDu cells were seeded into ULA plates and incubated for 24 hours to allow spheroid formation. Stearic acid was then added at either 0.03 µM and 1 µM. 24 hours after inhibitor treatment, spheroids were irradiated with 1 Gy or left unirradiated. Images of the spheroids were captured on days 3, 5, 8, 10, 12 and 15 post-seeding, which were used to measure the fold increase in growth over time. b) Images of spheroids on days 3 and 15 post-seeding after each different treatment condition.

The PDGFR inhibitor orantinib appeared to have no significant impact on spheroid growth at either 0.03 μM or 1 μM when used as a single-agent treatment, although between days 12 and 15 post-seeding there did appear to be some variation. On day 15, orantinib alone caused a reduced percentage growth of 70 % and 65 % at concentrations of 0.03 μM and 1 μM respectively. When combined with 1 Gy X-rays, 0.03 μM orantinib appeared to successfully radiosensitise spheroids, particularly after day 10. The overall percentage growth of spheroids treated with 0.03 μM orantinib plus X-rays was 44 %, compared to X-rays alone. Interestingly, the high concentration of 1 μM did not appear to reduce spheroid growth when combined with X-rays. In fact, this treatment actually increased spheroid growth at all time points, with an overall percentage growth of 125 % compared to spheroids treated with X-rays (figure 4.6).

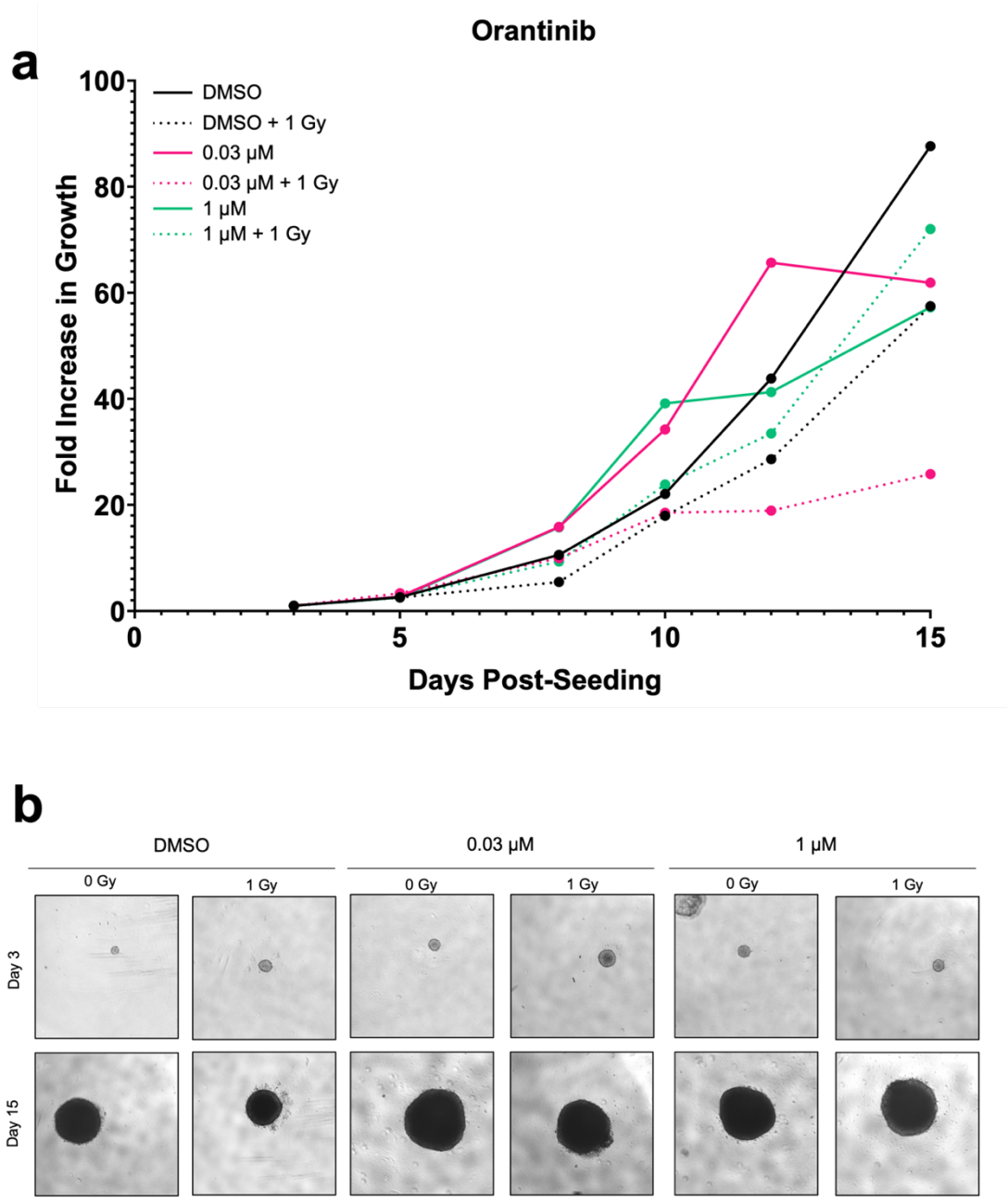

Figure 4.7: Spheroid growth following orantinib treatment

a) FaDu cells were seeded into ULA plates and incubated for 24 hours to allow spheroid formation. Orantinib was subsequently added at a concentration of either 0.03 μM and 1 μM. 24 hours after inhibitor treatment, spheroids were irradiated with 1 Gy or left unirradiated. Images of the spheroids were captured on days 3, 5, 8, 10, 12 and 15 post-seeding, which were used to measure the fold increase in growth over time. b) Images of spheroids on days 3 and 15 post-seeding after each different treatment condition.

Apremilast as a single agent treatment appeared to significantly promote spheroid growth. At a concentration of 0.03 μM, the drug consistently enhanced growth at all time points post-seeding, whereas 1 μM had an observable effect only after 8 days post-seeding. The overall growth of apremilast-treated spheroids relative to the DMSO controls was 134 % and 136 % following 0.03 μM and 1 μM treatment, respectively. 0.03 μM apremilast in combination with 1 Gy radiation suppressed growth between days 12 and 15 post-seeding, resulting in an overall growth of only 48 % compared to treatment with X-rays alone on day 15. As mentioned earlier, it is important to observe here that the spheroid treated with 0.03 μM apremilast plus X-rays was slightly larger on day 3 compared to the other treatments, so while the spheroids appear to be of similar sizes on day 15, the overall growth of this particular spheroid was notably less. On the other hand, 1 μM plus X-rays seemed to have little impact on spheroid growth initially, but from 10 days post-seeding appeared to significantly enhance growth, with an overall increase of 194 % compared to irradiated spheroids on day 15 (figure 4.7).

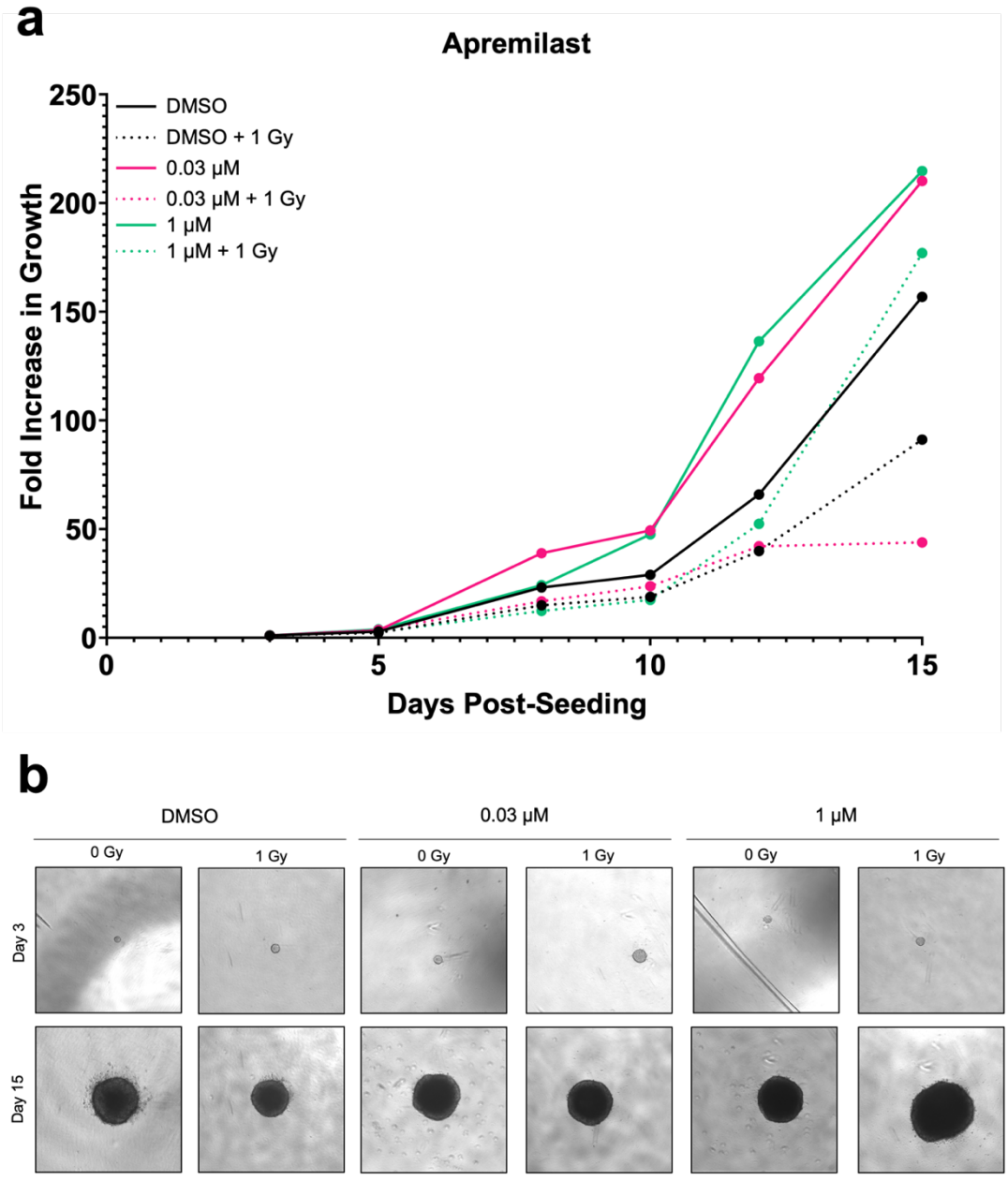

Figure 4.8: Spheroid growth following apremilast treatment

a) FaDu cells were seeded into ULA plates and incubated for 24 hours to allow spheroid formation. Apremilast was then added at either 0.03 µM and 1 µM, and 24 hours after inhibitor treatment, spheroids were irradiated with 1 Gy or left unirradiated. Images of the spheroids were captured on days 3, 5, 8, 10, 12 and 15 post-seeding, which were used to measure the fold increase in growth over time. b) Images of spheroids on days 3 and 15 post-seeding after each different treatment condition.

4.3.2. Chromatin Organisation Candidates

The addition of PTMs to histone subunits alters the structure of chromatin, influencing gene expression and allowing the cell to perform DNA-dependent processes, such as DNA damage repair. Due to the involvement of histone modifiers in the regulation of chromatin, inhibitors of these proteins can influence the response of cancer cells to radiotherapy and thus have the potential to increase cellular radiosensitivity. Four drugs with the same targets, HDACs, were identified as candidate radiosensitisers in this screen. These were CUDC-101, mocetinostat, pracinostat, and resminostat.

CUDC-101 is a multi-targeting inhibitor of HDACs, EGFR, and HER2. In the absence of radiation, 0.03 μM CUDC-101 treatment increased spheroid growth at all time points, resulting in a growth of 214 % relative to the DMSO controls. Until day 10 post-seeding, 1 μM treatment seemed to be comparable to controls, then there was a significant increase in growth at day 12, followed by a drop to a growth level 115 % relative to the DMSO-treated controls on day 15. The combination treatment of 0.03 μM CUDC-101 plus 1 Gy X-rays seemed to mildly promote growth until 12 days post-seeding, but then between days 12 and 15 there was a slight reduction in spheroid growth, but only bringing the overall growth down to 87 % relative to the irradiated spheroids. On the other hand, 1 μM CUDC-101 combined with X-rays had no impact on spheroid growth in the first 8 days post-seeding, but on days 12-15 the fold increase in growth reduced. As seen in other spheroids in this drug screen, the spheroid on day 3 following 1 μM CUDC-101 plus X-rays was observably larger than the other spheroids at this time point. While the spheroids on day 15 were a similar size, the overall growth of this spheroid was strikingly reduced to 33 % relative to spheroids treated with X-rays alone due to its larger starting volume (figure 4.8).

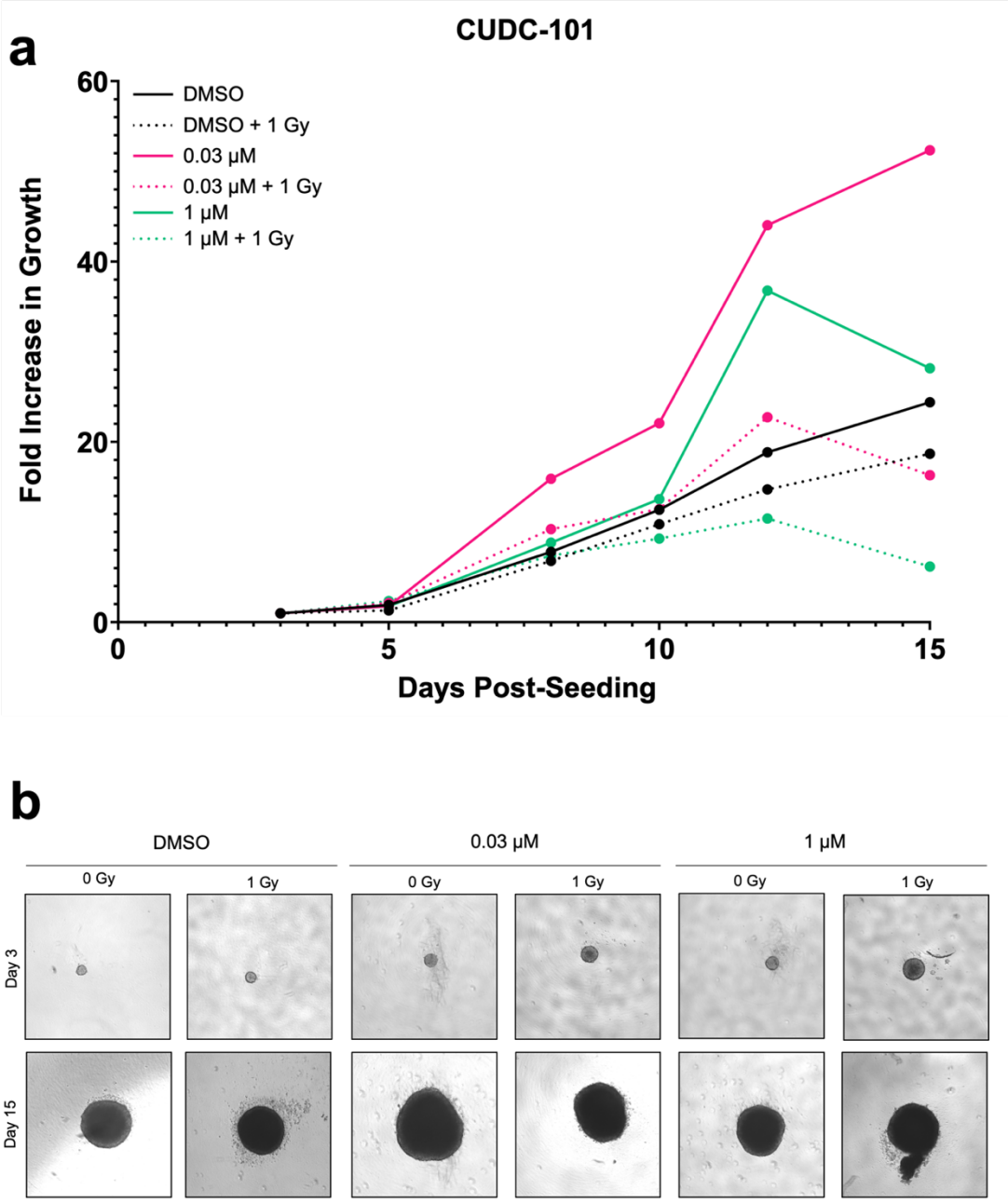

Figure 4.9: Spheroid growth following CUDC-101 treatment

a) FaDu cells were seeded into ULA plates and incubated for 24 hours to allow spheroid formation, and subsequently CUDC-101 was added at a concentration of either 0.03 µM and 1 µM. 24 hours after inhibitor treatment, spheroids were irradiated with 1 Gy or left unirradiated. Images of the spheroids were captured on days 3, 5, 8, 10, 12 and 15 post-seeding, which were used to measure the fold increase in growth over time. b) Images of spheroids on days 3 and 15 post-seeding after each different treatment condition.

Mocetinostat is a potent inhibitor of class I HDACs. As a single-agent treatment, mocetinostat did not reduce spheroid growth. In fact, while the rate of growth for spheroids treated with either concentration of mocetinostat was relatively comparable to the DMSO controls up to 8 days post-seeding, on days 10-12 there was a noticeable increase in spheroid growth using both concentrations of drug, particularly with 1 μM mocetinostat. By day 15 post-seeding, the overall increase in size of spheroids treated with mocetinostat alone was 98 % and 299 % relative to controls after either 0.03 μM or 1 μM treatment, respectively. In contrast, the combination of mocetinostat and 1 Gy X-rays appeared to be effective in reducing overall spheroid growth. 0.03 μM plus IR resulted in comparable growth to irradiated controls up to 10 days post-seeding, after which there was a size decrease, particularly between days 10 and 12. After day 15, the overall growth was 63 % relative to the spheroids treated with X-rays alone. 1 μM mocetinostat plus X-rays, on the other hand, consistently resulted in a lower rate of growth compared to irradiated spheroids across all time points, particularly noticeable on days 12 and 15 post-seeding. In fact, 1 μM mocetinostat combined with 1 Gy X-rays led to a spheroid growth of only 35 % relative to irradiated DMSO controls (figure 4.9).

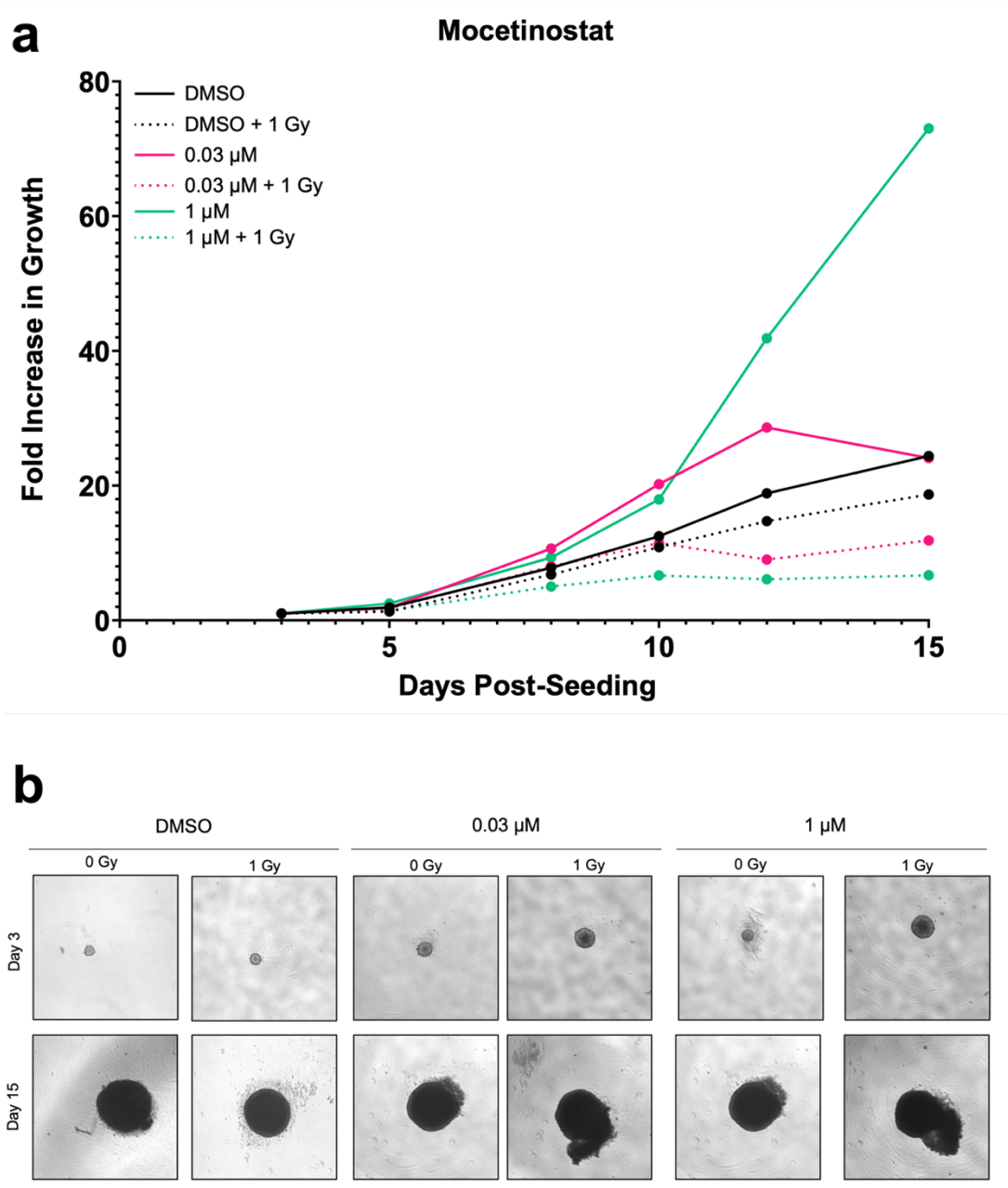

Figure 4.10: Spheroid growth following mocetinostat treatment

a) FaDu cells were seeded into ULA plates and incubated for 24 hours to allow spheroid formation. Following this, mocetinostat was then added at either 0.03 µM and 1 µM. 24 hours after inhibitor treatment, spheroids were irradiated with 1 Gy or left unirradiated. Images of the spheroids were captured on days 3, 5, 8, 10, 12 and 15 post-seeding, which were used to measure the fold increase in growth over time. b) Images of spheroids on days 3 and 15 post-seeding after each different treatment condition.

Pracinostat is a selective inhibitor of class I, II and IV HDACs. Similar to other HDAC inhibitors, pracinostat appeared to markedly enhance spheroid growth in the absence of radiation. Both 0.03 μM and 1 μM treatments caused an observable increase in growth compared to DMSO controls and followed a similar trend to one another. 0.03 μM treatment seemed to enhance growth slightly more than 1 μM treatment, and by day 15, the percentage growth relative to the controls was 245 % and 212 % for 0.03 μM and 1 μM, respectively. Intriguingly, 0.03 μM pracinostat also displayed enhanced spheroid growth when combined with IR, compared to X-rays alone. Up until day 8 post-seeding, growth rates of spheroids treated with 0.03 μM pracinostat plus 1 Gy X-rays were comparable to irradiated controls, however between days 8 and 15 post-seeding, the inhibitor-treated spheroids had a noticeably enhanced growth rate compared to controls. At day 15, the combination of 0.03 μM pracinostat and 1 Gy X-rays resulted in a 204 % increase in spheroid growth relative to DMSO plus X-rays. In contrast, 1 μM pracinostat appeared to be effectively radiosensitising the spheroids. The growth rates between the combination treatment and the control (X-rays only) spheroids were comparable up to 8 days post-seeding., However from day 10 onwards the rate of spheroid growth following 1 μM pracinostat treatment plus IR was noticeably lower than spheroids irradiated only. By 15 days post-seeding, the overall growth of spheroids treated with 1 μM pracinostat plus 1 Gy X-rays was 45 % relative to irradiated controls (figure 4.10).

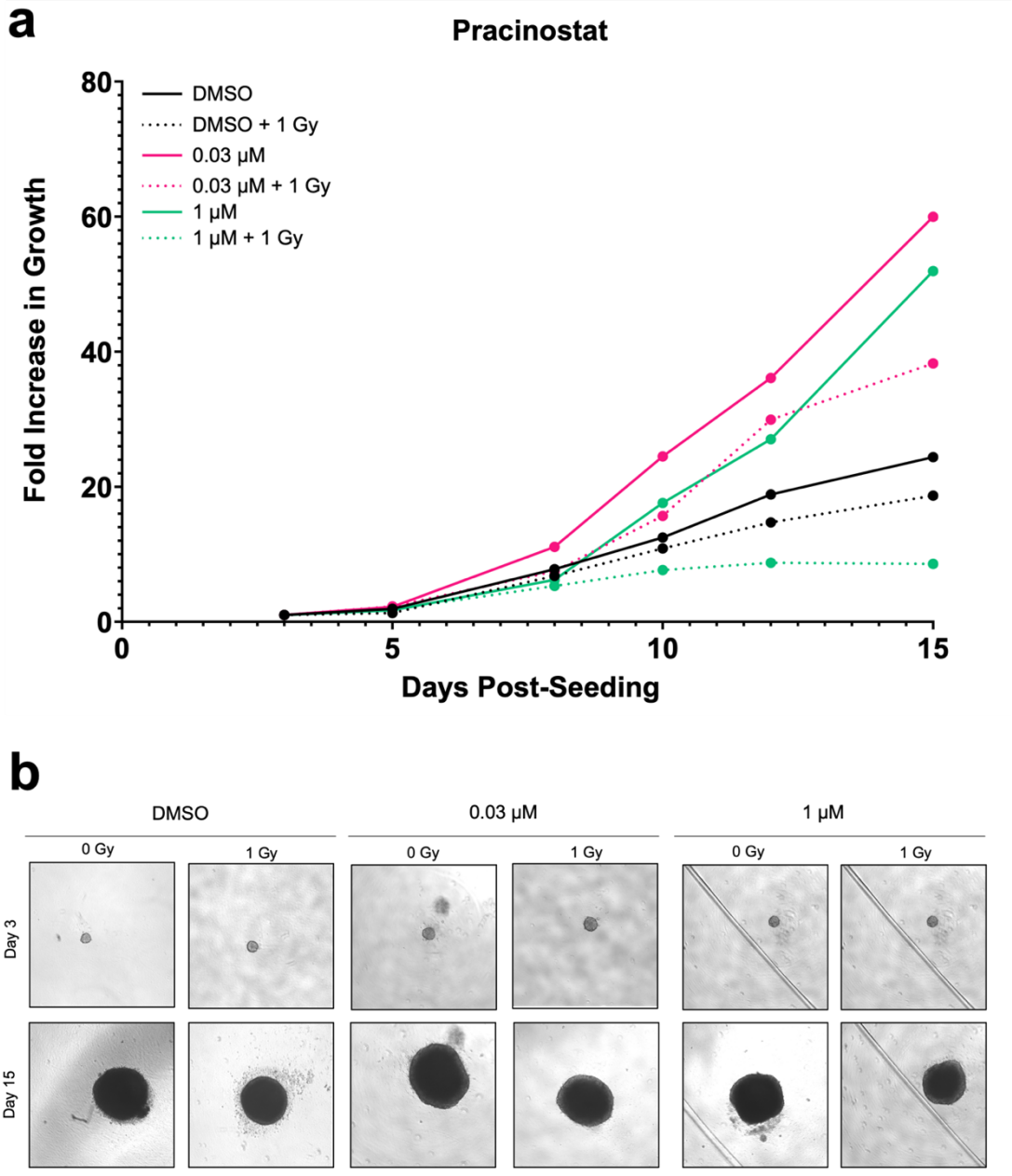

Figure 4.11: Spheroid growth following pracinostat treatment

a) FaDu cells were seeded into ULA plates and incubated for 24 hours to allow spheroid formation. Pracinostat was then added at either 0.03 μM and 1 μM. 24 hours after inhibitor treatment, spheroids were irradiated with 1 Gy or left unirradiated. Images of the spheroids were captured on days 3, 5, 8, 10, 12 and 15 post-seeding, which were used to measure the fold increase in growth over time. b) Images of spheroids on days 3 and 15 post-seeding after each different treatment condition.

Resminostat is a targeted inhibitor of class I, IIb and IV HDACs. In a consistent manner with the other HDACi in this screen, resminostat as a single agent treatment did not reduce spheroid growth, and in fact had a significant enhancement effect across all time points. The spheroids treated with 0.03 μM resminostat demonstrated a steep increase in growth between days 10 and 12 post-seeding, and the overall spheroid growth was 246 % relative to the DMSO controls on day 15. 1 μM resminostat had less of a marked impact, however still caused an enhancement of spheroid growth, particularly between days 10 and 12 post-seeding, however this was less prominent after 0.03 μM treatment. By day 15, spheroids treated with 1 μM resminostat alone had an overall growth of 142 % relative to the DMSO controls. In contrast, 0.03 μM resminostat combined with 1 Gy X-rays caused a marked decrease in spheroid growth relative to irradiated controls. The growth between the two conditions was comparable up to day 8 post-seeding, after which there was an observable decrease in size of the inhibitor-treated spheroids. This was most noticeable on day 15, when the growth of treated spheroids was only 36 % relative to the irradiated controls. Once again, it is key to note here that the spheroid was larger on day 3 than the spheroids treated under other conditions, so while the spheroid may not look drastically smaller on day 15, the overall growth was less. On the other hand, 1 μM interestingly did not have any significant impact on growth when combined with radiation. In fact, the growth rate was comparable to irradiated controls throughout the experiment, with a slight decrease on day 15 to 87 % growth relative to the controls (figure 4.11).

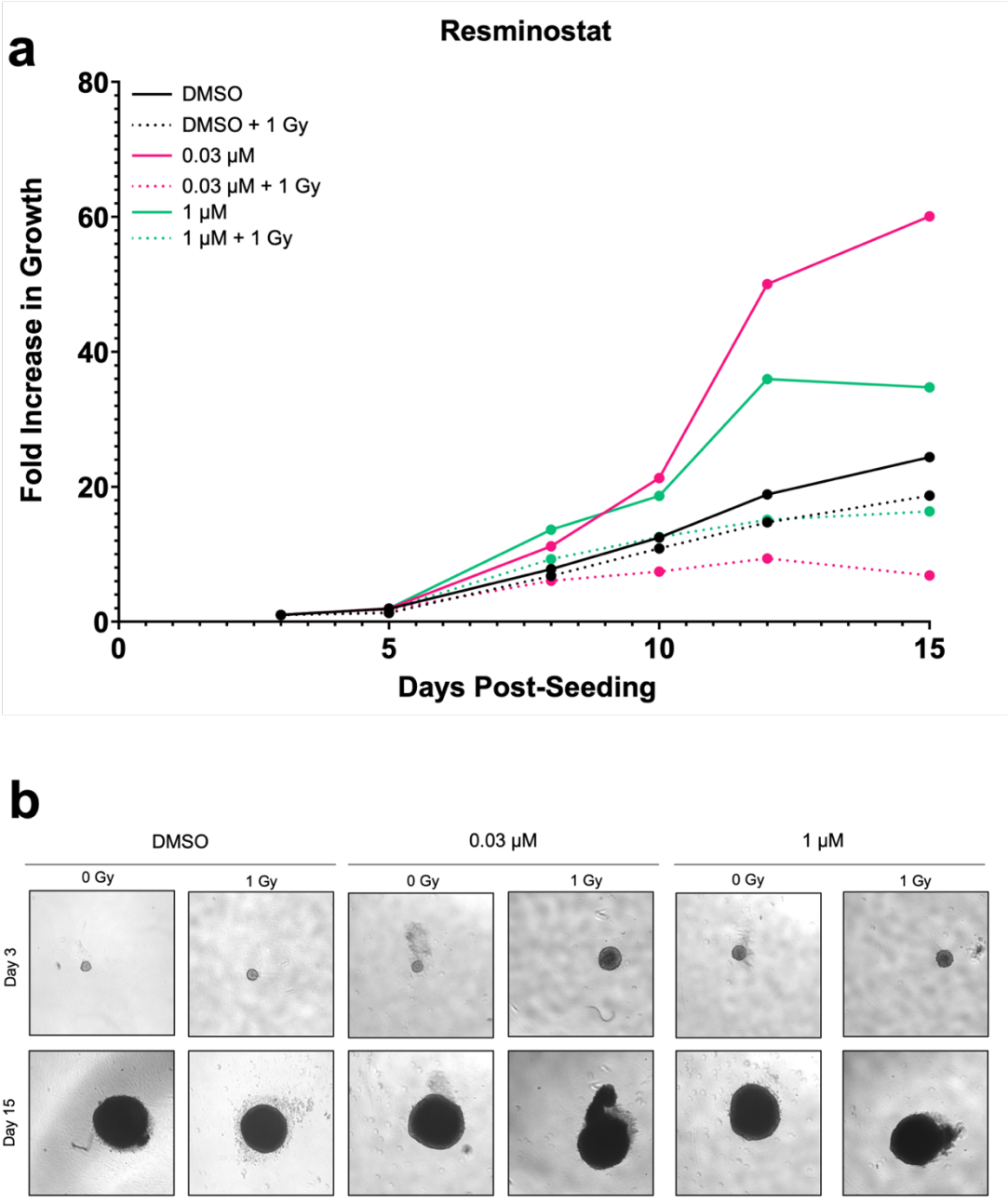

Figure 4.12: Spheroid growth following resminostat treatment

a) FaDu cells were seeded into ULA plates and incubated for 24 hours to allow spheroid formation. After this time, resminostat was added at a concentration of either 0.03 μM and 1 μM. 24 hours after inhibitor treatment, spheroids were irradiated with 1 Gy or left unirradiated. Images of the spheroids were captured on days 3, 5, 8, 10, 12 and 15 post-seeding, which were used to measure the fold increase in growth over time. b) Images of spheroids on days 3 and 15 post-seeding after each different treatment condition.

4.3.3. Cell Signalling Candidates

Signalling cascades frequently display aberrant activity in human cancers and are involved in almost all cellular functions, including proliferation, growth, and survival. Incorrect functioning of proteins at any level of a signalling cascade can have catastrophic effects, such as the induction and progression of tumourigenesis. Six of the candidates identified in this screen specifically inhibit EGFR, the transmembrane receptor capable of initiating multiple signalling cascades. These are icotinib, rociletinib, lidocaine HCl, CUDC-101 (see section 4.2.2), afatinib and genistein.

In the absence of IR, icotinib enhanced spheroid growth. At 0.03 μM, spheroids treated with icotinib had a markedly higher increase in growth compared to DMSO controls from days 8 – 12 post-seeding. However. between days 12 and 15, spheroid volume dropped dramatically to an overall fold increase lower than the controls, with a percentage growth of 82 %. On the other hand, spheroids treated with 1 μM icotinib displayed growth rates consistently higher than the DMSO controls at all time points. This was most observable on day 12 post-seeding, following a dramatic increase from day 10. By day 15, spheroids treated with 1 μM icotinib had a percentage growth of 125 % relative to the DMSO controls. An interesting observation was seen when icotinib was combined with 1 Gy X-rays. 0.03 μM plus IR seemed to be slightly enhancing spheroid growth in comparison to the irradiated controls up until day 12 post-seeding, after which there was a slight decline in growth and on day 15 the combination treatment resulted in a growth of 42 % relative to irradiated controls. 1 μM icotinib caused growth rates comparable to 0.03 μM icotinib with X-rays up to day 10 post-seeding. However, between days 10 and 12, spheroids treated with 1 μM icotinib plus X-rays had a noticeable increase in growth, followed by a growth plateau. Therefore, on day 15 post-seeding, the

irradiated 1 µM-treated spheroids ended with an overall growth of 85 % relative to irradiated only controls (figure 4.12).

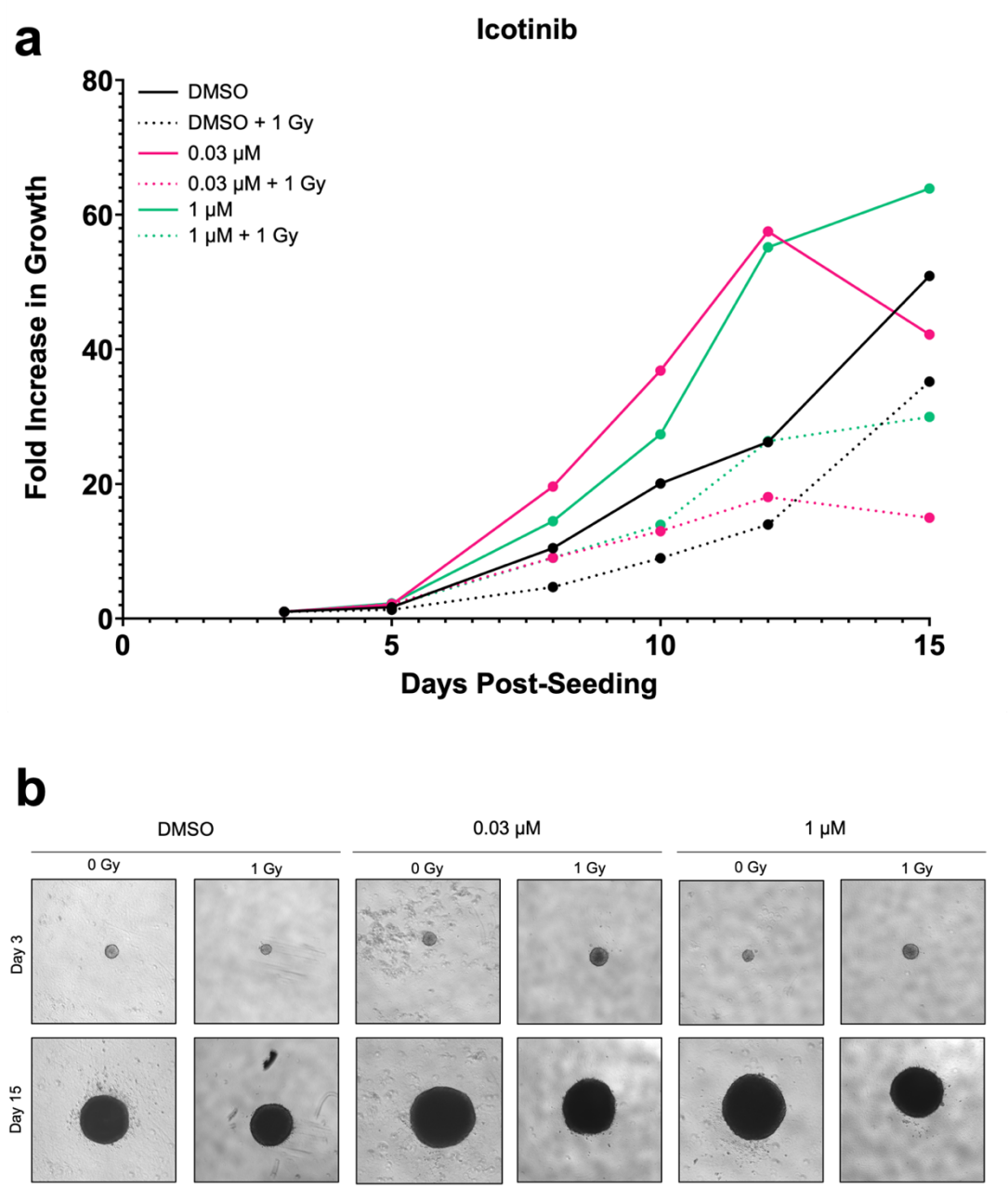

Figure 4.13: Spheroid growth following icotinib treatment

a) FaDu cells were seeded into ULA plates and incubated for 24 hours to allow spheroid formation. Icotinib was then added at either 0.03 µM and 1 µM. 24 hours after inhibitor treatment, spheroids were irradiated with 1 Gy or left unirradiated. Images of the spheroids were captured on days 3, 5, 8, 10, 12 and 15 post-seeding, which were used to measure the fold increase in growth over time. b) Images of spheroids on days 3 and 15 post-seeding after each different treatment condition.

In a contrast to many other drugs in this screen targeting EGFR, rociletinib caused a reduction in growth as a single agent treatment, particularly at 1 μM. 0.03 μM-treated spheroids actually displayed growth comparable to the DMSO controls up until day 10 post-seeding, but there were some minor differences on days 12 and 15, and by the latter of which the fold increase in growth had dropped to 86 % relative to the DMSO controls. 1 μM rociletinib, on the other hand, had a more observable negative effect on spheroid growth. While growth rates were comparable to the DMSO controls up to day 10 post-seeding, the drug significantly slowed growth between days 12 and 15. The overall percentage growth after 15 days was 72 % compared to the DMSO controls. When combined with 1 Gy X-rays, 0.03 μM rociletinib initially appeared to enhance growth in comparison to the irradiated controls at most time points between days 8-12. However, by day 15, the overall increase in growth was almost identical comparing both conditions, with a relative growth of 98 % for the spheroids treated with 0.03 μM plus IR. The combination of 1 μM rociletinib with X-rays appeared to have a similar effect as the lower drug combination treatment up until day 8 post-seeding. However, the rate of spheroid growth then slowed between days 8 and 12, and further dropped on day 15. This was significantly lower than the fold increase in growth of the irradiated controls, with the treatment of 1 μM rociletinib with X-rays only growing 24 % relative to these (figure 4.13).

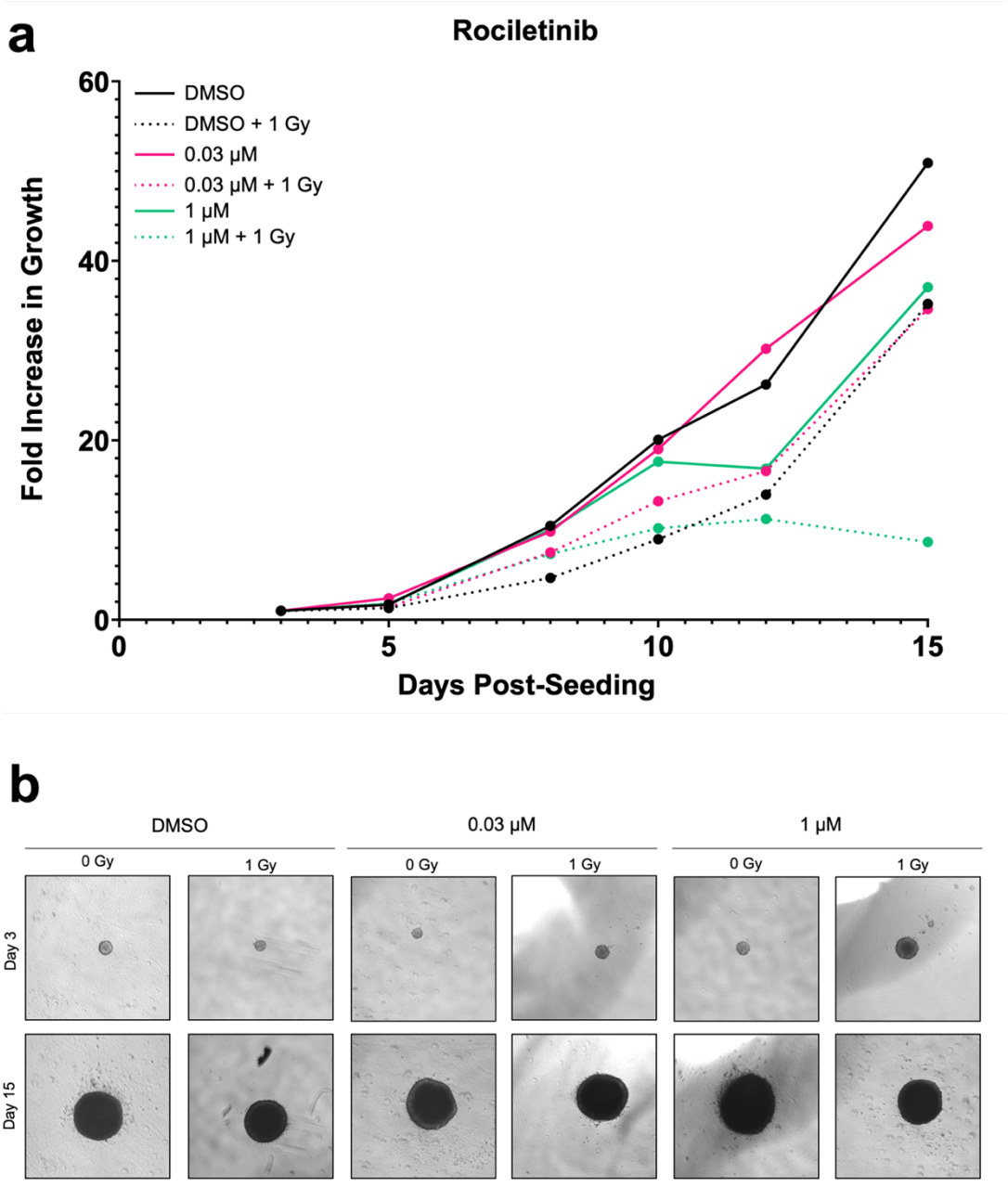

Figure 4.14: Spheroid growth following rociletinib treatment

a) FaDu cells were seeded into ULA plates and incubated for 24 hours to allow spheroid formation. After this time, rociletinib was added at either 0.03 µM and 1 µM. 24 hours after inhibitor treatment, spheroids were irradiated with 1 Gy or left unirradiated. Images of the spheroids were captured on days 3, 5, 8, 10, 12 and 15 post-seeding, which were used to measure the fold increase in growth over time. b) Images of spheroids on days 3 and 15 post-seeding after each different treatment condition.

Lidocaine HCl as a single agent treatment caused remarkable increases in overall spheroid growth. 0.03 μM Lidocaine HCl was comparable to the DMSO controls until 8 days post-seeding, however between days 8 and 12 there were steep increases in the fold increase in spheroid growth, to a significantly higher level than controls. There was a slight decrease between days 12 and 15, however the overall growth on day 15 following 0.03 μM lidocaine HCl treatment was still 163 % relative to DMSO controls. Similarly, 1 μM lidocaine HCl treatment also resulted in a dramatically higher rate of spheroid growth than controls. Between days 5 and 12, there was a significantly higher increase in growth of the spheroids compared to the DMSO controls. At 15 days post-seeding, spheroids treated with 1 μM lidocaine HCl had an overall growth of 194 % relative to the controls. In contrast, a reduction in spheroid growth was consistently observed upon combined treatment with lidocaine HCl and 1 Gy X-rays, compared to irradiation alone. 0.03 μM inhibitor plus IR had relatively little effect on spheroid growth until day 8, after which the increase in growth was noticeably lower than the irradiated controls. As a consequence, the overall increase in growth after this combined treatment was only 17 % relative to the irradiated controls. Interestingly, the effect observed following 1 μM lidocaine HCl plus IR treatment was not as drastic as the lower concentration. Up until day 12 post-seeding, the growth rate of spheroids treated with DMSO plus X-rays and spheroids treated with 1 μM lidocaine HCl plus X-rays was comparable at all time points. However, between days 12 and 15, there was a noticeable decrease in the inhibitor-treated spheroids, and their overall growth was 63 % compared to the irradiated controls (figure 4.14).

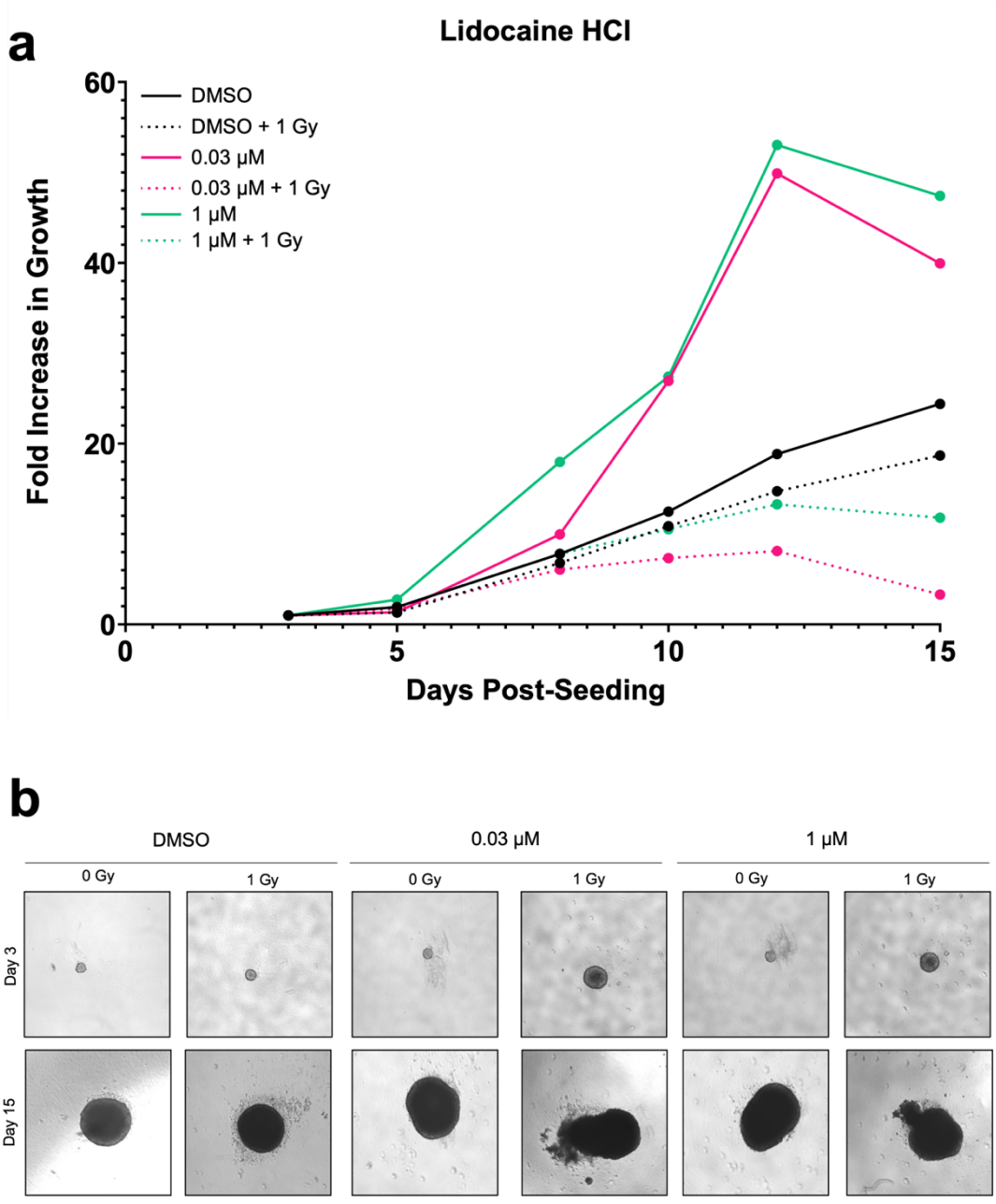

Figure 4.15: Spheroid growth following lidocaine HCl treatment

a) FaDu cells were seeded into ULA plates and incubated for 24 hours to allow spheroid formation. At this point lidocaine HCl was added at a concentration of either 0.03 µM and 1 µM. 24 hours after inhibitor treatment, spheroids were irradiated with 1 Gy or left unirradiated. Images of the spheroids were captured on days 3, 5, 8, 10, 12 and 15 post-seeding, which were used to measure the fold increase in growth over time. b) Images of spheroids on days 3 and 15 post-seeding after each different treatment condition.

Following the pattern of the other EGFR inhibitors, afatinib significantly enhanced spheroid growth when given as a single treatment. After 5 days post-seeding, spheroids treated with 0.03 μM afatinib displayed an exponential increase in growth rate that was consistently higher than spheroids treated with DMSO. In fact, by day 15, afatinib-treated spheroids displayed growth to a relative size of 411 % compared to the controls. 1 μM inhibitor also enhanced growth, but to a lesser extent. The fold increase in growth of spheroids treated with 1 μM afatinib was comparable to controls until day 8 post-seeding, after which it increased slowly until day 15. Overall, the spheroids grew 200 % relative to the DMSO controls. In contrast, 0.03 μM afatinib combined with 1 Gy X-rays caused a significant impairment in spheroid growth from day 8 post-seeding onwards. There was very little change in spheroid size from days 8 to 15, and the overall growth was only 29 % relative to the irradiated controls. 1 μM afatinib, meanwhile, was comparable to the irradiated controls at most time points when combined with IR. On day 10 post-seeding, there was a slight observable reduction in spheroid growth compared to controls, however on days 12 and 15 the growth rate actually increased compared to the irradiated DMSO controls. In fact, overall, the growth of spheroids treated with 1 μM afatinib with X-rays was 132 % relative to the spheroids treated with DMSO plus IR (figure 4.15).

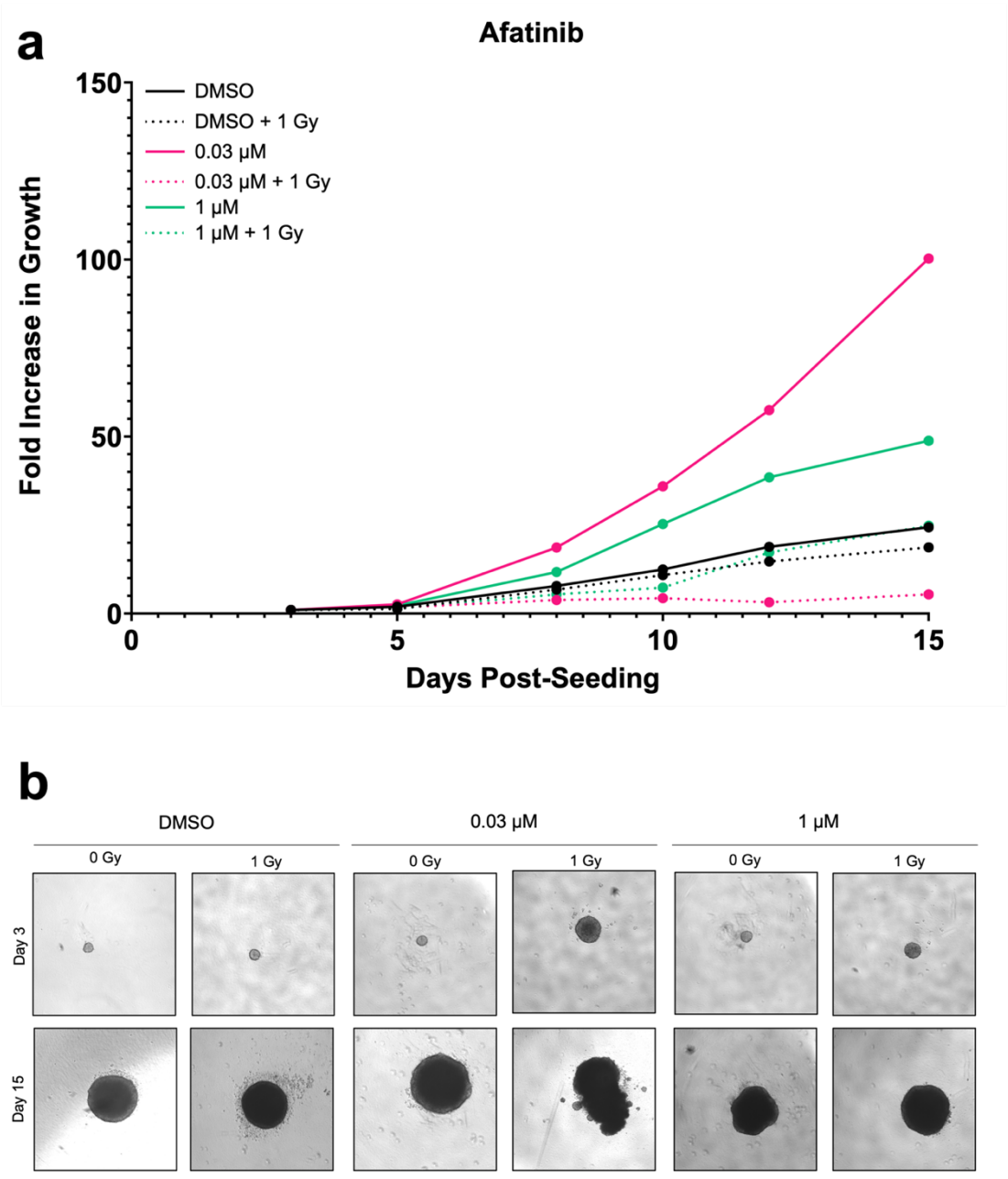

Figure 4.16: Spheroid growth following afatinib treatment

a) FaDu cells were seeded into ULA plates and incubated for 24 hours to allow spheroid formation, and afatinib was subsequently added at concentrations of either 0.03 μM and 1 μM. 24 hours after inhibitor treatment, spheroids were irradiated with 1 Gy or left unirradiated. Images of the spheroids were captured on days 3, 5, 8, 10, 12 and 15 post-seeding, which were used to measure the fold increase in growth over time. b) Images of spheroids on days 3 and 15 post-seeding after each different treatment condition.

Genistein alone was found to reduce the fold increase in spheroid growth, but only at day 15. Both concentrations of 0.03 μM and 1 μM genistein produced comparable growth rates from days 5 to day 12 post-seeding. However, with the steep drop in spheroid growth at day 15, the relative percentages of 56 % and 60 % following 0.03 μM or 1 μM treatment respectively reflect the negative impact of the drug on spheroid growth. Growth following 0.03 μM genistein in combination with 1 Gy X-rays followed a very similar pattern to growth following treatment with the drug alone. Up until day 12 post-seeding, the growth rate of inhibitor-treated spheroids was very similar, albeit slightly higher, than the irradiated controls. However, there was a significant drop in spheroid size between days 12 and 15, and therefore the overall growth of the combination treatment was 52 % relative to the irradiated controls. On the other hand, 1 μM genistein plus 1 Gy X-rays reduced spheroid growth compared to irradiation only. Growth rates were comparable until day 8, following which the inhibitor-treated spheroids grew very little over the final course of the experiment. The overall percentage growth of these spheroids was only 36 % relative to the irradiated controls (figure 4.16).

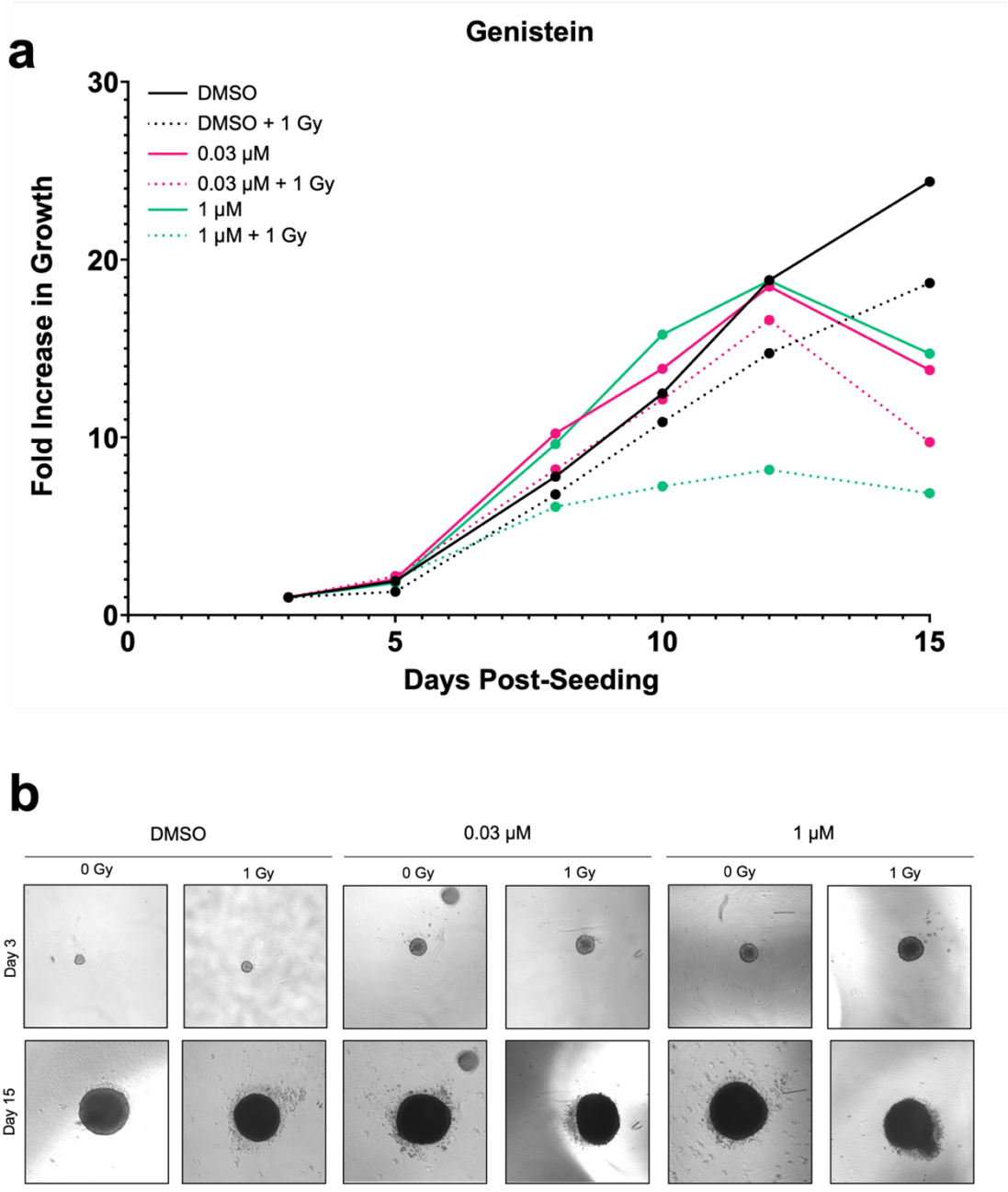

Figure 4.17: Spheroid increase following genistein treatment

a) FaDu cells were seeded into ULA plates and incubated for 24 hours to allow spheroid formation. At this point, genistein was added, using concentrations of either 0.03 µM and 1 µM. 24 hours after inhibitor treatment, spheroids were irradiated with 1 Gy or left unirradiated. Images of the spheroids were captured on days 3, 5, 8, 10, 12 and 15 post-seeding, which were used to measure the fold increase in growth over time. b) Images of spheroids on days 3 and 15 post-seeding after each different treatment condition.

4.3.4. Cell Cycle Regulation Candidates

Correct regulation of the cell cycle is vital to ensure cells remain healthy and do not contain any damage prior to cell division. There is a myriad of proteins involved in maintaining the cell cycle, and incorrect functioning of any of these proteins has the potential to disrupt the cycle and allow damaged cells to proliferate freely. Four of the candidate drugs identified in this screen inhibit topoisomerase enzymes, which are important enzymes that catalyses the unlinking of DNA strands during the S phase of the cell cycle. These specific enzymes are: genistein (see section 4.2.3), dexrazoxane HCl, novobiocin sodium, and enoxacin.

In the absence of IR, dexrazoxane HCl caused a dramatic enhancement of spheroid growth in comparison to the DMSO controls. The two drug concentrations were comparable in terms of spheroid size at most time points, and significant increases in growth compared to the DMSO controls were seen between days 5 and 15 post-seeding. On day 15, the overall growth of spheroids treated with 0.03 μM and 1 μM dexrazoxane HCl was 268 % and 262 % respectively, relative to the DMSO controls. Upon the addition of 1 Gy X-rays, 0.03 μM dexrazoxane HCl did not seem to alter the rate of spheroid growth from irradiated control levels up to 12 days post-seeding. However, between days 12 and 15, while the spheroids treated with DMSO plus IR displayed an increase in growth rate, those treated with 0.03 μM inhibitor plus IR seemed to level off, resulting in growth being only 44 % relative to the irradiated controls. On the other hand, 1 μM appeared to enhance growth when combined with X-rays. Up until day 8 post-seeding, the growth rate of the combination treatment was comparable to the irradiated controls, however, the fold increase in growth from days 10 – 15 was then consistently higher following 1 μM dexrazoxane HCl plus IR treatment. The overall growth

of spheroids with 1 µM dexrazoxane HCl and X-rays was 253 % relative to the irradiated controls (figure 4.17).

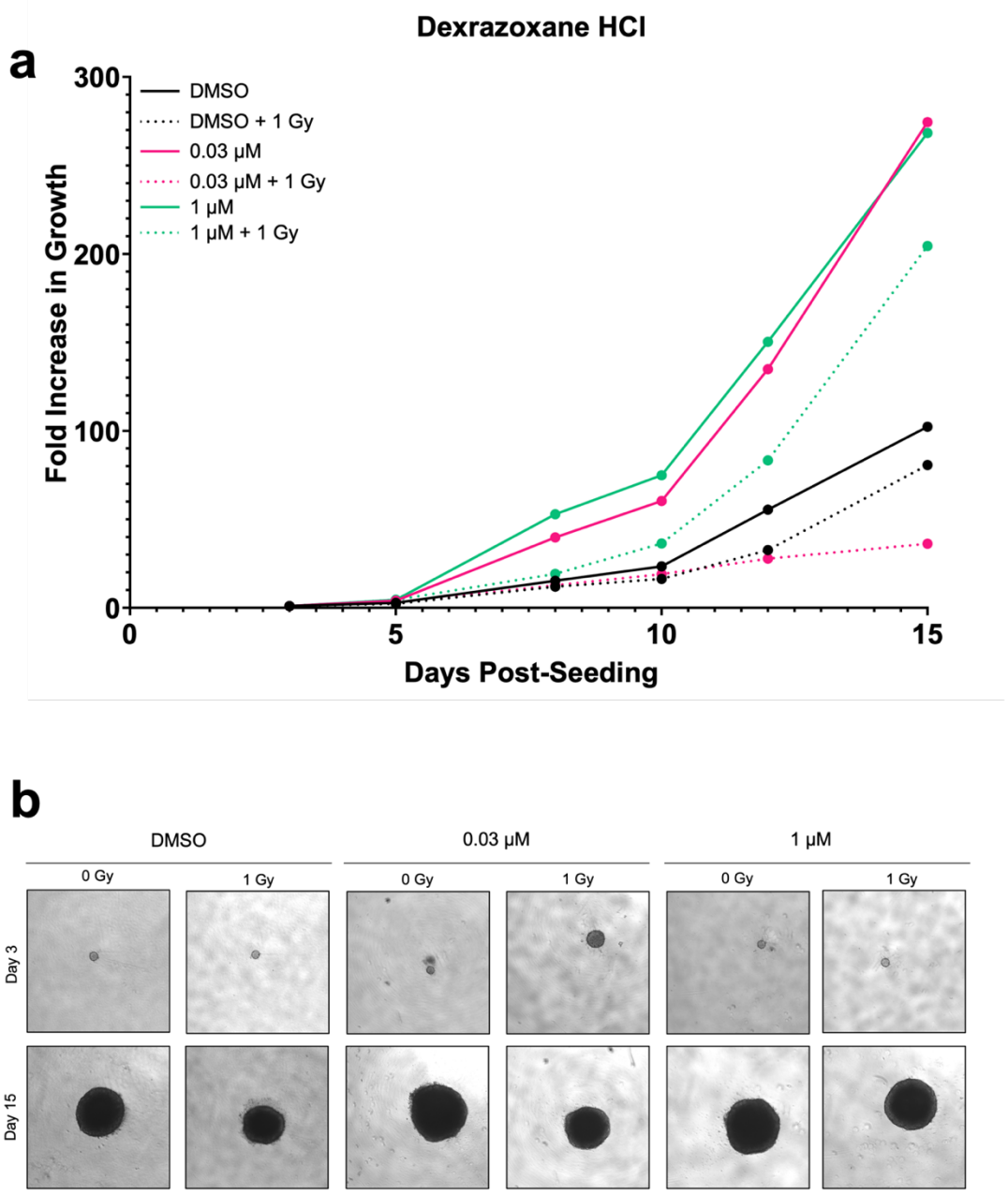

Figure 4.18: Spheroid growth following dexrazoxane HCl treatment

a) FaDu cells were seeded into ULA plates and incubated for 24 hours to allow spheroid formation. Dexrazoxane HCl was then added at either 0.03 µM and 1 µM. 24 hours after inhibitor treatment, spheroids were irradiated with 1 Gy or left unirradiated. Images of the spheroids were captured on days 3, 5, 8, 10, 12 and 15 post-seeding, which were used to measure the fold increase in growth over time. b) Images of spheroids on days 3 and 15 post-seeding after each different treatment condition.

In a similar manner to dexrazoxane HCl, novobiocin sodium enhanced growth when given as a single agent treatment. 0.03 μM treatment resulted in a higher growth rate from day 5 onwards, with a slow increase in spheroid size between days 5 and 10 post-seeding, followed by a sharp increase between days 10 and 15. This treatment caused an overall spheroid growth of 192 % relative to the DMSO controls. 1 μM had a similar effect, and spheroids displayed a growth rate comparable to those treated with 0.03 μM novobiocin sodium up to 10 days post-seeding. After this, the 1 μM drug-treated spheroids also displayed a sharp increase in growth, which was significantly higher than the DMSO-treated controls, leading to a percentage increase of 130 % on day 15. Meanwhile, 0.03 μM novobiocin sodium in combination with IR did cause a reduction in spheroid growth, although only later in the time course. The rate of growth of the combination treatment was comparable to the irradiated controls up to day 12 post-seeding. However, between days 12 and 15 post-seeding, there was a very little increase in spheroid size after novobiocin sodium plus IR treatment, and the overall growth was therefore 45 % relative to the irradiation only. On the other hand, 1 μM inhibitor in combination with X-rays actually promoted spheroid growth compared to treatment with X-rays only. In fact, there was a steep increase in spheroid growth from days 10 – 15 post-seeding, and the overall growth on day 15 after 1 μM novobiocin sodium plus IR was 195 % relative to the irradiated control spheroids (figure 4.18).

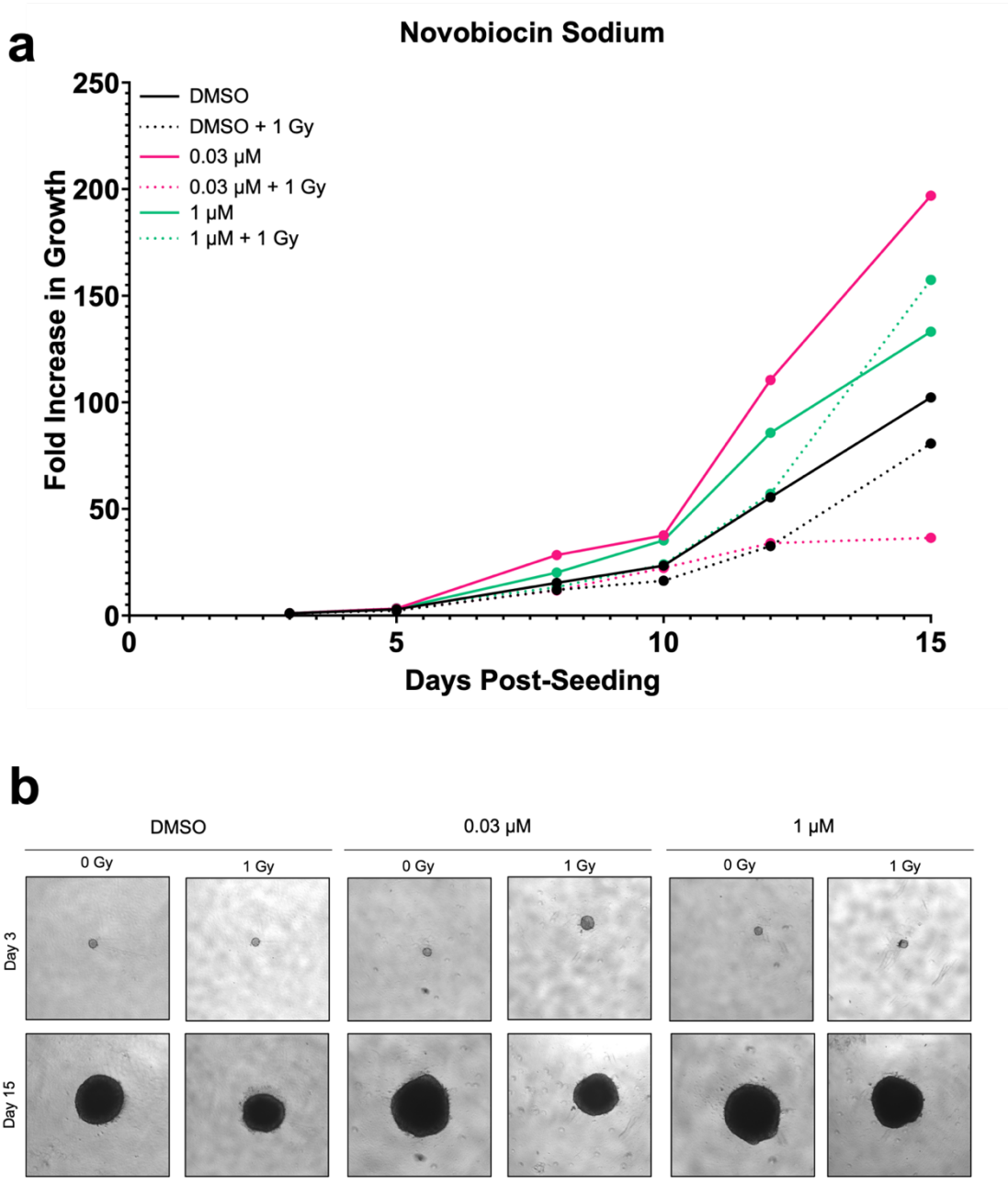

Figure 4.19: Spheroid growth following novobiocin sodium treatment

a) FaDu cells were seeded into ULA plates and incubated for 24 hours to allow spheroid formation, after which either 0.03 µM and 1 µM novobiocin sodium was then added. 24 hours after inhibitor treatment, spheroids were irradiated with 1 Gy or left unirradiated. Images of the spheroids were captured on days 3, 5, 8, 10, 12 and 15 post-seeding, which were used to measure the fold increase in growth over time. b) Images of spheroids on days 3 and 15 post-seeding after each different treatment condition.

Without the addition of IR, 0.03 μM enoxacin treatment produced comparable spheroid growth to the DMSO control treatment until day 10 post-seeding. On days 12 and 15, the increase in growth was then marginally lower in the inhibitor-treated spheroids. The overall percentage growth of spheroids on day 15 was 84 % relative to the DMSO controls. Similarly, 1 μM enoxacin treatment caused spheroid growth comparable to the controls until day 12, although no further changes in growth between days 12 and 15 was observed. Therefore, the overall change in percentage growth following 1 μM enoxacin treatment relative to the DMSO controls was 68 %. 0.03 μM enoxacin had a significant impact on spheroid growth at later times when combined with 1 Gy X-rays. Despite displaying a similar growth rate to irradiated control spheroids up to day 12 post-seeding, there was very little change in growth between days 12 and 15. On day 15, the 0.03 μM enoxacin-treated spheroids only had an overall growth of 29 % relative to irradiated controls. In stark contrast to this observation, 1 μM enoxacin seemed to enhance spheroid growth when combined with IR in comparison to irradiated controls. This was observed at almost every time point, until day 15, when the increase in growth was almost identical between the two treatments. As a consequence, the percentage growth of spheroids treated with 1 μM enoxacin plus 1 Gy X-rays was 97 % relative to irradiation alone (figure 4.19).

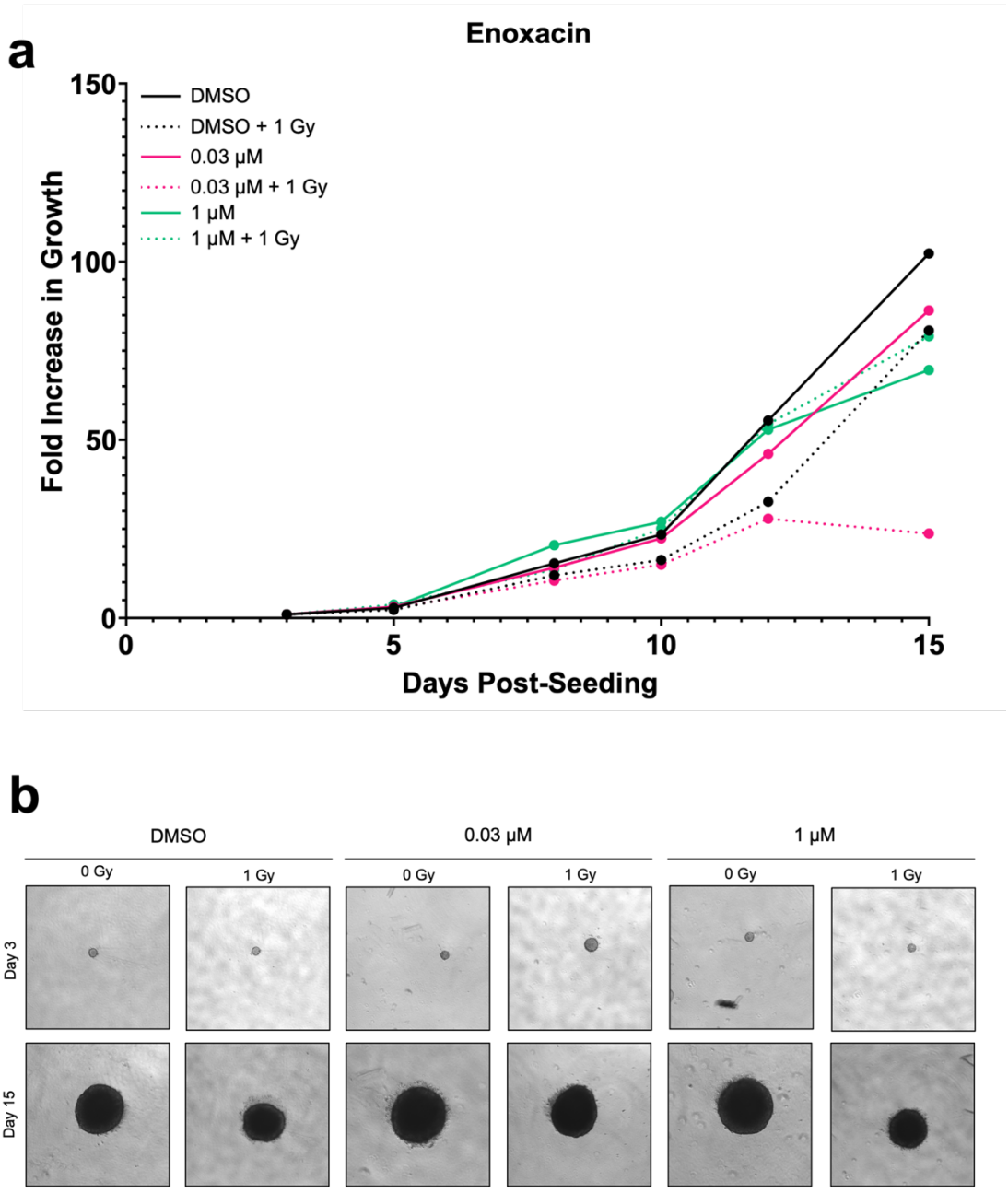

Figure 4.20: Spheroid growth following enoxacin treatment

a) FaDu cells were seeded into ULA plates and incubated for 24 hours to allow spheroid formation, after which either 0.03 μM and 1 μM enoxacin was then added. 24 hours after inhibitor treatment, spheroids were irradiated with 1 Gy or left unirradiated. Images of the spheroids were captured on days 3, 5, 8, 10, 12 and 15 post-seeding, which were used to measure the fold increase in growth over time. b) Images of spheroids on days 3 and 15 post-seeding after each different treatment condition.

4.3.5. DNA/RNA Synthesis Candidates

Two candidates identified in this screen, fidaxomicin and mupirocin, target DNA/RNA synthesis, and thus can impair efficient DNA damage repair in cancer cells. This contributes to the accumulation of damage and genomic instability, which further promotes tumourigenesis. Moreover, inability to synthesise new DNA to repair IR-induced damage can increase cellular radiosensitivity.

In the absence of radiation, 0.03 μM fidaxomicin appeared to be causing a significant enhancement of spheroid growth compared to the DMSO controls. This was evident from 5 days post-seeding onwards, with steep rises between days 5 and 10 post-seeding. There continued to be increases in spheroid growth following the drug treatment relative to the control, leading to an overall final percentage growth of 137 % relative to the spheroids treated with DMSO. Similar to the lower drug concentration, 1 μM fidaxomicin initially enhanced spheroid growth particularly on days 8 and 10 post-seeding where there were steep increases in growth rate. However, spheroid size dramatically decreased to a lower level comparable to the DMSO control on day 15. This led to an overall percentage growth of 105 % after 1 μM fidaxomicin treatment relative to the DMSO control-treated spheroids. When combined with 1 Gy X-rays, 0.03 μM fidaxomicin enhanced spheroid growth at all time points compared to the irradiated controls. On days 5 to 12 post-seeding, there was a steady increase in growth that lay approximately halfway between the growth rates of the unirradiated and irradiated controls. Between days 12 and 15, the spheroids treated with 0.03 μM plus IR dramatically increased in growth to a value significantly higher than the irradiated controls and almost identical to the unirradiated controls. The percentage growth of the combination treatment relative to the irradiated controls was 149 %. On

the other hand, a decrease in growth was observed when combining 1 μM fidaxomicin and 1 Gy X-rays, although only at the latest time point. In fact, the observed fold increase in growth of the drug-radiation treatment was actually higher than the irradiated controls on days 8 and 10 post-seeding. However, the spheroid size began to decrease from day 12 and on day 15, the inhibitor plus IR-treated spheroids had grown significantly less than the irradiated controls, with a relative overall growth of only 27 % (figure 4.20).

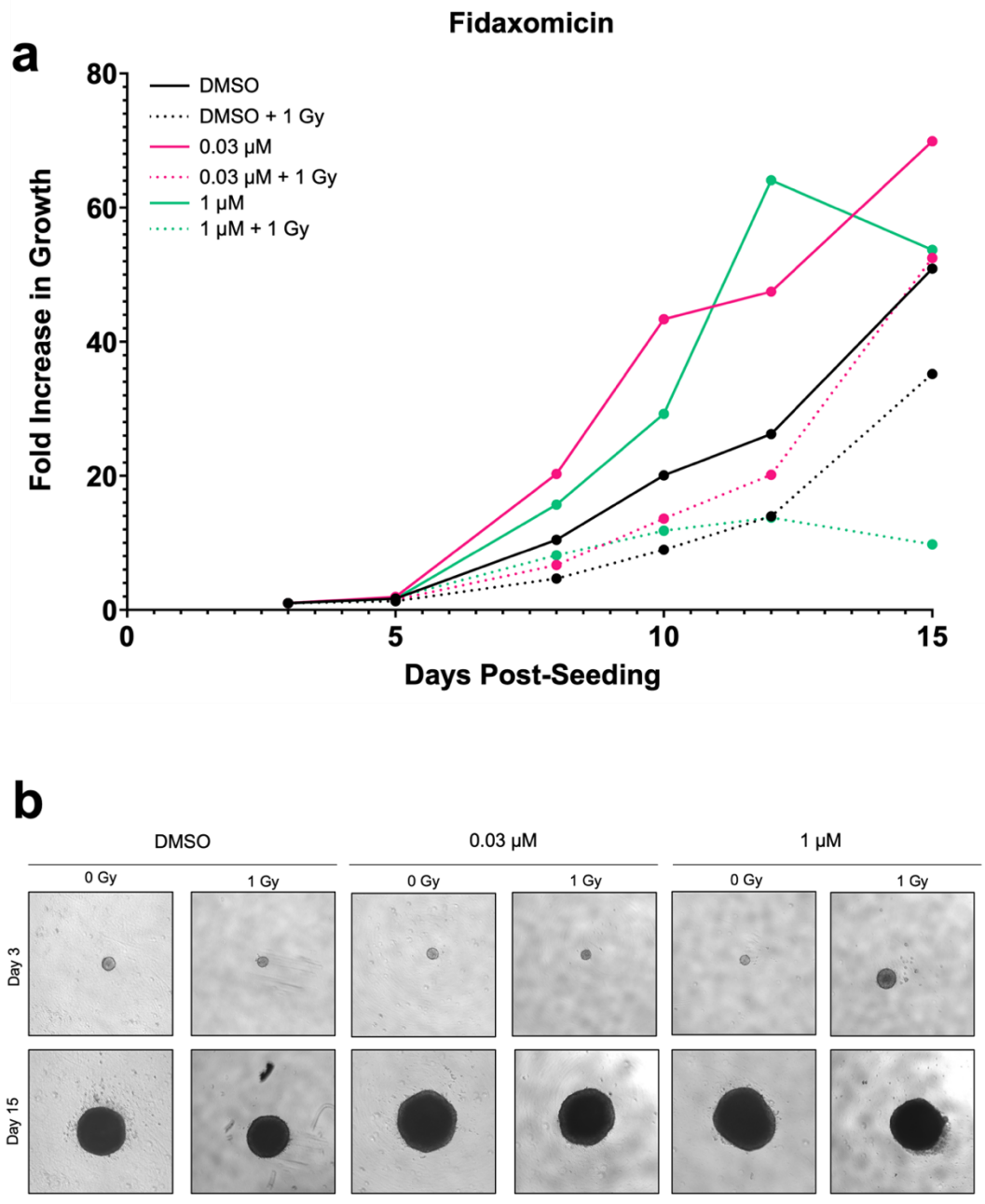

Figure 4.21: Spheroid growth following fidaxomicin treatment

a) FaDu cells were seeded into ULA plates and incubated for 24 hours to allow spheroid formation, after which either 0.03 µM and 1 µM novobiocin sodium was then added. 24 hours after inhibitor treatment, spheroids were irradiated with 1 Gy or left unirradiated. Images of the spheroids were captured on days 3, 5, 8, 10, 12 and 15 post-seeding, which were used to measure the fold increase in growth over time. b) Images of spheroids on days 3 and 15 post-seeding after each different treatment condition.

The final candidate identified in this drug screen, mupirocin, actually enhanced spheroid growth when used without radiation. 0.03 μM of the drug displayed consistently higher levels of growth across all time points when compared to the DMSO controls. There was an exponential rate of spheroid growth until day 12, although between days 12 and 15 post-seeding there was very little change in spheroid size. However, the overall growth of spheroids following drug treatment was still higher than the DMSO-treated controls, with a comparative percentage increased growth of 116 %. 1 μM mupirocin had a very similar effect than the lower concentration, following the same trend until day 12 post-seeding. Between days 12 and 15 however, the spheroids actually decreased in size, and at this point were in fact comparable to DMSO-treated spheroids, with a relative growth of 96 %. On the other hand, both concentrations of inhibitor reduced the overall growth of spheroids when combined with IR but only at day 15. Up until day 10 post-seeding, both concentrations actually seemed to promote growth compared to the irradiated controls. However, on day 12, the growth rate of spheroids treated with 0.03 μM mupirocin plus irradiation levelled off, leading by day 15 to cause an overall growth of 43 % relative to the irradiated controls. 1 μM mupirocin plus IR still caused a higher rate of growth on day 12 post-seeding, but this had decreased by day 15, causing the overall percentage growth relative to the irradiated controls to be 54 % (figure 4.21).

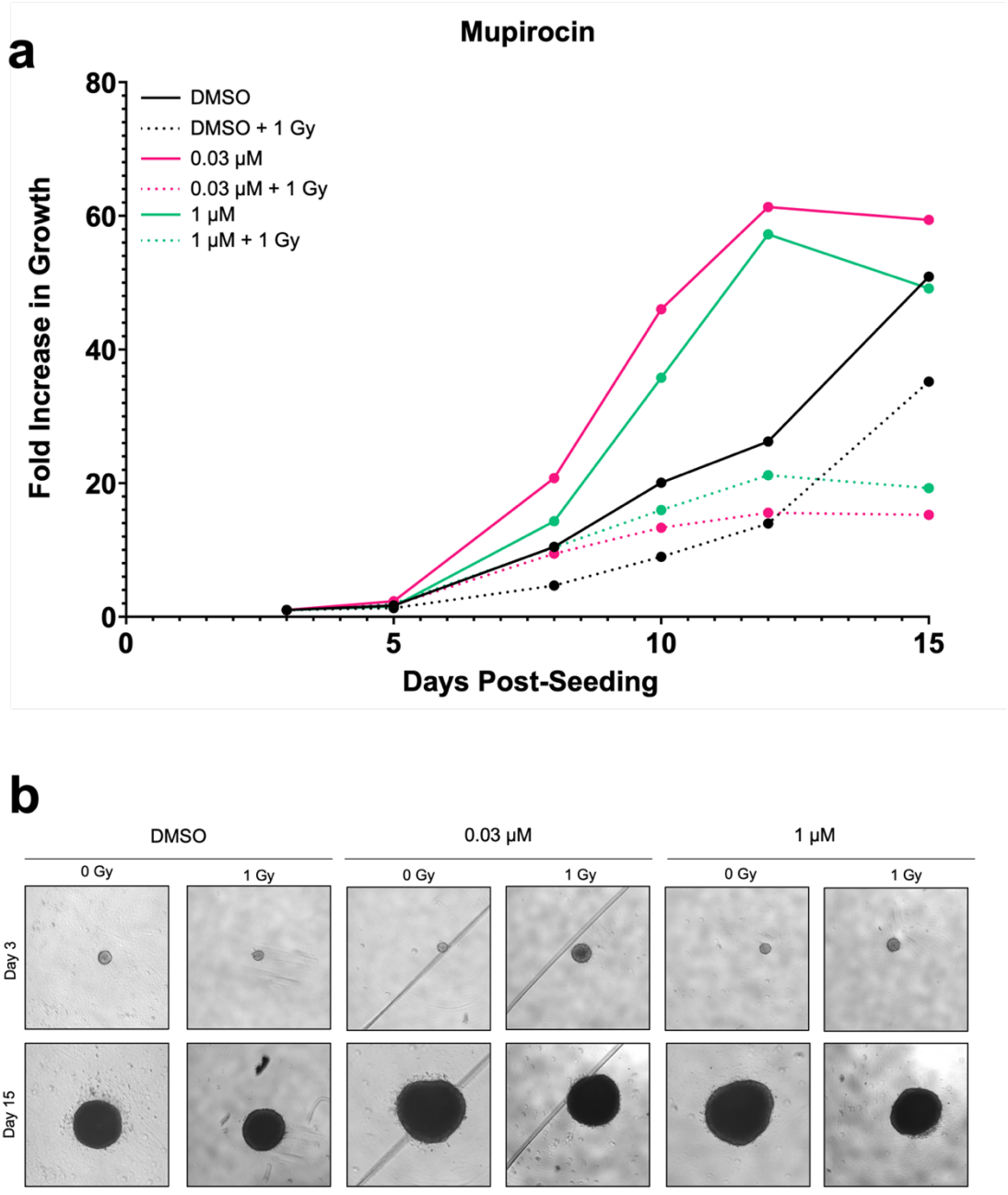

Figure 4.22: Spheroid growth following mupirocin treatment

a) FaDu cells were seeded into ULA plates and incubated for 24 hours to allow spheroid formation, after which either 0.03 µM and 1 µM mupirocin was then added. 24 hours after inhibitor treatment, spheroids were irradiated with 1 Gy or left unirradiated. Images of the spheroids were captured on days 3, 5, 8, 10, 12 and 15 post-seeding, which were used to measure the fold increase in growth over time. b) Images of spheroids on days 3 and 15 post-seeding after each different treatment condition.

4.4. Summary

Using a 3D spheroid model of HNSCC, 183 FDA-approved drugs were screened for potential radiosensitisation ability. Spheroids were treated with 0.03 μM or 1 μM of each drug alone, in combination with either no irradiation or with 1 Gy X-rays. On days 3, 5, 8, 10, 12 and 15 post-seeding, images of the spheroids were captured, and spheroid volume was calculated at each time point. Overall fold increase in growth over 15 days was used as the endpoint to determine which candidates to take forward for further experimentation.

In this chapter, I have identified 17 drugs as potential candidate radiosensitisers of HPV-negative HNSCC. These drugs have a variety of cellular targets, inhibiting proteins involved in processes such as cell growth and survival, chromatin remodelling, cell signalling, cell cycle regulation, and DNA/RNA synthesis. As this initial screen only utilised one spheroid per treatment condition, it was crucial to then validate these findings using replicate samples and independent biological experiments to eliminate any false positive candidates and narrow down the list of true radiosensitisers of HNSCC cells *in vitro*.

CHAPTER 5: RESULTS II

Validation of candidate drugs and identification of three novel radiosensitisers of HNSCC *in vitro*

5.1. Introduction

Based on the results from the initial drug screen, I chose 17 candidate radiosensitisers to take forward for further study (see table 4.1). These 17 drugs covered a variety of cellular targets, including NF-κB, PDGFR, TNF-α, HDACs, EGFR, topoisomerases, and DNA/RNA synthesis.

The NF-κB signalling pathway is implicated in a number of cellular processes, including stimulating the expression of anti-apoptosis genes, and human cancers are thought to utilise elevated levels of NF-κB signalling to avoid apoptosis and maintain tumour cell proliferation. This has been demonstrated in multiple types of HNSCC, for example one study of patients with OSCC showed that NF-κB levels were increased in tumour tissue compared to healthy tissue, and this increase correlated with high rates of tumour infiltration and decreased patient survival (439). Moreover, another study demonstrated through whole genome sequencing that NF-κB signalling is aberrantly regulated in 41 % of cases of nasopharyngeal carcinoma (52). In addition to contributing to tumour development and progression, NF-κB signalling has also been shown to play a role in intrinsic cellular sensitivity to IR. Upon exposure to IR, tumour cells have been shown to activate NF-κB signalling in order to reduce apoptosis (418), and research has demonstrated the effectiveness of inhibiting NF-κB in enhancing cellular radiosensitivity in several cancer types *in vitro*, including colorectal cancer, laryngeal squamous cell carcinoma, hepatocellular carcinoma, lung cancer, and transformed

prostate cells (419, 420, 440-442). One of the drugs identified in the initial drug screen was stearic acid, which has been shown to reduce the activation of NF-κB (443). To date, there has been no research carried out into the radiosensitising ability of stearic acid, however it has been shown that it may be an effective therapy for colon cancer when combined with 5-FU (444) and can significantly inhibit the colony formation ability of rat hepatoma cell lines (445).

PDGFR-α and -β are signalling receptors activated by platelet-derived growth factors (PDGFs) (446). Activation of the receptor initiates a cascade of downstream signalling through either the MAPK pathway, the PI3K/AKT/mTOR pathway, or the phospholipase-γ pathway, all of which contribute to the balance of pro- and anti-apoptotic signalling in the cell (447), and thus mutations and incorrect activity of PDGFR can contribute to the progression and maintenance of cancers. Indeed, an overexpression of PDGFR-α has been observed in invasive breast cancers, where it is correlated with lymph node metastasis and expression of *HER2* and *BCL2* (448). More recently, a study of OSCCs demonstrated an increase in PDGFR-β expression in the cancer cells, which was associated with lymph node metastasis and a decrease in overall survival (449). Increases in PDGFR expression have also been observed in colorectal cancer, gastric cancer, and thyroid cancer, where increased PDGFR expression significantly reduced patient survival (450-452). Building on this, the inhibition of PDGFR-β has been shown to enhance radiosensitivity in glioblastoma cells both *in vitro* and *in vivo* in multiple studies, as well as increasing sensitivity in lower grade astrocytoma cells (453-455). Furthermore, initial research into the multi-kinase inhibitors sorafenib and sunitinib, both of which block the activity of PDGFRs, demonstrates their potential as radiosensitisers in HNSCC cell lines (423). In the initial drug screen, orantinib, a potent inhibitor of PDGFR, was identified as a potential

radiosensitiser. Previous research has shown that orantinib can effectively radiosensitise endothelial cancer, prostate cancer, and glioblastoma cells to IR both *in vitro* and *in vivo* (456-458). The radiosensitising potential of orantinib has also been shown in a murine squamous cell carcinoma model (459), but to date, no research has been carried out into the specific effects of orantinib in HNSCCs.

TNF-α is a transmembrane protein that can induce signalling through a variety of signalling cascades, including the ERK, MAPK, PI3K and NF-κB pathways (460). These pathways can influence survival and apoptosis signalling within the cell, thus TNF-α can have a significant role in tumourigenesis. Indeed, it has been shown that TNF-α has a tumour-promoting effect in breast cancers. One study demonstrated that TNF-α was expressed at the tumour site in breast cancer patients, and as the tumour grade increased, so did the number of cancer cells expressing the protein (461). Furthermore, TNF-α has been observed in the bloodstream of breast cancer patients, and levels of TNF-α correlated with lymph node involvement, suggesting there may be a role for TNF-α in metastasis (462). On the contrary, TNF-α has also been shown to have tumour-suppressive qualities and can be used as a therapeutic target. The addition of TNF-α can enhance the permeability of cancer cell vasculature, which increases the effectiveness of chemotherapeutic cytostatic drugs (463, 464). It has been proposed that significantly elevated levels of TNF-α can be an effective treatment, while lower levels are tumourigenic (465). Thus, both TNF-α inhibitors and TNF-α itself have been utilised as anti-cancer therapies. Apremilast, the TNF-α inhibitor identified in the initial stages of this research, has been shown to induce apoptosis in human colorectal cancer cells (466), however has not been investigated for its impact on radiosensitivity. In fact, the literature suggests that treatment with TNF-α itself can increase radiosensitivity of oesophageal

squamous cell carcinoma, melanoma, and lung cancer cells *in vitro* (467-469). To date, TNF-α inhibition has not been demonstrated to have any radiosensitising potential.

HDACs alter gene expression by modifying the structure of chromatin (see section 1.4.2.). The acetylation status of histones has been implicated in DNA DSB repair pathways, both HR and NHEJ, and thus can influence the development of cancer and response to treatments (286, 287). For example, HDAC1/2-depleted cells have been shown to display significant defects in the NHEJ pathway, specifically resulting in the persistence of Ku70 and Artemis at DNA damage sites (387). Furthermore, HDAC4 interacts with 53BP1 during DSB repair (390), and HDAC6 interacts with two key MMR proteins, MLH1 and MSH2, and can inhibit the MMR pathway (391). HDAC9 and HDAC10 have been implicated in the HR pathways, as one study demonstrated that a reduction of HDAC9/10 led to significantly less HR activity and sensitised cells to mitomycin C (393). The role of HDACs in the DDR provides a solid basis for their potential as radiosensitisers. Indeed, multiple HDACi have been studied for their radiosensitising effects, including one of the inhibitors identified in this research: the class I HDACi mocetinostat. When given alongside X-ray irradiation, mocetinostat significantly reduced survival of bladder cancer cells *in vitro*, and decreased levels of MRE11, implying that this effect could be due to impaired DNA damage repair (405). This research also identified CUDC-101, a combined inhibitor of HDACs and EGFR, as a potential radiosensitiser. Research has shown that CUDC-101 has significant radiosensitising potential in pancreatic cancer, glioblastoma, and breast cancer cell lines (402, 403). To date there has been no evidence suggesting CUDC-101 can radiosensitise HNSCC cells, although another HDACi, VPA, has been demonstrated to effectively radiosensitise oesophageal SCC cells *in vitro* (397).

EGFR is a transmembrane receptor and an upstream activator of a multitude of cellular signalling pathways, including MAPK, PI3K/AKT/mTOR and JNK pathways (470). These pathways control vital activities in the cell, including proliferation, angiogenesis, and survival, thus dysregulation of any protein in the cascade can lead to the development of the hallmarks of cancer and tumourigenesis. An overexpression of EGFR has been observed in 80 – 90 % of HNSCCs and is associated with poor survival rates (471, 472), making it a popular target for therapeutic inhibition. EGFR inhibitors have been used successfully to increase radiosensitivity of a variety of cancer types, and of the six EGFR inhibitors identified as candidates in this drug screen, four have been shown to act as radiosensitisers. Icotinib was demonstrated to radiosensitise lung cancer cells *in vitro* via the inhibition of MAPK and AKT activation (473), while CUDC-101 enhances the radiosensitivity of pancreatic cancer, breast cancer, and glioblastoma cells (402, 403). Afatinib has been shown to radiosensitise HNSCC and nasopharyngeal carcinoma cells (430, 474), and genistein improves radiosensitivity of oesophageal SCC cells *in vitro* (475). Despite the success of EGFR inhibitors *in vitro*, clinical trials have failed to replicate this effect, and EGFR inhibition does not appear to be an effective treatment in practice.

Topoisomerase enzymes catalyse the unlinking of DNA strands to ensure correct separation during DNA replication, allowing DNA polymerases to move down the replication fork (476). Inhibitors of topoisomerase therefore lead to stalled replication forks, DSB induction, and cell cycle arrest, and have consequently been used as an anti-cancer therapeutic (477). Four of the drugs identified as candidates in this drug screen inhibit topoisomerases: genistein, dexrazoxane HCl, novobiocin sodium and enoxacin, but to date only genistein – which also inhibits EGFR – has previously been shown to act as a radiosensitiser. The radiosensitising potential of genistein has been

demonstrated in a large number of cancer types, including oesophageal, colorectal, breast, prostate, and hepatocellular cancers, plus sarcoma and NSCLC cells (475, 478-483). Although this has not been demonstrated in HNSCC to date, research does suggest that genistein as a single agent treatment can induce apoptosis and reduce growth of HNSCC tumours (484-486).

In recent years, there has been significant development in the use of antibiotics as anticancer agents. The ability of antibiotics to inhibit DNA/RNA synthesis means they can effectively inhibit cell cycle progression and exert an anti-proliferative effect on cancerous cells. It has also been shown that antibiotics have the potential to impede EMT, thus reducing the metastatic potential of cells (487). Two of the drugs identified in this screen, fidaxomicin and mupirocin, are antibiotics that interfere with DNA/RNA synthesis. The potential anticancer effect of fidaxomicin has not been investigated to date, however, it has been suggested that mupirocin may be cytotoxic to melanoma cells (488). Currently, there has been no research into how antibiotics can impact cancer cell radiosensitivity.

The initial drug screen identified 17 candidate radiosensitisers, inhibiting the targets discussed above. Only one spheroid per treatment condition was used in this drug screen, and thus these candidates needed to be validated to ensure the observed radiosensitisation effect was genuine. In this chapter, I aimed to validate the findings of the drug screen through repeated spheroid experiments, and to further confirm these findings using clonogenic survival assays.

5.1. Validation of 17 Candidate Radiosensitisers

The initial approach to validate the findings of the drug screen was to repeat the spheroid experiments. Once again, as described in section 3.6, FaDu cells were seeded at a density of 500 cells/well into ultra-low attachment 96-well plates and left overnight to form spheroids. 0.03 and 1 μM concentrations of the 17 candidate drugs were used to treat the spheroids on day 2, and 24 hours later they were irradiated with X-rays at 1 Gy. Spheroid volume and fold increase in growth was calculated on days 3, 5, 8, 10, 12 and 15 post-seeding analyse the radiosensitisation ability of the drugs. The results of these validation experiments were surprising. Contrary to what was observed in the initial drug screen, the drugs did not exert a potent radiosensitisation effect. It was expected that some of the drugs identified in the screen may have been false positives, however it was anticipated that some of the drugs would show evidence of radiosensitisation. One explanation for these observations could be the stability and potency of the drugs, and therefore I repeated the spheroid experiments with higher concentrations of drugs, 5 μM and 10 μM, and an additional dose of X-rays, 2 Gy. All data was analysed using a two-tailed t-test, all p-values can be found in supplementary section 10.1.

From all 17 candidate drugs, only two, CUDC-101 and pracinostat, seemed to be successfully radiosensitising FaDu spheroids when used at the higher concentrations of 5 μM and 10 μM. These experiments are detailed below. The remaining 15 candidate experiments are discussed in Appendix I.

5.1.1. CUDC-101

In the initial drug screen, CUDC-101 appeared to have a significant radiosensitisation effect at a concentration of 1 μM, however this was not replicated in the first set of validation experiments (figure 5.4a). 0.03 μM CUDC-101 as a single agent treatment enhanced spheroid growth at all time points compared to DMSO controls and had an overall increase of 140 % relative to the unirradiated controls on day 15 post-seeding. Meanwhile 10 μM alone slightly decreased overall growth, again consistently across all time points, but only to a relative 84 % overall growth. However, this was statistically significant on day 8 ($p < 0.05$; *t-test*, supplementary table 10.4). Upon addition of 1 Gy X-rays, both concentrations of CUDC-101 increased spheroid growth in comparison to the irradiated controls. 0.03 μM plus 1 Gy X-rays was comparable to 1 Gy controls up to 10 days post-seeding, following an observable – but not significant – increase on days 10 and 15 to an overall increase in growth of 123 % relative to controls. 1 μM plus 1 Gy caused a slight decrease in spheroid growth until day 12 post-seeding, and between day 2 and 15 there was a slight increase compared to irradiated controls, but only to a relative 105 % overall growth. In contrast, 5 μM as a single agent treatment markedly reduced spheroid growth in comparison to DMSO controls across all time points of the experiment and was statistically significant at all time points (figure 5.4b; *t-test*, supplementary table 10.4). The spheroid growth rate was slow in the first 8 days post-seeding, followed by a steady increase between days 8 and 12. From day 12 to day 15, there was a sharper increase in growth, and the overall percentage growth following 5 μM CUDC-101 treatment was 55 % relative to the control treatment. In sharp contrast to this, 10 μM CUDC-101 was extremely toxic, and inhibited any spheroid growth across the 15 days post-seeding. By the end of the experiment, these spheroids had only grown to 3 % relative to controls, and as expected this was

statistically significant on all days except day 5 post-seeding. 5 μM CUDC-101 combined with X-rays significantly reduced spheroid growth at both 1 Gy and 2 Gy consistently across all time points. The two radiation doses produced almost identical growth rates up to 12 days post-seeding, however on day 15 the spheroids treated with 5 μM CUDC-101 plus 1 Gy X-rays actually had the lower overall increase. Compared to the corresponding irradiated controls, 5 μM CUDC-101 caused an overall growth increase of 23 % and 30 % at 1 Gy and 2 Gy respectively, and these differences were statistically significant on days 5 – 12 post-seeding (1 Gy) and days 8 and 10 post-seeding (2 Gy) (*t-test*, supplementary table 10.4). As predicted based on the observation of the high concentration of CUDC-101 alone, 10 μM plus IR was extremely toxic to the spheroids, with growth only reaching 5 % and 7 % relative to the controls following 1 Gy and 2 Gy respectively – this was statistically significant at all time points (*t-test*, supplementary table 10.4). From this data, it appears that CUDC-101 can radiosensitise FaDu spheroids.

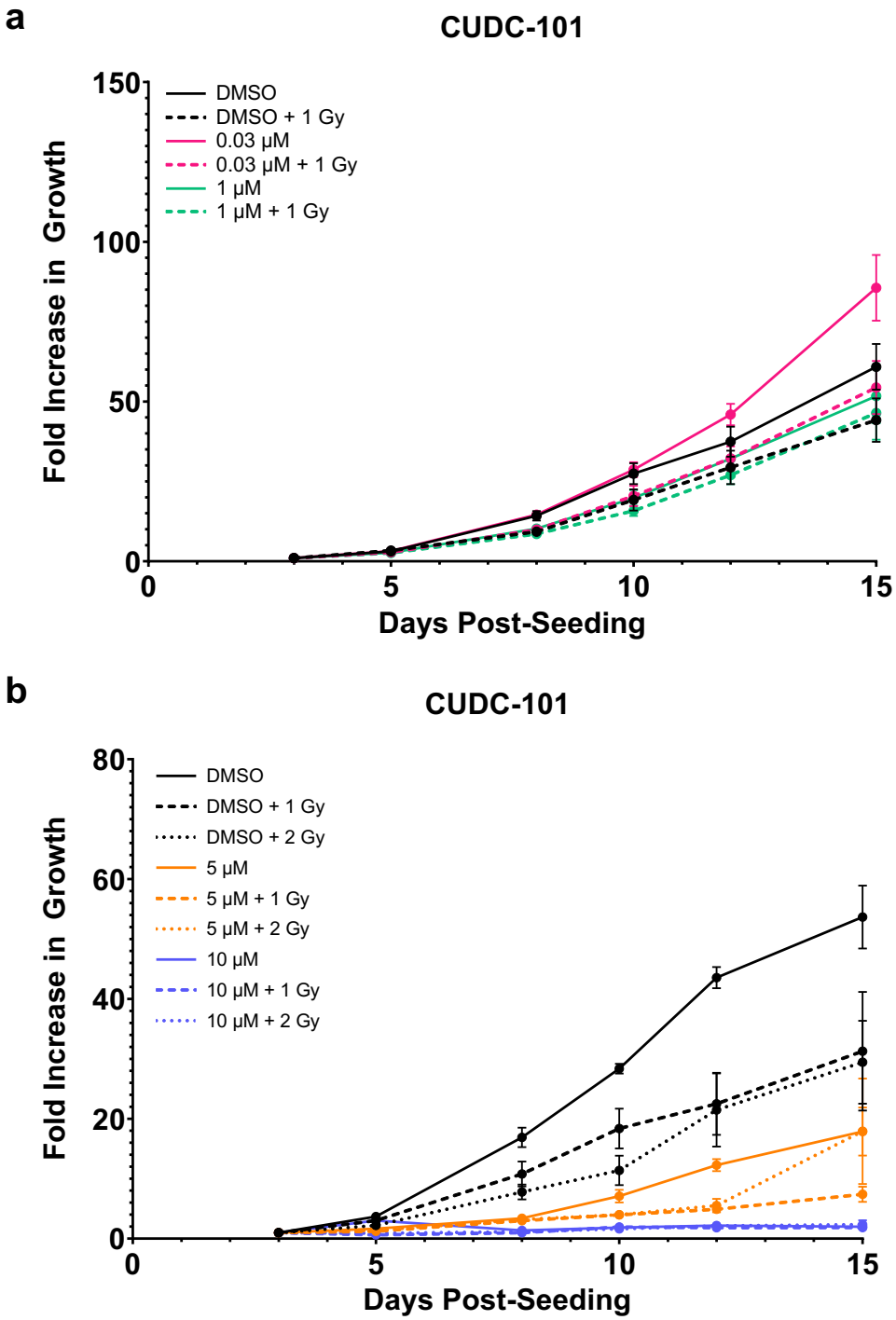

Figure 5.1: Spheroid growth after CUDC-101 treatment

FaDu cells were seeded into ULA plates and incubated for 24 hours to allow spheroid formation, after which CUDC-101 was added at either (a) 0.03 µM and 1 µM or (b) 5 µM and 10 µM. Following 24 hours of inhibitor treatment, spheroids were irradiated with either (a) 1 Gy or (b) 1 Gy and 2 Gy X-rays. Images of the spheroids were captured on days 3, 5, 8, 10, 12 and 15 post-seeding, which were used to measure the fold increase in growth over time. The data are presented as mean ± SEM of triplicate wells and are representative of three independent experiments.

5.1.2. Pracinostat

Pracinostat also appeared to be radiosensitising spheroids at 1 μM in the initial drug screen. In the first set of validation experiments (figure 5.6a), 0.03 μM caused an enhancement of growth at 0 Gy from day 8 post-seeding onwards, with an overall increase in growth of 138 % relative to unirradiated controls at day 15 post-seeding. In contrast, 1 μM caused a slight reduction in the growth of spheroids at all time points, to 85 % relative to the DMSO controls – this was statistically significant on days 8 and 10 post-seeding ($p < 0.05$; *t-test*, supplementary table 10.6). 0.03 μM plus 1 Gy X-rays caused an enhancement of growth compared to irradiated controls, with a relative percentage growth on day 15 of 116 %. 1 μM plus IR caused a reduction in growth rate up to 12 days post-seeding, but on day 15 was comparable to controls, with an overall relative growth of 95 %. This was in contrast to the dramatic reduction seen in the initial drug screen. However, 5 μM pracinostat as a single agent treatment markedly reduced spheroid growth compared to the DMSO control at all time points across the experiment (figure 5.6b). By day 15, spheroids grew to an overall size of 57 % relative to the controls, and the difference was statistically significant on days 8 – 15 post-seeding. Interestingly, 10 μM pracinostat had a contrasting effect, causing an overall increase in spheroid growth of 107 % relative to the control. In combination with 1 Gy X-rays, 5 μM pracinostat significantly radiosensitised FaDu spheroids. Growth was steady – but much slower than control conditions – across all time points and consistently lower than the DMSO plus 1 Gy controls. Statistically, the difference between the spheroids treated with DMSO plus 1 Gy and 5 μM pracinostat plus 1 Gy was significant on days 5 – 10 post-seeding, with $p < 0.05$ at each time point (*t-test*, supplementary table 10.6). By day 15, the spheroids treated with 5 μM pracinostat plus 1 Gy X-rays had an overall percentage growth of 48 % relative to controls. Conversely, 10 μM pracinostat plus 1 Gy X-rays enhanced growth

compared to the irradiated controls. Up to 10 days post-seeding, the growth was actually lower following inhibitor treatment combined with 1 Gy, however there was a steep increase in growth between days 10 and 12 post-seeding to a value observably higher than the irradiated controls. On day 15, inhibitor treated spheroids had an overall growth of 114 % relative to 1 Gy controls. When combined with 2 Gy X-rays, 5 μM pracinostat again significantly reduced spheroid growth. By day 15, the relative percentage growth to the 2 Gy irradiated controls was 21 %, and the difference between the two conditions was statistically significant on days 8 and 10 post-seeding (*t-test,* supplementary table 10.6). Meanwhile, 10 μM did slightly reduce growth compared to irradiated controls when combined with 2 Gy X-rays, however not to a significant level nor the extent of 5 μM combined with IR. In fact, the growth of spheroids treated with 10 μM pracinostat plus 2 Gy followed a very similar trend to the spheroids treated with 5 μM alone. Overall, 10 μM plus 2 Gy resulted in a total spheroid growth of 83 % relative to irradiated controls. From this data, I can conclude that 5 μM pracinostat can radiosensitise FaDu spheroids.

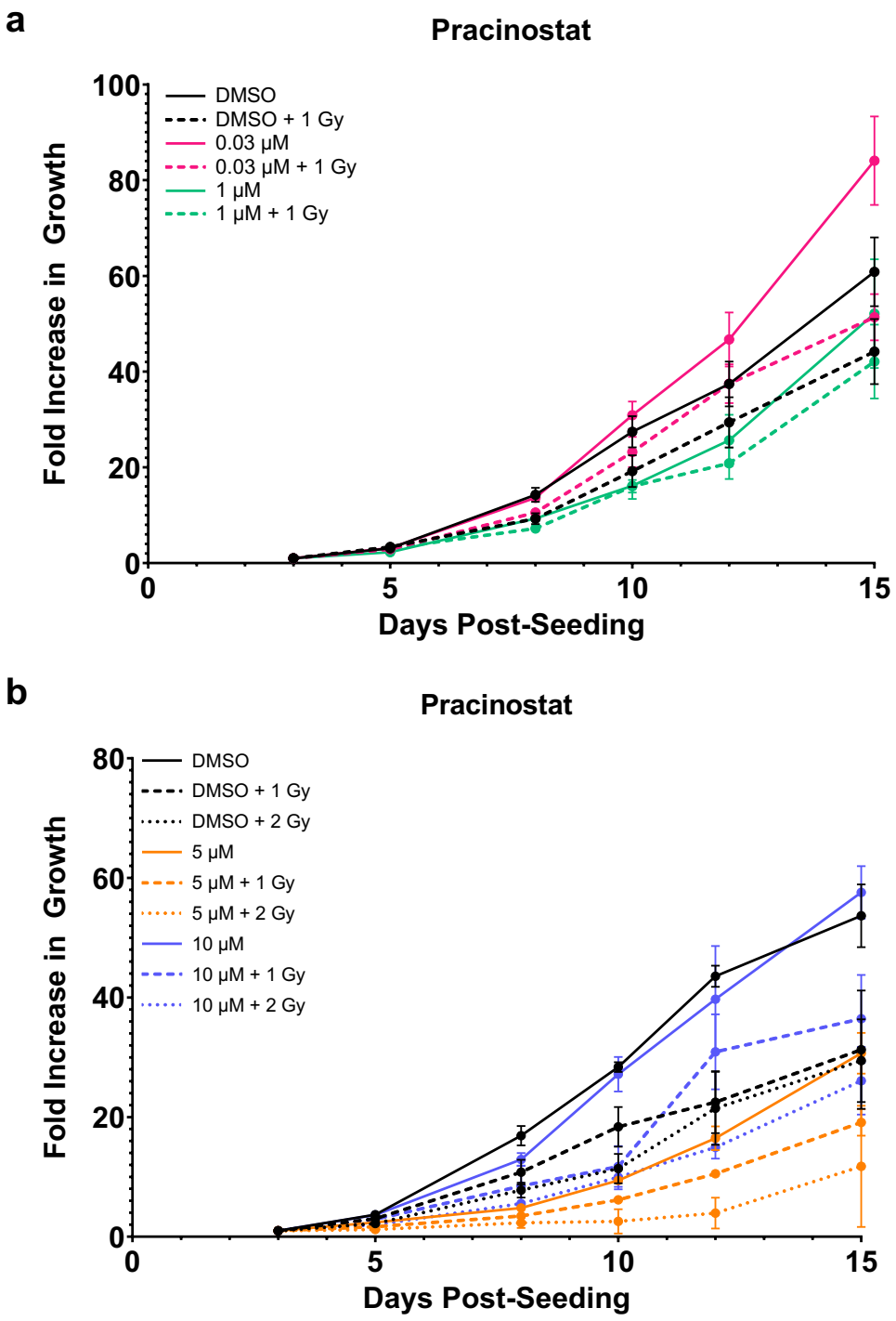

Figure 5.2: Spheroid growth following pracinostat treatment

FaDu cells were seeded into ULA plates and incubated for 24 hours to allow spheroid formation. Following this, pracinostat was added at either (a) 0.03 µM and 1 µM or (b) 5 µM and 10 µM. Following 24 hours of inhibitor treatment, spheroids were irradiated with either (a) 1 Gy or (b) 1 Gy and 2 Gy X-rays. Images of the spheroids were captured on days 3, 5, 8, 10, 12 and 15 post-seeding, which were used to measure the fold increase in growth over time. The data are presented as mean ± SEM of triplicate wells and are representative of three independent experiments.

5.1.3. Summary

In summary, these validation experiments highlighted that many of the inhibitors identified in the initial drug screen were in fact false positives. Out of the 17 candidates, only two appeared to be acting as radiosensitisers: CUDC-101 and pracinostat. Although these results do not conclusively prove that pracinostat and CUDC-101 are acting as radiosensitisers, the data is promising. Therefore, I carried out further experimentation using these inhibitors to gain more insight into their radiosensitisation potential.

5.2. Confirmation of pracinostat and CUDC-101 as radiosensitisers

5.2.1. Overview

To further validate the roles of pracinostat and CUDC-101 as radiosensitisers, I carried out additional spheroid experiments along with clonogenic survival assays using multiple HPV-negative HNSCC cell lines. As CUDC-101 is a multi-targeting inhibitor of HDACs and EGFR, I elected to also investigate two EGFR inhibitors – lidocaine HCl and genistein - and one other HDAC inhibitor – mocetinostat. These drugs were chosen as, in the initial drug screen, they were all identified as possible radiosensitisers, and in the initial validation experiments, all three appeared to cause some slight radiosensitisation. Spheroid growth assays were performed using FaDu cells, as in earlier experiments. As new stocks of the 5 inhibitors of interest were used, the spheroids were treated using the original concentrations of 0.03 μM or 1 μM, combined with either 0 Gy, 1 Gy or 2 Gy X-rays. In addition, clonogenic assays were carried out in 6 HPV-negative HNSCC cell lines (see table 3.5), four of which had mutated *p53* – FaDu, A253, UM-SCC-12 and UM-SCC-11b – and

two of which had wild-type *p53* –UM-SCC-6 and UM-SCC-17A. A253, UM-SCC-12, UM-SCC-11b and UM-SCC-17A cells all originated from the oral cavity, while UM-SCC-6 cells came from the tongue, and FaDu from the hypopharynx. UM-SCC-11b cells were used following the conclusion that only CUDC-101 and pracinostat were acting as radiosensitisers, and therefore only these two inhibitors were tested in this cell line. All cell lines were seeded at a density of 1000 cells per well for 0 Gy, with this value doubling for each subsequent dose of radiation. After allowing the cells to attach to the plate, fresh media containing 0.5 μM inhibitor was added to each well. 0.5 μM was chosen after a series of dose response experiments showing that 1 μM was too toxic to the cells at 0 Gy, while 0.3 μM did not have an observable impact on survival. 24 hours after inhibitor treatment, the plates were irradiated with 1, 2 or 4 Gy X-rays, fresh media was added, and the cells were then left for 6-10 days to allow colony formation to occur. The CFAssay was used for statistical analysis across the whole dataset for each cell line/inhibitor combination. Clonogenic survival assays are a gold standard for analysing radiosensitivity, and thus provide more confidence in the results.

5.2.2. EGFR Inhibitors

Lidocaine HCl

Lidocaine HCl was tested once more in spheroid growth assays (figure 5.18a). Inhibitor treatment in the absence of IR seemed to enhance growth relative to DMSO controls at 0.03 μM, consistently across all 15 days post-seeding. By day 15, 0.03 μM lidocaine HCl as a single-agent treatment caused an overall growth of 123 % relative to DMSO controls. 1 μM alone caused growth to be observably higher than controls on days 8 to 12 post-seeding, however on day

15 the inhibitor-treated spheroids grew slightly less, to a relative 97 %. Both 0.03 μM and 1 μM lidocaine HCl enhanced spheroid growth when combined with IR. The spheroids treated with 0.03 μM lidocaine HCl plus X-rays followed a similar growth trend to the unirradiated DMSO controls, which was markedly higher than the 1 Gy controls. Overall, 0.03 μM lidocaine HCl plus 1 Gy resulted in a percentage growth of 149 % relative to DMSO plus 1 Gy. 1 μM lidocaine HCl plus 1 Gy resulted in a similar trend in growth, just to a lower level compared to the 0.03 μM plus IR treatment. There was still an enhancement of spheroid growth, with an overall 131 % relative to the irradiated controls. 0.03 μM lidocaine HCl plus 2 Gy X-rays caused growth that was comparable to DMSO plus 2 Gy up to day 12 post-IR. Between day 12 and 15, there was an increase to an overall 179 % relative to DMSO plus 2 Gy controls. Spheroids treated with 1 μM plus 2 Gy X-rays grew to a comparable rate to the 2 Gy controls, just slightly lower at all time points. The overall percentage growth was 97 % relative to 2 Gy controls. Across this experiment, there was no statistical significance (*t-test*, table 5.1). Spheroid growth was also analysed as a function of X-ray dose (figure 5.18b). By comparing the increase in volume on day 15 relative to day 3 for each drug-radiation combination, then normalising this to volume increase with the drug alone (set to 1.0), it was clear that there was no difference between the effects of DMSO and 0.03 μM lidocaine HCl on radiosensitivity. Interestingly 1 μM lidocaine HCl appeared to promote some degree of radioresistance.

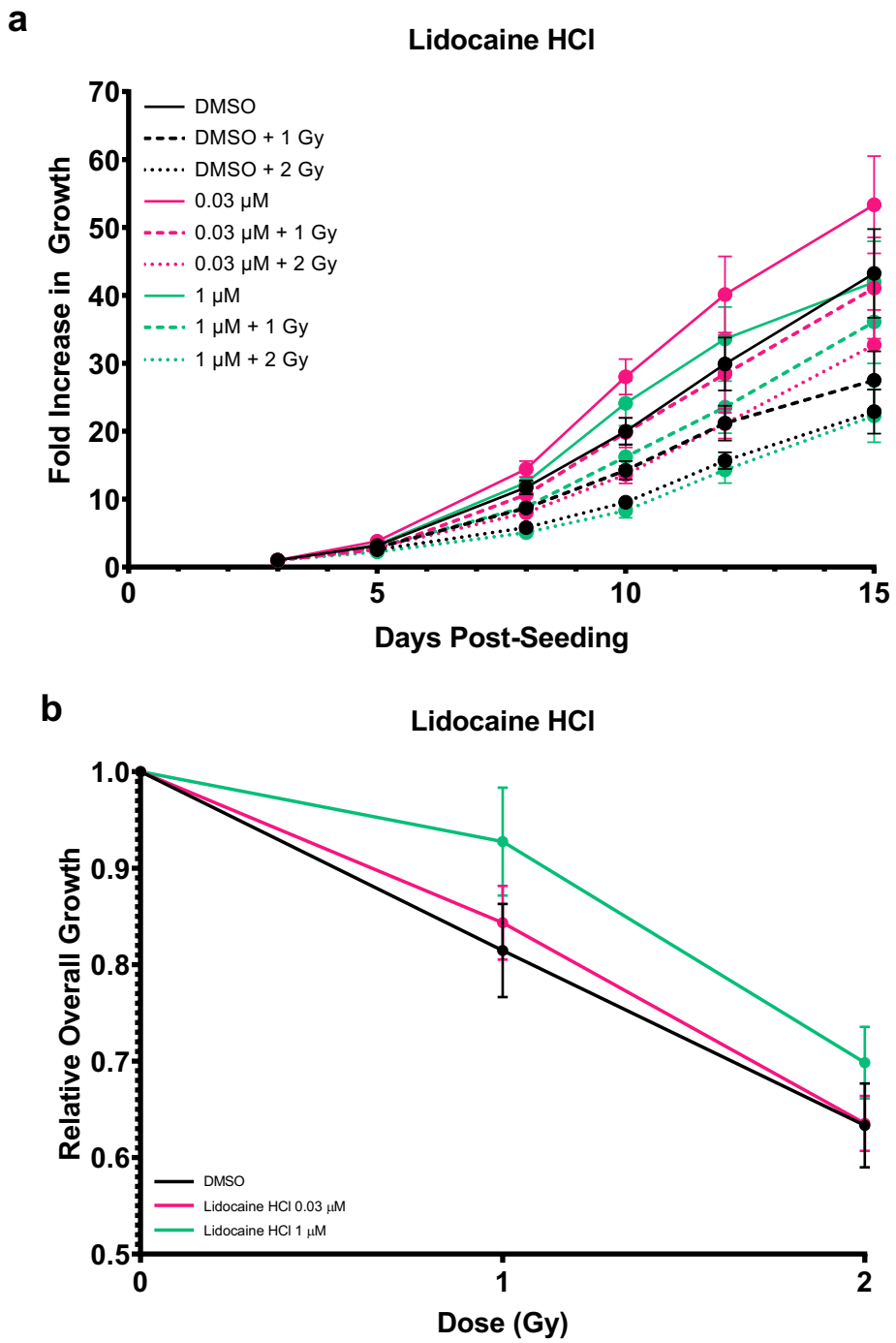

Figure 5.3: Effect of lidocaine HCl on spheroid growth

a) FaDu cells were seeded into ULA plates and incubated for 24 hours to allow spheroid formation. After this time, lidocaine HCl was added at either 0.03 µM and 1 µM. Following 24 hours of inhibitor treatment, spheroids were irradiated with either 1 Gy or 2 Gy X-rays. Images of the spheroids were captured on days 3, 5, 8, 10, 12 and 15 post-seeding, which were used to measure the fold increase in growth over time. b) Spheroid growth was also analysed as a function of X-ray dose by comparing the increase in volume on day 15 relative to day 3 for each drug-radiation combination, then normalising this to volume increase with the drug alone. All data are presented as mean ± SEM of triplicate wells and are representative of three independent experiments.

Table 5.1: Statistical significance of lidocaine HCl treatment on spheroid growth

Day	0.03 μM	0.03 μM + 1 Gy	0.03 μM + 2 Gy	1 μM	1 μM + 1 Gy	1 μM + 2 Gy
5	0.21153992	0.71285928	0.732152	0.24106104	0.90834872	0.67385212
8	0.34893746	0.69502625	0.75984541	0.67343778	0.9133153	0.97670867
10	0.13647202	0.40173528	0.76056719	0.50169061	0.53227226	0.82152742
12	0.37324364	0.8518666	0.97648129	0.65147717	0.62943251	0.82191946
15	0.77674837	0.29765355	0.9114881	0.90451681	0.28597579	0.58053382

A two-tailed t-test was used to compare various conditions of lidocaine HCl treatment with DMSO controls on FaDu spheroids. The p-values are based on triplicate wells in three independent experiments.

Lidocaine HCl was also tested in clonogenic survival assays in FaDu, A253, UM-SCC-12, UM-SCC-6, and UM-SCC-17A cell lines (figure 5.19, all p-values in table 5.4). In FaDu cells, there was very little change in survival following lidocaine HCl treatment, regardless of the dose of X-rays. In A253 cells, lidocaine HCl treatment considerably reduced SF when combined with IR, with SF values of 0.633, 0.553, and 0.278 for 1, 2 and 4 Gy respectively. At 1 and 2 Gy, this was a reduction in survival compared to DMSO-treated cells, which had SFs of 0.973 and 0.789 for each respective radiation dose. However, at 4 Gy, the SF of DMSO-treated cells dropped to 0.252, which was slightly lower than the corresponding SF after lidocaine HCl treatment. Across the whole dataset, lidocaine HCl did not cause a significant decrease in SF of A253 cells (CFAssay, table 5.4). In UM-SCC-12 cells, lidocaine HCl treated-cells had lower SFs compared to DMSO-treated cells at all doses of X-rays. The SFs for lidocaine HCl-treated cells were 0.703, 0.367 and 0.081 following 1, 2 and 4 Gy respectively, while DMSO-treated cells had respective SFs of 0.858, 0.502 and 0.120. While this suggests a slight radiosensitisation effect of the inhibitor, this was not statistically significant (CFAssay, table 5.2). In UM-SCC-17A cells, lidocaine HCl treatment resulted in an enhancement of survival at 1 Gy compared to DMSO controls, with respective SF values of 0.571 and 0.451. At 2 Gy, the SF was comparable in the two treatment conditions, while at 4 Gy

the inhibitor-treated cells had a very slight reduction in survival, with a SF value of 0.042 compared to 0.051 following DMSO treatment. Again, there was no statistical significance across this dataset (CFAssay, table 5.4). Finally, in UM-SCC-6 cells, lidocaine HCl slightly enhanced survival at 1 Gy, with a SF of 0.675 compared to a value of 0.579 for DMSO-treated cells. However, the SF at 2 Gy was lower following inhibitor treatment compared to controls, with SFs of 0.397 and 0.334 for DMSO- and lidocaine HCl-treated cells, respectively. At 4 Gy, the SFs were slightly higher in cells treated with the inhibitor. As in other cell lines, there was no statistical significance between the inhibitor and DMSO treatments (CFAssay, table 5.4). These data suggest that lidocaine HCl cannot radiosensitise HNSCC cells, regardless of cell line and dose of X-rays.

Table 5.2: Statistical significance of lidocaine HCl treatment on clonogenic survival

Cell Line	**P-value**
FaDu	0.9134
A253	0.3296
UM-SCC-12	0.7337
UM-SCC-17A	0.5884
UM-SCC-6	0.6204

The CFAssay was used to compare DMSO and lidocaine HCl treatments across 4 doses of X-rays (0-4 Gy) in 5 cell lines. The P-values are based on three independent experiments.

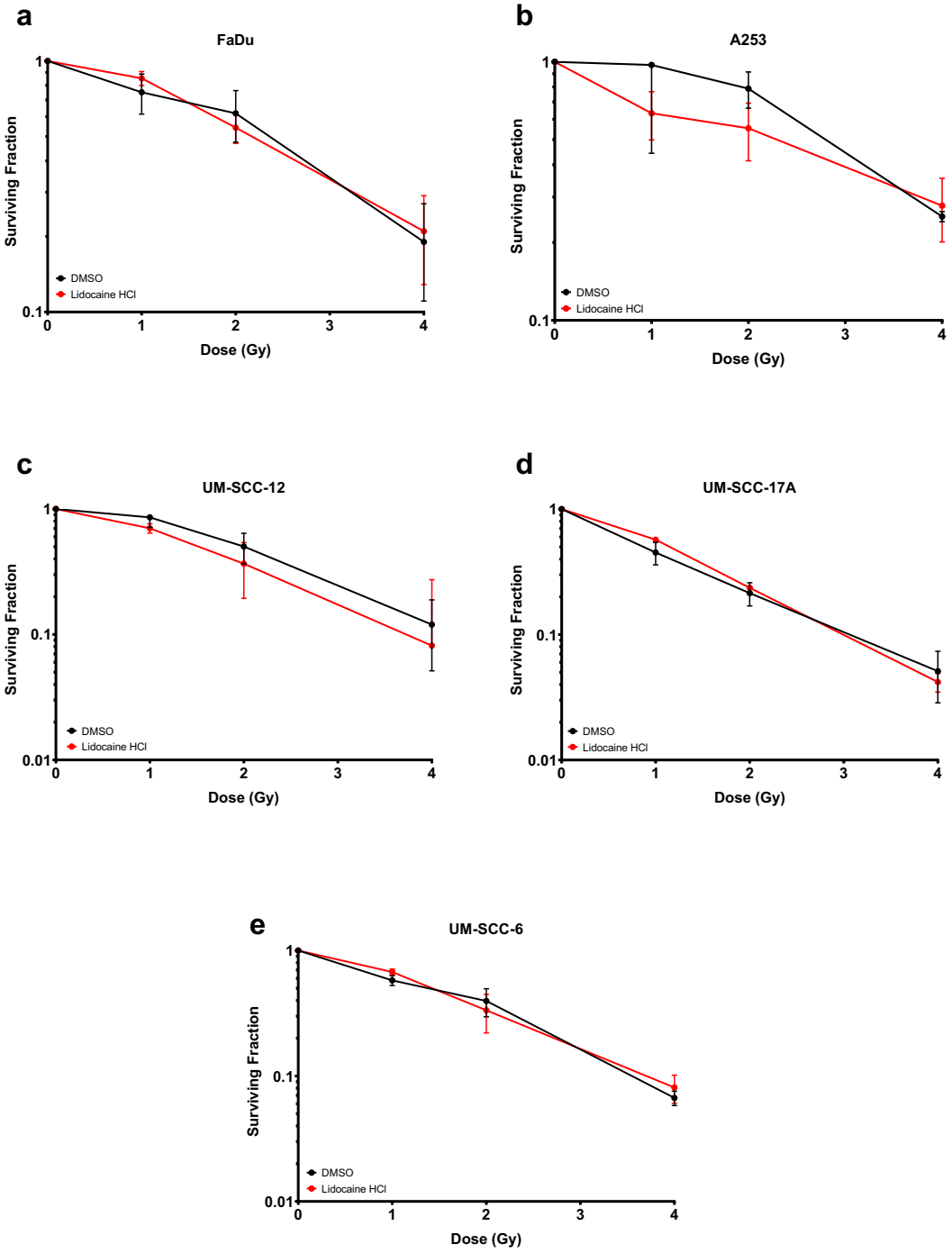

Figure 5.4: Clonogenic survival following lidocaine HCl treatment

Clonogenic survival in a) FaDu cells, b) A253 cells, c) UM-SCC-12 cells, d) UM-SCC-17A cells and e) UM-SCC-6 cells following DMSO and lidocaine HCl treatments. Cells were seeded at a density of 1000 cells per well for 0 Gy, and this was doubled for each subsequent dose of radiation. Cells were allowed to attach to the plate, then fresh media containing 0.5 µM lidocaine HCl was added. 24 hours later, plates were irradiated with 1, 2 or 4 Gy X-rays and the cells were then left for 6-10 days to allow colony formation to occur. Data is based on three independent experiments ± SEM, and statistical analysis was performed using the CFAssay.

Genistein

In spheroid assays (figure 5.20a), genistein alone at a concentration of 0.03 μM caused growth comparable to DMSO controls up to 8 days post-seeding, after which there was a slight increase compared to controls between days 8 and 10. The spheroids in the two conditions were comparable on day 12, and on day 15 there was a small but observable decrease in growth of the spheroids treated with genistein. Overall, the percentage growth following 0.03 μM genistein treatment after day 15 was 86 % relative to DMSO controls. 1 μM genistein, on the other hand, considerably enhanced spheroid growth compared to DMSO controls, particularly on days 10, 12 and 15 post-seeding. The overall percentage growth relative to controls was 113 %. In combination with 1 Gy X-rays, 0.03 μM genistein was comparable to DMSO plus 1 Gy up to 12 days post-seeding, after which inhibitor-treated spheroids grew to an overall higher level, with 122 % relative growth. Following the same trend as the unirradiated control treatment, 1 μM plus 1 Gy X-rays markedly increased spheroid growth compared to 1 Gy controls. This was evident from day 8 onwards, and by day 15 the relative percentage growth was 149 %. 0.03 μM plus 2 Gy was comparable to the 2 Gy irradiated controls at all time points, with a slight increase to a relative 105 % on day 15. 1 μM plus 2 Gy X-rays followed a similar growth trend to the spheroids treated with 2 Gy up to day 10 post-seeding. On day 12, there was a slight enhancement of growth in the spheroids treated with 1 μM plus 2 Gy X-rays, and by day 15 these spheroids had increased to an overall percentage growth of 117 % relative to the spheroids treated with DMSO plus 2 Gy. There were no statistically significant differences between genistein and DMSO treatments, regardless of X-ray dose and inhibitor concentration (*t-test*, table 5.3). I also analysed spheroid growth as a function of X-ray dose (figure 5.20b). This analysis demonstrated that genistein does not cause synergistic radiosensitivity, and at the lower

concentration of 0.03 μM, there even appears to be an increase of radioresistance.

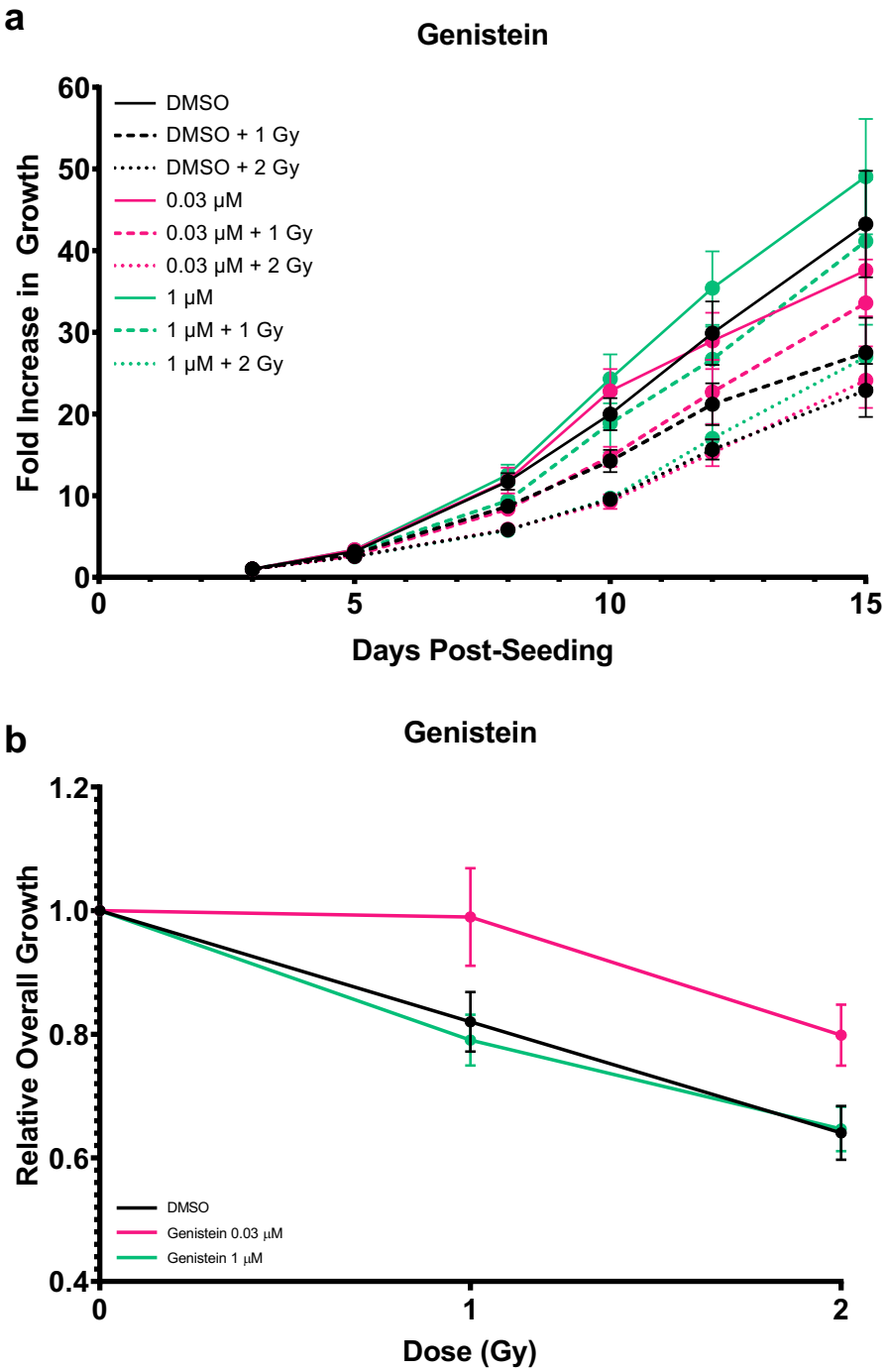

Figure 5.5: Effect of genistein on spheroid growth

a) FaDu cells were seeded into ULA plates and incubated for 24 hours to allow spheroid formation. After this time, genistein was added at either 0.03 μM and 1 μM. Following 24 hours of inhibitor treatment, spheroids were irradiated with either 1 Gy or 2 Gy X-rays. Images of the spheroids were captured on days 3, 5, 8, 10, 12 and 15 post-seeding, which were used to measure the fold increase in growth over time. b) Spheroid growth was also analysed as a function of X-ray dose by comparing the increase in volume on day 15 relative to day 3 for each drug-radiation combination, then normalising this to volume increase with the drug alone. All data are presented as mean ± SEM of triplicate wells and are representative of three independent experiments.

Table 5.3: Statistical significance of genistein treatment on spheroid growth

Day	0.03 μM	0.03 μM + 1 Gy	0.03 μM + 2 Gy	1 μM	1 μM + 1 Gy	1 μM + 2 Gy
5	0.55450575	0.70643321	0.94089792	0.5865096	0.34130247	0.80822881
8	0.95405874	0.68443756	0.93792258	0.6132709	0.53380707	0.92698124
10	0.41002129	0.77683951	0.81640677	0.24711387	0.24650336	0.88679998
12	0.85679749	0.67872882	0.83749894	0.36738794	0.26294	0.54639049
15	0.51894771	0.38677032	0.79508076	0.62215201	0.13459529	0.43735136

A two-tailed t-test was used to compare various conditions of genistein treatment with DMSO controls on FaDu spheroids. The p-values are based on triplicate wells in three independent experiments.

As with lidocaine HCl, genistein was also tested in clonogenic survival assays in FaDu, A253, UM-SCC-12, UM-SCC-6, and UM-SCC-17A cell lines (figure 5.21, all p-values in table 5.4). In FaDu cells, genistein had very little impact on colony survival in comparison to DMSO treatment at all doses of IR. At 1 Gy, DMSO-treated cells had an SF of 0.751, while cells treated with genistein had a slightly higher SF of 0.866. At both 2 and 4 Gy X-rays, genistein slightly reduced SF compared to controls, with values of 0.543 and 0.209 for the respective radiation doses. In comparison, DMSO-treated cells had SFs of 0.619 and 0.190 at 2 and 4 Gy, respectively. Across the dataset, there was no statistical significance (CFAssay, table 5.4). In A253 cells, SF following genistein treatment plus 1 Gy X-rays was slightly lower than DMSO controls, with values of 0.777 and 0.973 respectively. At 2 Gy, DMSO-treated cells had an SF of 0.788, which was higher than the SF in genistein-treated cells, which was 0.655. However, at 4 Gy, genistein appeared to increase survival, increasing the SF from 0.252 following DMSO treatment to 0.392 after inhibitor treatment. Although there was some trend towards sensitisation, there was no statistical significance across this dataset (CFAssay, table 5.4). Similarly, genistein slightly enhanced survival in UM-SCC-12 cells irradiated with 1 Gy X-rays in comparison to DMSO plus 1 Gy treatment, with SF values of 0.922 and 0.858 following genistein and DMSO treatment, respectively. However, at

doses of both 2 Gy and 4 Gy, genistein considerably reduced survival compared to controls. At 2 Gy, the SF following DMSO treatment was 0.503, while genistein-treated cells had an SF of 0.400. The difference between the treatment conditions was more evident at a radiation dose of 4 Gy, where DMSO treatment resulted in an SF of 0.120, whereas genistein treatment reduced SF to 0.073. Once again, there was no statistical significance across this dataset (CFAssay, table 5.4). In UM-SCC-17A cells, genistein enhanced survival at all doses of radiation compared to the DMSO controls. At 1, 2 and 4 Gy, genistein-treated cells had respective SF values of 0.755, 0.327 and 0.082, while DMSO treatment resulted in SFs of 0.451 at 1 Gy, 0.214 and 2 Gy and 0.051 at 4 Gy. Although this difference was not significant across the dataset (CFAssay, table 5.4), there is a trend towards enhanced radioresistance. Finally, in UM-SCC-6 cells, at a radiation dose of 1 Gy, the SF between genistein- and DMSO-treated cells was comparable, with values of 0.579 for DMSO-treated cells, and a slightly higher value of 0.626 for genistein-treated cells. An important observation here was at 2 Gy, where there was a reduction in SF following genistein treatment compared to controls, with values of 0.397 and 0.291, respectively. In fact, at this radiation dose, genistein reduced survival more than any other inhibitor tested. Interestingly, at 4 Gy X-rays, genistein considerably enhanced survival, with SFs of 0.067 and 0.209 for DMSO- and genistein-treated cells, respectively. Again, no statistical significance was observed (CFAssay, table 5.4). Taken together, these data suggest that genistein does not radiosensitise HNSCC cells to X-rays, although in A253 cells, there was a trend towards radiosensitisation at 1 Gy and 2 Gy.

Table 5.4: Statistical significance of genistein treatment on clonogenic survival

Cell Line	P-value
FaDu	0.8842
A253	0.812
UM-SCC-12	0.5696
UM-SCC-17A	0.3884
UM-SCC-6	0.3025

The CFAssay was used to compare DMSO and genistein treatments across 4 doses of X-rays (0-4 Gy) in 5 cell lines. The P-values are based on three independent experiments.

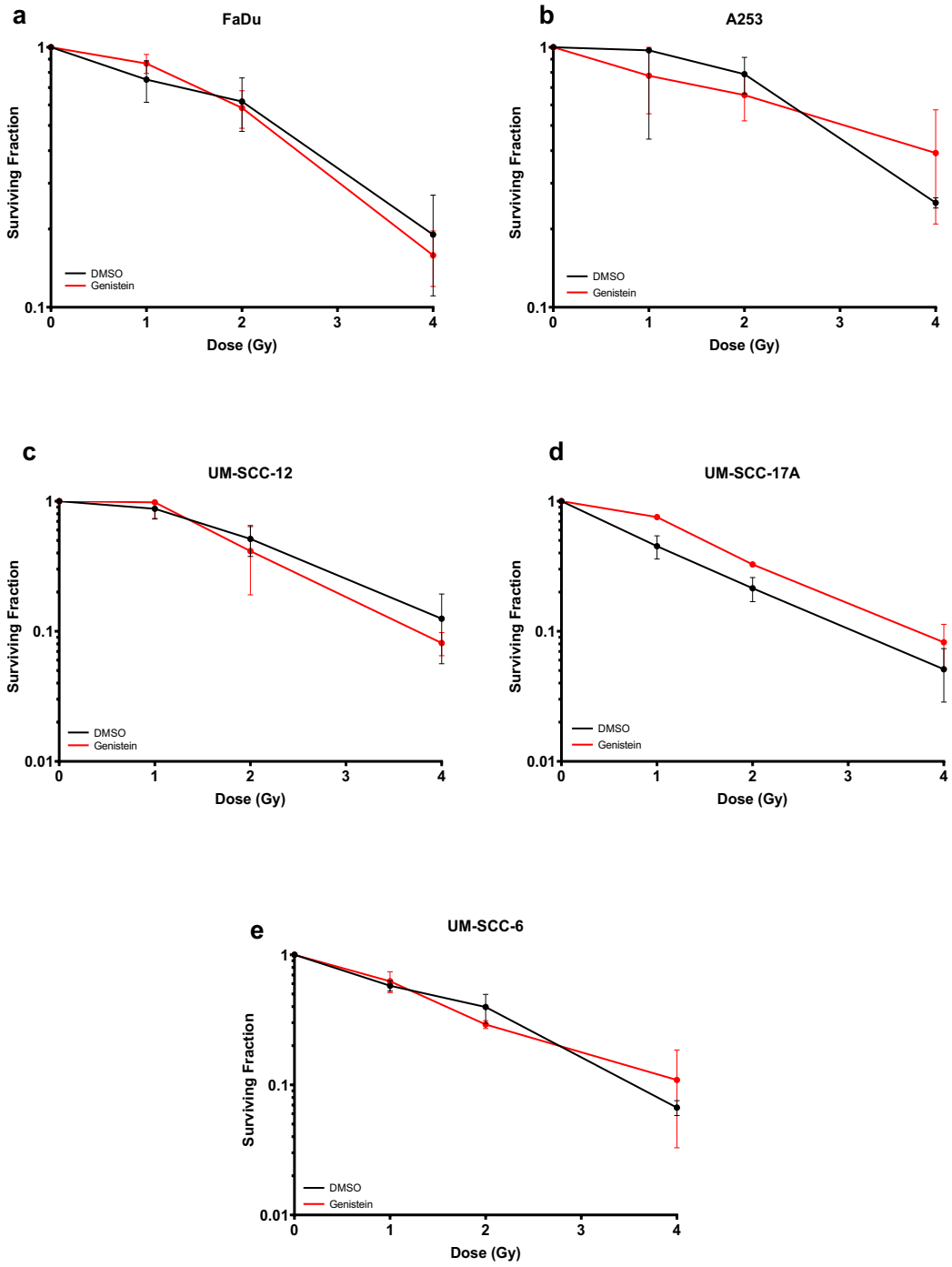

Figure 5.6: Clonogenic survival following genistein treatment

Clonogenic survival in a) FaDu cells, b) A253 cells, c) UM-SCC-12 cells, d) UM-SCC-17A cells and e) UM-SCC-6 cells following DMSO and genistein treatments. Cells were seeded at a density of 1000 cells per well for 0 Gy, and this was doubled for each subsequent dose of radiation. Cells were allowed to attach to the plate, then fresh media containing 0.5 μM genistein was added. 24 hours later, plates were irradiated with 1, 2 or 4 Gy X-rays and the cells were then left for 6-10 days to allow colony formation to occur. Data is based on three independent experiments ± SEM, and statistical analysis was performed using the CFAssay.

5.2.3. HDAC Inhibitors

Mocetinostat

In the final spheroid growth assays (figure 5.22a), 0.03 μM mocetinostat alone slightly enhanced spheroid growth relative to controls at all time points up to 12 days post-seeding. Between days 12 and 15, while the DMSO-treated spheroids continued to grow, the growth of mocetinostat-treated spheroids levelled off. At 15 days post-seeding, these spheroids grew to 89 % relative to the controls. 1 μM mocetinostat reduced spheroid growth at all time points, most starkly on days 12 and 15 post-seeding. The overall growth following 1 μM inhibitor treatment alone was 73 % relative to the controls. 0.03 μM mocetinostat seemed to have a protective effect against 1 Gy X-rays, as spheroids following this treatment grew better compared to the 1 Gy controls consistently across the experiment. Overall, these spheroids grew to 125 % relative to the spheroids treated with DMSO plus 1 Gy. Meanwhile, 1 μM mocetinostat plus 1 Gy X-rays initially seemed to be slightly reducing spheroid growth, but on days 12 and 15 post-seeding had almost identical growth to the DMSO plus 1 Gy controls, with the overall relative growth being 101 %. In combination with 2 Gy X-rays, 0.03 μM caused a very slight reduction in spheroid growth compared to DMSO; however, the relative overall growth was only lowered to 94 % after day 15. In contrast, from 8 days post-seeding onwards, 1 μM mocetinostat plus 2 Gy X-rays reduced spheroid growth compared to the irradiated controls. This difference was statistically significant on days 8, 10 and 12, with p-values of < 0.05 (*t-test,* table 5.5), and most evident on days 10, 12 and 15. Although a statistical significance was observed, by the end of the experiment the treatment had only reduced overall spheroid growth to 64 %, which was greater than the 50 % cut-off used throughout this research. Moreover, when looking at the change in spheroid

growth relative to IR dose for each condition (figure 5.22b), it became clear that mocetinostat works additively with IR to reduce growth, rather than working synergistically.

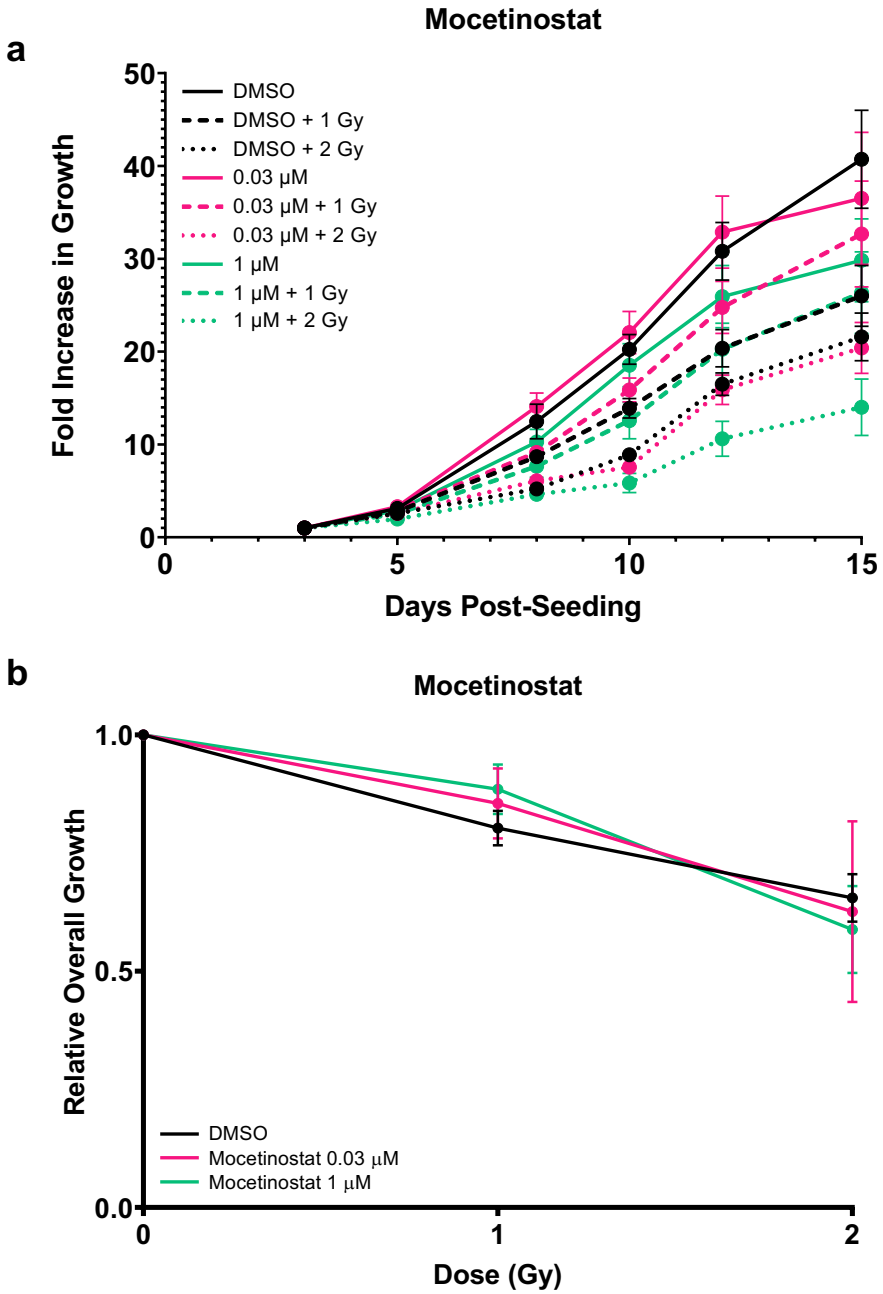

Figure 5.7: Effect of mocetinostat on spheroid growth

a) FaDu cells were seeded into ULA plates and incubated for 24 hours to allow spheroid formation. After this time, mocetinostat was added at either 0.03 μM and 1 μM. Following 24 hours of inhibitor treatment, spheroids were irradiated with either 1 Gy or 2 Gy X-rays. Images of the spheroids were captured on days 3, 5, 8, 10, 12 and 15 post-seeding, which were used to measure the fold increase in growth over time. b) Spheroid growth was also analysed as a function of X-ray dose by comparing the increase in volume on day 15 relative to day 3 for each drug-radiation combination, then normalising this to volume increase with the drug alone. All data are presented as mean ± SEM of triplicate wells and are representative of three independent experiments.

Table 5.5: Statistical significance of mocetinostat treatment on spheroid growth

Day	0.03 μM	0.03 μM + 1 Gy	0.03 μM + 2 Gy	1 μM	1 μM + 1 Gy	1 μM + 2 Gy
5	0.412634	0.308769	0.957516	0.96293	0.910247	0.157694
8	0.740122	0.596569	0.8983	0.117245	0.928804	0.015742
10	0.740122	0.249234	0.409909	0.549674	0.972242	0.014395
12	0.681945	0.217074	0.760574	0.556883	0.517197	0.040842
15	0.896864	0.320337	0.892221	0.237248	0.433409	0.232713

A two-tailed t-test was used to compare various conditions of mocetinostat treatment with DMSO controls on FaDu spheroids. The p-values are based on triplicate wells in three independent experiments, and significant values are highlighted.

Mocetinostat was also tested in clonogenic survival assays in FaDu, A253, UM-SCC-12, UM-SCC-6, and UM-SCC-17A cell lines (figure 5.23, all p-values in table 5.6). In FaDu clonogenics, mocetinostat only had slight impact on survival. At a dose of 1 Gy X-rays, mocetinostat actually reduced survival more than any other inhibitor, however only to a SF of 0.609 compared to DMSO treated cells, which had a SF of 0.751. At 2 Gy, the difference between the two treatment conditions was even less, with SFs of 0.619 and 0.574 for DMSO- and mocetinostat-treated cells, respectively. At 4 Gy, there was an observable difference in survival following inhibitor treatment. The cells treated with mocetinostat had a SF of 0.125, while DMSO treatment resulted in a SF of 0.190. However, the difference between the two dose response curves was not significant (CFAssay, table 5.6). In A253 cells, mocetinostat markedly reduced survival at both 1 and 2 Gy compared to controls. The SF of mocetinostat-treated cells was 0.419 and 0.367 for 1 and 2 Gy respectively, while in DMSO-treated cells these values were 0.973 and 0.788. At 4 Gy, there was much less difference between the survival following either treatment condition, with SFs of 0.252 and 0.245 for DMSO and mocetinostat, respectively. These differences, however, were not statistically significant (CFAssay, table 5.6). In UM-SCC-12 cells, mocetinostat-treated cells had smaller SF values at each radiation dose than DMSO-treated cells. At 1, 2 and

4 Gy, mocetinostat treatment resulted in SFs of 0.648, 0.348 and 0.089 for each respective dose. In contrast, DMSO-treated cells had SFs of 0.858, 0.503 and 0.120, respectively. While observable, these differences were not statistically significant (CFAssay, table 5.6). In UM-SCC-17A cells, at doses of 1 Gy and 2 Gy X-rays, mocetinostat-treated cells had a decrease in survival relative to controls, but these differences were not extensive. Mocetinostat treatment resulted in SFs of 0.378 and 0.159 at 1 and 2 Gy, respectively, while DMSO caused SFs of 0.451 and 0.214. However, at 4 Gy, the SF of cells treated with mocetinostat was slightly higher than DMSO, with SFs of 0.064 and 0.051, respectively. Across the dataset, there was no significant difference in survival (CFAssay, table 5.6). Finally, in UM-SCC-6 cells, the SF at 1 Gy in mocetinostat-treated cells was slightly higher than controls, with values of 0.579 following DMSO treatment and 0.681 following mocetinostat. At 2 Gy, the survival was slightly lower in cells treated with mocetinostat, with SFs of 0.397 and 0.310 for control and treated cells, respectively. However, at 4 Gy, mocetinostat appeared to considerably enhance survival, as the cells had a SF of 0.129 compared to 0.068 in DMSO-treated cells. However, there was no statistical significance (CFAssay, table 5.6). Overall, mocetinostat appears to be exerting a slight radiosensitising effect in all cell lines except UM-SCC-6, however not to a significant degree.

Table 5.6: Statistical significance of mocetinostat treatment on clonogenic survival

Cell Line	**P-value**
FaDu	0.8206
A253	0.1645
UM-SCC-12	0.651
UM-SCC-17A	0.6981
UM-SCC-6	0.06031

The CFAssay was used to compare DMSO and mocetinostat treatments across 4 doses of X-rays (0-4 Gy) in 5 cell lines. The P-values are based on three independent experiments.

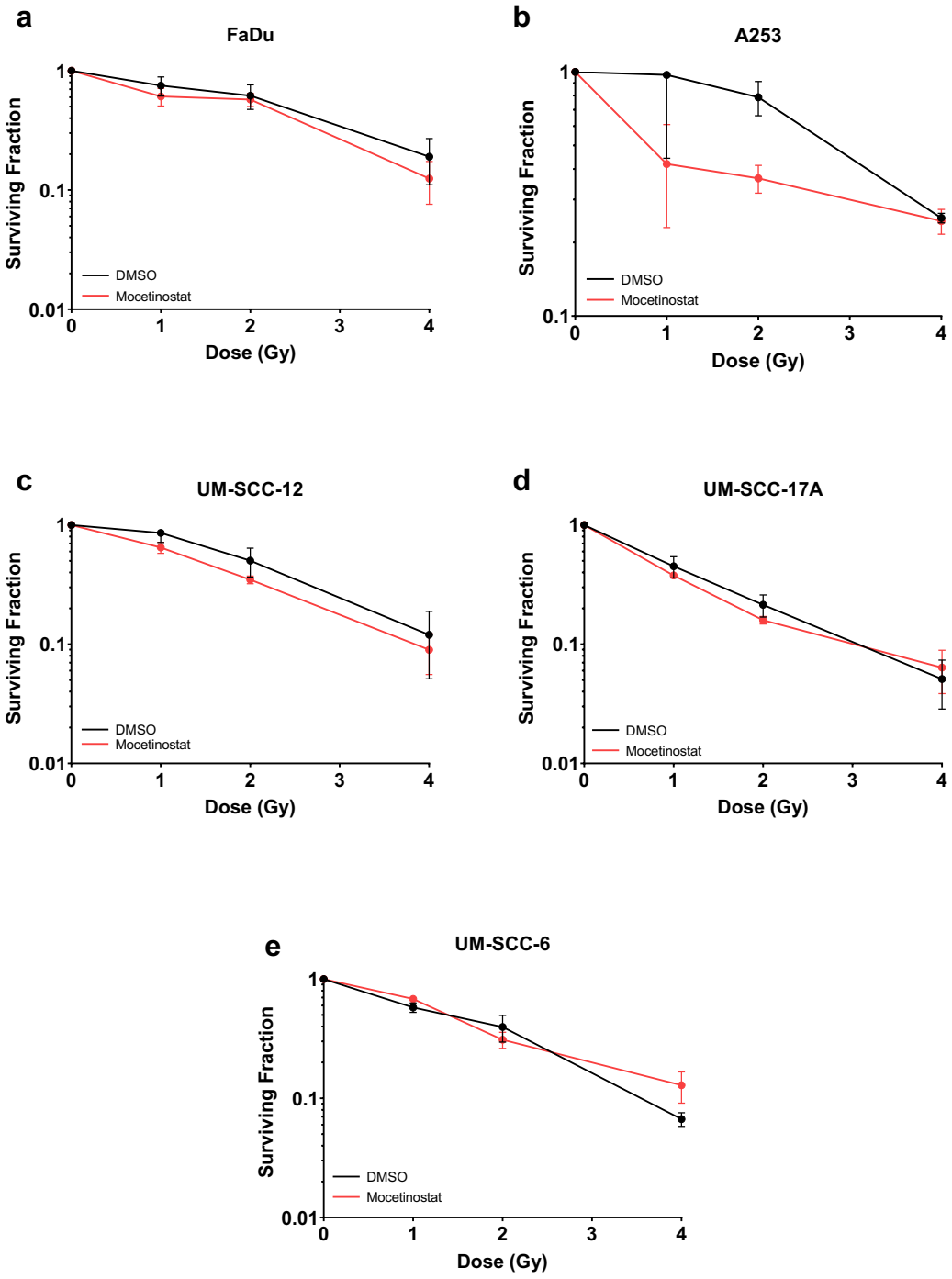

Figure 5.8: Clonogenic survival following mocetinostat treatment

Clonogenic survival in a) FaDu cells, b) A253 cells, c) UM-SCC-12 cells, d) UM-SCC-17A cells and e) UM-SCC-6 cells following DMSO and mocetinostat treatments. Cells were seeded at a density of 1000 cells per well for 0 Gy, and this was doubled for each subsequent dose of radiation. Cells were allowed to attach to the plate, then fresh media containing 0.5 μM mocetinostat was added. 24 hours later, plates were irradiated with 1, 2 or 4 Gy X-rays and the cells were then left for 6-10 days to allow colony formation to occur. Data is based on three independent experiments ± SEM, and statistical analysis was performed using the CFAssay.

CUDC-101

In spheroid experiments (figure 5.24a), CUDC-101 alone had very little impact on growth compared to the DMSO controls. Growth following 0.03 μM CUDC-101 alone was comparable – in fact very slightly higher – than controls, until day 15, when there was a reduction in overall growth. 1 μM CUDC-101 alone, on the other hand, markedly reduced spheroid growth in comparison to DMSO treatment at all time points, and by day 15, the overall growth relative to DMSO controls was 94 % and 84 % following 0.03 μM and 1 μM treatment, respectively. 0.03 μM CUDC-101 plus 1 Gy X-rays enhanced spheroid growth compared to controls at all time points, resulting in an overall growth of 122 % relative to spheroids treated with DMSO plus 1 Gy. 1 μM CUDC-101, similar to the drug alone, reduced growth compared to the irradiated controls, but only up to 12 days post-seeding, after which there was an increase to a relative 100 % compared to controls. In combination with 2 Gy, 0.03 μM CUDC-101 was comparable to the irradiated controls at each time point, having no impact on overall growth – the percentage growth relative to DMSO plus 2 Gy was in fact 100 %. 1 μM CUDC-101 plus 2 Gy was comparable to the irradiated controls until 8 days post-seeding, after which it observably reduced spheroid growth, to 68 % relative to the X-ray only controls on day 15. The difference between spheroids treated with DMSO plus 2 Gy and 1 μM CUDC-101 plus 2 Gy was statistically significant on days 8 and 10 post seeding, with p-values of < 0.05 (*t-test*, table 5.7). When examining the overall change in spheroid growth relative to radiation dose following either 0.03 μM or 1 μM CUDC-101 treatment (figure 5.24b), at the higher concentration of 1 μM there was a noticeable reduction in growth relative to the DMSO controls - this is a clear indication that at 1 μM, CUDC-101 is working synergistically with IR in reducing spheroid growth.

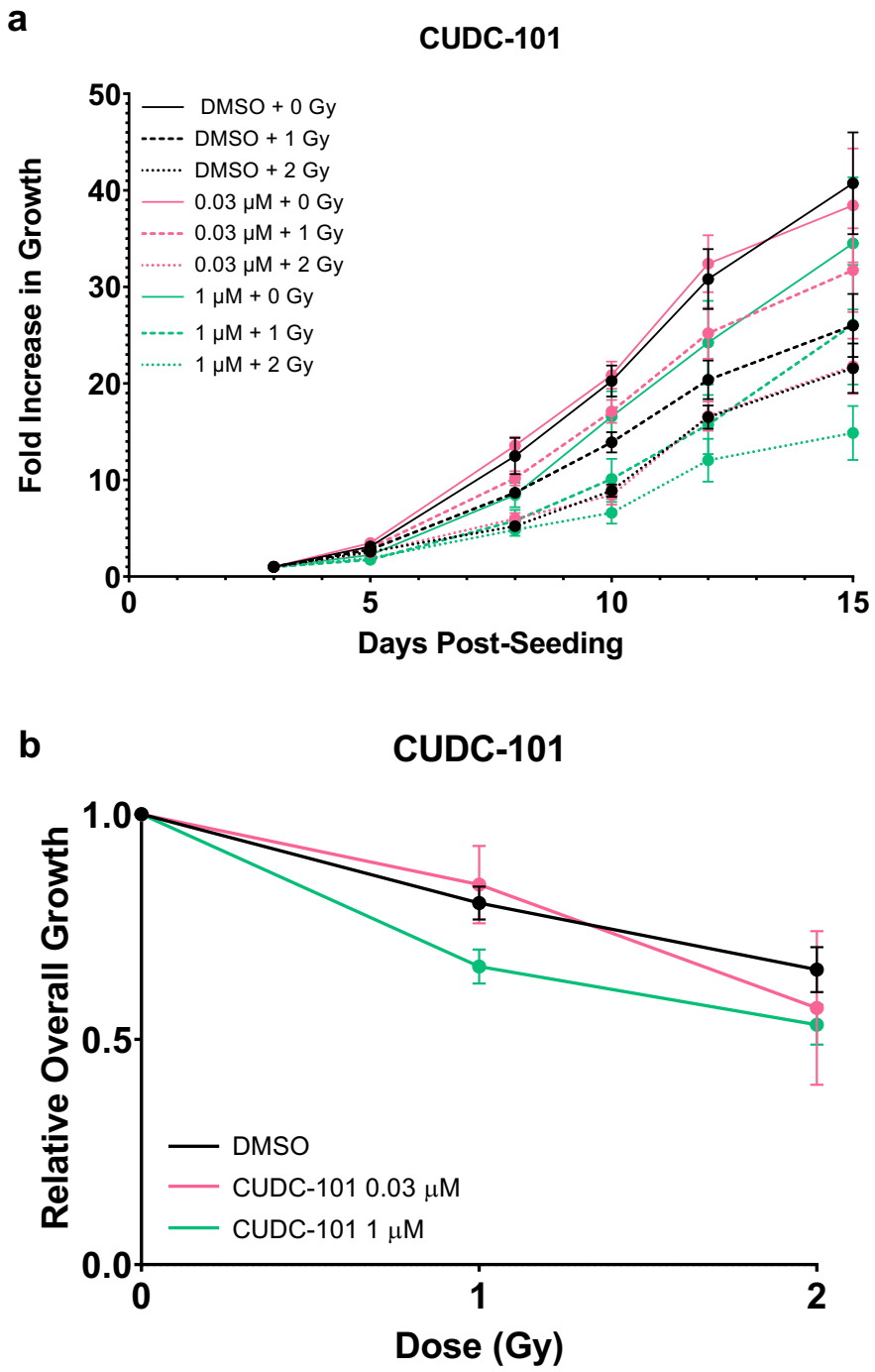

Figure 5.9: Effect of CUDC-101 on spheroid growth

a) FaDu cells were seeded into ULA plates and incubated for 24 hours to allow spheroid formation. After this time, CUDC-101 was added at either 0.03 µM and 1 µM. Following 24 hours of inhibitor treatment, spheroids were irradiated with either 1 Gy or 2 Gy X-rays. Images of the spheroids were captured on days 3, 5, 8, 10, 12 and 15 post-seeding, which were used to measure the fold increase in growth over time. b) Spheroid growth was also analysed as a function of X-ray dose by comparing the increase in volume on day 15 relative to day 3 for each drug-radiation combination, then normalising this to volume increase with the drug alone. All data are presented as mean ± SEM of triplicate wells and are representative of three independent experiments.

Table 5.7: Statistical significance of CUDC-101 treatment on spheroid growth

Day	0.03 μM	0.03 μM + 1 Gy	0.03 μM + 2 Gy	1 μM	1 μM + 1 Gy	1 μM + 2 Gy
5	0.1647838	0.419389	0.002126	0.065686	0.00145	0.08261
8	0.530542	0.107326	0.796399	0.018715	0.031281	0.01263
10	0.530542	0.055425	0.868178	0.244076	0.125562	0.033398
12	0.713276	0.159265	0.952465	0.399695	0.203267	0.102995
15	0.9079212	0.303199	0.604402	0.703292	0.975815	0.131578

A two-tailed t-test was used to compare various conditions of CUDC-101 treatment with DMSO controls on FaDu spheroids. The p-values are based on triplicate wells in three independent experiments, and significant values are highlighted.

CUDC-101 was also tested for its effect on survival in clonogenic assays using FaDu, A253, UM-SCC-12, UM-SCC-17A, UM-SCC-6 and UM-SCC-11b cells (figure 5.25, all p-values in table 5.8). In FaDu cells, there was little difference between the survival of DMSO- and CUDC-101-treated cells at 1 Gy and 2 Gy, with a slight decrease at 2 Gy. The SF values following CUDC-101 treatment were 0.778 and 0.535 at 1 and 2 Gy respectively, while DMSO-treated cells had values of 0.751 and 0.619. However, at 4 Gy, there was a dramatically reduced survival of FaDu cells treated with CUDC-101 compared to cells treated with DMSO. The SF following DMSO treatment was 0.190, and in comparison, the CUDC-101-treated cells had a SF of 0.057. This was a statistically significant difference, with a p-value of 0.04104 (CFAssay, table 5.8). In A253 cells, CUDC-101 markedly reduced cell survival at 1 Gy and 2 Gy, with SF values of 0.721 and 0.419 for each respective dose. In comparison, DMSO-treated cells had SFs of 0.973 and 0.788 at 1 Gy and 2 Gy, respectively. At 4 Gy, the SFs were remarkably similar, with values of 0.252 following DMSO treatment and 0.250 following CUDC-101. Despite the observable difference at 1 Gy and 2 Gy, the overall results of A253 clonogenics were not statistically significant (CFAssay, table 5.8). In UM-SCC-12 cells, survival following CUDC-101 treatment was comparable to controls at a dose of 1 Gy X-rays, with SFs of 0.858 for controls and 0.838 for CUDC-101. At 2 Gy and 4 Gy, CUDC-101 treatment slightly

reduced survival compared to controls, however not to a considerable nor statistically significant degree (CFAssay, table 5.8). The relative SF values for CUDC-101-treated cells at 2 and 4 Gy were 0.348 and 0.090, while the cells treated with DMSO had respective SFs of 0.503 and 0.120. In UM-SCC-17A cells, survival following both treatments was comparable at a dose of 1 Gy X-rays, with SFs of 0.451 and 0.481 following DMSO and CUDC-101 treatment, respectively. At both 2 and 4 Gy, CUDC-101 markedly reduced SF compared to DMSO. Following CUDC-101 treatment, the SF at 2 Gy and 4 Gy was 0.117 and 0.040 respectively, while the SF following DMSO treatment was 0.214 and 0.051 at 2 and 4 Gy, respectively. In spite of these considerable differences, there was no statistical significance observed for this cell line (CFAssay, table 5.8). In contrast to all other results for this inhibitor, I observed an enhancement of growth following CUDC-101 treatment in UM-SCC-6 cells at all doses of IR. At 1 Gy, CUDC-101 actually promoted survival relative to the 0 Gy cells, with an SF of 1.029. In comparison, DMSO-treated cells had an SF of 0.579 at 1 Gy. At 2 Gy, the SF values were 0.397 an 0.539 following DMSO and CUDC-101 treatment, respectively, while at 4 Gy the values were 0.067 and 0.111. However, there was no statistical significance observed (CFAssay, table 5.8). CUDC-101 did appear to be acting as a radiosensitiser in *p53-mut* cell lines (FaDu; A253; UM-SCC-12), although it is worth noting there was only statistical significance in FaDu cells, and there seemed to be some kind of response in *p53-WT* UM-SCC-17A cells, and thus the effect may be dependent on factors other than p53 status. CUDC-101 was also tested in another *p53-mut* cell line, UM-SCC-11b, to gain a deeper insight into the effects of p53. However, CUDC-101 appeared to enhance survival compared to controls in this cell line at all doses of X-rays, with SF values of 0.746, 0.322 and 0.098 at 1, 2 and 4 Gy respectively. Meanwhile, the DMSO-treated cells had SF values of 0.539, 0.275 and 0.082 for each respective dose. Overall, these data suggest that CUDC-101 does have radiosensitising potential in FaDu, A253, UM-SCC-12

and UM-SCC-17A cells, although only to a significant degree in FaDu (CFAssay, table 5.8).

Table 5.8: Statistical significance of CUDC-101 treatment on clonogenic survival

Cell Line	**CUDC-101**
FaDu	0.04104
A253	0.5328
UM-SCC-12	0.6052
UM-SCC-17A	0.4828
UM-SCC-6	0.9308
UM-SCC-11b	0.6461

The CFAssay was used to compare DMSO and CUDC-101 treatments across 4 doses of X-rays (0-4 Gy) in 5 cell lines. The P-values are based on three independent experiments. Statistically significant results are highlighted.

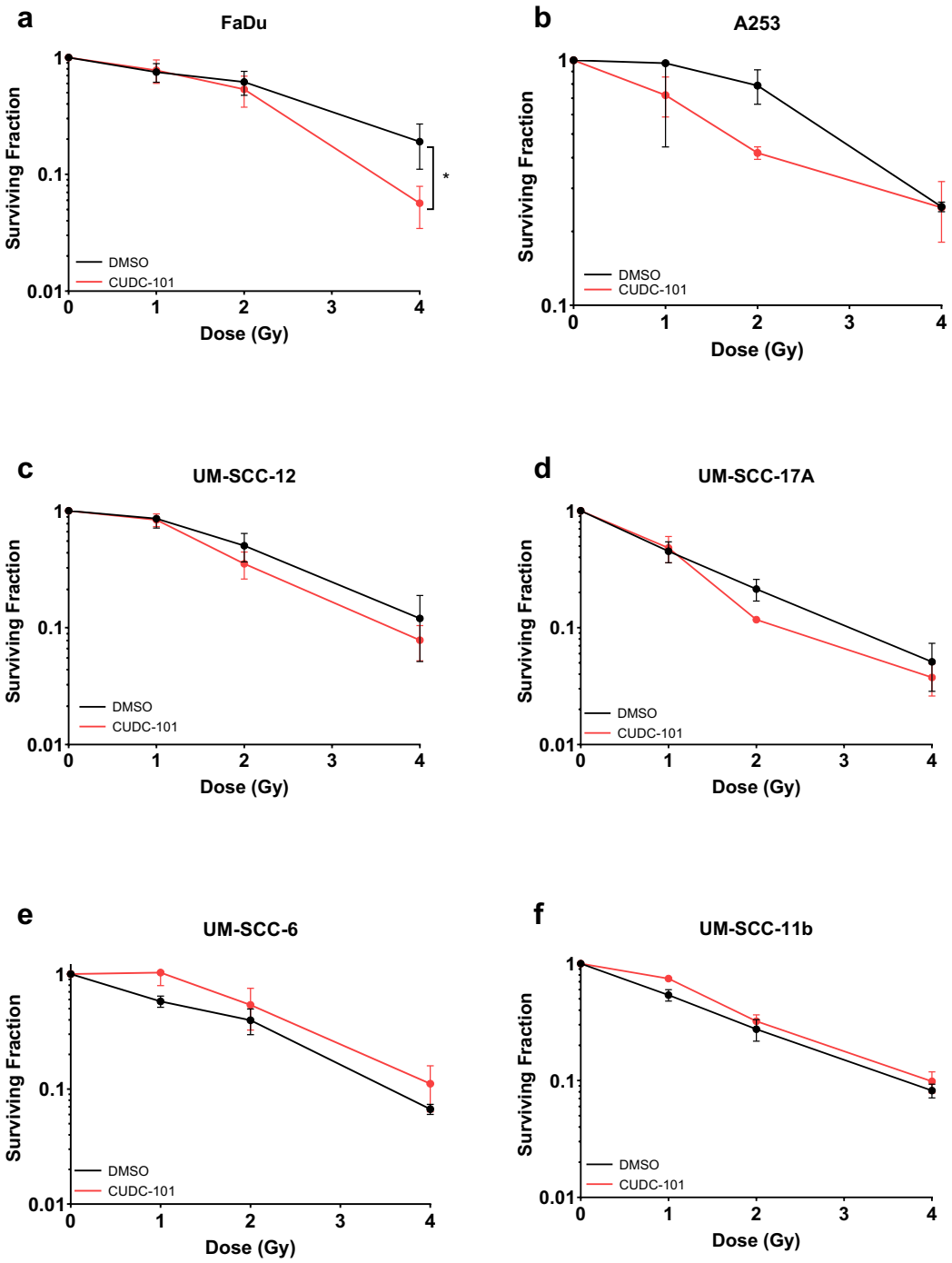

Figure 5.10: Clonogenic survival following CUDC-101 treatment

Clonogenic survival in a) FaDu cells, b) A253 cells, c) UM-SCC-12 cells, d) UM-SCC-17A cells e) UM-SCC-6 cells and f) UM-SCC-11b cells following DMSO and CUDC-101 treatments. Cells were seeded at a density of 1000 cells per well for 0 Gy, and this was doubled for each subsequent dose of radiation. Cells were allowed to attach to the plate, then fresh media containing 0.5 μM CUDC-101 was added. 24 hours later, plates were irradiated with 1, 2 or 4 Gy X-rays and the cells were then left for 6-10 days to allow colony formation to occur. Data is based on three independent experiments ± SEM, and statistical analysis was performed using the CFAssay (* = $p < 0.05$).

Pracinostat

In spheroid experiments (figure 5.26a), treatment with 0.03 μM pracinostat slightly increased spheroid growth at all time points post-seeding compared to controls, with an overall growth of 102 % relative to the spheroids treated with DMSO. In contrast, 1 μM alone considerably reduced growth at all time points, reducing the overall growth to 79 % relative to the DMSO controls. In combination with 1 Gy X-rays, 0.03 μM pracinostat enhanced spheroid growth compared to the spheroids treated with DMSO plus 1 Gy. In fact, the growth was more comparable to unirradiated spheroids treated with 1 μM pracinostat, particularly on days 8 and 10 post-seeding. By day 15, the overall growth following 0.03 μM plus 1 Gy was 132 % relative to controls. 1 μM pracinostat plus 1 Gy did reduce growth compared to the irradiated controls, but not to a dramatic extent. By day 15, the growth of both treatments was almost identical, with a relative overall growth of 97 %. As expected, 0.03 μM pracinostat plus 2 Gy X-rays did not reduce spheroid growth compared to the irradiated controls. The growth between the two conditions was comparable, particularly on day 10 post-seeding, and slightly higher following pracinostat treatment on days 12 and 15. The overall growth of the combination treatment relative to the irradiated controls was 115 %. In contrast, 1 μM pracinostat plus 2 Gy X-rays significantly reduced spheroid growth compared to the irradiated controls, notably on days 10, 12 and 15 post-seeding. The difference between DMSO plus 2 Gy and 1 μM pracinostat plus 2 Gy was statistically significant on days 8, 10 and 12 post-seeding, with p-values < 0.05 on days 8 and 10, and < 0.01 on day 12 (*t-test*, table 5.9). When analysing spheroid growth relative to the X-ray dose (figure 5.26b), it appears that pracinostat does radiosensitise FaDu spheroids at 1 μM, however, does not work in a synergistic manner with the IR and instead appears to be working additively.

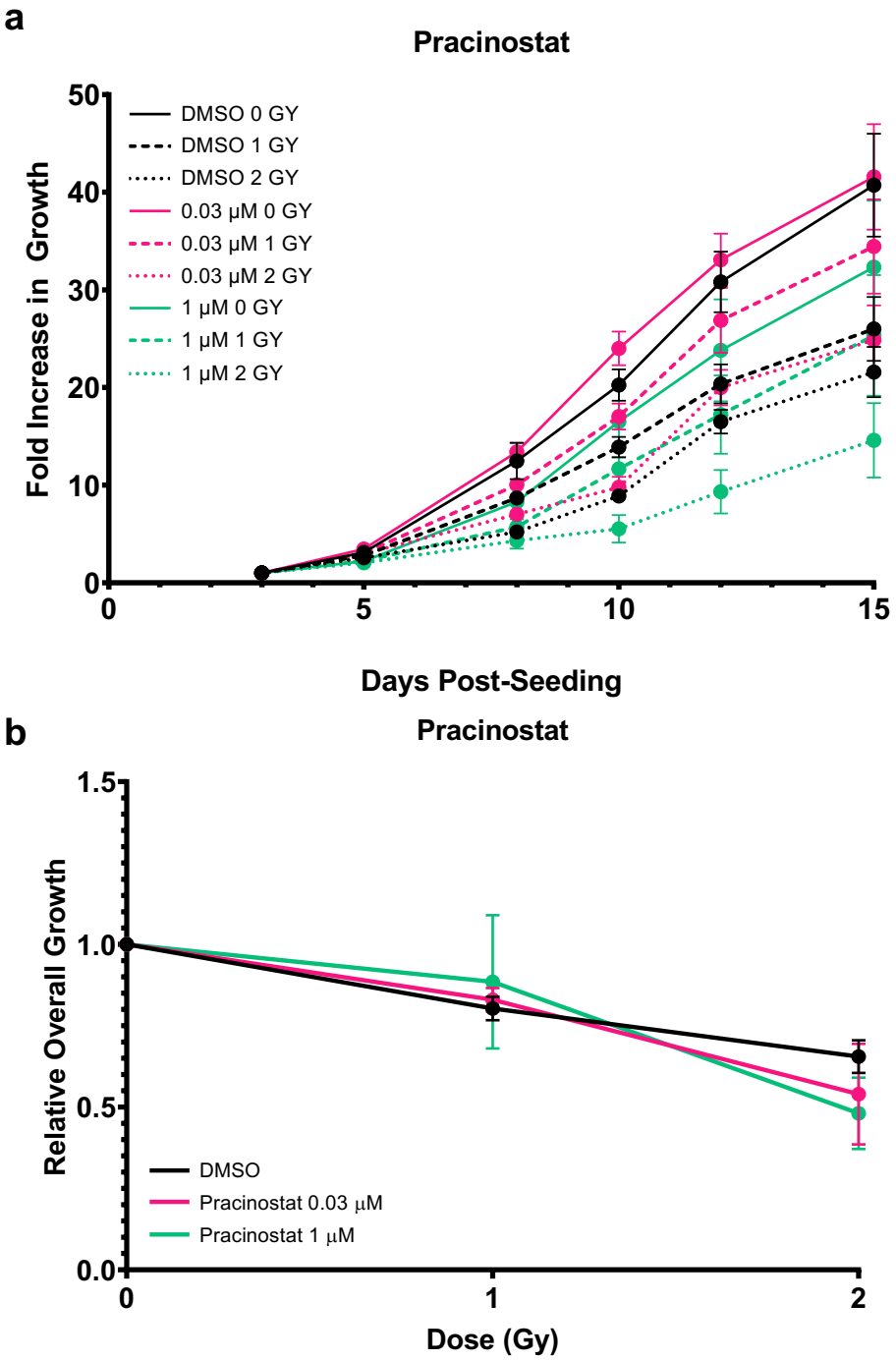

Figure 5.11: Effect of pracinostat on spheroid growth

a) FaDu cells were seeded into ULA plates and incubated for 24 hours to allow spheroid formation. After this time, pracinostat was added at either 0.03 μM and 1 μM. Following 24 hours of inhibitor treatment, spheroids were irradiated with either 1 Gy or 2 Gy X-rays. Images of the spheroids were captured on days 3, 5, 8, 10, 12 and 15 post-seeding, which were used to measure the fold increase in growth over time. b) Spheroid growth was also analysed as a function of X-ray dose by comparing the increase in volume on day 15 relative to day 3 for each drug-radiation combination, then normalising this to volume increase with the drug alone. All data are presented as mean ± SEM of triplicate wells and are representative of three independent experiments.

Table 5.9: Statistical significance of pracinostat treatment on spheroid growth

Day	0.03 μM	0.03 μM + 1 Gy	0.03 μM + 2 Gy	1 μM	1 μM + 1 Gy	1 μM + 2 Gy
5	0.133205	0.182758	0.123585	0.071673	0.120715	0.129321
8	0.482013	0.130822	0.244306	0.031308	0.020843	0.011002
10	0.482013	0.07883	0.169487	0.361461	0.443102	0.014702
12	0.585303	0.108384	0.126496	0.416711	0.506611	0.00994
15	0.562283	0.161549	0.234793	0.514624	0.943016	0.144848

A two-tailed t-test was used to compare various conditions of pracinostat treatment with DMSO controls on FaDu spheroids. The p-values are based on triplicate wells in three independent experiments, and significant values are highlighted.

Pracinostat was also examined in clonogenic assays to test its effect on cell survival (figure 5.27, all p-values in table 5.10). In FaDu cells, pracinostat slightly enhanced survival when combined with 1 Gy X-rays, with an SF of 0.924. DMSO-treated cells had an SF of 0.751 at the same IR dose. At 2 Gy, the survival was comparable, with SF values of 0.619 and 0.565 following DMSO and pracinostat treatment respectively. However, pracinostat reduced cell survival at a radiation dose of 4 Gy, bringing the SF down to 0.019 compared to DMSO, which resulted in an SF of 0.190. Using the CFAssay statistical analysis, this difference was statistically significant, with a p-value of 0.00231. In A253 cells, pracinostat did reduce survival at both 1 Gy and 2 Gy, however by 4 Gy the growth was comparable to the DMSO controls. The SF values following pracinostat treatment were 0.633, 0.434 and 0.247 for 1, 2 and 4 Gy respectively, while DMSO treatment resulted in values of 0.973, 0.788 and 0.252 at each dose. While observable, these differences were not statistically significant (CFAssay, table 5.10). Similarly, pracinostat appeared to slightly reduce survival in UM-SCC-12 cells at all doses of IR. Following DMSO treatment, the SF was 0.858, 0.503 and 0.120 for doses of 1, 2 and 4 Gy respectively. In comparison, pracinostat-treated cells had values of 0.690, 0.335 and 0.092. As in the A253 cells, these differences were not statistically

significant (CFAssay, table 5.10). In contrast, pracinostat mildly enhanced survival in UM-SCC-17A cells at IR doses of 1 Gy and 2 Gy. At 1 Gy, the SFs were 0.451 and 0.587 following either DMSO or pracinostat treatment respectively, while at 2 Gy the values were more similar, at 0.214 following DMSO and 0.266 following pracinostat. Pracinostat though, did actually reduce survival of UM-SCC-17A cells at 4 Gy, with SFs of 0.051 and 0.238 for DMSO and pracinostat, respectively. However, the differences were not statistically significant (CFAssay, table 5.10). In UM-SCC-6 cells, pracinostat enhanced survival at all doses of IR, most notably at 4 Gy. For pracinostat-treated cells, the SF values were 0.915, 0.429 and 0.165 for 1, 2 and 4 Gy, respectively. Meanwhile, DMSO-treated cells had SFs of 0.579. 0.397 and 0.067 at the respective radiation doses. Once again, no statistical significance was observed (CFAssay, table 5.10). As with CUDC-101, pracinostat was also investigated for its effect in UM-SCC-11b cells. At 1 Gy, the SFs were almost identical between the treatment conditions, with values of 0.539 and 0.547 for DMSO and pracinostat, respectively. However, pracinostat markedly reduced cell survival at both 2 and 4 Gy, with SF values of 0.152 and 0.035 for each radiation dose, respectively, while DMSO-treated cells had values of 0.275 and 0.082. This difference was statistically significant, with a p-value of 0.01991. Overall, these data suggest that pracinostat has strong potential as a radiosensitiser for HNSCC, albeit in a cell line-dependent manner.

Table 5.10: Statistical significance of pracinostat treatment on clonogenic survival

Cell Line	**Pracinostat**
FaDu	0.00231
A253	0.5391
UM-SCC-12	0.717
UM-SCC-17A	0.2662
UM-SCC-6	0.8564
UM-SCC-11b	0.01991

The CFAssay was used to compare DMSO and pracinostat treatments across 4 doses of X-rays (0-4 Gy) in 5 cell lines. The P-values are based on three independent experiments. Statistically significant results are highlighted.

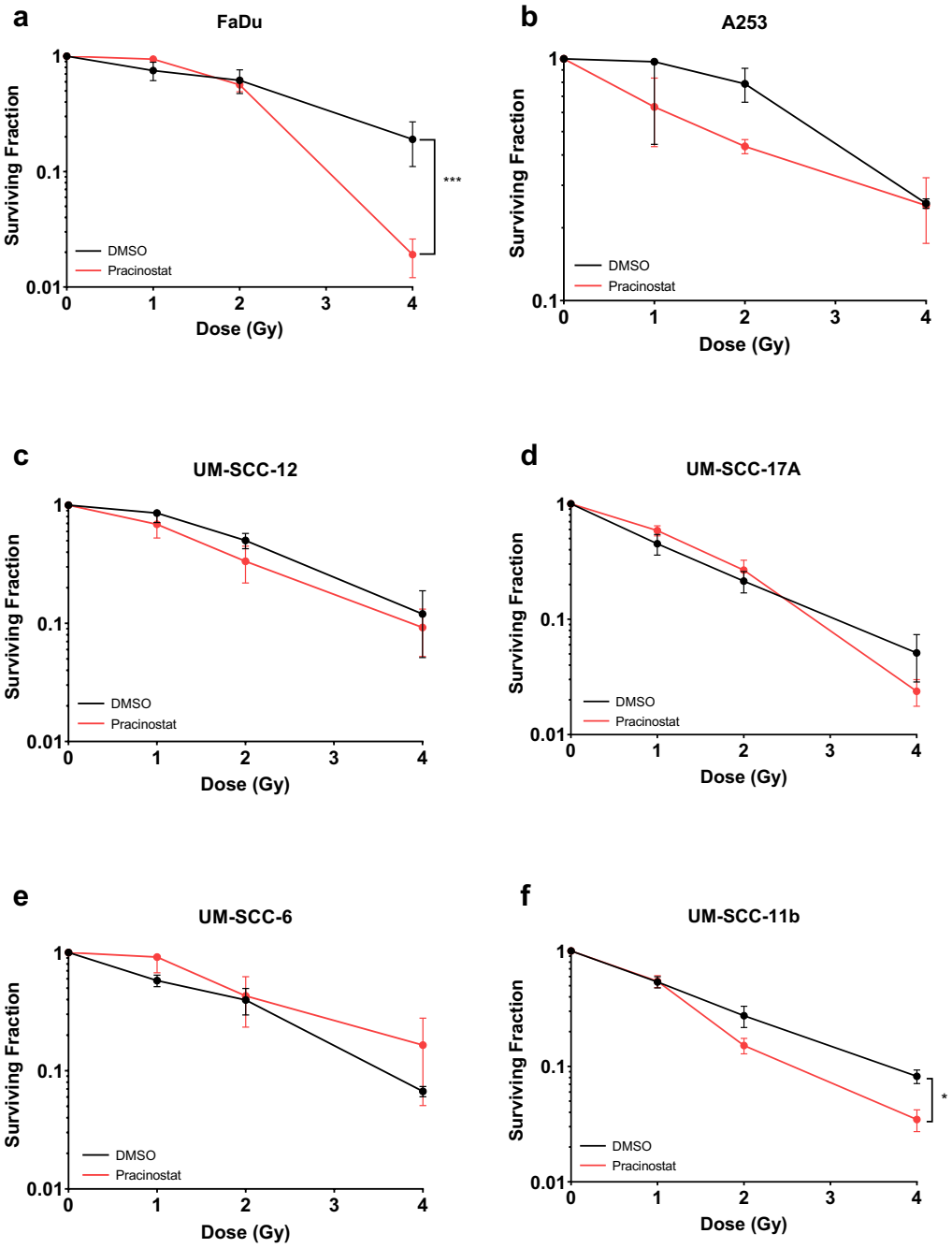

Figure 5.12: Clonogenic survival following pracinostat treatment

Clonogenic survival in a) FaDu cells, b) A253 cells, c) UM-SCC-12 cells, d) UM-SCC-17A cells e) UM-SCC-6 cells and f) UM-SCC-11b cells following DMSO and pracinostat treatments. Cells were seeded at a density of 1000 cells per well for 0 Gy, and this was doubled for each subsequent dose of radiation. Cells were allowed to attach to the plate, then fresh media containing 0.5 μM pracinostat was added. 24 hours later, plates were irradiated with 1, 2 or 4 Gy X-rays and the cells were then left for 6-10 days to allow colony formation to occur. Data is based on three independent experiments ± SEM, and statistical analysis was performed using the CFAssay (* = $p < 0.05$; ** = $p < 0.01$).

5.3. Summary

In this chapter, I have revealed the novel finding that the multi-targeting EGFR and HDAC inhibitor CUDC-101 and the class I, II and IV HDAC inhibitor pracinostat can radiosensitise selected HNSCC cells in both 3D spheroid models and 2D clonogenic survival assays. The variability in response between different HNSCC cell lines was an interesting development in this research. There are several factors that could be influencing the response of the cells to inhibitor treatment, including p53 status but also the site of origin of the tumour the cells were derived from. FaDu, A253 and UM-SCC-12 cells are all *p53-mut* cell lines, while UM-SCC-6 and UM-SCC17A are *p53-WT*. The positive results in FaDu spheroids and clonogenics suggest that CUDC-101 works in a cell-line dependent manner, which may also be linked to the p53 status of the cells. In the *p53-mut* cell lines, CUDC-101 did reduce clonogenic survival - although disappointingly this was not statistically significant in A253 or UM-SCC-12 - while CUDC-101 enhanced survival in the *p53-WT* UM-SCC-6 following exposure to IR. However, arguing against this theory, in UM-SCC-17A cells, which are also *p53-WT*, CUDC-101 reduced cell survival, and actually enhanced survival in the *p53-mut* UM-SCC-11b cells. A similar effect was seen following pracinostat treatment, however this inhibitor also significantly radiosensitised UM-SCC-11b cells. Therefore, it is clear that p53 is not the only important factor in radiosensitisation following CUDC-101 or pracinostat treatment. The HDAC inhibitor mocetinostat appears to have a slight negative impact on survival of *p53-mut* FaDu, A253 and UM-SCC-12 cells post-irradiation, however this was not a statistically significant effect. Mocetinostat seemed to enhance survival in UM-SCC-6 cells, also *p53-WT*, and had no effect on FaDu spheroid response to IR. Moreover, I also confirmed that, in neither 2D nor 3D models, the EGFR inhibitors lidocaine HCl and

genistein do not effectively radiosensitise HNSCC cells, regardless of the cell line, concentration or dose of X-rays. This implies that it is the HDAC-inhibiting potential of CUDC-101 that causes any radiosensitisation effect.

The findings that HDAC inhibition with CUDC-101 or pracinostat can radiosensitise HNSCC are novel results. CUDC-101 has been shown to radiosensitise other cancer types, but no research to date has been published showing its effectiveness in HNSCC. Even more novel is the finding that pracinostat can significantly radiosensitise multiple HNSCC cell lines, as there has been no evidence to date of the radiosensitising ability of pracinostat in any cancer type. After confirming that these HDACi do in fact effectively increase radiosensitivity in HNSCC cells, I then wanted to elucidate the mechanisms behind this radiosensitisation.

CHAPTER 6: RESULTS III

In vitro investigation of the mechanisms behind HDAC inhibitor-induced radiosensitisation of HNSCC cells

6.1. Introduction

In chapter 5, I demonstrated that the HDAC inhibitors pracinostat and CUDC-101 were effectively radiosensitising HNSCC cells *in vitro*.

Pracinostat (SB939) is an extremely potent inhibitor of class I, II and IV HDACs. Early studies involving pracinostat demonstrated that it is approximately 2-fold more potent than other HDACis, such as vorinostat, and selectively accumulates in tumour tissue (489, 490). Multiple clinical trials have shown that pracinostat is well-tolerated in patients (491, 492), and it has been suggested that pracinostat is more effective against solid tumours than other HDACis due to its accumulation in tumour tissue, superior pharmacokinetic properties, and less dose-limiting side effects (489). Most research carried out to date focuses on the effect of pracinostat in haematological malignancies, and multiple studies have demonstrated that pracinostat effectively induces cell death in chronic myeloid leukaemia (CML) cells expressing the BCR-ABL fusion protein, and can overcome resistance to BCR-ABL kinase inhibitors (493, 494). Phase I and II clinical trials have confirmed that pracinostat is tolerated well and has modest single-agent activity in patients with haematological malignancies (495-497). More recently, there has been some investigation into pracinostat's effects in solid tumours. In xenograft models of colorectal cancer, pracinostat has superior anti-tumour activity in comparison to other HDACis, and works in synergy with 5-FU to cause colorectal cancer cell death *in vitro* (489). Another study demonstrated that

pracinostat, at concentrations of 0.5 μM – 1 μM, inhibits the metastatic potential of breast cancer cells *in vitro* through altering the expression of EMT proteins such as E-cadherin and N-cadherin. This study also revealed that pracinostat inhibits the activity of signal transducer and activator of transcription 3 (STAT3), which is implicated in the formation of malignant tumours. These *in vitro* findings were also replicated in an *in vivo* mouse model (498). Most recently, pracinostat has been shown to inhibit the proliferation, migration, and invasion of glioblastoma multiforme (GBM) cells. In this study, it was found that treatment with pracinostat can inhibit angiogenesis and the expression of VEGF and HIF-1α, as well as altering expression of metastasis proteins MMP2 and MMP9 (499). To date, there has been no research into the potential of pracinostat as a radiosensitiser in any type of cancer.

CUDC-101 inhibits HDAC1-10, EGFR, and HER2 in a potent and synergistic manner, and has been shown to have anti-cancer effects against a wide variety of cancer types, including head and neck cancer. Due to the inhibition of EGFR and HER2 activation, downstream signalling pathways, such as the PI3K/AKT pathway, are also repressed after CUDC-101 treatment (500). Similar to pracinostat, CUDC-101 has been shown to influence cancer cell migration and invasion. A 2013 study by Wang *et al.* showed that in lung and gastric cancer cells with amplifications of the oncogene *MET*, CUDC-101 treatment increased E-cadherin expression and induced changes in cell morphology to impair cell migration (501). In research involving anaplastic thyroid cancer, CUDC-101 was shown to inhibit proliferation, and induce cell cycle arrest and caspase-dependent apoptosis. Moreover, this study provided further evidence that CUDC-101 increases the expression of E-cadherin, and prevents tumour metastasis *in vivo* (502). In clinical trials of patients with advanced solid tumours, CUDC-101 has been shown to be well tolerated, and there is evidence of antitumour activity in patients (503). Unlike pracinostat, CUDC-101 has

been shown to have radiosensitisation potential. In pancreatic cancer cell lines, treatment with 0.5 μM CUDC-101 significantly radiosensitised cells to 5 Gy X-rays in both clonogenic and spheroid models. This study also revealed that after combined CUDC-101 and X-ray treatment, there was an increase in apoptotic cells (402). Evidence from a scientific conference report suggests that treatment with CUDC-101 enhances the radiosensitivity of GBM and breast cancer cell lines, and this effect may be associated with a delay DSB repair (403). Currently, there is no data for the effects of CUDC-101 on the radiosensitivity of HNSCC cells.

There is little to no research into the effects of pracinostat and CUDC-101 on the DNA damage response, however there is extensive research showing the impact of individual HDACs on DNA repair (385). For example, HDAC1 and HDAC2 have been shown to influence expression levels of key DDR proteins such as ATM, ATR and BRCA1 (386), as well as localising to sites of IR-induced DNA damage, where they regulate H3K56 acetylation (387). This is supported by data showing that siRNA-mediated depletion of HDAC1/2 leads to hypersensitivity to radiation and elevated phosphorylation levels of γH2AX, CHK1/2 and p53. Moreover, cells with reduced levels of HDAC1 and HDAC2 exhibit persistence of Ku70 and Artemis at DNA damage sites, leading to severe deficiencies in DSB repair (387). Furthermore, the inactivation of HDAC3 in MEFs has been shown to cause inefficient DNA repair, potentially through the alteration of chromatin structure (388, 389). Meanwhile, HDAC4 and 53BP1 colocalise to nuclear foci post-irradiation during DSB repair, and it has been suggested that HDAC4 and 53BP1 may maintain the stability of one another (390). HDAC6 interacts with the DDR proteins MLH1 and MSH2 to repress MMR (391, 392), and a decrease in HDAC9 and HDAC10 represses HR, though the mechanism behind this is yet to be elucidated (393).

Based on these findings, an assumption can be made that the radiosensitisation seen after HDACi treatment could be a consequence of impaired DNA damage repair. Thus, in this chapter, I used neutral comet assays and immunofluorescent staining to investigate repair kinetics post-treatment and used western blotting to gain more in-depth insights into the cellular effects of HDAC inhibition.

6.2. Confirmation of HDACi activity

To support investigation into the mechanisms behind CUDC-101- and pracinostat-induced radiosensitisation, I confirmed that the inhibitors were in fact working in the expected way. Due to the time constraints in this work, I was only able to partially investigate this. FaDu and UM-SCC-11b cells were seeded into 10 cm dishes and left 24 hours to attach. 5 μM pracinostat was then added, and 24 hours later the cells were either irradiated with 4 Gy X-rays or left unirradiated. Unirradiated cells were harvested at 24 hours post-inhibitor treatment, while for the irradiated cells, fresh media was added at 24 hours post-inhibitor treatment before exposure to 4 Gy X-rays, and the cells were harvested 4 hours post-IR. Following this, the cell pellet was resuspended in 100 μl of hypotonic buffer and incubated for 30 minutes at 4 °C on a shaker. The suspension was subsequently centrifuged at 10,000 x g for 10 minutes, the supernatant removed and the pellet – which contained the nuclei – was resuspended in 80 μl of 0.4 M sulfuric acid and incubated overnight at 4 °C. The next day, samples were centrifuged at 16,000 x g. Trichloroacetic acid was added dropwise to the supernatant and the samples were then incubated on ice for 30 minutes and centrifuged again at 16,000 x g to pellet the histones. The histone pellets were washed with 100 μl ice-cold acetone, centrifuged again at 16,000 x g, and the wash was repeated. The pellets were then left at

room temperature for 10 – 15 minutes to air dry, dissolved in 50 μl of dH_2O, and protein concentration was measured by Nanodrop. Western blot was then performed (see section 3.6). As mentioned above, time constraints hindered the progress of these experiments, and I was only able to analyse various acetylation sites in FaDu and UM-SCC-11b cells following pracinostat treatment, and not after treatment with CUDC-101. From these experiments (figure 6.1) there is clear evidence in both FaDu and UM-SCC-11b cells that pracinostat successfully inhibits the activity of HDACs. Interestingly, in both cell lines, H4K5 appears to have an increased level of acetylation compared to other sites even in control conditions. Although more investigation is required to fully elucidate the effects of pracinostat – and also CUDC-101 – treatment on HNSCC cells, these immunoblots are sufficient to confirm that pracinostat is effectively inhibiting HDAC activity.

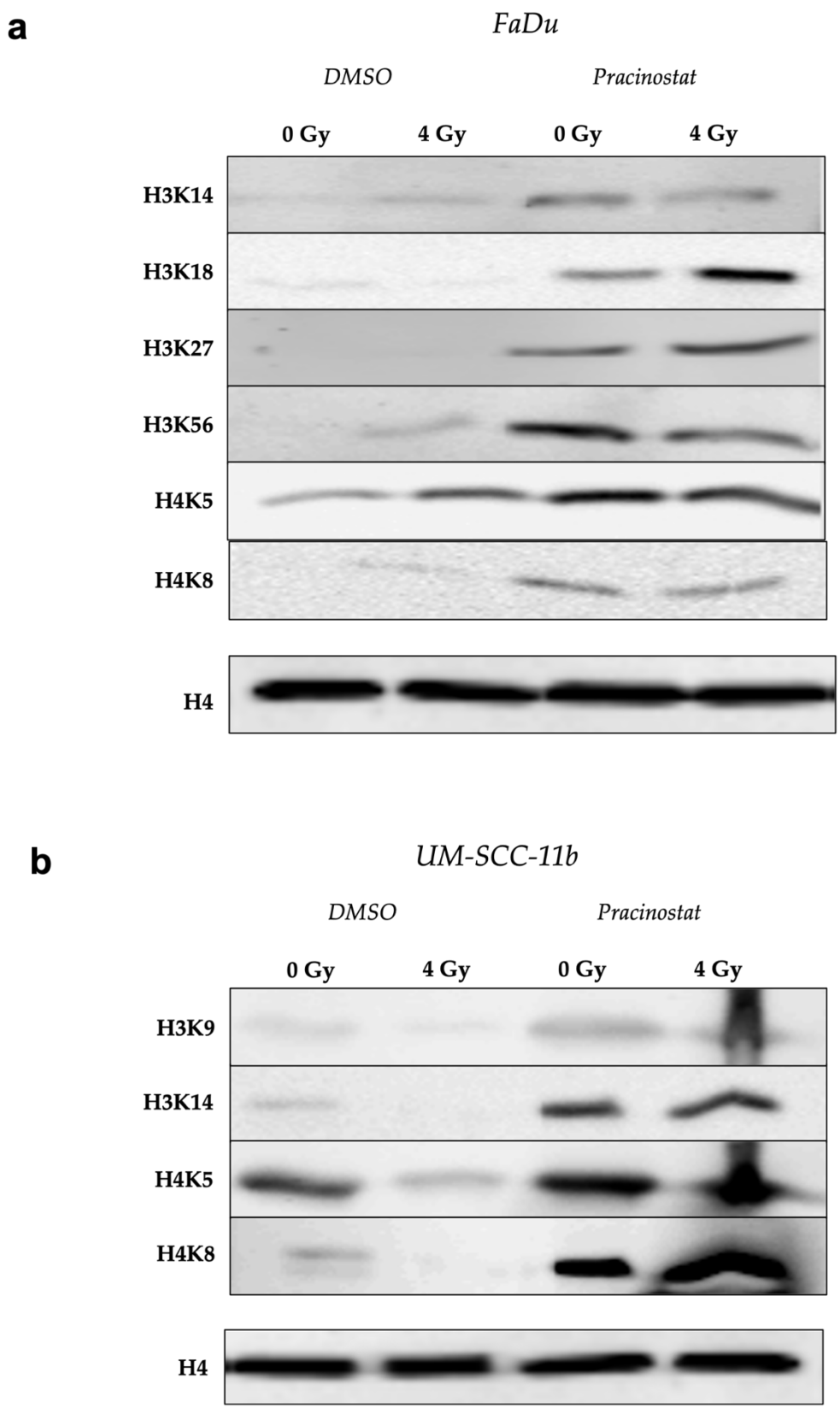

Figure 6.1: Western blot analysis of histone acetylation sites

a) FaDu and b) UM-SCC-11b cells were treated with 5 μM pracinostat or a DMSO control, and either irradiated with 4 Gy X-rays or left unirradiated. Acid extraction was used to isolate the histones, and western blot was performed to visualise acetylation of specific histone sites. Data shown is from one experiment.

6.3. Investigation of DSB repair kinetics after HDACi treatment

As the results of chapter 5 show, pracinostat and CUDC-101 appear to be radiosensitising two HNSCC cell lines, FaDu (pracinostat and CUDC-101) and UM-SCC-11b (pracinostat only), *in vitro*. Previous research has suggested a role for HDACs in the DDR, and thus I investigated the impact of HDACi on the repair kinetics of DNA DSBs following irradiation using the neutral comet assay. Cells were seeded into 6 cm dishes and grown until 70 – 80 % confluent, when they were then treated with either DMSO or 0.5 μM pracinostat or CUDC-101. After 24-hour drug treatment, DNA damage was induced with 4 Gy X-rays and cells were then embedded in agarose on microscope slides. Cells were incubated for set time points to allow DNA repair to occur and following this were lysed. Electrophoresis was performed, cells were stained with SYBR Gold the following day and subsequently imaged using the BX61 Olympus microscope at 10 x magnification. Analysis was performed using Komet 6.0 software.

6.3.1. Neutral comet assay in UM-SCC-12 cells

To further support the theory that radiosensitisation is caused, in part, by impaired DSB repair, I also performed the neutral comet assay using UM-SCC-12 cells (figure 6.2), which are not radiosensitised by HDACi, as demonstrated in chapter 5. Neither pracinostat nor CUDC-101 was sufficient to significantly impair DSB damage repair in the UM-SCC-12 cells. The inhibitor-treated cells did have an increased level of damage in the unirradiated control condition and displayed only a slight delay in DSB repair compared to DMSO-treated cells, however these differences were not statistically significant (*t-test*, table 6.1). Most DSBs in UM-SCC-12 cells were repaired during the first 2 hours

post-IR, and the majority of DSBs were repaired by 4 hours post-IR. These results give further proof to the theory that HDACi-induced radiosensitisation is linked to DSB repair, as the lack of significant difference in DSB repair in UM-SCC-12 cells corroborates the observed lack of radiosensitisation after HDACi treatment in clonogenic assays.

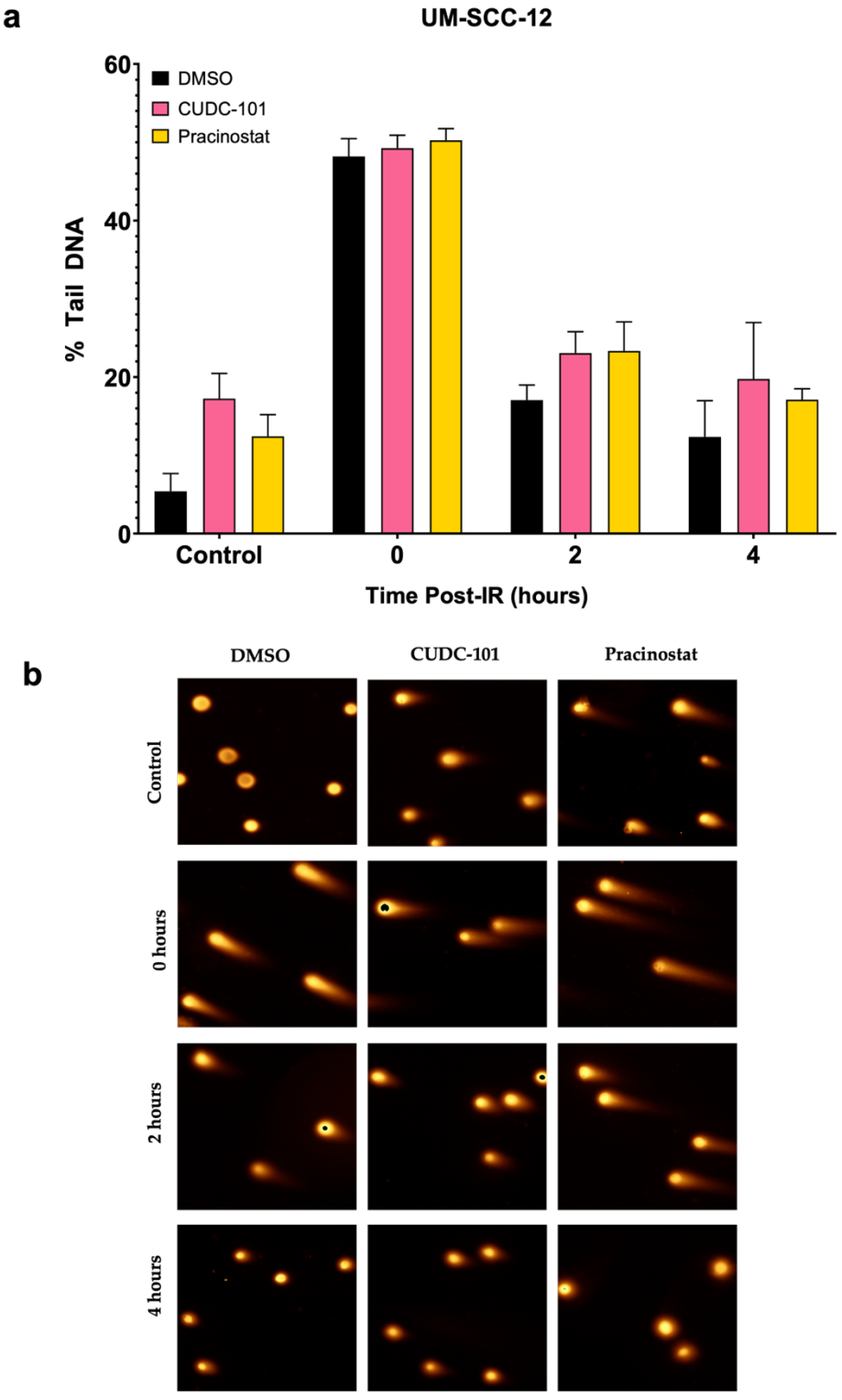

Figure 6.2: Neutral comet assay in UM-SCC-12 cells

UM-SCC-12 cells were treated with either DMSO or 0.5 μM pracinostat/CUDC-101. 24 hours later, DNA damage was induced with 4 Gy X-rays and cells were then embedded in agarose on microscope slides. Cells were lysed at 0-, 2- and 4-hours post-IR, plus an unirradiated control. Electrophoresis was performed, cells were stained with SYBR Gold the following day and subsequently imaged using the BX61 Olympus microscope. Analysis of tail DNA was performed using Komet 6.0 software. Data is based on three independent experiments ± SEM, and statistical analysis was performed using the t-test.

Table 6.1: Statistical significance of inhibitor treatment in UM-SCC-12 comets

Time Post-IR	P-Value	
	CUDC-101	Pracinostat
Control	0.226762	0.101948
0 hours	0.690039	0.435154
2 hours	0.127819	0.192792
4 hours	0.414093	0.301007

A t-test was used to compare the effect of DMSO treatment with either CUDC-101 or pracinostat on DSB repair in UM-SCC-12 cells. The P-values are based on three independent experiments.

6.3.2. Neutral comet assay in FaDu cells

As shown in figure 6.3, in the FaDu cells treated with DMSO, the vast majority of radiation-induced DNA DSBs were repaired by 4 hours post-IR, shown by a restoration of percentage tail DNA to levels similar to those of the unirradiated control. Most of this repair occurred within the first 2 hours following irradiation. Treatment with CUDC-101 or pracinostat prior to irradiation led to a significant depletion in DSB repair capacity in the FaDu cells, and interestingly both drugs also resulted in an increased amount of DNA damage in the control conditions. This implies that pracinostat and CUDC-101 are causing an impairment of the repair of endogenous DNA damage in FaDu cells. Immediately after irradiation, the levels of DNA damage in the inhibitor-treated cells were comparable to those treated with DMSO, suggesting that neither inhibitor impacts the amount of initial damage induced by IR. However, at 2 hours post-irradiation, there were significantly higher levels of DNA damage in the inhibitor-treated cells. This was more evident in the cells treated with CUDC-101, which had a 2.1-fold increase in the level of DNA damage compared to the DMSO treated cells at the same timepoint. Pracinostat still had a marked effect on DNA repair at this time point, causing a 1.7-fold increase in damage compared to DMSO. These differences were statistically significant, as shown by p-values of 0.003 (CUDC-101) and 0.03 (pracinostat) (*t-test*, table 6.2). At 4 hours post-

irradiation, HDACi treated cells still had significantly higher levels of DNA damage than the DMSO treated cells, which had returned to control levels. Unlike at 2 hours, the difference between the two inhibitors was marginal, with CUDC-101 and pracinostat respectively causing a 2.8- and 3-fold increase in DNA repair compared to controls. Once again, this was statically significant, as shown by p-values of 0.014 for both treatment conditions (*t-test*, table 6.2). These results demonstrate that in FaDu cells, inhibition of HDACs with pracinostat, and the dual inhibition of HDACs and EGFR with CUDC-101, result in higher levels of DNA DSBs without irradiation, and 2 hours after irradiation the HDACi-treated cells display decreased levels of damage repair compared to DMSO-treated cells. By 4 hours post-IR, levels of damage had returned to levels similar to the unirradiated controls, however this was still significantly higher in the inhibitor-treated cells (*t-test,* table 6.2). Taken together, these results implicate a role for impaired DSB repair in the HDACi-induced radiosensitisation of FaDu cells.

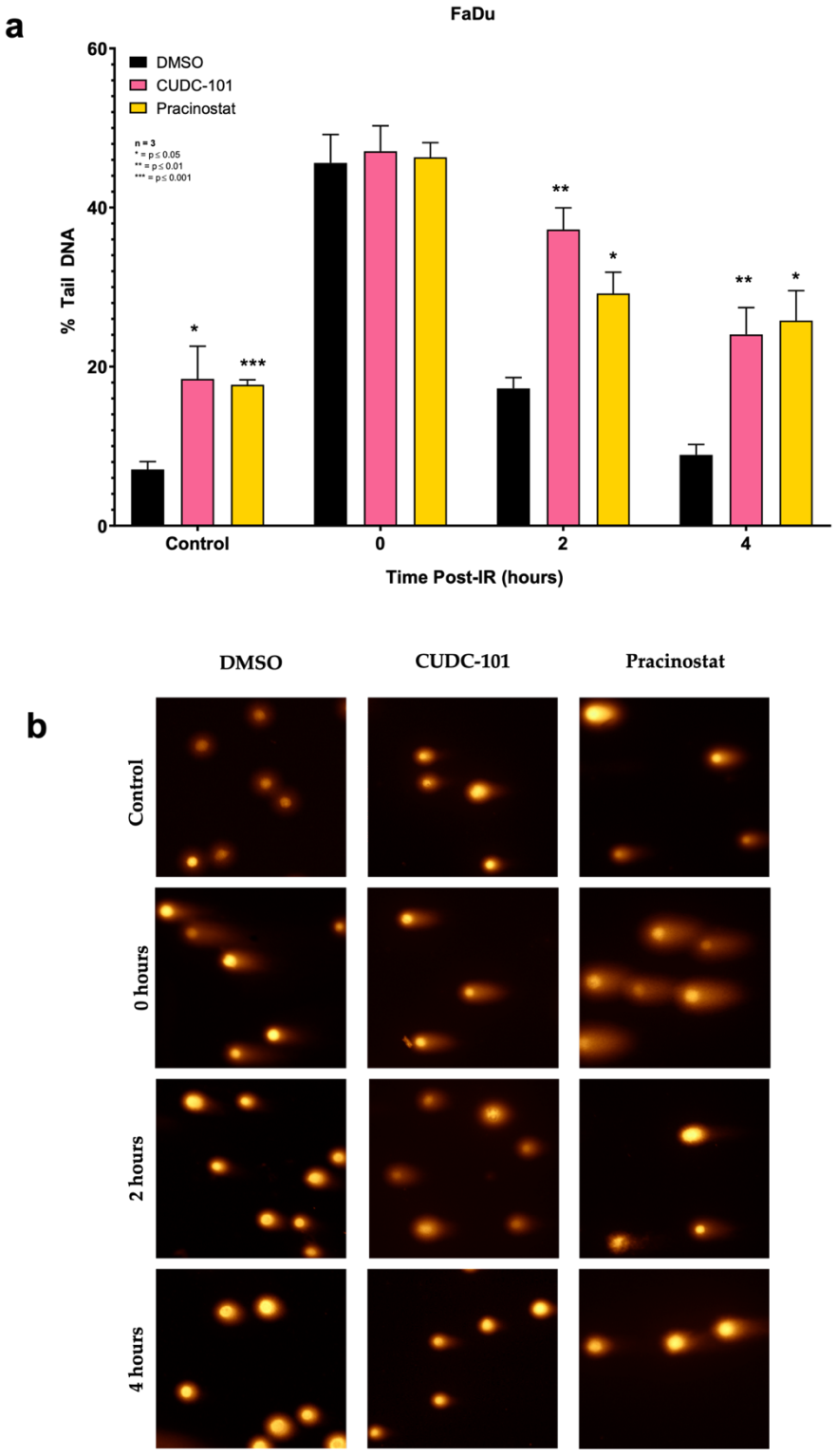

Figure 6.3: Neutral comet assay in FaDu cells

FaDu cells were treated with either DMSO or 0.5 μM pracinostat/CUDC-101. 24 hours later, DNA damage was induced with 4 Gy X-rays and cells were then embedded in agarose on microscope slides. Cells were lysed at 0-, 2- and 4-hours post-IR, plus an unirradiated control. Electrophoresis was performed, cells were stained with SYBR Gold the following day and subsequently imaged using the BX61 Olympus microscope. Analysis of tail DNA was performed using Komet 6.0 software. Data is based on three independent experiments ± SEM, and statistical analysis was performed using the t-test (* = $p < 0.05$; ** = $p < 0.01$, *** = $p < 0.001$).

Table 6.2: Statistical significance of inhibitors in FaDu comets

Time Post-IR	P-Value	
	CUDC-101	Pracinostat
Control	0.030005	0.000366
0 hours	0.725454	0.838698
2 hours	0.001304	0.0081
4 hours	0.006495	0.006264

A t-test was used to compare the effect of DMSO treatment with either CUDC-101 or pracinostat on DSB repair in FaDu cells. The P-values are based on three independent experiments. Statistically significant values are highlighted.

6.3.3. Neutral comet assay in UM-SCC-11b cells

In UM-SCC-11b cells, pracinostat appeared to induce DNA DSB damage independent of the addition of X-rays, with damage levels 2.3-fold higher after pracinostat treatment in comparison to DMSO controls (figure 6.4). Immediately following irradiation with 4 Gy X-rays, the amount of DSB damage in both treatment conditions markedly increased to comparable levels as expected. However, at 2-hours post-IR, while damage levels in DMSO-treated cells dropped by 60 %, pracinostat treatment caused the DSB damage to persist, with levels 1.5-fold higher than controls. 4 hours following irradiation, the damage levels in the DMSO control-treated conditions had returned to control levels, however this was still significantly higher in cells treated with pracinostat. The difference in damage levels between the two treatment conditions at all time points except immediately post-IR were statistically significant, with p-values of 0.017, 0.03 and 0.004 for the unirradiated controls, 2-hours post-IR and 4-hours post-IR respectively (*t-test*, table 6.3).

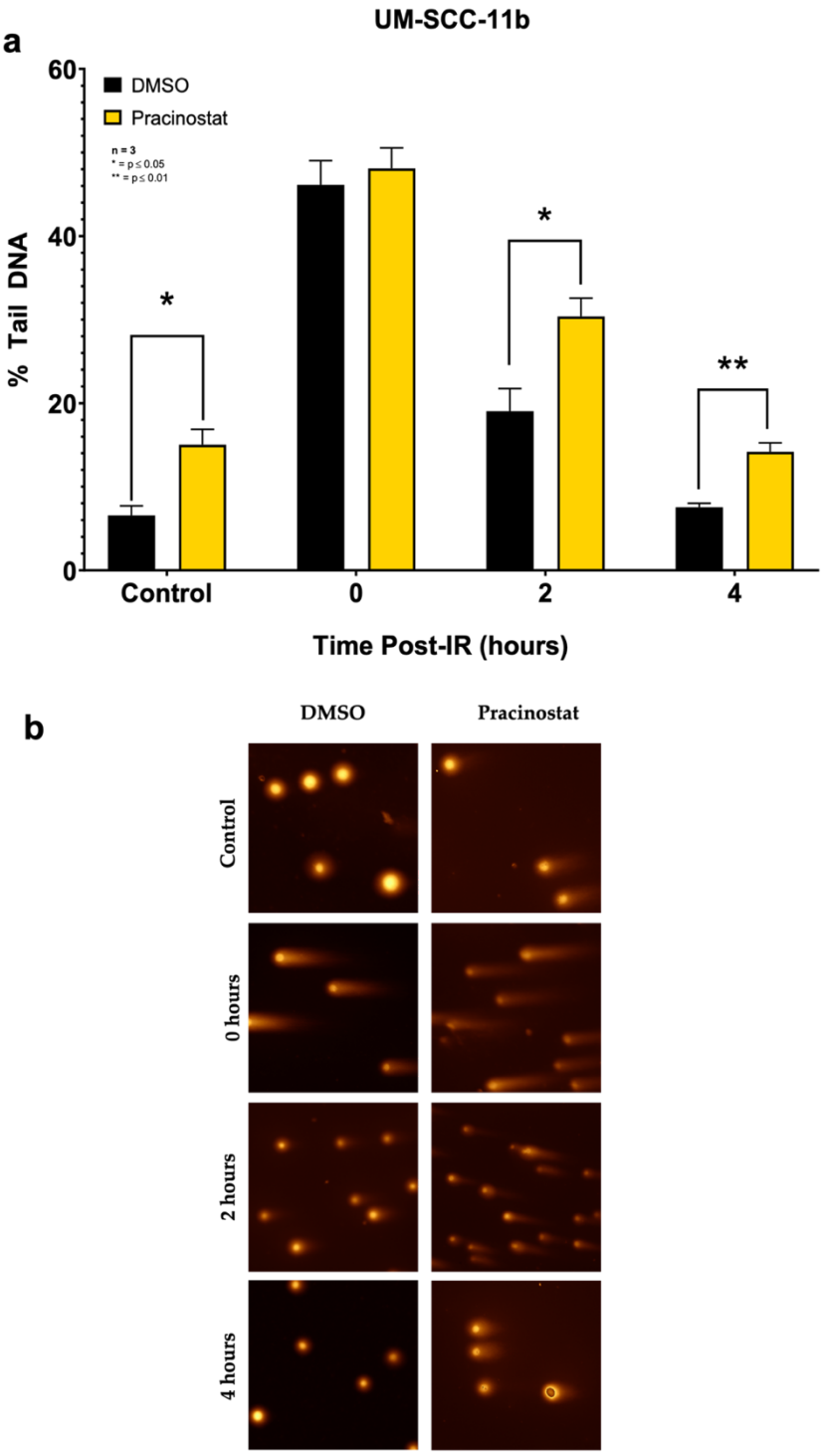

Figure 6.4: Neutral comet assay in UM-SCC-11b cells

UM-SCC-11b cells were treated with either DMSO or 0.5 μM pracinostat. 24 hours later, DNA damage was induced with 4 Gy X-rays and cells were then embedded in agarose on microscope slides. Cells were lysed at 0-, 2- and 4-hours post-IR, plus an unirradiated control. Electrophoresis was performed, cells were stained with SYBR Gold the following day and subsequently imaged using the BX61 Olympus microscope. Analysis of tail DNA was performed using Komet 6.0 software. Data is based on three independent experiments ± SEM, and statistical analysis was performed using the t-test (* = $p < 0.05$; ** = $p < 0.01$).

Table 6.3: Statistical significance of pracinostat treatment in UM-SCC-11b comets

Time Post-IR	P- Value
	Pracinostat
Control	0.017364
0 hours	0.629842
2 hours	0.030959
4 hours	0.004833

A t-test was used to compare the effect of DMSO treatment with pracinostat on DSB repair in UM-SCC-11b cells. The P-values are based on three independent experiments. Statistically significant values are highlighted.

6.4. Investigation of γH2AX foci after HDACi treatment

To further prove that the radiosensitising effect of HDACi treatment is related to an impairment in DNA DSB repair, I analysed γH2AX foci in FaDu and UM-SCC-11b cells following treatment with HDACi. The cells were seeded on to glass coverslips in the bottom of 3.5 cm dishes, and left to attach for 24 hours, after which fresh media containing DMSO or 0.5 μM inhibitor was added. After 24-hour drug treatment, the dishes were irradiated with 4 Gy X-rays, and the media was replaced. At defined time points post-irradiation, the cells were fixed, permeabilised with Triton x-100, and the coverslips were then incubated with 2 % BSA solution to prevent non-specific binding. The primary antibody was then added, and coverslips were incubated overnight at 4 °C. The following day, coverslips were incubated with the secondary antibody for 1 hour at room temperature in a light protected environment. The coverslips were then washed in PBS, left to dry for at least 1 hour, and then mounted on to a microscope slide using Fluoroshield containing DAPI (Sigma-Aldrich, St Louis, USA). A BX61 Olympus microscope (Olympus, Shinjuku, Japan) was used to capture images of the slides. 5 representative images were captured for each coverslip, and 2 coverslips from each condition were imaged. γH2AX foci were counted using ImageJ.

6.4.1. Immunofluorescent staining in FaDu cells

As shown in figure 6.5, the average number of γH2AX foci per cell remains less than 5 in unirradiated cells regardless of control or inhibitor treatment. The number is slightly higher in cells treated with CUDC-101, with an average 4.2 foci per cell compared to 2.4 foci per cell following both DMSO and pracinostat treatment. However, this difference was not statistically significant (*t-test*, table 6.4). 1-hour post-irradiation, average foci numbers dramatically increased in all treatment conditions, to average foci counts of 16.1 (DMSO), 14.9 (CUDC-101) and 18.4 (pracinostat). Again, there was no statistically significant difference between the treatment conditions (*t-test*, table 6.4). By 4 hours post-irradiation, the number of γH2AX foci in DMSO-treated cells dropped to an average of 7.3 foci per cell, while both CUDC-101 and pracinostat caused a persistence in foci number, with averages of 10.8 and 13.3 respectively. These differences were both statistically significant, with p-values of < 0.05 (*t-test*, table 6.4). At 8 hours post-irradiation, DMSO-treated cells had average foci counts of 6.2 per cell, and this was comparable in the CUDC-101-treated cells, which had 7.1 γH2AX foci per cell on average. However, average foci numbers remained higher in the pracinostat treated cells, with approximately 9.1 foci per cell. The difference between DMSO- and pracinostat-treated cells was statistically significant, with a p-value of < 0.05 (*t-test*, table 6.4). At 24 hours post-irradiation, the average number of foci/cell had returned to levels comparable to the unirradiated controls in all three treatment conditions. This data is consistent with that from the neutral comet assay, described in section 6.3.1., and suggests that HDACi treatment causes an impairment of DSB repair in FaDu cells, resulting in a persistence of DSBs and γH2AX foci up to 8 hours post-irradiation compared to DMSO-treated control cells.

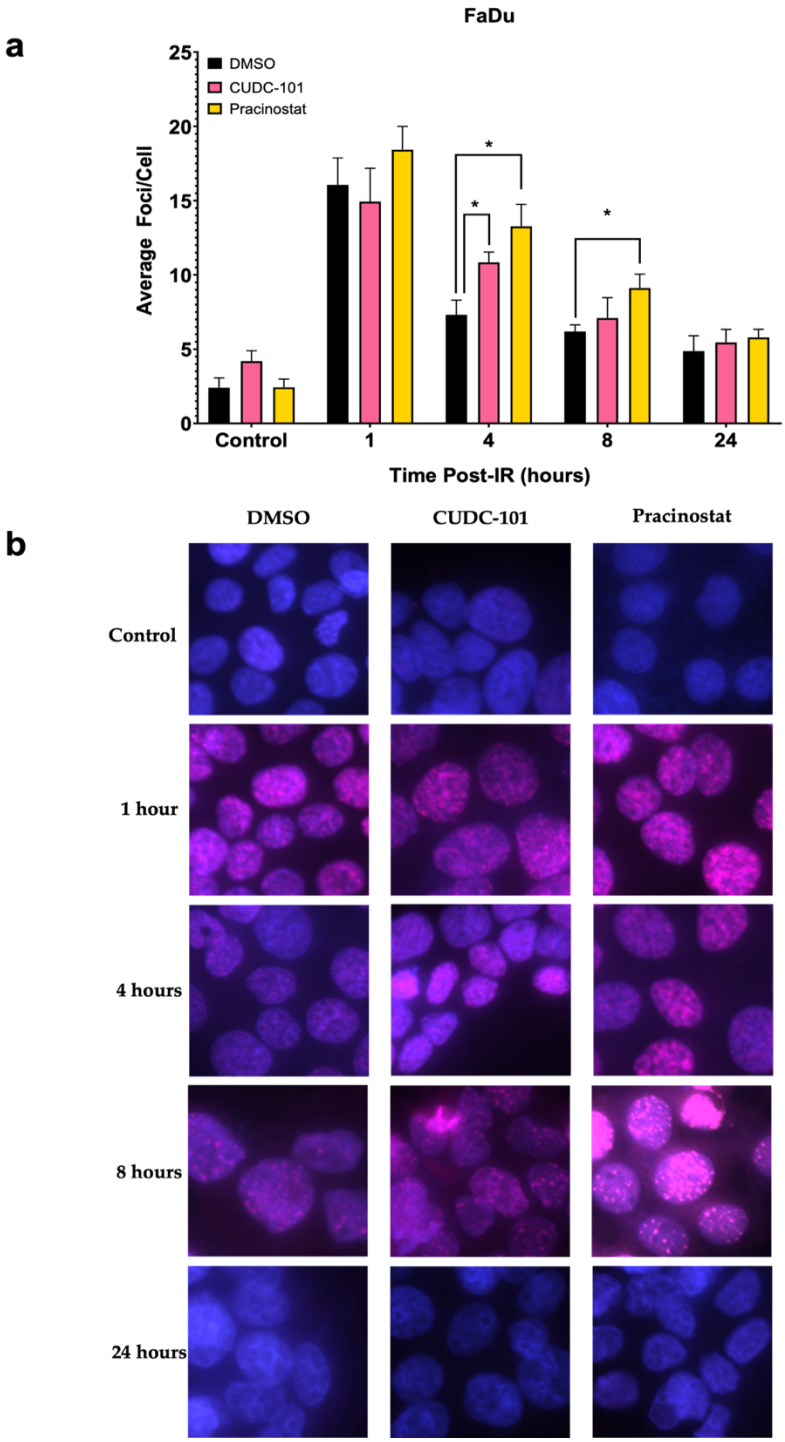

Figure 6.5: γH2AX staining in FaDu cells

FaDu cells were seeded on to glass coverslips incubated to allow attachment, after which DMSO or 0.5 μM inhibitor was added. After 24-hour drug treatment, cells were irradiated with 4 Gy X-rays or left unirradiated, and at 1-, 4-, 8- and 24-hours post-IR, the cells were fixed, permeabilised with Triton x-100, and the coverslips were then incubated with 2 % BSA solution. The coverslips were then incubated overnight at 4°C with the primary antibody, and the following day were incubated with the secondary antibody for 1 hour at room temperature. The coverslips were then washed in PBS and mounted on to a microscope slide using Fluoroshield containing DAPI (Sigma-Aldrich, St Louis, USA). A BX61 Olympus microscope (Olympus, Shinjuku, Japan) was used to capture images of the slides, and γH2AX foci were counted using ImageJ. Data is based on three independent experiments ± SEM, and statistical analysis was performed using the t-test (* = $p < 0.05$).

Table 6.4: Statistical significance of inhibitor treatment on γH2AX foci in FaDu cells

Time Post-IR	P-Value	
	CUDC-101	**Pracinostat**
Control	0.11208461	0.97519629
1 hour	0.71041763	0.3606694
4 hours	0.026692	0.01546016
8 hours	0.549083	0.03815005
24 hours	0.71057686	0.4580992

A t-test was used to compare the effect of DMSO treatment with either CUDC-101 or pracinostat on the average number of γH2AX foci in FaDu cells. The P-values are based on three independent experiments. Statistically significant values are highlighted.

6.4.2. Immunofluorescent staining in UM-SCC-11b cells

As in FaDu cells, the average number of γH2AX foci per cell remains less than 5 in unirradiated cells regardless of control or inhibitor treatment in UM-SCC-11b cells (figure 6.6). The average number of γH2AX foci per cell following DMSO treatment was only 1 foci on average, while pracinostat-treated cells had an average of 2.6 foci per cell. 1-hour post-irradiation with 4 Gy X-rays, the average number of foci markedly increased in both treatment conditions, to average numbers of 10.2 and 12.3 foci per cell for DMSO- and pracinostat-treated cells, respectively. Despite the observable differences in both unirradiated cells and 1-hour post-irradiation, no statistical significance was observed (*t-test*, table 6.5). After 4 hours, the DMSO-treated cells had repaired approximately half of the DNA DSB damage, as the average number of foci dropped to 6.2 per cell. Pracinostat, on the other hand, caused a significant persistence of γH2AX foci, with only a small decrease compared to 1-hour post-irradiation, with an average of 11.2 foci per cell. A similar pattern was seen at 8 hours post-IR, with DMSO-treated cells having an average count of 3.9 and pracinostat-treated cells maintaining a higher count of 9.1 foci per cell. By 24 hours, DMSO-treated cells had decreased to an average foci count comparable to control levels, but cells treated with pracinostat still maintained

a higher level of damage, with an average of 7.2 foci per cell. The differences at 4-, 8- and 24-hours post-IR were significant, with p-values of 0.04, 0.002 and 0.02 for each respective timepoint (*t-test,* table 6.5). As in the FaDu cells, this data is consistent with the results of neutral comet assays as another measurement of DSBs, as described in section 6.3.2. In UM-SCC-11b cells, it is clear that treatment with pracinostat is sufficient to induce DNA DSB damage as a single agent, and repair of this damage is significantly slowed in comparison to DMSO treatment, even at 24-hours post-irradiation.

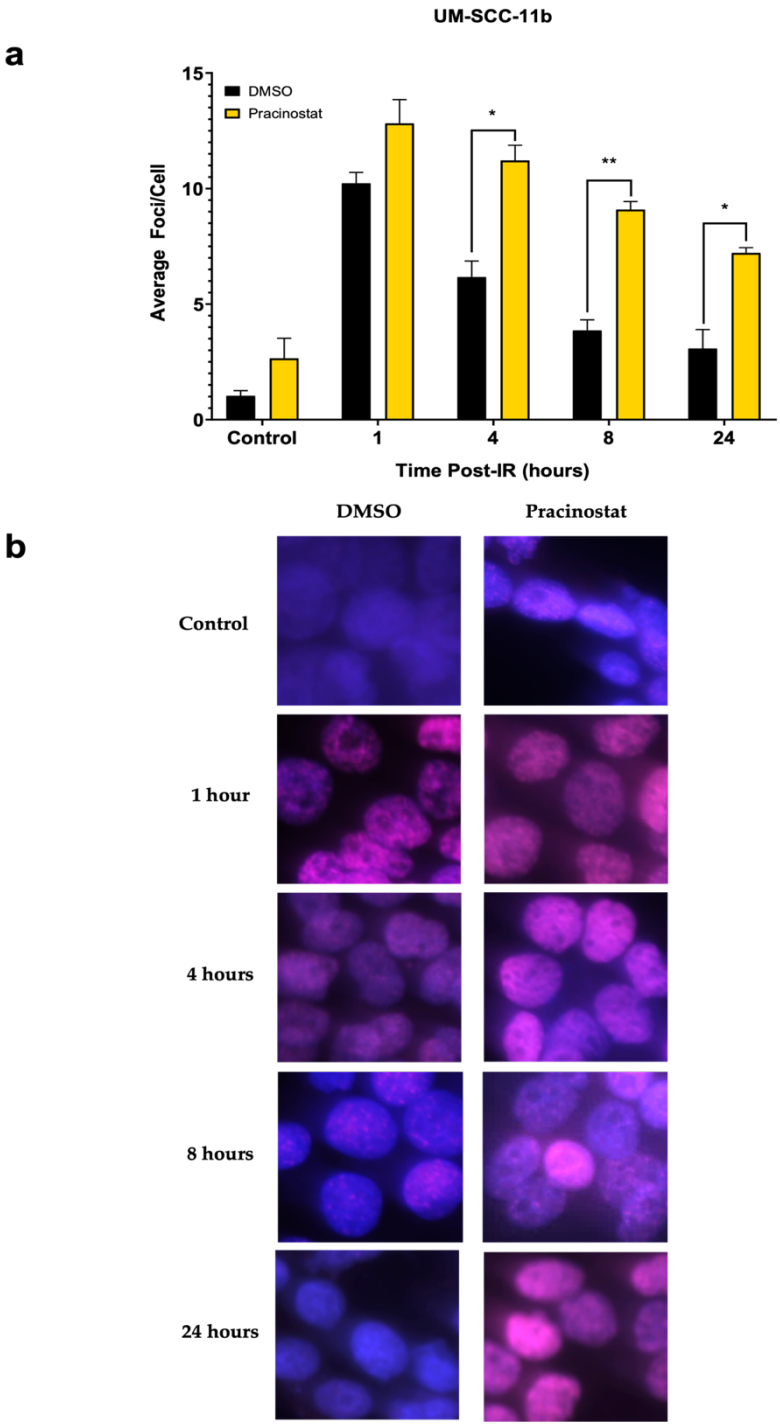

Figure 6.6: γH2AX staining in UM-SCC-11b cells

UM-SCC-11b cells were seeded on to glass coverslips incubated to allow attachment, after which DMSO or 0.5 μM pracinostat was added. After 24-hour drug treatment, cells were irradiated with 4 Gy X-rays or left unirradiated, and at 1-, 4-, 8- and 24-hours post-IR, the cells were fixed, permeabilised with Triton x-100, and the coverslips were then incubated with 2 % BSA solution. The coverslips were then incubated overnight at 4°C with the primary antibody, and the following day were incubated with the secondary antibody for 1 hour at room temperature. The coverslips were then washed in PBS and mounted on to a microscope slide using Fluoroshield containing DAPI (Sigma-Aldrich, St Louis, USA). A BX61 Olympus microscope (Olympus, Shinjuku, Japan) was used to capture images of the slides, and γH2AX foci were counted using ImageJ. Data is based on three independent experiments ± SEM, and statistical analysis was performed using the t-test (* = $p < 0.05$; ** = $p < 0.01$).

Table 6.5: Statistical significance of pracinostat treatment on γH2AX foci in UM-SCC-11b cells

Time Post-IR	P-Value
	Pracinostat
Control	0.28122081
1 hour	0.55938343
4 hours	0.04369577
8 hours	0.00202102
24 hours	0.02249499

A t-test was used to compare the effect of DMSO treatment with pracinostat on the average number of γH2AX foci in UM-SCC-11b cells. The P-values are based on three independent experiments. Statistically significant values are highlighted.

6.5. Summary

In this chapter, I initially demonstrated that pracinostat can inhibit HDAC activity, by showing through Western blot analysis that acetylation levels of key histone sites are maintained following HDACi treatment. Due to technical problems and time constrains, I was unable to examine each acetylation site in multiple cell lines, and I was also unable to look at the effects of CUDC-101. Furthermore, I have effectively demonstrated exert a radiosensitisation effect via an impairment of the cellular DDR. Using both the neutral comet assay and immunofluorescent staining, I confirmed that there is a persistence of DNA DSBs and γH2AX foci in HDACi-treated FaDu and UM-SCC-11b cells following exposure to 4 Gy X-rays, suggesting that DSB repair is impacted in some manner upon HDAC inhibition.

CHAPTER 7: DISCUSSION

7.1.Overview

Head and neck cancer (HNC) is the sixth most common cancer worldwide. According to data from 2020, there are approximately 890,000 new cases and 470,000 deaths caused by HNC every year (103). The incidence of HNC is rising – on average, there has been a 24 % increase over the last decade (105). Survival of patients with HNC can vary, with 10- and 5-year survival ranging between 19 – 59 % and 28 – 67 % respectively (105). Most HNCs are squamous cell carcinomas and arise in the epithelial linings of several regions in the head and neck, including the oral cavity, nasal cavity, pharynx, larynx, salivary glands, and sinuses. The main risk factors for HNSCC are tobacco and alcohol consumption, and infection with HPV, particularly HPV type 16. The HPV genome carries two tumour-promoting genes, called *E6* and *E7*. The E6 protein has a role in sustaining proliferative signalling in cells via the degradation of the p53 protein (127), while the E7 protein alters the activity of the Rb tumour suppressor protein (130, 131). Together, disruption of the p53 and Rb proteins results in the uncontrolled proliferation of cells carrying DNA damage, thus contributing to carcinogenesis (132). Infection with HPV-16 leads to a 14-fold increase in risk for developing HNSCC, particularly in the oropharynx, however HPV-positive HNSCC has a better prognosis than its HPV-negative counterpart (133). Treatment modalities for HNSCC are chemotherapy, radiotherapy, and surgical resection. Radiotherapy is used in both curative and a palliative setting, and normally utilises IMRT, in which the radiation beam is shaped to accurately fit the tumour and minimise dose to healthy tissue (143). Although radiotherapy can be a success, radioresistance is a common occurrence and patients can experience either a lack of response, a

partial response, or recurrence after an initial response to radiation treatment (152). Research shows that approximately 25 % of HNSCC patients exhibit local relapses after treatment, and if radiotherapy treatment fails, patients must often undergo surgical salvage (153). A variety of characteristics have been implicated in HNSCC radiosensitivity, including an enhancement of the DDR (154-158), the p53 status of the tumour (159), overexpression of EGFR and its downstream pathways (161-164), and tumour hypoxia (165-167). HPV-negative HNSCCs also display increased radioresistance compared to their HPV-positive counterparts. This could be linked to mutations in the *TP53* gene (160), and, as has been shown previously in the Parsons laboratory, changes in the DDR (504). However, the full relationship between HPV and radiosensitivity is yet to be uncovered. IR deposits energy in cells as it passes through the tissues in the body during radiotherapy. This causes DNA damage, predominantly base damage and SSBs, but also DSBs and complex DNA damage (CDD) which are considered the major contributors to IR-induced cell death (144). The DDR is activated upon the generation of damage. The BER pathway is utilised for the repair of base damage and SSBs (199), while DSBs are repaired by NHEJ or HR (216). The repair mechanism for CDD is yet to be elucidated, however the Parsons laboratory have recently demonstrated a critical role for proteins involved in SSB repair (414, 505).

The research presented in this thesis aimed to carry out a targeted drug screen to identify candidate radiosensitisers of HPV-negative HNSCC, to validate these findings in both 2D and 3D cell models, and to elucidate the mechanisms behind any observed radiosensitisation effects.

7.2. Screening of FDA-approved drugs

The significant number of patients that have radioresistant tumours and therefore experience disease recurrence means there is a critical need for identifying new treatment modalities to improve the response to radiotherapy. With this in mind, the first stage of my research comprised a targeted drug screen of 183 FDA-approved inhibitors, aiming to identify those that could be repurposed as novel HNSCC radiosensitisers.

For the drug screen, I utilised a 3D model of HNSCC in the form of FaDu spheroids. FaDu cells were chosen as they grow well as spheroids *in vitro*, meaning there is a large scope to examine relative changes in growth after inhibitor and radiation treatments. Moreover, FaDu spheroids display a relatively higher radioresistance compared to other HNSCC cell lines, and previous work in our laboratory by Dr. Chumin Zhou had established FaDu cells as a successful spheroid model (413). Spheroid models are highly beneficial for the purposes of drug screening, as they more closely mimic and the structure and environment of *in vivo* tumours in comparison to 2D cell culture. Spheroids are composed of three layers: a necrotic core, a quiescent intermediate layer made up of non-proliferating cells, and finally an outer layer of proliferating cells. Due to this composition, there is active transport of oxygen and nutrients through the spheroid comparable to that of tumours (506). Importantly, the growth kinetics, proliferation and oxygen gradients that are generated in spheroids cannot be replicated in 2D models but have significant impacts on the response of the cells to drug and radiation treatment (438). This is comparable to the treatment resistance observed in solid tumours, and therefore provides more confidence in the data. In the preliminary drug screen, 183 drugs covering 29 different cellular targets were investigated for radiosensitisation potential. A number of the proteins

targeted in this screen had previously been associated with radiosensitivity in different cancer types, while others were related to the hallmarks of cancer but had no previous links to radiosensitivity (table 7.1).

Table 7.1: Drug screen targets and their links to radiosensitivity

Target	Radiosensitisation ability	Reference
Bcl-2	Bcl-2 inhibitors AT-101 and venetoclax both shown to radiosensitise HNSCCs *in vitro* and *in vivo*.	(416, 417)
Caspase	Caspase-8 loss linked to radioresistance in HNSCC, loss of caspase-8 sensitises HNSCC cells to radiosensitisation by the IAP inhibitor birinapant, caspase-9 activated by high-LET radiation to induce apoptosis.	(507, 508)
IAP	Birinapant sensitises GBM cells to IR, combined IAP and WEE1 inhibition increases TNF-α-induced cell death following IR.	(509, 510)
NF-κB	Inhibition of NF-κB increases radiosensitivity in hepatocellular, renal cell and laryngeal SC carcinomas	(440, 511, 512)
PPAR	Rosiglitazone increases radiosensitivity in pancreatic and colorectal cancer cells by acting as an agonist of PPAR	(422, 513)
PDGFR	Inhibition of multiple tyrosine kinase receptors, including PDGFR, radiosensitises breast cancer cells, glioma cells, and nasopharyngeal SCC cells	(453, 514, 515)
TNF-α	Blocking of TNF-α signalling increases radiosensitivity in tumour-associated macrophages	(516)
CDK	Inhibiting various CDKs increases radiosensitivity in HNSCC, NSCLC and oesophageal SCC *in vitro*	(424, 517, 518)
GSK-3	Restoration of GSK-3 expression in GBM cells increases radiosensitivity, indirectly inhibiting GSK-3 activity through PDK1 inhibition radiosensitises nasopharyngeal cells	(519, 520)
MDM2	Oesophageal SCC and lung cancer cells are both radiosensitised by impairment of MDM2 function	(521, 522)
PLK-1	Pharmacological inhibition of PLK-1 radiosensitises breast cancer, medulloblastoma and HNSCCs *in vitro*	(523-526)

Aurora kinase	Aurora kinase inhibition has been shown to radiosensitise OSCC, colorectal cancer, NSCLC, hepatocellular carcinoma and androgen-resistant prostate cancer	(428, 429, 527-531)
PI3K-AKT-mTOR pathway	Many cancer types, including nasopharyngeal carcinoma, HNSCC, rectal cancer, pancreatic cancer, oesophageal SCC, gastric cancer, OSCC, GBM and lung cancer, amongst many others, are radiosensitised by blocking the PI3K-AKT-mTOR pathway	(431, 473, 532-539)
MEK	Pancreatic and prostate cancers, rhabdomyosarcomas and lung cancers are all radiosensitised by MEK inhibition	(432, 540-542)
CK2	Lung cancer cells are radiosensitised by CK2 inhibition	(434, 543)
MTH1	MTH1 inhibition radiosensitises colorectal cancer cells in hypoxia	(544)
PARP	3D models of HNSCC are effectively radiosensitised by PARP inhibition	(413)
Topoisomerase	Topoisomerase inhibitor etoposide impairs the DDR and radiosensitises HNSCC cells, while amrubicin induces necrosis and increases the radiosensitivity of lung cancer cells *in vitro*	(545, 546)
DNMT	GBM and lung cancer cells were radiosensitised by DNMT inhibitor MA17	(547, 548)
HnMT	No evidence of radiosensitisation potential	

Many of the inhibitors screened in this initial stage of research target components involved in cell growth, cell survival and the regulation of apoptosis, such as Bcl-2, caspases, IAPs, NF-κB, PPARs, PDGFR and TNF-α. Bcl-2 proteins regulate Bax and Bak, which induce apoptosis. Overexpression of Bcl-2 is commonly seen in many cancers, and results in a decreased level of apoptosis. Specifically in HNSCCs, Bcl-2 overexpression is a marker of a more aggressive form of the disease – albeit with a more favourable prognosis (549), and Bcl-2 inhibitors have previously been shown to successfully radiosensitise HNSCC *in vitro* and *in vivo* (416, 417). Caspase proteins have a paradoxical role in tumour radiosensitivity, as IR activates the caspase cascade to induce apoptosis in cancer cells, however the caspase cascade can also stimulate the

repopulation of tumour cells, and thus reduce the success of radiotherapy (550). Caspase-8 is frequently mutated in HNSCCs and is associated with radioresistance and poor survival (507, 551). High-LET radiation has been shown to activate caspase-9 to increase apoptosis in *p53-mut* oral SCC Ca9-22 cells (508), however it is also interesting to note that the loss of caspase-8 has been shown to increase the susceptibility of HNSCC cells to birinapant, an inhibitor of IAPs, in combination with IR (507). IAP bind to caspases, blocking their activation and thus preventing the initiation of pro-apoptotic pathways (45). Increased expression of IAP proteins has been associated with tumour progression and treatment failure (46), and in GBM cells, IAP inhibition with birinapant increases radiosensitivity via the activation of TNF-α (509). A similar result was seen in HNSCCs, in which TNF-α-induced cell death was enhanced following combined inhibition of IAP and WEE1 (510). NF-κB stimulates the expression of anti-apoptosis genes, such as caspase inhibitors and IAPs (50), and thus increased expression of these proteins results in cell proliferation and tumour development (51). NF-κB is therefore elevated in a variety of cancer types, including approximately 41 % of nasopharyngeal cancers (52). Moreover, research has demonstrated that suppression of the NF-κB pathway in a large number of cancers, including hepatocellular carcinoma, renal cell carcinoma, and laryngeal SCC increases radiosensitivity both *in vitro* and *in vivo* (440, 511, 512). PPARs are nuclear receptor proteins that perform complex, cell-specific regulation of cell survival, proliferation, and differentiation (552). PPAR-γ expression in tongue SCC patients was found to be elevated in cases with reduced invasion depth, no evidence of muscular infiltration, and was associated with improved survival (553). Furthermore, rosiglitazone, an agonist of PPAR, has been shown to enhance radiosensitivity in pancreatic and colorectal cancer cells (422, 513). PDGFRs are tyrosine kinase receptors involved in the regulation of many cellular processes. Activation of PDGFR-mediated signalling pathways has been demonstrated to suppress

apoptosis in oral SCC (554), and inhibition of PDGFR along with other tyrosine kinase receptors has been shown to radiosensitise breast cancer cells (514). Furthermore, silencing of PDGFR increases radiosensitivity of glioma cells both *in vitro* and *in vivo* (453), and research has also demonstrated that the tyrosine kinase inhibitor famitinib can augment the radiosensitivity of nasopharyngeal carcinoma by decreasing PDGFR phosphorylation (515). The TNF-α receptor is involved in the extrinsic apoptosis pathway, where it recruits adaptor proteins, which in turn bind to procaspase-8 and procaspase-10 to form the DISC (38), activates caspase-8 to trigger cell death (39). Studies show that blocking TNF-α signalling in tumour-associated macrophages can increase radiosensitivity (516).

Furthermore, several of the cellular targets are involved in maintaining correct regulation of the cell cycle, including CDKs, GSK-3, MDM2, PLK-1, and aurora kinases. CDKs, small kinases that rely on cyclin binding to function, phosphorylate crucial cellular substrates to stimulate progression through the cell cycle (2). *CDKN2A* is one of the most frequently altered genes in HNSCC, in 22 % of cases, according to The Cancer Genome Atlas (115). CDK inhibitors have previously been shown to increase radiosensitivity in HNSCC, NSCLC and oesophageal SCC in *in vitro* studies (424, 517, 518). GSK-3 is a protein kinase involved in a number of different cellular processes, including cell cycle regulation. One study revealed that 73 % of HNSCC samples displayed erroneous expression of GSK-3, while another revealed that GSK-3 is involved in Rab1A-mediated radioresistance in nasopharyngeal carcinomas (555, 556). Interestingly, GSK-3 is downregulated in radioresistant GBM cells and its restoration has been shown to increase radiosensitivity, while indirect impairment of GSK-3 function in nasopharyngeal carcinoma by PDK1 inhibition increases sensitivity to IR (519, 520). MDM2 is a negative regulator of TP53, and is frequently upregulated in between 40 – 80 % of HNSCC cases

(557). Targeting MDM2 has been shown to increase cancer cell radiosensitivity. For example. An antagonist of MDM2 increases the radiosensitivity of *p53-WT* oesophageal SCC cells, while siRNA-mediated blocking of MDM2 activity radiosensitises A549 lung cancer cells (521, 522). PLK-1 is a serine/threonine protein kinase involved in G2/M transition, with roles in centrosome and spindle establishment and maintenance (6, 7). With such a key function in cell cycle regulation, PLK-1 is broadly implicated in cancer development, and numerous studies have focused on the anti-cancer effects of PLK-1 inhibition. Pharmacologically inhibiting PLK-1 has been demonstrated to increase sensitivity to IR in a variety of cancer types, including breast cancer, medulloblastoma, and HNSCC (523-526). Aurora kinase enzymes AURKA and AURKB are key enzymes involved in cycle progression and cellular proliferation, with roles in entering mitosis and attachment of the mitotic spindle (9, 10). Increases in the expression of aurora kinases therefore causes genetic instability, and increased levels of AURKA have been linked to a decrease in overall and disease-free survival in HNSCC patients (16). Inhibition of AURKB by Tanshinone IIA has been shown to radiosensitise OSCC in *in vivo* mouse models, while knockdown of AURKA increases the sensitivity of colorectal cancers to IR (527, 529). Aurora kinase inhibition has also been demonstrated to increase radiosensitivity in NSCLC, hepatocellular carcinoma, and androgen-resistant prostate cancer (428, 429, 528, 530, 531).

In addition, proteins involved in various cell signalling pathways were also selected for targeting during this screen, including the PI3K-AKT-mTOR pathway and MEKs. The PI3K-AKT-mTOR pathway is a key signalling pathway that is overactive in many cancers, including HNSCCs, where it is related to radiotherapy responses (558, 559). Inhibition of signalling through this pathway can radiosensitise a huge variety of cancers, including but not

limited to nasopharyngeal carcinoma, HNSCC, rectal cancer, pancreatic cancer, oesophageal SCC, gastric cancer, OSCC, GBM and lung cancer (431, 473, 532-539). Mitogen-activated protein kinase (MAPK) signalling cascades exert control over several cellular pathways, including proliferation, growth and survival, and are overactivated in many cancers, including over 50 % of OSCCs (560). MEKs are one of the downstream proteins in MAPK cascades, and inhibition of MEK – and therefore the entire signalling cascade – can induce radiosensitivity. For example, one study demonstrated the effectiveness of inhibiting MEK on the radiation response in pancreatic cancer cells *in vitro* (432). Moreover, disruption of MEK signalling can radiosensitise prostate cancer cells both *in vitro* and *in vivo* and increase sensitivity to IR in rhabdomyosarcomas (540, 541). Interestingly, combining trametinib, a MEK inhibitor, with Temsirolimus, an mTOR inhibitor, can radiosensitise lung cancer xenografts (542).

DNA associated proteins have also been selected for this drug screen. For example, drugs targeting DDR-associated proteins such as CK2, MTH1, and PARPs, were all selected, as well as topoisomerase enzymes and other DNA/RNA synthesis proteins. CK2 is a serine/threonine-selective protein kinase that regulates important phosphorylation events – such as that of p53 or MAPK – that can alter the DDR (561). CK2 expression has been shown to be altered in many cancer types, including HNSCC (562-564). CK2 has also been shown to play an important role in the radiation response of nasopharyngeal carcinoma cells (565), and inhibition of CK2 in lung cancer cells increases the response to IR (434, 543). MTH1 is an enzyme involved in the hydrolysation of oxidised purines, preventing their addition into the DNA chain (566). It is well known that cancer cells have higher levels of ROS than normal cells, and thus MTH1 is a crucial enzyme for cancer cell survival (567). Increased expression of MTH1 has been found in gastric cancer, osteosarcoma, lung

cancer, breast cancer, renal cell carcinoma and colorectal cancer (568-572). Furthermore, MTH1 inhibition increases the sensitivity of colorectal cancer cells to IR (544). The PARP family of enzymes are crucial for the DDR. Upon the induction of DNA damage, there is an increase in PARP activity, and it is well known that PARP1 is a key component of the BER pathway, where it catalyses the PARylation of repair proteins including Polβ and XRCC1, increasing the efficiency of their recruitment to damage sites (232, 573). The effectiveness of inhibiting PARP in 3D models of HNSCC has previously been demonstrated in the Parsons laboratory (413). Topoisomerase enzymes catalyse any changes in the topology of DNA during processes such as replication and transcription. Topoisomerase-IIα has a been demonstrated to have a high expression level in HNSCC and is related to tumour differentiation. There is also an association of topoisomerase-IIα expression with disease stage, recurrence, and survival of HNSCC patients – however this was not statistically significant (546). Building on this, topoisomerase-IIα inhibition by the drug etoposide has been shown to radiosensitise FaDu HNSCC cells *in vitro* by impairing the DNA damage response (545). Moreover, the topoisomerase-II inhibitor amrubicin has been demonstrated to increase the radiosensitivity of lung cancer cells *in vitro* as a result of necrosis induction (574).

Finally, I also chose to screen drugs targeting proteins involved in the regulation of chromatin organisation, including DNA methyltransferases (DNMTs) and HnMTs. DNMTs and HnMTs catalyse the addition of a methyl group onto cytosine residues of DNA or histone tails, respectively, altering chromatin architecture and thus modifying expression patterns. It is well understood that hypermethylation occurs on the promoter regions of tumour suppressor genes, thus silencing their activity (575). Furthermore, the activity of DNMTs has been linked to alcohol consumption, which is a key risk factor

for developing a multitude of cancer types, including HNSCC (576). There are several studies highlighting the importance of DNA/histone methylation on the tumour radiation response (577-581), and the DNMT inhibitor MA17 has been demonstrated to enhance radiosensitivity in lung cancer and GBM cells (547, 548). However, there is currently no evidence of HnMT inhibitors increasing radiosensitivity.

7.3. Identification of novel radiosensitisers of HPV-negative HNSCC

7.3.1. Validation of candidate radiosensitisers

Through this screen, 17 initial candidate drugs (table 4.1) were identified as possible radiosensitisers. These drugs covered a variety of the targets discussed above, with some previously being shown to successfully act as radiosensitisers. For example, the PDGFR inhibitor orantinib has been shown to increase radiosensitivity in murine carcinoma models, as well as in lung cancer, endothelial cancer, prostate cancer and GBM both *in vitro* and *in vivo* (456-459). Furthermore, the HDACi mocetinostat radiosensitises bladder cancer cells, while resminostat has previously been demonstrated to increase radiosensitivity in HNSCC (394, 405). Icotinib, an EGFR inhibitor, has been shown to radiosensitise lung cancer cells, and the combined EGFR and HDAC inhibitor CUDC-101 radiosensitises pancreatic cancer, breast cancer and glioblastoma cells *in vitro* (402, 403, 473). Further research has revealed that afatinib, another EGFR inhibitor, can radiosensitise HNSCC and nasopharyngeal carcinomas *in vitro*, and the non-specific tyrosine kinase inhibitor genistein radiosensitises many cancer types in experimental settings, including oesophageal SCC, colorectal cancer, sarcoma, prostate cancer,

hepatocellular carcinoma and NSCLC (430, 474, 475, 478-483). However, several of the drugs in the screen have not previously been linked to cancer cell radiosensitivity, including orantinib, apremilast, pracinostat, lidocaine HCl, dexrazoxane HCl, enoxacin, novobiocin sodium, fidaxomicin and mupirocin. These candidates were used to repeat the spheroid experiments; however, the results were largely negative, and it appeared that the inhibitors were false positive results. This could have been a result of the inhibitors losing their stability, so higher concentrations of 5 μM and 10 μM were used to repeat the experiments, along with a higher dose of X-rays.

Disappointingly, these results revealed that the majority of candidates did not in fact exert a radiosensitising effect on FaDu spheroids (appendix I). However, two inhibitors, CUDC-101 and pracinostat, did appear to be increasing radiosensitivity. CUDC-101 is a multitargeting inhibitor of EGFR and HDACs, while pracinostat is a potent HDACi.

7.3.2. Histone deacetylases and EGFR

HDACs are important enzymes that can modify the structure of chromatin, the condensed structure in which genomic DNA is packaged in eukaryotic cells. At its basic level, chromatin is formed from ~145 – 147 base pairs of DNA wrapped around a histone octamer (237). Histone subunits can carry PTMs which regulate and remodel the chromatin structure (242). There are a variety of histone PTMs, and of these, histone acetylation is one of the most well understood. Histone acetylation and deacetylation is controlled by HATs and HDACs. The addition of acetyl groups by HATs weakens the interaction between the histone and DNA, thus activating gene expression. Conversely, HDACs remove the acetyl groups, which restores the strong interaction between the histone and DNA and therefore silences gene expression. The

acetylation and deacetylation of histones has also been associated with the regulation of DNA repair, in particular the repair of DSBs (286, 287). In response to IR, histone acetylation levels change to allow repair factors to access the DNA, and once repair is complete, chromatin is restored to its original state. HDACs have been implicated in the maintenance of dynamic acetylation equilibrium of DDR proteins (385, 387, 389-391, 393). Aberrant HDAC expression has been associated with a large variety of cancer types (see table 1.1), including gastric, pancreatic, colorectal, prostate, hepatocellular, lung, breast, cervical, oesophageal, and ovarian cancers, as well as GBM, leukaemia and neuroblastoma (293-360). Importantly HDAC6, HDAC7 and HDAC9 have all been linked to HNSCC (340, 343, 350). Based on this evidence, it appears logical to combine HDACi with IR, resulting in altered DNA accessibility and a change in either the induction or repair efficiency of DNA damage, or changes in the gene expression profile to improve radiosensitivity in cancer cells. EGFR is a transmembrane protein with key functions in many cellular processes. Expression levels of EGFR have been associated with tumour radioresistance (161-164), and as a result there has been a large amount of research into targeting EGFR for radiosensitisation.

Both HDACis and EGFR inhibitors have been studied for radiosensitisation potential (table 7.2). EGFR inhibition has been demonstrated to radiosensitise HNSCCs, colorectal cancer, nasopharyngeal carcinoma, oesophageal SCC, GBM and breast cancer cells (474, 478, 514, 533, 534, 582). Furthermore, HDACi have been shown to be effective radiosensitisers in a variety of cancer types (table 1.2). For example, the class I HDACi VPA has been shown to effectively radiosensitise colorectal, oesophageal and thyroid cancer to photons, as well as increasing the response of hepatocellular carcinoma cells to protons (395-398). Vorinostat is a non-selective HDACi, and increases the sensitivity of melanomas as well as lung, breast, and colorectal cancer cells to photons (399-

401). Another non-selective HDACi, panobinostat, has also been shown to increase the sensitivity of hepatocellular carcinoma cells to protons, as well as bladder and prostate cancer cells to photons (404-406). Romidepsin and mocetinostat are both class I HDACi that radiosensitise bladder cancer cells to photons, and the non-selective HDACi belinostat increases the radiosensitivity of rhabdomyosarcoma, cervical and colorectal cancer cells (405, 410, 411).

Table 7.2: EGFR and HDAC inhibition and the links to radiosensitivity

Target	Radiosensitisation ability	Reference
EGFR	Inhibiting EGFR can radiosensitise many cancer types, including HNSCCs, colorectal cancer, nasopharyngeal carcinoma, oesophageal SCC, GBM and breast cancer	(474, 478, 514, 533, 534, 582)
HDAC	A variety of HDACi can sensitise colorectal, oesophageal, thyroid, lung, breast, pancreatic, prostate, bladder, and cervical cancers, as well as GBM, melanoma, hepatocellular carcinoma, HNSCC and rhabdomyosarcoma to both photons and protons	(394-407, 410, 411)

7.3.2.1. CUDC-101

CUDC-101 is a small-molecule multi-targeting inhibitor of HDAC1-10, EGFR and HER2. In pancreatic cancer cells, CUDC-101 treatment increased radiosensitivity of 3D spheroids, reduced PARP-1 levels and increased the population of apoptotic cells compared to either inhibitor or radiation treatment alone (402). Evidence from a scientific conference report also suggests that CUDC-101 can radiosensitise glioblastoma and breast cancer cells, and this effect may be associated with a delay in DSB repair (403).

7.3.2.2. Pracinostat

Pracinostat is a potent inhibitor of class I, II and IV HDACs that selectively accumulates in tumour tissue and has been shown to be approximately 2-fold more potent than other HDACi (489, 490). To date, there has been no research published into the potential of pracinostat has a radiosensitiser, however it has been demonstrated to have anti-cancer effects, and has been tested in clinical trials, particularly in haematological malignancies (493-497). More recently, there has been some investigation into pracinostat's effects in solid tumours, revealing that pracinostat can cause cell death and inhibit migration and invasion in colorectal cancer, breast cancer, and GBM cells (489, 498, 499).

7.4. Confirmation of radiosensitisers

Further validation experiments were carried out in both 2D and 3D models to confirm the observation that CUDC-101 and pracinostat can act as radiosensitisers (summarised in Table 7.3). In spheroid experiments, 1 μM CUDC-101 observably reduced spheroid growth in combination with a clinically relevant dose of 2 Gy X-rays to a statistically significant level. Similarly, 1 μM pracinostat plus 2 Gy X-rays significantly reduced spheroid growth compared to the irradiated controls. Analysis of spheroid growth relative to radiation dose following inhibitor treatment revealed that 1 μM CUDC-101 caused a clear reduction in growth relative to the DMSO controls, indicating that CUDC-101 is working synergistically with IR to reducing spheroid growth. On the other hand, this similar method of analysis shows that pracinostat does radiosensitise FaDu spheroids at 1 μM, but in an additive manner. Clonogenic survival assays were also used to assess the potential of CUDC-101 and pracinostat as radiosensitisers, using multiple HPV-negative

HNSCC cell lines: FaDu, A253, UM-SCC-11b and UM-SCC-12 (*p53-mut*), UM-SCC-6 and UM-SCC-17A (*p53-WT*). In FaDu cells, CUDC-101 dramatically reduced colony survival, particularly at a dose of 4 Gy X-rays, and this was statistically significant across the whole dataset. In a similar manner, pracinostat also dramatically reduced SF compared to controls, particularly at a 4 Gy dose, and this was statistically significant. In A253 cells, both inhibitors reduced SF compared to controls, however the differences were not statistically significant for either drug, most likely as a result of variation in the results. In UM-SCC-12 cells, CUDC-101 treatment slightly reduced survival compared to controls, however not to a statistically significant degree. Pracinostat appeared to slightly reduce SF in UM-SCC-12 cells at all doses of IR, although the difference was not statistically significant. In UM-SCC-17A cells, CUDC-101 markedly reduced SF compared to controls, and pracinostat caused a decrease in SF particularly at 4 Gy, albeit neither of these were significant. In UM-SCC-6 cells at all doses of IR, both CUDC-101 and pracinostat treatments enhanced survival compared to controls – although neither to a statistically significant degree. CUDC-101 enhanced SF in UM-SCC-11b cells at all doses of X-rays, again not to a significant degree, while in contrast pracinostat markedly reduced SF in UM-SCC-11b cells at IR doses to a statistically significant degree.

As CUDC-101 is a multi-targeting inhibitor of HDACs and EGFR, two EGFR inhibitors were also analysed, as was the HDACi mocetinostat. In both 2D and 3D models, the EGFR inhibitors lidocaine HCl and genistein did not exert any radiosensitisation effect on HNSCC cells, regardless of the cell line, inhibitor concentration or dose of X-rays. This observation replicates what has been seen in clinical trials, in which EGFR inhibitors plus IR results in inferior survival in comparison to the standard of care, cisplatin plus IR (583, 584). Mocetinostat only slightly radiosensitised FaDu spheroids, and also

somewhat reduced clonogenic survival in FaDu, A253 and UM-SCC-12 cells, although not to a significant degree. These data imply that the radiosensitisation of FaDu cells seen following CUDC-101 treatment is likely due to the HDAC-inhibiting activity of the drug, as opposed to the EGFR-inhibiting capacity. Furthermore, the cell line-dependent manner in which CUDC-101 and pracinostat appear to be working seems to be linked to the p53 status of the cells. In the *p53-mut* cell lines FaDu, A253, and UM-SCC-12, both pracinostat and CUDC-101 did reduce clonogenic survival - although disappointingly the overall reduction in SF was not statistically significant in either A253 or UM-SCC-12 cell lines. Both inhibitors enhanced survival in the *p53-WT* cell line UM-SCC-6, however, in UM-SCC-17A cells, which are also *p53-WT*, both CUDC-101 and pracinostat seemed to exert a slight radiosensitisation effect – albeit not significantly. Interestingly, CUDC-101 enhanced survival in *p53-mut* UM-SCC-11b cells, while pracinostat caused a significant radiosensitisation effect. These observations suggest that, while p53 status may be an important factor in the effectiveness of CUDC-101 and pracinostat treatments, there are other conditions involved that are influencing the cell line-dependent manner in which these inhibitors are working.

These observations have generated some interesting and novel findings. CUDC-101 has been shown to radiosensitise other cancer types (402, 403), but no research to date has been published showing its effectiveness in HNSCC. Here, I have demonstrated its effectiveness in radiosensitising FaDu cells *in vitro*. The radiosensitising potential of pracinostat has not been shown experimentally in any tumour type, and in this research, I have demonstrated its ability to significantly radiosensitise both FaDu and UM-SCC-11b cell lines *in vitro*.

Table 7.3: Summary of inhibitors in various cell models

Summary of the effects of each of the five final drugs tested in each of the various cell models. + : radiosensitisation observed to a statistically significant degree; - : no radiosensitisation observed

Drug	Spheroids	Clonogenics					
	FaDu	FaDu	A253	UM-SCC-12	UM-SCC-6	UM-SCC-17A	UM-SCC-11b
Lidocaine HCl	-	-	-	-	-	-	-
Genistein	-	-	-	-	-	-	-
CUDC-101	+	+	-	-	-	-	-
Mocetinostat	-	-	-	-	-	-	-
Pracinostat	+	+	-	-	-	-	+

7.5. HDACi Alter the DNA Damage Response in HNSCC Cells

As mentioned above, HDACs have been implicated in the regulation of the DDR. HDAC1 and HDAC2 swiftly localise to sites of IR-induced DNA damage, where they regulate H3K56 acetylation, which decreases following damage induction. Class I/II HDAC inhibitors can impact this localisation (387). Moreover, siRNA-mediated depletion of HDAC1/2 has been shown to cause hypersensitivity to IR, DNA damage-induced phosphorylation of CHK1/2 and p53, and increased levels of γH2AX. In the same study, it was found that in HDAC1/2-depleted cells, there is a persistence of Ku70 and Artemis at DNA damage sites (387). Research has also demonstrated the importance of HDAC3 function for efficient DSB repair. In MEFs, the inactivation of HDAC3 results in a higher sensitivity to DNA-damaging agents doxorubicin and cisplatin (388). Interestingly, research also shows that HDAC3 is not recruited to sites of DNA damage, nor does the loss of HDAC3 affect the localisation of key DDR proteins, including RAD51, BRCA1, and MRE11, suggesting that the loss of HDAC3 impedes the DDR by targeting the chromatin structure rather than impacting specific repair proteins (389). Meanwhile, HDAC4 has been shown to localise to nuclear foci post-irradiation, and these foci demonstrate similar kinetics to 53BP1 foci. In fact, further investigation revealed that HDAC4 and 53BP1 colocalise to sites of

DSBs and may maintain the stability of one another, as a reduction in levels of 53BP1 were observed upon HDAC4 silencing, and vice versa. Additionally, either HDAC4 or 53BP1 silencing decreases 53BP1 foci upon DNA damage, further supporting the notion that HDAC4 is involved in the repair of DSBs (390). HDAC6 has been demonstrated to have a significant role in DNA MMR, via interactions with MLH1 and MSH2, while HDAC9/10 have been implicated in the HR pathway, as siRNA-mediated reduction of HDAC9/10 reduced HR activity and sensitised cells to mitomycin C (393). The mechanisms behind the roles of HDAC9/10 in HR, however, are yet to be elucidated.

Despite the lack of evidence regarding CUDC-101 and pracinostat specifically, there is research suggesting that inhibition of HDAC1 and HDAC3 with the drug entinostat alters the expression of several DDR proteins, including BRCA1, PolB, MRE11A and RPA1 (585). HDAC1 has also been linked to the expression of ATM, ATR and BRCA1 (387). Another HDACi, vorinostat, has been shown to downregulate BRCA1, CHK1, Rad51, Rad50 and MRE11 in cancer cells (586, 587) and deacetylates MLH1 on lysines 33, 241, 361 and 377, which prevents the formation of the MutLα-MutSα complex, thus inhibiting the MMR pathway (391). In addition to this, HDAC6 has been reported to reduce the stability of the MSH2 via its deacetylation (392). Finally, there is some evidence to suggest that HDAC9 and HDAC10 are involved in the DDR, specifically HR. One study demonstrated that an siRNA-mediated decrease in levels of HDAC9/10 significantly reduced the activity of the HR pathways, and sensitised cells to mitomycin C (393). However, the mechanism behind this is currently unclear. As both CUDC-101 and pracinostat are broad spectrum inhibitors of HDACs, their activity could therefore be impairing correct expression of DDR proteins, which could then be linked to the observed

radiosensitisation seen following CUDC-101 and pracinostat treatments in HNSCC. There has been some previous research to suggest that CUDC-101 can impair the DDR, for example, data from a scientific conference report showed that γH2AX foci were retained in breast cancer and GBM cells following combined CUDC-101 and IR treatment (403). On the other hand, there has been no research to date linking pracinostat to impaired DNA repair. However, as discussed in chapter 6, my research uncovered the novel finding that in HNSCC cells, both pracinostat and CUDC-101 impair the DDR, specifically DSB repair, following X-ray irradiation.

Utilising the neutral comet assay, I demonstrated that DSB repair is delayed in FaDu cells following HDACi treatment via CUDC-101 and pracinostat. Intriguingly, the data also showed that HDACi induces DNA damage in an IR-independent manner, as the amount of endogenous DNA damage in unirradiated cells was significantly higher in both CUDC-101 and pracinostat-treated cells in comparison to controls. A similar result was observed in UM-SCC-11b cells, in that pracinostat caused a significant impairment of DSB repair following X-ray irradiation. To further support the theory that impairments in the DDR were causing the observed HDACi-induced radiosensitisation, I also carried out neutral comet assays using UM-SCC-12 cells, which were not radiosensitised by HDAC inhibition. As expected, there was no significant difference in DSB repair kinetics between the cells treated with HDACi and the DMSO controls. As well as analysing DSB repair kinetics with the neutral comet assay, I also assessed γH2AX foci as a marker of DNA damage. In FaDu cells, both pracinostat and CUDC-101 treatment resulted in a persistence of γH2AX foci. Cells treated with either inhibitor had a significantly higher number of foci per cell compared to controls, specifically at 4-hours post-IR. These data strongly support the data from neutral comet

assays, proving that these inhibitors do impair the DDR in FaDu cells. In UM-SCC-11b cells, the differences observed between pracinostat-treated cells and controls were even more striking. At all the time points analysed post-IR, there were significantly higher numbers of γH2AX foci per cell after pracinostat treatment in comparison to DMSO controls. Again, this provides further validation that pracinostat alters the DDR in UM-SCC-11b cells. Thus, I can conclude that pracinostat and CUDC-101 impair DSB repair following IR in a cell line-dependent manner. Moreover, there is also evidence to suggest that these inhibitors may induce DNA damage as a single-agent therapy.

CHAPTER 8: CONCLUSIONS AND FUTURE PERSPECTIVES

8.1. Conclusions

In summary, over the course of this research I have successfully performed a screen of 183 FDA-approved drugs, examining their impact on the radiosensitivity of HPV-negative HNSCC. Following multiple validation experiments in both 2D and 3D models, I confirmed the novel observation that two drugs, pracinostat – a potent HDAC inhibitor – and CUDC-101 – a multitargeting HDAC and EGFR inhibitor – can successfully radiosensitise FaDu (both inhibitors) and UM-SCC-11b (pracinostat only) cells. Further investigation into the mechanisms behind this observation revealed that both drugs had a significant impact on the cellular DDR, causing an impairment of repair and persistence of DSB damage.

At the start of this research, I hypothesised that, by analysing an FDA-approved drug library, I could identify specific inhibitors that had potential to be used as effective radiosensitisers of relatively radioresistant HPV-negative HNSCC. Within this project, I have successfully completed the aims I set out to achieve:

- Utilising a 3D spheroid model, through drug screening I identified 17 candidate inhibitors that seemed to be radiosensitising FaDu cells.
- I used 2D and 3D models to validate the effects of these candidates, and identified two inhibitors, CUDC-101 and pracinostat, that appeared to act as radiosensitisers.

- I successfully demonstrated that CUDC-101 radiosensitises FaDu cells in both a 3D spheroid model and a 2D clonogenic model, however, does not exert a significant radiosensitisation effect on other HNSCC cell lines tested.
- I successfully revealed the novel finding that pracinostat can radiosensitise FaDu spheroids, as well as reduce survival in FaDu and UM-SCC-11b cells following IR exposure.
- Through analysis of DNA repair kinetics, I showed that CUDC-101 and pracinostat can induce damage as single agent treatments, as well as impairing the repair of DNA DSBs following exposure to X-rays.

8.2. Future Perspectives

This research has provided crucial advancements in the field of HNSCC radiosensitivity. It is vital that more methods of improving patient response to radiotherapy are identified to improve survival and quality of life. The next stages of this work would be to carry out further investigation of the mechanisms behind the impairment of DNA repair following HDACi, and to test the effects of these drugs on healthy cells. Ideally, these inhibitors would be tested in non-cancerous cell lines from the same sites of origin as the HNSCC cells, allowing for direct comparisons in survival. Previous research has suggested that HDACi can alter the expression of several key DDR proteins (385, 387, 389-391, 393), and it would be crucial to understand the specific manner in which CUDC-101 and pracinostat could be altering the DDR. For example, techniques such as immunoblotting can be used to analyse the impact of HDAC inhibition on the expression or activation of key proteins involved in the DDR. Furthermore, CUDC-101 and pracinostat, through their HDAC-inhibiting activity, can alter the structure of chromatin, which is highly dynamic depending on the needs of the cell. PTMs alter the structure of chromatin by changing the amount of interaction between the double helix

and histone complexes. Histone acetylation neutralises the positive charge of the histone octamer, thus weakening the histone-DNA interactions and resulting in the open, euchromatic structure (285). On the other hand, deacetylation preserves the stronger attraction between the DNA and the histones, maintaining a closed heterochromatic structure. Upon exposure to IR, any DNA within euchromatic regions is more accessible, and consequently much more sensitive to IR-induced damage. In order to elucidate the structure of chromatin to confirm this hypothesis, a variety of sequencing techniques can be used, including chromatin immunoprecipitation followed by sequencing (ChIP-seq), in which DNA sequences associated with specific histone modifications can be identified, allowing the determination of either euchromatin or heterochromatin structure (588). Moreover, the assay for transpose-accessible chromatin using sequencing (ATAC-seq) allows for the assessment of chromatin accessibility at a genome wide level (589). There has been a significant number of studies linking cellular radiosensitivity to chromatin structure (590-594). HDAC inhibitors, by preventing the removal of acetyl groups and the transition to the closed heterochromatin structure, increase the proportion of DNA that is exposed to IR, thus increasing cellular radiosensitivity. In fact, the results from neutral comet assays and immunofluorescent staining carried out in this research did suggest that CUDC-101 and pracinostat as single-agent treatments are sufficient to increase DNA damage, and this could be a result of increased susceptibility to endogenous sources of damage.

As a cell line-dependent effect was seen in this research, it will be important to fully understand the conditions under which CUDC-101 and pracinostat can effectively radiosensitise HNSCC cells. This will involve testing a wider variety of cell lines, including those from more sites of origin – the majority of cell lines used in this research came from the oral cavity, with the exception of

FaDu and UM-SCC-6, which originated in the hypopharynx and tongue, respectively. Moreover, it is important to study the effects of these inhibitors in cell lines with differing p53 statuses, as this research revealed that *p53-mut* cell lines may be more sensitive to HDACi – however it is clear more factors are involved, such as the origin site of the tumour. This research only focused on HPV-negative cell lines, as HPV-negative cases of HNSCC are known to be more radioresistant. However, CUDC-101 and pracinostat may also be effective at radiosensitising HPV-positive HNSCCs, and thus it is important that these cell lines are also represented in future experiments. Utilising more advanced 3D models of HNSCC will be highly beneficial for future research, as the observations would be more representative of those seen in patient tumours. This includes the use of patient-derived organoids, which have previously been successfully established, and have been shown to predict drug sensitivity as well as accurately represent the original tumours from which they were derived (595). This would eventually develop into *in vivo* animal models, particularly xenografts on mice, followed by human clinical trials in the future.

Furthermore, researching the activity of these drugs under hypoxic conditions will also be of high importance, due to the hypoxic cores present in most solid tumours. Tumour hypoxia develops as a result of imbalances between oxygen supply and demand. In HNSCC, hypoxia has been shown to contribute to radioresistance and treatment failure (596), and hypoxic conditions in the tumour core result in reduced levels of IR-induced DNA damage (165-168). Experimentally, cells should be grown and irradiated under different hypoxic conditions, such as mild and severe (1 % and 0.1 % O_2, respectively), and compared to normoxia (21 % O_2), and the effects of CUDC-101 and pracinostat on growth, survival, and the expression of hypoxia-related proteins, such as HIF, should be analysed.

These inhibitors should also be investigated with other forms of radiotherapy, including PBT and ultra-high dose FLASH radiotherapy, both of which can reduce normal tissue toxicity and thus have a significant impact on patient quality of life. PBT is a more targeted treatment than conventional radiotherapy due to the low entrance dose, which then increases along the radiation track, and peaks at the Bragg peak, after which there is a rapid distal fall-off of energy (144). This allows the dose to be targeted to specific regions, as well as minimising the dose deposited in healthy tissues. Particle therapy, such as PBT, has an increasing LET at and around the Bragg peak, meaning there is a large energy deposit within a short distance (597, 598). This is directly opposed to low LET radiation, such as X-rays, which deposits a small amount of energy over a small distance. Higher LET radiation increases the formation of DSBs and CDD compared to low LET radiation, which mostly generates base lesions and SSBs (144, 414, 599, 600). There are many biological uncertainties associated with PBT as a result of the variable LET, resulting in changes to the DNA damage profile induced by the radiation (144, 414). The HDACi VPA and panobinostat have previously been shown to radiosensitise hepatocellular carcinoma to protons (398, 404), and thus there is justification for testing the effects of CUDC-101 and pracinostat in combination with PBT for HNSCC. FLASH radiotherapy utilises ultra-high dose rates greater than 40 Gy/s – this is a stark contrast to conventional dose rates, which are approximately 2 Gy/min (601). This ultra-high dose rate results in the so-called 'FLASH effect', which is the decrease in IR-induced toxicities in normal tissue with the maintenance of tumour cytotoxicity compared to conventional radiotherapy (602, 603). The mechanisms behind this FLASH effect are yet to be fully elucidated, although there are a number of hypotheses, including the oxygen depletion hypothesis, the involvement of ROS, and the inflammatory and immune responses (604-611). There are still several uncertainties

surrounding FLASH radiotherapy and its potential for clinical translation, as there are a variety of factors that must be taken into consideration, including: source of radiation, overall radiation dose, pulse rate, duration, width, and number, and the total delivery time (601).

In conclusion, the identification of two novel radiosensitisers of HPV-negative HNSCC through this research is a key step in improving patient treatment, and the cell line-dependent manner in which these inhibitors work presents an opportunity for developing personalised radiosensitisation treatment in the future.

CHAPTER 9: REFERENCES

1. Hanahan D, Weinberg RA. Hallmarks of Cancer: The Next Generation. Cell. 2011;144(5):646-74.
2. Barnum KJ, O'Connell MJ. Cell cycle regulation by checkpoints. Methods Mol Biol. 2014;1170:29-40.
3. Peter M. The regulation of cyclin-dependent kinase inhibitors (CKIs). Prog Cell Cycle Res. 1997;3:99-108.
4. Rayess H, Wang MB, Srivatsan ES. Cellular senescence and tumor suppressor gene p16. Int J Cancer. 2012;130(8):1715-25.
5. Kanellou P, Zaravinos A, Zioga M, Spandidos DA. Deregulation of the tumour suppressor genes p14(ARF), p15(INK4b), p16(INK4a) and p53 in basal cell carcinoma. Br J Dermatol. 2009;160(6):1215-21.
6. van de Weerdt BC, Medema RH. Polo-Like Kinases: A Team in Control of the Division. Cell Cycle. 2006;5(8):853-64.
7. Malumbres M, Barbacid M. Cell cycle kinases in cancer. Curr Opin Genet Dev. 2007;17(1):60-5.
8. Chen X-H, Lan B, Qu Y, Zhang X-Q, Cai Q, Liu B-Y, et al. Inhibitory effect of Polo-like kinase 1 depletion on mitosis and apoptosis of gastric cancer cells. World J Gastroenterol. 2006;12(1):29-35.
9. Hannak E, Kirkham M, Hyman AA, Oegema K. Aurora-A kinase is required for centrosome maturation in Caenorhabditis elegans. J Cell Biol. 2001;155(7):1109-16.
10. Hauf S, Cole RW, LaTerra S, Zimmer C, Schnapp G, Walter R, et al. The small molecule Hesperadin reveals a role for Aurora B in correcting kinetochore-microtubule attachment and in maintaining the spindle assembly checkpoint. J Cell Biol. 2003;161(2):281-94.
11. Gopalan G, Chan CSM, Donovan PJ. A Novel Mammalian, Mitotic Spindle–associated Kinase Is Related to Yeast and Fly Chromosome Segregation Regulators J Cell Biol. 1997;138(3):643-56.
12. Hartwell L, Kastan M. Cell Cycle Control and Cancer. Science. 1994;266(5192):1821-8.
13. Network TCGA. Comprehensive genomic characterization of head and neck squamous cell carcinomas. Nature. 2015;517(7536):576-82.
14. de Boer V, Martens-de Kemp SR, Buijze M, Stiger-van Walsum M, Bloemena E, Dietrich R, et al. Targeting PLK1 as a novel chemopreventive approach to eradicate preneoplastic mucosal changes in the head and neck. Oncotarget. 2017;8(58):97928-40.
15. Marumoto T, Zhang D, Saya H. Aurora-A - a guardian of poles. Nat Rev Cancer. 2005;5(1):42-50.
16. Reiter R, Gais P, Jutting U, Steuer-Vogt MK, Pickhard A, Bink K, et al. Aurora kinase A messenger RNA overexpression is correlated with tumor progression and shortened survival in head and neck squamous cell carcinoma. Clin Cancer Res. 2006;12(17):5136-41.
17. Otto T, Sicinski P. Cell cycle proteins as promising targets in cancer therapy. Nat Rev Cancer. 2017;17(2):93-115.
18. Wang LH, Wu CF, Rajasekaran N, Shin YK. Loss of Tumor Suppressor Gene Function in Human Cancer: An Overview. Cell Physiol Biochem. 2018;51(6):2647-93.
19. Cowell JK. Tumour suppressor genes. Ann Oncol. 1992;3(9):693-8.
20. Knudson AG. Mutation and Cancer: Statistical Study of Retinoblastoma. Proc Nat Acad Sci USA. 1971;68(4):820-3.
21. Cavenee WK, Dryja TP, Phillips RA, Benedict WF, Godbout R, Gallie BL, et al. Expression of recessive alleles by chromosomal mechanisms in retinoblastoma. Nature. 1983;305:779-84.
22. Weinberg RA. The Retinoblastoma Protein and Cell Cycle Control. Cell. 1995;81:323-30.
23. Dyson N. The regulation of E2F by pRB-family proteins. Genes and Development. 1998;12:2245-62.
24. Adams PD, Kaelin Jr WG. Transcriptional control by E2F. Seminars in Cancer Biology. 1995;6:99-108.
25. Olivier M, Hollstein M, Hainaut P. TP53 mutations in human cancers: origins, consequences, and clinical use. Cold Spring Harb Perspect Biol. 2010;2(1):a001008.
26. Malkin D, Li FP, Strong LC, Fraumeni Jr JF, Nelson CE, Kim DH, et al. Germ line p53 mutations in a familial synfrome of breast cancer, sarcomas and other neoplasms. Science. 1990;250(4985):1233-8.

27. Hickman ES, Moroni MC, Helin K. The role of p53 and pRB in apoptosis and cancer. Current Opinion in Genetics & Development. 2002;12:60-6.
28. Lakin ND, Jackson SP. Regulation of p53 in response to DNA damage. Oncogene. 1999;18:7644-55.
29. Williams AB, Schumacher B. p53 in the DNA-Damage-Repair Process. Cold Spring Harb Perspect Med. 2016;6(5).
30. Kuerbitz SJ, Plunkett BS, Walsh WV, Kastan MB. Wild-type p53 is a cell cycle checkpoint determinant following irradiation. Proc Nat Acad Sci USA. 1992;89(7491-7495).
31. Scully R, Chen J, Plug A, Xiao Y, Weaver D, Feunteun J, et al. Association of BRCA1 with Rad51 in Mitotic and Meiotic Cells. Cell. 1997;88(2):265-75.
32. Chen L, Nievera CJ, Lee AY, Wu X. Cell cycle-dependent complex formation of BRCA1.CtIP.MRN is important for DNA double-strand break repair. J Biol Chem. 2008;283(12):7713-20.
33. Moynahan ME, Pierce AJ, Jasin M. BRCA2 is Required for Homology-Directed Repair of Chromosomal Breaks. Molecular Cell. 2001;7:263-72.
34. Roy R, Chun J, Powell SN. BRCA1 and BRCA2: different roles in a common pathway of genome protection. Nat Rev Cancer. 2011;12(1):68-78.
35. Elmore S. Apoptosis: A Review of Programmed Cell Death. Toxicol Pathol. 2007;35(4):495-516.
36. Adams JM, Cory S. The Bcl-2 apoptotic switch in cancer development and therapy. Oncogene. 2007;26(9):1324-37.
37. Locksley RM, Killeen N, Lenardo MJ. The TNF and TNF receptor superfamilies: integrating mammalian biology. Cell. 2001;104:487-501.
38. Kischkel F, Hellbardt S, Behrmann I, Germer M, Pawlita M, Krammer P, et al. Cytotoxicity-dependent APO-1 (Fas/CD95)-associated proteins form a death-inducing signaling complex (DISC) with the receptor. EMBO J. 1995;14(22):5579-88.
39. Green DR, Llambi F. Cell Death Signaling. Cold Spring Harb Perspect Biol. 2015;7(12).
40. Lopez J, Tait SW. Mitochondrial apoptosis: killing cancer using the enemy within. Br J Cancer. 2015;112(6):957-62.
41. Evan G, T L. A Matter of Life and Cell Death. Science. 1998;281(5381):1317-22.
42. Oltersdorf T, Elmore SW, Shoemaker AR, Armstrong RC, Augeri DJ, Belli BA, et al. An inhibitor of Bcl-2 family proteins induces regression of solid tumours. Nature. 2005;435(7042):677-81.
43. Philchenkov A, Zavelevich M, Kroczak TJ, Los M. Caspases and Cancer: Mechanisms of Inactivation and New Treatment Modalities. Exp Oncol. 2004;26(2):82-97.
44. Chaudhary PM, Eby MT, Jasmin A, Kumar A, Liu L, Hood L. Activation of the NF-kB pathway by Caspase 8 and its homologs. Oncogene. 2000;19(39):4451-60.
45. Fulda S, Vucic D. Targeting IAP proteins for therapeutic intervention in cancer. Nat Rev Drug Discov. 2012;11(2):109-24.
46. Owens TW, Gilmore AP, Streuli CH, Foster FM. Inhibitor of Apoptosis Proteins: Promising Targets for Cancer Therapy. J Carcinog Mutagen. 2013;Suppl 14.
47. Sah NK, Khan Z, Khan GJ, Bisen PS. Structural, functional and therapeutic biology of survivin. Cancer Lett. 2006;244(2):164-71.
48. Ambrosini G, C A, Altieri D. A novel anti-apoptosis gene, survivin, expressed in cancer and lymphoma. Nat Med. 1997;3(8):917-2.
49. Rong L, Guo H, Liu K. The role of survivin in oral squamous cell carcinoma. Biomedical Research. 2018;29(4):780-3.
50. Xia Y, Shen S, Verma IM. NF-kappaB, an active player in human cancers. Cancer Immunol Res. 2014;2(9):823-30.
51. Vlahopoulos SA. Aberrant control of NF-kappaB in cancer permits transcriptional and phenotypic plasticity, to curtail dependence on host tissue: molecular mode. Cancer Biol Med. 2017;14(3):254-70.
52. Li YY, Chung GT, Lui VW, To KF, Ma BB, Chow C, et al. Exome and genome sequencing of nasopharynx cancer identifies NF-kappaB pathway activating mutations. Nat Commun. 2017;8:14121.
53. Hayflick L, Moorhead PS. The Serial Cultivation of Human Diploid Cell Strains. Experimental Cell Research. 1961;25:585-621.
54. de Lange T. Shelterin: the protein complex that shapes and safeguards human telomeres. Genes Dev. 2005;19(18):2100-10.
55. Harley CB, Futcher AB, Greider CW. Telomeres shorten during ageing of human fibroblasts. Nature. 1990;345:458-60.

56. Reddel RR. Telomere Maintenance Mechanisms in Cancer: Clinical Implications. Curr Pharm Des. 2014;20(41):6361-74.
57. Shay JW, Bacchetti S. A Survey of Telomerase Activity in Human Cancer. European Journal of Cancer. 1997;33(5):787-91.
58. Blackburn EH, Greider CW, Szostak JW. Telomeres and telomerase: the path from maize, *Tetrahymena* and yeast to human cancer and aging. Nat Med. 2006;12:1133-8.
59. Collins K, Mitchell JR. Telomerase in the human organism. Oncogene. 2002;21:564-79.
60. Akincilar SC, Unal B, Tergaonkar V. Reactivation of telomerase in cancer. Cell Mol Life Sci. 2016;73(8):1659-70.
61. Dunham MA, Neumann AA, Fasching CL, Reddel RR. Telomere maintenance by recombination in human cells. Nature Genetics. 2000;26:447-50.
62. Hanahan D, Folkman J. Patterns and Emerging Mechanisms of the Angiogenic Switch during Tumourigenesis. Cell. 1996;86:353-64.
63. De Francesco EM, Lappano R, Santolla MF, Marsico S, Caruso A, Maggiolini M. HIF-1alpha/GPER signaling mediates the expression of VEGF induced by hypoxia in breast cancer associated fibroblasts (CAFs). Breast Cancer Res. 2013;15(4):R64.
64. Carmeliet P. VEGF as a key mediator of angiogenesis in cancer. Oncology. 2005;69 Suppl 3:4-10.
65. Kazerounian S, Yee KO, Lawler J. Thrombospondins in cancer. Cell Mol Life Sci. 2008;65(5):700-12.
66. Raica M, Cimpean AM, Ribatti D. Angiogenesis in pre-malignant conditions. Eur J Cancer. 2009;45(11):1924-34.
67. Baeriswyl V, Christofori G. The angiogenic switch in carcinogenesis. Semin Cancer Biol. 2009;19(5):329-37.
68. Kleiner DE, Stetler-Stevenson WG. Matrix metalloproteinases and metastasis. Cancer Chemother Pharmacol. 1999;43:(suppl)S42-S51.
69. Navarro P, Gomez M, Pizarro A, Gamallo C, Quintanilla M, Cano A. A role for the E-cadherin cell-cell adhesion molecule during tumour progression of mouse epidermal carcinogenesis. J Cell Biol. 1991;115:517-33.
70. Mendonsa AM, Na TY, Gumbiner BM. E-cadherin in contact inhibition and cancer. Oncogene. 2018;37(35):4769-80.
71. Yang J, Weinberg RA. Epithelial-mesenchymal transition: at the crossroads of development and tumor metastasis. Dev Cell. 2008;14(6):818-29.
72. De Craene B, Berx G. Regulatory networks defining EMT during cancer initiation and progression. Nat Rev Cancer. 2013;13(2):97-110.
73. Hong T, Watanabe K, Ta CH, Villarreal-Ponce A, Nie Q, Dai X. An Ovol2-Zeb1 Mutual Inhibitory Circuit Governs Bidirectional and Multi-step Transition between Epithelial and Mesenchymal States. PLoS Comput Biol. 2015;11(11):e1004569.
74. Zhang J, Tian X, Zhang H, Teng Y, Li R, Bai F, et al. TGF-b–induced epithelial-to-mesenchymaltransition proceeds through stepwise activation ofmultiple feedback loops. Sci Signal. 2015;7(ra91).
75. Rankin EB, Giaccia AJ. Hypoxic control of metastasis. Science. 2016;352(6282):175-80.
76. Pastushenko I, Brisebarre A, Sifrim A, Fioramonti M, Revenco T, Boumahdi S, et al. Identification of the tumour transition states occurring during EMT. Nature. 2018;556(7702):463-8.
77. Aceto N, Bardia A, Miyamoto DT, Donaldson MC, Wittner BS, Spencer JA, et al. Circulating tumor cell clusters are oligoclonal precursors of breast cancer metastasis. Cell. 2014;158(5):1110-22.
78. Fares J, Fares MY, Khachfe HH, Salhab HA, Fares Y. Molecular principles of metastasis: a hallmark of cancer revisited. Signal Transduct Target Ther. 2020;5(1):28.
79. Roche J. The Epithelial-to-Mesenchymal Transition in Cancer. Cancers (Basel). 2018;10(2).
80. Warburg O. On respiratory impairment in cancer cells. Science. 1956;124:269-70.
81. Vander Heiden MG, Cantley LC, Thompson CB. Understanding the Warburg effect: the metabolic requirements of cell proliferation. Science. 2009;324(5930):1029-33.
82. Jones RG, Thompson CB. Tumor suppressors and cell metabolism: a recipe for cancer growth. Genes Dev. 2009;23(5):537-48.
83. Semenza GL. HIF-1: upstream and downstream of cancer metabolism. Curr Opin Genet Dev. 2010;20(1):51-6.

84. Vajdic CM, van Leeuwen MT. Cancer incidence and risk factors after solid organ transplantation. Int J Cancer. 2009;125(8):1747-54.
85. Gonzales H, Hagerling C, Werb Z. Roles of the immune system in cancer: from tumour initiation to metastatic progression. Genes and Development. 2018;32(19-20):1267-84.
86. McGranahan N, Rosenthal R, Hiley CT, Rowan AJ, Watkins TBK, Wilson GA, et al. Allele-Specific HLA Loss and Immune Escape in Lung Cancer Evolution. Cell. 2017;171(6):1259-71 e11.
87. Tran E, Robbins PF, Lu YC, Prickett TD, Gartner JJ, Jia L, et al. T-Cell Transfer Therapy Targeting Mutant KRAS in Cancer. N Engl J Med. 2016;375(23):2255-62.
88. Chowell D, Morris LGT, Grigg CM, Weber JK, Samstein RM, Makarov V, et al. Patient HLA class I genotype influences cancer response to checkpoint blockade immunotherapy. Science. 2018;359(6375):582-7.
89. Lanier LL. Up on the tightrope: natural killer cell activation and inhibition. Nat Immunol. 2008;9(5):495-502.
90. Gras Navarro A, Bjorklund AT, Chekenya M. Therapeutic potential and challenges of natural killer cells in treatment of solid tumors. Front Immunol. 2015;6:202.
91. Lopez-Soto A, Gonzalez S, Smyth MJ, Galluzzi L. Control of Metastasis by NK Cells. Cancer Cell. 2017;32(2):135-54.
92. Malladi S, Macalinao DG, Jin X, He L, Basnet H, Zou Y, et al. Metastatic Latency and Immune Evasion through Autocrine Inhibition of WNT. Cell. 2016;165(1):45-60.
93. Becker JC, Andersen MH, Schrama D, Thor Straten P. Immune-suppressive properties of the tumor microenvironment. Cancer Immunol Immunother. 2013;62(7):1137-48.
94. Chew V, Toh HC, Abastado JP. Immune microenvironment in tumor progression: characteristics and challenges for therapy. J Oncol. 2012;2012:608406.
95. Ostrand-Rosenberg S, Sinha P. Myeloid-derived suppressor cells: linking inflammation and cancer. J Immunol. 2009;182(8):4499-506.
96. Mantovani A, Schioppa T, Porta C, Allavena P, Sica A. Role of tumor-associated macrophages in tumor progression and invasion. Cancer Metastasis Rev. 2006;25(3):315-22.
97. Chew V, Chen J, Lee D, Loh E, Lee J, Lim KH, et al. Chemokine-driven lymphocyte infiltration: an early intratumoural event determining long-term survival in resectable hepatocellular carcinoma. Gut. 2012;61(3):427-38.
98. Tosolini M, Kirilovsky A, Mlecnik B, Fredriksen T, Mauger S, Bindea G, et al. Clinical impact of different classes of infiltrating T cytotoxic and helper cells (Th1, th2, treg, th17) in patients with colorectal cancer. Cancer Res. 2011;71(4):1263-71.
99. Balkwill F. Cancer and the chemokine network. Nat Rev Cancer. 2004;4(7):540-50.
100. Wilson J, Balkwill F. The role of cytokines in the epithelial cancer microenvironment. Semin Cancer Biol. 2002;12(2):113-20.
101. Bhowmick NA, Neilson EG, Moses HL. Stromal fibroblasts in cancer initiation and progression. Nature. 2004;432(7015):332-7.
102. Mohseny AB, Hogendoorn PC. Concise review: mesenchymal tumors: when stem cells go mad. Stem Cells. 2011;29(3):397-403.
103. Sung H, Ferlay J, Siegel RL, Laversanne M, Soerjomataram I, Jemal A, et al. Global Cancer Statistics 2020: GLOBOCAN Estimates of Incidence and Mortality Worldwide for 36 Cancers in 185 Countries. CA Cancer J Clin. 2021;71(3):209-49.
104. Mody MD, Rocco JW, Yom SS, Haddad RI, Saba NF. Head and neck cancer. Lancet. 2021;398(10318):2289-99.
105. CRUK. Head and neck cancers statistics 2021 [Available from: https://www.cancerresearchuk.org/health-professional/cancer-statistics/statistics-by-cancer-type/head-and-neck-cancers#heading-Two.
106. Talamini R, Bosetti C, La Vecchia C, Dal Maso L, Levi F, Bidoli E, et al. Combined effect of tobacco and alcohol on laryngeal cancer risk: a case-control study. Cancer Causes and Control. 2002;13:957-64.
107. Blot WJ, McLaughin JK, Winn DM, Austin DF, Greenberg RS, Preston-Martin S, et al. Smoking and Drinking in Relation to Oral and Pharyngeal Cancer. Cancer Res. 1988;48:3282-7.
108. Zhang LW, Li J, Cong X, Hu XS, Li D, Wu LL, et al. Incidence and mortality trends in oral and oropharyngeal cancers in China, 2005-2013. Cancer Epidemiol. 2018;57:120-6.
109. Research NWC. Head and Neck Cancer. 2023.

110. Gillison ML, Chaturvedi AK, Anderson WF, Fakhry C. Epidemiology of Human Papillomavirus-Positive Head and Neck Squamous Cell Carcinoma. J Clin Oncol. 2015;33(29):3235-42.
111. Chaturvedi AK, Graubard BI, Broutian T, Pickard RK, Tong ZY, Xiao W, et al. NHANES 2009-2012 Findings: Association of Sexual Behaviors with Higher Prevalence of Oral Oncogenic Human Papillomavirus Infections in U.S. Men. Cancer Res. 2015;75(12):2468-77.
112. Veeramachaneni R, Walker T, Revil T, Weck A, Badescu D, O'Sullivan J, et al. Analysis of head and neck carcinoma progression reveals novel and relevant stage-specific changes associated with immortalisation and malignancy. Sci Rep. 2019;9(1):11992.
113. Califano J, van der Reet P, Westra W, Nawroz H, Clayman G, Piantadosi S, et al. Genetic Progression Model for Head and Neck Cancer: Implications for Field Characterization. Cancer Res. 1996;56:2488-92.
114. Yagyu T, Ohira T, Shimizu R, Morimoto M, Murakami Y, Hanaki T, et al. Human chromosome 3p21.3 carries TERT transcriptional regulators in pancreatic cancer. Sci Rep. 2021;11(1):15355.
115. Cancer Genome Atlas N. Comprehensive genomic characterization of head and neck squamous cell carcinomas. Nature. 2015;517(7536):576-82.
116. Parfenov M, Pedamallu CS, Gehlenborg N, Freeman SS, Danilova L, Bristow CA, et al. Characterization of HPV and host genome interactions in primary head and neck cancers. Proc Natl Acad Sci U S A. 2014;111(43):15544-9.
117. Zhou G, Liu Z, Myers JN. TP53 Mutations in Head and Neck Squamous Cell Carcinoma and Their Impact on Disease Progression and Treatment Response. J Cell Biochem. 2016;117(12):2682-92.
118. Boyle JO, Hakim J, Koch W, Riet Pvd, Hruban RH, Roa RA, et al. The incidence of p53 mutations increases with progression of head and neck cancer. Cancer research. 1993;53(19):4477-80.
119. Vousden KH, Prives C. Blinded by the light: the growing complexity of p53. Cell. 2009;137(3):413-31.
120. Muller PA, Vousden KH. p53 mutations in cancer. Nature cell biology. 2013;15(1):2-8.
121. Haupt S, Raghu D, Haupt Y. Mutant p53 Drives Cancer by Subverting Multiple Tumor Suppression Pathways. Front Oncol. 2016;6:12.
122. Neskey DM, Osman AA, Ow TJ, Katsonis P, McDonald T, Hicks SC, et al. Evolutionary Action Score of TP53 Identifies High-Risk Mutations Associated with Decreased Survival and Increased Distant Metastases in Head and Neck Cancer. Cancer Res. 2015;75(7):1527-36.
123. Zhou G, Wang J, Zhao M, Xie T-X, Tanaka N, Sano D, et al. Gain-of-function mutant p53 promotes cell growth and cancer cell metabolism via inhibition of AMPK activation. Molecular cell. 2014;54(6):960-74.
124. Schiller JT, Day PM, Kines RC. Current understanding of the mechanism of HPV infection. Gynecol Oncol. 2010;118(1 Suppl):S12-7.
125. Graham SV. Human papillomavirus: gene expression, regulation and prospects for novel diagnostic methods and antiviral therapies. Future Microbiol. 2010;5(10):1493-506.
126. Münger K, Howley PM. Human papillomavirus immortalization and transformation functions. Virus Research. 2002;89:213-28.
127. Crook T, Tidy JA, Vousden KH. Degradation of p53 Can Be Targeted by HPV E6 Sequences Distinct from Those Required for p53 Binding and Trans-Activation. Cell. 1991;67:547-56.
128. Yim E-K, Park J-S. The Role of HPV E6 and E7 Oncoproteins in HPV-associated Cervical Carcinogenesis. Cancer Res Treat. 2005;37(6):319-24.
129. Lipinski MM, Jacks T. The retinoblastoma gene family in differentiation and development. Oncogene. 1999;17:7873–82.
130. Jones DL, Münger K. Interactions of the human papillomavirus E7 protein with cell cycle regulators. Semin Cancer Biol. 1996;7:327–37.
131. Chellappan S, Kraus VB, Kroger B, Münger K, Howley PM, Phelps WC, et al. Adeno virus E1A, simian virus 40 tumor antigen, and human papillomavirus E7 protein share the capacity to disrupt the interaction between transcription factor E2F and the retinoblastoma gene product. Proc Nat Acad Sci USA. 1992;89:4549-53.
132. Murphree AL, Benedict WF. Retinoblastoma: Clues to human oncogenesis. Science. 1984;223:1028–33.
133. Lowy DR, Münger K. Prognostic implications of HPV in oropharyngeal cancer. N Engl J Med. 2010;363:82-4.
134. de Martel C, Plummer M, Vignat J, Franceschi S. Worldwide burden of cancer attributable to HPV by site, country and HPV type. Int J Cancer. 2017;141(4):664-70.

135. Lee NCJ, Kelly JR, Park HS, An Y, Judson BL, Burtness BA, et al. Patterns of failure in high-metastatic node number human papillomavirus-positive oropharyngeal carcinoma. Oral Oncol. 2018;85:35-9.
136. Cooper JS, Pajak TF, Forastiere AA, Jacobs J, Campbell BH, Saxman SB, et al. Postoperative concurrent radiotherapy and chemotherapy for high-risk squamous-cell carcinoma of the head and neck. N Engl J Med. 2004;350:1937–44.
137. Forastiere AA, Zhang Q, Weber RS, Maor MH, Goepfert H, Pajak TF, et al. Long-term results of RTOG 91-11: a comparison of three nonsurgical treatment strategies to preserve the larynx in patients with locally advanced larynx cancer. J Clin Oncol. 2013;31(7):845-52.
138. Eastman A. The formation, isolation and characterisation of DNA adducts produced by anticancer platinum complexes. Pharmac Ther. 1987;34:155-66.
139. Fink D, Aebi S, Howell SH. The Role of DNA Mismatch Repair in Drug Resistance. Clin Cancer Res. 1998;4:1-6.
140. Siddik ZH. Cisplatin: mode of cytotoxic action and molecular basis of resistance. Oncogene. 2003;22(47):7265-79.
141. Shapiro G, Harper J. Anticancer drug targets: cell cycle and checkpoint control. J Clin Invest. 1999;104:1645-53.
142. Appella E, Anderson CW. Post-translational modifications and activation of p53 by genotoxic stresses. Eur J Biochem. 2001;268:2764–72.
143. Taylor A, Powell ME. Intensity-modulated radiotherapy--what is it? Cancer Imaging. 2004;4(2):68-73.
144. Vitti ET, Parsons JL. The Radiobiological Effects of Proton Beam Therapy: Impact on DNA Damage and Repair. Cancers (Basel). 2019;11(7).
145. Baskar R, Lee KA, Yeo R, Yeoh KW. Cancer and radiation therapy: current advances and future directions. Int J Med Sci. 2012;9(3):193-9.
146. Lomax ME, Folkes LK, O'Neill P. Biological consequences of radiation-induced DNA damage: relevance to radiotherapy. Clin Oncol (R Coll Radiol). 2013;25(10):578-85.
147. Cadet J, Douki T, Ravanat J. Oxidatively generated damage to the guanine moiety of DNA: mechanistic aspects and formation in cells. Acc Chem Res. 2008;41(8):1075-83.
148. Dynan W, Takeda Y, Roth D, Bao G. Understanding and re-engineering nucleoprotein machines to cure human disease. Nanomedicine (Lond). 2008;3(1):93-105.
149. Begg AC, Stewart FA, Vens C. Strategies to improve radiotherapy with targeted drugs. Nat Rev Cancer. 2011;11(4):239-53.
150. Bonm A, Kesari S. DNA Damage Response in Glioblastoma: Mechanism for Treatment Resistance and Emerging Therapeutic Strategies. The Cancer Journal. 2021;27(5):379-85.
151. Jackson SP, Bartek J. The DNA-damage response in human biology and disease. Nature. 2009;461(7267):1071-8.
152. Perri F, Pacelli R, Della Vittoria Scarpati G, Cella L, Giuliano M, Caponigro F, et al. Radioresistance in head and neck squamous cell carcinoma: Biological bases and therapeutic implications. Head Neck. 2015;37(5):763-70.
153. De Crevoisier R, Domenge C, Wibault P, Koscielny S, Lusinchi A, Janot F, et al. Full Dose Reirradiation Combined with Chemotherapy after Salvage Surgery in Head and Neck Carcinoma. Cancer. 2001;91(11):2071-6.
154. Banerjee R, Russo N, Liu M, Basrur V, Bellile E, Palanisamy N, et al. TRIP13 promotes error-prone nonhomologous end joining and induces chemoresistance in head and neck cancer. Nat Commun. 2014;5:4527.
155. Chang HW, Kim SY, Yi SL, Son SH, Song DY, Moon SY, et al. Expression of Ku80 correlates with sensitivities to radiation in cancer cell lines of the head and neck. Oral Oncol. 2006;42(10):979-86.
156. Moeller BJ, Yordy JS, Williams MD, Giri U, Raju U, Molkentine DP, et al. DNA repair biomarker profiling of head and neck cancer: Ku80 expression predicts locoregional failure and death following radiotherapy. Clin Cancer Res. 2011;17(7):2035-43.
157. Chen BP, Uematsu N, Kobayashi J, Lerenthal Y, Krempler A, Yajima H, et al. Ataxia telangiectasia mutated (ATM) is essential for DNA-PKcs phosphorylations at the Thr-2609 cluster upon DNA double strand break. J Biol Chem. 2007;282(9):6582-7.
158. Mansour WY, Bogdanova NV, Kasten-Pisula U, Rieckmann T, Kocher S, Borgmann K, et al. Aberrant overexpression of miR-421 downregulates ATM and leads to a pronounced DSB repair defect and clinical hypersensitivity in SKX squamous cell carcinoma. Radiother Oncol. 2013;106(1):147-54.

159. Hutchinson MND, Mierzwa M, D'Silva NJ. Radiation resistance in head and neck squamous cell carcinoma: dire need for an appropriate sensitizer. Oncogene. 2020;39(18):3638-49.
160. Stransky N, Egloff AM, Tward AD, Kostic AD, Cibulskis K, Sivachenko A, et al. The mutational landscape of head and neck squamous cell carcinoma. Science. 2011;333(6046):1157-60.
161. Harari PM, Wheeler DL, Grandis JR. Molecular target approaches in head and neck cancer: epidermal growth factor receptor and beyond. Semin Radiat Oncol. 2009;19(1):63-8.
162. Eriksen JG, Steiniche T, Askaa J, Alsner J, Overgaard J. The prognostic value of epidermal growth factor receptor is related to tumor differentiation and the overall treatment time of radiotherapy in squamous cell carcinomas of the head and neck. Int J Radiat Oncol Biol Phys. 2004;58(2):561-6.
163. Zhan M, Han ZC. Phosphatidylinositide 3-kinase/AKT in radiation responses. Histol Histopathol. 2004;19(3):915-23.
164. Skinner HD, Sandulache VC, Ow TJ, Meyn RE, Yordy JS, Beadle BM, et al. TP53 disruptive mutations lead to head and neck cancer treatment failure through inhibition of radiation-induced senescence. Clin Cancer Res. 2012;18(1):290-300.
165. Bristow RG, Hill RP. Hypoxia and metabolism. Hypoxia, DNA repair and genetic instability. Nat Rev Cancer. 2008;8(3):180-92.
166. Meijer TW, Kaanders JH, Span PN, Bussink J. Targeting hypoxia, HIF-1, and tumor glucose metabolism to improve radiotherapy efficacy. Clin Cancer Res. 2012;18(20):5585-94.
167. Olcina M, Lecane PS, Hammond EM. Targeting hypoxic cells through the DNA damage response. Clin Cancer Res. 2010;16(23):5624-9.
168. Hill RM, Rocha S, Parsons JL. Overcoming the Impact of Hypoxia in Driving Radiotherapy Resistance in Head and Neck Squamous Cell Carcinoma. Cancers (Basel). 2022;14(17).
169. Watson JD, Crick FHC. Molecular Structure of Nucleic Acids: A Structure for Deoxyribose Nucleic Acid. Nature. 1953;171:737-8.
170. Chargaff E, Lipshitz R, Green C, Hodes ME. The Composition of the Desoxyribonucleic Acid of Salmon Sperm. Journal of Biological Chemistry. 1951;192(1):223-30.
171. Friedberg EC, McDaniel LD, Schultz RA. The role of endogenous and exogenous DNA damage and mutagenesis. Curr Opin Genet Dev. 2004;14(1):5-10.
172. Hoeijmakers JHJ. DNA damage, aging and cancer. N Engl J Med. 2009;361(15):1475-85.
173. Arjunan KP, Sharma VK, Ptasinska S. Effects of atmospheric pressure plasmas on isolated and cellular DNA-a review. Int J Mol Sci. 2015;16(2):2971-3016.
174. Lindahl T, Karlström O. Heat-induced depyrimidination of deoxyribonucleic acid in neutral solution. Biochemistry. 1973;12(25):5151-4.
175. Kokoska RJ, McCulloch SD, Kunkel TA. The efficiency and specificity of apurinic/apyrimidinic site bypass by human DNA polymerase eta and Sulfolobus solfataricus Dpo4. J Biol Chem. 2003;278(50):50537-45.
176. Lindahl T. Instability and decay of the primary structure of DNA. Nature. 1993;362(6422):709-15.
177. Croteau DL, Bohr VA. Repair of oxidative damage to nuclear and mitochondrial DNA in mammalian cells. J Biol Chem. 1997;272(41):25409-12.
178. Steenken S, Jovanovic SV. How easily oxidisable is DNA? One-electron reduction potentials of adenosine and guanosine radicals in aqueous solution. J Am Chem Soc. 1997;119(3):617-8.
179. Klaunig JE, Xu Y, Isenberg JS, Bachowski S, Kolaja KL, Jiang J, et al. The role of oxidative stress in chemical carcinogenesis. Environ Health Perspect 1998;106:289-95.
180. Markkanen E, van Loon B, Ferrari E, Parsons JL, Dianov GL, Hubscher U. Regulation of oxidative DNA damage repair by DNA polymerase lambda and MutYH by cross-talk of phosphorylation and ubiquitination. Proc Natl Acad Sci U S A. 2012;109(2):437-42.
181. van Loon B, Markkanen E, Hubscher U. Oxygen as a friend and enemy: How to combat the mutational potential of 8-oxo-guanine. DNA Repair (Amst). 2010;9(6):604-16.
182. Drabløs F, Feyzi E, Aas PA, Vaagbo CB, Kavli B, Bratlie MS, et al. Alkylation damage in DNA and RNA--repair mechanisms and medical significance. DNA Repair (Amst). 2004;3(11):1389-407.
183. Fu D, Calvo JA, Samson LD. Balancing repair and tolerance of DNA damage caused by alkylating agents. Nat Rev Cancer. 2012;12(2):104-20.
184. Kondo N, Takahashi A, Ono K, Ohnishi T. DNA damage induced by alkylating agents and repair pathways. J Nucleic Acids. 2010;2010:543531.
185. Soll JM, Sobol RW, Mosammaparast N. Regulation of DNA Alkylation Damage Repair: Lessons and Therapeutic Opportunities. Trends Biochem Sci. 2017;42(3):206-18.

186. Rydberg B, Lindahl T. Nonenzymatic methylation of DNA by the intracellular methyl group donor S-adenosyl-L-methionine is a potentially mutagenic reaction. EMBO J. 1982;1(2):211-6.
187. Sedgwick B, Bates PA, Paik J, Jacobs SC, Lindahl T. Repair of alkylated DNA: recent advances. DNA Repair (Amst). 2007;6(4):429-42.
188. Shrivastav N, Li D, Essigmann JM. Chemical biology of mutagenesis and DNA repair: cellular responses to DNA alkylation. Carcinogenesis. 2010;31(1):59-70.
189. Borrego-Soto G, Ortiz-Lopez R, Rojas-Martinez A. Ionizing radiation-induced DNA injury and damage detection in patients with breast cancer. Genet Mol Biol. 2015;38(4):420-32.
190. Morgan WF, Sowa MB. Effects of ionizing radiation in nonirradiated cells. Proc Natl Acad Sci U S A. 2005;102(40):14127-8.
191. Khanna KK, Jackson SP. DNA double-strand breaks: signaling, repair and the cancer connection. Nature Genetics. 2001;27:247-54.
192. Santivasi WL, Xia F. Ionizing radiation-induced DNA damage, response, and repair. Antioxid Redox Signal. 2014;21(2):251-9.
193. Caldecott KW. Single-strand break repair and genetic disease. Nat Rev Genet. 2008;9(8):619-31.
194. Tubbs A, Nussenzweig A. Endogenous DNA Damage as a Source of Genomic Instability in Cancer. Cell. 2017;168(4):644-56.
195. Kouzminova EA, Kuzminov A. Fragmentation of replicating chromosomes triggered by uracil in DNA. J Mol Biol. 2006;355(1):20-33.
196. Kuzminov A. Single-strand interruptions in replicating chromosomes cause double-strand breaks. Proc Natl Acad Sci U S A. 2001;98(15):8241-6.
197. O'Connor MJ. Targeting the DNA Damage Response in Cancer. Mol Cell. 2015;60(4):547-60.
198. Pearl LH, Schierz AC, Ward SE, Al-Lazikani B, Pearl FM. Therapeutic opportunities within the DNA damage response. Nat Rev Cancer. 2015;15(3):166-80.
199. Carter RJ, Parsons JL. Base Excision Repair, a Pathway Regulated by Posttranslational Modifications. Mol Cell Biol. 2016;36(10):1426-37.
200. Dantuma NP, van Attikum H. Spatiotemporal regulation of posttranslational modifications in the DNA damage response. EMBO J. 2016;35(1):6-23.
201. Aplan PD. Causes of oncogenic chromosomal translocation. Trends Genet. 2006;22(1):46-55.
202. Kohl KP, Sekelsky J. Meiotic and mitotic recombination in meiosis. Genetics. 2013;194(2):327-34.
203. Maizels N. Immunoglobulin gene diversification. Annu Rev Genet. 2005;39:23-46.
204. Lieber MR. The mechanism of human nonhomologous DNA end joining. J Biol Chem. 2008;283(1):1-5.
205. Pannunzio N, Wantanabe G, Lieber MR. Nonhomologous DNA end-joining for repair of DNA double-strand breaks. J Biol Chem. 2018;293(27):10512-23.
206. Jackson SP. Sensing and repairing DNA double-strand breaks. Carcinogenesis. 2002;23(5):687-96.
207. Shrivastav M, De Haro LP, Nickoloff JA. Regulation of DNA double-strand break repair pathway choice. Cell Res. 2008;18(1):134-47.
208. Meek K, Douglas P, Cui X, Ding Q, Lees-Miller SP. trans Autophosphorylation at DNA-dependent protein kinase's two major autophosphorylation site clusters facilitates end processing but not end joining. Mol Cell Biol. 2007;27(10):3881-90.
209. Ma Y, Lu H, Tippin B, Goodman MF, Shimazaki N, Koiwai O, et al. A biochemically defined system for mammalian nonhomologous DNA end joining. Mol Cell. 2004;16(5):701-13.
210. Lu H, Shimazaki N, Raval P, Gu J, Watanabe G, Schwarz K, et al. A biochemically defined system for coding joint formation in V(D)J recombination. Mol Cell. 2008;31(4):485-97.
211. Chappell C, Hanakahi LA, Karimi-Busheri F, Weinfeld M, West SC. Involvement of human polynucleotide kinase in double-strand break repair by non-homologous end joining. EMBO J. 2002;21(11):2827-32.
212. Della-Maria J, Zhou Y, Tsai MS, Kuhnlein J, Carney JP, Paull TT, et al. Human Mre11/human Rad50/Nbs1 and DNA ligase IIIalpha/XRCC1 protein complexes act together in an alternative nonhomologous end joining pathway. J Biol Chem. 2011;286(39):33845-53.
213. Daley JM, Laan RL, Suresh A, Wilson TE. DNA joint dependence of pol X family polymerase action in nonhomologous end joining. J Biol Chem. 2005;280(32):29030-7.
214. Lieber MR. The mechanism of double-strand DNA break repair by the nonhomologous DNA end-joining pathway. Annu Rev Biochem. 2010;79:181-211.

215. Frit P, Barboule N, Yuan Y, Gomez D, Calsou P. Alternative end-joining pathway(s): bricolage at DNA breaks. DNA Repair (Amst). 2014;17:81-97.
216. Mao Z, Bozzella M, Seluanov A, Gorbunova V. DNA repair by nonhomologous end joining and homologous recombination during cell cycle in human cells. Cell Cycle. 2008;7(18):2902-6.
217. Orthwein A, Noordermeer SM, Wilson MD, Landry S, Enchev RI, Sherker A, et al. A mechanism for the suppression of homologous recombination in G1 cells. Nature. 2015;528(7582):422-6.
218. van den Bosch M, Bree RT, Lowndes NF. The MRN complex: coordinating and mediating the response to broken chromosomes. EMBO Rep. 2003;4(9):844-9.
219. Chang HHY, Pannunzio NR, Adachi N, Lieber MR. Non-homologous DNA end joining and alternative pathways to double-strand break repair. Nat Rev Mol Cell Biol. 2017;18(8):495-506.
220. Ciccia A, Elledge SJ. The DNA damage response: making it safe to play with knives. Mol Cell. 2010;40(2):179-204.
221. Benson FE, Stasiak A, West SC. Purification and characterization of the human Rad51 protein, an analogue of E. coli RecA. EMBO J. 1994;13(23):5764-71.
222. Masson JY, Tarsounas MC, Stasiak AZ, Stasiak A, Shah R, McIlwraith MJ, et al. Identification and purification of two distinct complexes containing the five RAD51 paralogs. Genes Dev. 2001;15(24):3296-307.
223. Zhao W, Steinfeld JB, Liang F, Chen X, Maranon DG, Jian Ma C, et al. BRCA1-BARD1 promotes RAD51-mediated homologous DNA pairing. Nature. 2017;550(7676):360-5.
224. Kowalczykowski SC. An Overview of the Molecular Mechanisms of Recombinational DNA Repair. Cold Spring Harb Perspect Biol. 2015;7(11).
225. Ranjha L, Howard SM, Cejka P. Main steps in DNA double-strand break repair: an introduction to homologous recombination and related processes. Chromosoma. 2018;127(2):187-214.
226. Szostak JW, Orr-Weaver TL, Rothstein RJ, Stahl FW. The double-strand-break repair model for recombination. Cell. 1983;33(1):25-35.
227. Boiteux S, Coste F, Castaing B. Repair of 8-oxo-7,8-dihydroguanine in prokaryotic and eukaryotic cells: Properties and biological roles of the Fpg and OGG1 DNA N-glycosylases. Free Radic Biol Med. 2017;107:179-201.
228. Parsons JL, Dianov GL. Co-ordination of base excision repair and genome stability. DNA Repair (Amst). 2013;12(5):326-33.
229. Jacobs AL, Schar P. DNA glycosylases: in DNA repair and beyond. Chromosoma. 2012;121(1):1-20.
230. Demple B, Herman T, Chen DS. Cloning and expression of APE, the cDNA encoding the major human apurinic endonuclease: definition of a family of DNA repair enzymes. Proc Nat Acad Sci USA. 1991;88(24):11450-4.
231. Robson CN, Hickson ID. Isolation of cDNA clones encoding a human apurinic/apyrimidinic endonuclease that corrects DNA repair and mutagenesis defects in E. coli xth (exonuclease III) mutants. Nucleic Acids Res. 1991;19(20):5519-23.
232. Horton JK, Stefanick DF, Prasad R, Gassman NR, Kedar PS, Wilson SH. Base excision repair defects invoke hypersensitivity to PARP inhibition. Mol Cancer Res. 2014;12(8):1128-39.
233. Grundy GJ, Parsons JL. Base excision repair and its implications to cancer therapy. Essays Biochem. 2020;64(5):831-43.
234. Wallace SS. Base excision repair: a critical player in many games. DNA Repair (Amst). 2014;19:14-26.
235. Wallace SS, Murphy DL, Sweasy JB. Base excision repair and cancer. Cancer Lett. 2012;327(1-2):73-89.
236. Markkanen E. Not breathing is not an option: How to deal with oxidative DNA damage. DNA Repair (Amst). 2017;59:82-105.
237. Luger K, Mäder AW, Richmond RK, Sargent DF, Richmond TJ. Crystal structure of the nucleosome core particle at 2.8 A resolution. Nature. 1997;389:251-60.
238. Davey CA, Sargent DF, Luger K, Maeder AW, Richmond TJ. Solvent Mediated Interactions in the Structure of the Nucleosome Core Particle at 1.9Å Resolution. Journal of Molecular Biology. 2002;319(5):1097-113.
239. Woodcock CL, Dimitrov S. Higher-order structure of chromatin and chromosomes. Curr Op Genet Dev. 2001;11:130-5.
240. Finch JT, Klug A. Solenoidal model for superstructure in chromatin. Proc Nat Acad Sci USA. 1976;73(6):1897-901.

241. Gilbert N, Allan J. Supercoiling in DNA and chromatin. Curr Opin Genet Dev. 2014;25:15-21.
242. Allfrey VG, Faulkner R, Mirskey A. Acetylation and Methylation of Histones and Their Possible Role in the Regulation of RNA Synthesis. Proc Nat Acad Sci USA. 1964;51(5):786-94.
243. Morales V, Richard-Foy H. Role of Histone N-Terminal Tails and Their Acetylation in Nucleosome Dynamics. Mol Cell Biol. 2000;20(19):7230-7.
244. Clapier CR, Cairns BR. The biology of chromatin remodeling complexes. Annu Rev Biochem. 2009;78:273-304.
245. Arents G, Burlingame RW, Wang BC, Love WE, Moudrianakis EN. The nucleosomal core histone octamer at 3.1 A resolution: a tripartite protein assembly and a left-handed superhelix. Proc Nat Acad Sci USA. 1991;88(22):10148-52.
246. Arents G, Moudrianakis EN. The histone fold: a ubiquitous architechtural motif utilized in DNA compaction and protein dimerization. Proc Nat Acad Sci USA. 1995;92(24):11170-4.
247. McGinty RK, Tan S. Nucleosome structure and function. Chem Rev. 2015;115(6):2255-73.
248. Langmore JP, Schutt C. The higher order structure of chicken erythrocyte chromosomes in vivo. Nature. 1980;288(5791):620-2.
249. McGhee JD, Nickol JM, Felsenfeld G, Rau DC. Higher Order Structure of Chromatin: Orientation of Nucleosomes within the 30 nm Chromatin Solenoid Is Independent of Species and Spacer Length. Cell. 1983;33(3):831-41.
250. Renz M, Nehls P, Hozier J. Involvement of histone H1 in the organization of the chromatin fiber. Proc Nat Acad Sci USA. 1977;74(5):1879-83.
251. Williams SP, Athey BD, Muglia LJ, Schappe RS, Gough AH, Langmore JP. Chromatin fibers are left-handed double helices with diameter and mass per unit length that depend on linker length. Biophys J. 1986;49(1):233-48.
252. Woodcock CL, Frado LL, Rattner JB. The higher-order structure of chromatin: evidence for a helical ribbon arrangement. J Cell Biol. 1984;99(1):42-52.
253. Worcel A, Strogatz S, Riley D. Structure of chromatin and the linking number of DNA. Proc Nat Acad Sci USA. 1981;78(3):1461-5.
254. Paulson JR, Laemmli UK. The structure of histone-depleted metaphase chromosomes. Cell. 1977;12(3):817-28.
255. Müller WG, Rieder D, Kreth G, Cremer C, Trajanoski Z, McNally JG. Generic features of tertiary chromatin structure as detected in natural chromosomes. Mol Cell Biol. 2004;24(21):9359-70.
256. Eltsov M, Maclellan KM, Maeshima K, Frangakis AS, Dubochet J. Analysis of cryo-electron microscopy images does not support the existence of 30-nm chromatin fibers in mitotic chromosomes in situ. Proc Natl Acad Sci U S A. 2008;105(50):19732-7.
257. Tremethick DJ. Higher-order structures of chromatin: the elusive 30 nm fiber. Cell. 2007;128(4):651-4.
258. Fussner E, Ching RW, Bazett-Jones DP. Living without 30nm chromatin fibers. Trends Biochem Sci. 2011;36(1):1-6.
259. Luger K, Dechassa ML, Tremethick DJ. New insights into nucleosome and chromatin structure: an ordered state or a disordered affair? Nat Rev Mol Cell Biol. 2012;13(7):436-47.
260. Oberdoerffer P, Miller KM. Histone H2A variants: Diversifying chromatin to ensure genome integrity. Semin Cell Dev Biol. 2023;135:59-72.
261. Kuo LJ, Yang LX. Gamma-H2AX - a novel biomarker for DNA double-strand breaks. In Vivo. 2008;22(3):305-9.
262. Hota SK, Bruneau BG. ATP-dependent chromatin remodeling during mammalian development. Development. 2016;143(16):2882-97.
263. Flaus A, Martin DM, Barton GJ, Owen-Hughes T. Identification of multiple distinct Snf2 subfamilies with conserved structural motifs. Nucleic Acids Res. 2006;34(10):2887-905.
264. Clapier CR, Iwasa J, Cairns BR, Peterson CL. Mechanisms of action and regulation of ATP-dependent chromatin-remodelling complexes. Nat Rev Mol Cell Biol. 2017;18(7):407-22.
265. Corona DF, Tamkun JW. Multiple roles for ISWI in transcription, chromosome organization and DNA replication. Biochim Biophys Acta. 2004;1677(1-3):113-9.
266. Boyer LA, Latek RRP, Craig L. . The SANT domain: a unique histone-tail-binding module? Nat Rev Mol Cell Biol. 2004;5:158-63.
267. Dang W, Bartholomew B. Domain architecture of the catalytic subunit in the ISW2-nucleosome complex. Mol Cell Biol. 2007;27(23):8306-17.

268. Xiao H, Sandaltzopoulos R, Wang H-M, Hamiche A, Ranallo R, Lee K-M, et al. Dual Functions of Largest NURF Subunit NURF301 in Nucleosome Sliding and Transcription Factor Interactions. Mol Cell. 2001;8(3):531-43.
269. Tran HG, Steger DJ, Iyer VR, Johnson AD. The chromo domain protein chd1p from budding yeast is an ATP-dependent chromatin-modifying factor. EMBO J. 2000;19(10):2323-31.
270. Hauk G, McKnight JN, Nodelman IM, Bowman GD. The chromodomains of the Chd1 chromatin remodeler regulate DNA access to the ATPase motor. Mol Cell. 2010;39(5):711-23.
271. Ryan DP, Sundaramoorthy R, Martin D, Singh V, Owen-Hughes T. The DNA-binding domain of the Chd1 chromatin-remodelling enzyme contains SANT and SLIDE domains. EMBO J. 2011;30(13):2596-609.
272. Lusser A, Urwin DL, Kadonaga JT. Distinct activities of CHD1 and ACF in ATP-dependent chromatin assembly. Nat Struct Mol Biol. 2005;12(2):160-6.
273. Murawska M, Brehm A. CHD chromatin remodelers and the transcription cycle. Transcription. 2011;2(6):244-53.
274. Konev AY, Tribus M, Park SY, Podhraski V, Lim CY, Emelyanov AV, et al. CHD1 motor protein is required for deposition of histone variant H3.3 into chromatin in vivo. Science. 2007;317(5841):1087-90.
275. Szerlong H, Hinata K, Viswanathan R, Erdjument-Bromage H, Tempst P, Cairns BR. The HSA domain binds nuclear actin-related proteins to regulate chromatin-remodeling ATPases. Nat Struct Mol Biol. 2008;15(5):469-76.
276. Mizuguchi G, Shen X, Landry J, Wu W-H, Sen S, Wu C. ATP-driven exchange of histone H2AZ variant catalyzed by SWR1 chromatin remodeling complex. Science. 2004;303(5656):343-8.
277. Papamichos-Chronakis M, Watanabe S, Rando OJ, Peterson CL. Global regulation of H2A.Z localization by the INO80 chromatin-remodeling enzyme is essential for genome integrity. Cell. 2011;144(2):200-13.
278. Mohrmann L, Verrijzer CP. Composition and functional specificity of SWI2/SNF2 class chromatin remodeling complexes. Biochim Biophys Acta. 2005;1681(2-3):59-73.
279. Schubert HL, Wittmeyer J, Kasten MM, Hinata K, Rawling DC, Heroux A, et al. Structure of an actin-related subcomplex of the SWI/SNF chromatin remodeler. Proc Natl Acad Sci U S A. 2013;110(9):3345-50.
280. Bannister AJ, Kouzarides T. Regulation of chromatin by histone modifications. Cell Res. 2011;21(3):381-95.
281. Michalak EM, Burr ML, Bannister AJ, Dawson MA. The roles of DNA, RNA and histone methylation in ageing and cancer. Nat Rev Mol Cell Biol. 2019;20(10):573-89.
282. Kouzarides T. Histone methylation in transcriptional control. Curr Op Genet Dev. 2002;12(2):198-209.
283. Black JC, Van Rechem C, Whetstine JR. Histone lysine methylation dynamics: establishment, regulation, and biological impact. Mol Cell. 2012;48(4):491-507.
284. Rogakou EP, Pilch DR, Orr AH, Ivanova VS, Bonner WM. DNA double-stranded breaks induce histone H2AX phosphorylation on serine 139. J Biol Chem. 1998;273(10):5858-68.
285. Garcia-Ramirez M, Rocchini C, Ausio J. Modulation of chromatin folding by histone acetylation. J Biol Chem. 1995;270(30):17923-8.
286. Tamburini BA, Tyler JK. Localized histone acetylation and deacetylation triggered by the homologous recombination pathway of double-strand DNA repair. Mol Cell Biol. 2005;25(12):4903-13.
287. Robert C, Nagaria PK, Pawar N, Adewuyi A, Gojo I, Meyers DJ, et al. Histone deacetylase inhibitors decrease NHEJ both by acetylation of repair factors and trapping of PARP1 at DNA double-strand breaks in chromatin. Leuk Res. 2016;45:14-23.
288. de Ruijter AJ, van Gennip AH, Caron HN, Kemp S, van Kuilenburg AB. Histone deacetylases (HDACs): characterization of the classical HDAC family. Biochem J. 2003;15(370):737-49.
289. Muslin AJ, Xing H. 14-3-3 proteins: regulation of subcellular localization by molecular interference. Cell Signal. 2000;12(11-12):703-9.
290. Jayathilaka N, Han A, Gaffney KJ, Dey R, Jarusiewicz JA, Noridomi K, et al. Inhibition of the function of class IIa HDACs by blocking their interaction with MEF2. Nucleic Acids Res. 2012;40(12):5378-88.
291. Blander G, Guarente L. The Sir2 family of protein deacetylases. Annu Rev Biochem. 2004;73:417-35.

292. Dai Y, Faller DV. Transcription Regulation by Class III Histone Deacetylases (HDACs)—Sirtuins. Transl Oncogenomics. 2008;3:53-65.
293. Ammanamanchi S, Freeman JW, Brattain MG. Acetylated sp3 is a transcriptional activator. J Biol Chem. 2003;278(37):35775-80.
294. Ashburner BP, Westerheide SD, Baldwin AS, Jr. The p65 (RelA) subunit of NF-kappaB interacts with the histone deacetylase (HDAC) corepressors HDAC1 and HDAC2 to negatively regulate gene expression. Mol Cell Biol. 2001;21(20):7065-77.
295. Huang Y, Myers SJ, Dingledine R. Transcriptional repression by REST: recruitment of Sin3A and histone deacetylase to neuronal genes. Nat Neurosci. 1999;2(10):867-72.
296. Hung JJ, Wang YT, Chang WC. Sp1 deacetylation induced by phorbol ester recruits p300 to activate 12(S)-lipoxygenase gene transcription. Mol Cell Biol. 2006;26(5):1770-85.
297. Miyake K, Yoshizumi T, Imura S, Sugimoto K, Batmunkh E, Kanemura H, et al. Expression of Hypoxia-Inducible Factor-1α, Histone Deacetylase 1, and Metastasis-Associated Protein 1 in Pancreatic Carcinoma
Correlation With Poor Prognosis With Possible Regulation. Pancreas. 2008;36:e1-e9.
298. Qiu Z, Ghosh A. A calcium-dependent switch in a CREST-BRG1 complex regulates activity-dependent gene expression. Neuron. 2008;60(5):775-87.
299. Weichert W, Röske A, Gekeler V, Beckers T, Ebert MPA, Pross M, et al. Association of patterns of class I histone deacetylase expression with patient prognosis in gastric cancer: a retrospective analysis. The Lancet Oncology. 2008;9(2):139-48.
300. Choi J-H, Kwon HJ, Yoon B-I, Kim J-H, Han SU, Joo HJ, et al. Expression Profile of Histone Deacetylase 1 in Gastric Cancer Tissues. Jpn J Cancer Res. 2001;92:1300-4.
301. Weichert W, Roske A, Gekeler V, Beckers T, Stephan C, Jung K, et al. Histone deacetylases 1, 2 and 3 are highly expressed in prostate cancer and HDAC2 expression is associated with shorter PSA relapse time after radical prostatectomy. Br J Cancer. 2008;98(3):604-10.
302. Weichert W, Roske A, Niesporek S, Noske A, Buckendahl AC, Dietel M, et al. Class I histone deacetylase expression has independent prognostic impact in human colorectal cancer: specific role of class I histone deacetylases in vitro and in vivo. Clin Cancer Res. 2008;14(6):1669-77.
303. Halkidou K, Gaughan L, Cook S, Leung HY, Neal DE, Robson CN. Upregulation and nuclear recruitment of HDAC1 in hormone refractory prostate cancer. Prostate. 2004;59(2):177-89.
304. Rikimaru T, Taketomi A, Yamashita Y, Shirabe K, Hamatsu T, Shimada M, et al. Clinical significance of histone deacetylase 1 expression in patients with hepatocellular carcinoma. Oncology. 2007;72(1-2):69-74.
305. Cao LL, Song X, Pei L, Liu L, Wang H, Jia M. Histone deacetylase HDAC1 expression correlates with the progression and prognosis of lung cancer: A meta-analysis. Medicine (Baltimore). 2017;96(31):e7663.
306. Zhang Z, Yamashita H, Toyama T, Sugiura H, Ando Y, Mita K, et al. Quantitation of HDAC1 mRNA expression in invasive carcinoma of the breast*. Breast Cancer Res Treat. 2005;94(1):11-6.
307. Cong L, Pakala SB, Ohshiro K, Li DQ, Kumar R. SUMOylation and SUMO-interacting motif (SIM) of metastasis tumor antigen 1 (MTA1) synergistically regulate its transcriptional repressor function. J Biol Chem. 2011;286(51):43793-808.
308. Harms KL, Chen X. Histone deacetylase 2 modulates p53 transcriptional activities through regulation of p53-DNA binding activity. Cancer Res. 2007;67(7):3145-52.
309. Rountree MR, Bachman KE, Baylin SB. DNMT1 binds HDAC2 and a new co-repressor, DMAP1, to form a complex at replication foci. Nature Genetics. 2000;25:269-77.
310. Huang BH, Laban M, Leung CH, Lee L, Lee CK, Salto-Tellez M, et al. Inhibition of histone deacetylase 2 increases apoptosis and p21Cip1/WAF1 expression, independent of histone deacetylase 1. Cell Death Differ. 2005;12(4):395-404.
311. Müller BM, Jana L, Kasajima A, Lehmann A, Prinzler J, Budczies J, et al. Differential expression of histone deacetylases HDAC1, 2 and 3 in human breast cancer - overexpression of HDAC2 and HDAC3 is associated with clinicopathological indicators of disease progression. BMC Cancer. 2013;13(215).
312. Atsumi A, Tomita A, Kiyoi H, Naoe T. Histone deacetylase 3 (HDAC3) is recruited to target promoters by PML-RARalpha as a component of the N-CoR co-repressor complex to repress transcription in vivo. Biochem Biophys Res Commun. 2006;345(4):1471-80.
313. Martin D, Li Y, Yang J, Wang G, Margariti A, Jiang Z, et al. Unspliced X-box-binding protein 1 (XBP1) protects endothelial cells from oxidative stress through interaction with histone deacetylase 3. J Biol Chem. 2014;289(44):30625-34.

314. Hatzi K, Jiang Y, Huang C, Garrett-Bakelman F, Gearhart MD, Giannopoulou EG, et al. A hybrid mechanism of action for BCL6 in B cells defined by formation of functionally distinct complexes at enhancers and promoters. Cell Rep. 2013;4(3):578-88.
315. Ji H, Zhou Y, Zhuang X, Zhu Y, Wu Z, Lu Y, et al. HDAC3 Deficiency Promotes Liver Cancer through a Defect in H3K9ac/H3K9me3 Transition. Cancer Res. 2019;79(14):3676-88.
316. Spurling CC, Godman CA, Noonan EJ, Rasmussen TP, Rosenberg DW, Giardina C. HDAC3 overexpression and colon cancer cell proliferation and differentiation. Mol Carcinog. 2008;47(2):137-47.
317. Li J, Hu M, Liu N, Li H, Yu Z, Yan Q, et al. HDAC3 deteriorates colorectal cancer progression via microRNA-296-3p/TGIF1/TGFbeta axis. J Exp Clin Cancer Res. 2020;39(1):248.
318. Cui Z, Xie M, Wu Z, Shi Y. Relationship Between Histone Deacetylase 3 (HDAC3) and Breast Cancer. Med Sci Monit. 2018;24:2456-64.
319. Lee H, Sengupta N, Villagra A, Rezai-Zadeh N, Seto E. Histone deacetylase 8 safeguards the human ever-shorter telomeres 1B (hEST1B) protein from ubiquitin-mediated degradation. Mol Cell Biol. 2006;26(14):5259-69.
320. Wilson BJ, Tremblay AM, Deblois G, Sylvain-Drolet G, Giguere V. An acetylation switch modulates the transcriptional activity of estrogen-related receptor alpha. Mol Endocrinol. 2010;24(7):1349-58.
321. Oehme I, Deubzer HE, Wegener D, Pickert D, Linke JP, Hero B, et al. Histone deacetylase 8 in neuroblastoma tumorigenesis. Clin Cancer Res. 2009;15(1):91-9.
322. An P, Chen F, Li Z, Ling Y, Peng Y, Zhang H, et al. HDAC8 promotes the dissemination of breast cancer cells via AKT/GSK-3beta/Snail signals. Oncogene. 2020;39(26):4956-69.
323. Qian DZ, Kachhap SK, Collis SJ, Verheul HM, Carducci MA, Atadja P, et al. Class II histone deacetylases are associated with VHL-independent regulation of hypoxia-inducible factor 1 alpha. Cancer Res. 2006;66(17):8814-21.
324. Bryant DW, Haynes RH. Endonuclease a from Saccharomyces cerevisiae shows increased activity on ultraviolet irradiated native DNA. Mol Gen Genet. 1978;167:139-45.
325. Zeng L-S, Yang X-Z, Wen Y-F, Mai S-J, Wang M-H, Zhang M-Y, et al. Overexpressed HDAC4 is associated with poor survival and promotes tumor progression in esophageal carcinoma. Aging. 2016;8(6):1236-48.
326. Cai JY, Xu TT, Wang Y, Chang JJ, Li J, Chen XY, et al. Histone deacetylase HDAC4 promotes the proliferation and invasion of glioma cells. Int J Oncol. 2018;53(6):2758-68.
327. Kang ZH, Wang CY, Zhang WL, Zhang JT, Yuan CH, Zhao PW, et al. Histone deacetylase HDAC4 promotes gastric cancer SGC-7901 cells progression via p21 repression. PLoS One. 2014;9(6):e98894.
328. Wilson AJ, Byun D-S, Nasser S, Murray LB, Auyyanar K, Arango D, et al. HDAC4 Promotes Growth of Colon Cancer Cells via Repression of p21. Molecular Biology of the Cell. 2008;19:4062-75.
329. Kang HJ, Lee MH, Kang HL, Kim SH, Ahn JR, Na H, et al. Differential regulation of estrogen receptor alpha expression in breast cancer cells by metastasis-associated protein 1. Cancer Res. 2014;74(5):1484-94.
330. Lee DY, Lin TE, Lee CI, Zhou J, Huang YH, Lee PL, et al. MicroRNA-10a is crucial for endothelial response to different flow patterns via interaction of retinoid acid receptors and histone deacetylases. Proc Natl Acad Sci U S A. 2017;114(8):2072-7.
331. Wein MN, Spatz J, Nishimori S, Doench J, Root D, Babij P, et al. HDAC5 controls MEF2C-driven sclerostin expression in osteocytes. J Bone Miner Res. 2015;30(3):400-11.
332. Zhou Y, Jin X, Ma J, Ding D, Huang Z, Sheng H, et al. HDAC5 Loss Impairs RB Repression of Pro-Oncogenic Genes and Confers CDK4/6 Inhibitor Resistance in Cancer. Cancer Res. 2021;81(6):1486-99.
333. Feng G-W, Dong L-D, Shang W-J, Pang X-L, Li JF, Liu L, et al. HDAC5 promotes cell proliferation in human hepatocellular carcinoma by up-regulating Six1 expression. Eur Rev Med Pharmacol Sci. 2014;18(6):811-6.
334. He P, Liang J, Shau T, Guo Y, Hou Y, Li Y. HDAC5 promotes colorectal cancer cell proliferation by up-regulating DLL4 expression. Int J Clin Exp Med. 2015;8(4):6510-6.
335. Li A, Liu Z, Li M, Zhou S, Xu Y, Xiao Y, et al. HDAC5, a potential therapeutic target and prognostic biomarker, promotes proliferation, invasion and migration in human breast cancer. Oncotarget. 2016;7(25):37966-78.
336. Zhong L, Sun S, Yao S, Han X, Gu M, Shi J. Histone deacetylase 5 promotes the proliferation and invasion of lung cancer cells. Oncol Rep. 2018;40(4):2224-32.

337. Olzmann JA, Li L, Chudaev MV, Chen J, Perez FA, Palmiter RD, et al. Parkin-mediated K63-linked polyubiquitination targets misfolded DJ-1 to aggresomes via binding to HDAC6. J Cell Biol. 2007;178(6):1025-38.
338. Bazzaro M, Lin Z, Santillan A, Lee MK, Wang MC, Chan KC, et al. Ubiquitin proteasome system stress underlies synergistic killing of ovarian cancer cells by bortezomib and a novel HDAC6 inhibitor. Clin Cancer Res. 2008;14(22):7340-7.
339. Zhang Z, Yamashita H, Toyama T, Sugiura H, Omoto Y, Ando Y, et al. HDAC6 expression is correlated with better survival in breast cancer. Clin Cancer Res. 2004;10:6962-8.
340. Sakuma T, Uzawa K, Onda T, Shiiba M, Yokoe H, Shiabahara T, et al. Aberrant expression of histone deacetylase 6 in oral squamous cell carcinoma. Int J Oncol. 2006;29(1):117-24.
341. Lei Y, Liu L, Zhang S, Guo S, Li X, Wang J, et al. Hdac7 promotes lung tumorigenesis by inhibiting Stat3 activation. Mol Cancer. 2017;16(1):170.
342. Li B, Samanta A, Song X, Iacono KT, Bembas K, Tao R, et al. FOXP3 interactions with histone acetyltransferase and class II histone deacetylases are required for repression. Proc Natl Acad Sci U S A. 2007;104(11):4571-6.
343. Li QG, Xiao T, Zhu W, Yu ZZ, Huang XP, Yi H, et al. HDAC7 promotes the oncogenicity of nasopharyngeal carcinoma cells by miR-4465-EphA2 signaling axis. Cell Death Dis. 2020;11(5):322.
344. Uzelac B, Krivokuca A, Susnjar S, Milovanovic Z, Supic G. Histone Deacetylase 7 Gene Overexpression Is Associated with Poor Prognosis of Triple-Negative Breast Cancer Patients. Genet Test Mol Biomarkers. 2021;25(3):227-35.
345. Yu Y, Cao F, Yu X, Zhou P, Di Q, Lei J, et al. The expression of HDAC7 in cancerous gastric tissues is positively associated with distant metastasis and poor patient prognosis. Clin Transl Oncol. 2017;19(8):1045-54.
346. Haberland M, Arnold MA, McAnally J, Phan D, Kim Y, Olson EN. Regulation of HDAC9 gene expression by MEF2 establishes a negative-feedback loop in the transcriptional circuitry of muscle differentiation. Mol Cell Biol. 2007;27(2):518-25.
347. Kanki K, Watanabe R, Nguyen Thai L, Zhao CH, Naito K. HDAC9 Is Preferentially Expressed in Dedifferentiated Hepatocellular Carcinoma Cells and Is Involved in an Anchorage-Independent Growth. Cancers (Basel). 2020;12(10).
348. He W, Wu Y, Tang X, Xia Y, He G, Min Z, et al. HDAC inhibitors suppress c-Jun/Fra-1-mediated proliferation through transcriptionally downregulating MKK7 and Raf1 in neuroblastoma cells. Oncotarget. 2016;7(6):6727-47.
349. Okudela K, Mitsui H, Suzuki T, Woo T, Tateishi Y, Umeda S, et al. Expression of HDAC9 in lung cancer – potential role in lung carcinogenesis. Int J Clin Exp Pathol. 2014;7(1):213-20.
350. Rastogi B, Raut SK, Panda NK, Rattan V, Radotra BD, Khullar M. Overexpression of HDAC9 promotes oral squamous cell carcinoma growth, regulates cell cycle progression, and inhibits apoptosis. Mol Cell Biochem. 2016;415(1-2):183-96.
351. Salgado E, Bian X, Feng A, Shim H, Liang Z. HDAC9 overexpression confers invasive and angiogenic potential to triple negative breast cancer cells via modulating microRNA-206. Biochem Biophys Res Commun. 2018;503(2):1087-91.
352. Ridinger J, Koeneke E, Kolbinger FR, Koerholz K, Mahboobi S, Hellweg L, et al. Dual role of HDAC10 in lysosomal exocytosis and DNA repair promotes neuroblastoma chemoresistance. Sci Rep. 2018;8(1):10039.
353. Tao X, Yan Y, Lu L, Chen B. HDAC10 expression is associated with DNA mismatch repair gene and is a predictor of good prognosis in colon carcinoma. Oncol Lett. 2017;14(4):4923-9.
354. Duan B, Ye D, Zhu S, Jia W, Lu C, Wang G, et al. HDAC10 promotes angiogenesis in endothelial cells through the PTPN22/ERK axis. Oncotarget. 2017;8(37):61338-49.
355. Yang Y, Huang Y, Wang Z, Wang H-T, Duan B, Ye D, et al. HDAC10 promotes lung cancer proliferation via AKT phosphorylation. Oncotarget. 2016;7(37):59388-401.
356. Islam MM, Banerjee T, Packard CZ, Kotian S, Selvendiran K, Cohn DE, et al. HDAC10 as a potential therapeutic target in ovarian cancer. Gynecol Oncol. 2017;144(3):613-20.
357. Liu X, Wang Y, Zhang R, Jin T, Qu L, Jin Q, et al. HDAC10 Is Positively Associated With PD-L1 Expression and Poor Prognosis in Patients With NSCLC. Front Oncol. 2020;10:485.
358. Bi L, Ren Y, Feng M, Meng P, Wang Q, Chen W, et al. HDAC11 Regulates Glycolysis through the LKB1/AMPK Signaling Pathway to Maintain Hepatocellular Carcinoma Stemness. Cancer Res. 2021;81(8):2015-28.

359. Thole TM, Lodrini M, Fabian J, Wuenschel J, Pfeil S, Hielscher T, et al. Neuroblastoma cells depend on HDAC11 for mitotic cell cycle progression and survival. Cell Death Dis. 2017;8(3):e2635.
360. Wang W, Fu L, Li S, Xu Z, Li X. Histone deacetylase 11 suppresses p53 expression in pituitary tumor cells. Cell Biol Int. 2017;41(12):1290-5.
361. Antrobus J, Parsons JL. Histone Deacetylases and Their Potential as Targets to Enhance Tumour Radiosensitisation. Radiation. 2022;2(1):149-67.
362. Watson PJ, Millard CJ, Riley AM, Roberston NS, Wright LC, Godage HY, et al. Insights into the activation mechanism of class I HDAC complexes by inositol phosphates. Nature Communications. 2016;48(7):829-34.
363. Lin CL, Tsai ML, Lin CY, Hsu KW, Hsieh WS, Chi WM, et al. HDAC1 and HDAC2 Double Knockout Triggers Cell Apoptosis in Advanced Thyroid Cancer. Int J Mol Sci. 2019;20(2).
364. Chen Z, Pei L, Zhang D, Xu F, Zhou E, Chen X. HDAC3 increases HMGB3 expression to facilitate the immune escape of breast cancer cells via down-regulating microRNA-130a-3p. Int J Biochem Cell Biol. 2021;135:105967.
365. Vannini A, Volpari C, Filocamo G, Casavola EC, Brunetti M, Renzoni D, et al. Crystal structure of a eukaryotic zinc-dependent histone deacetylase, human HDAC8, complexed with a hydroxamic acid inhibitor. Proc Natl Acad Sci U S A. 2004;101(42):15064-9.
366. Lemercier C, Verdel A, Galloo B, Curtet S, Brocard MP, Khochbin S. mHDA1/HDAC5 histone deacetylase interacts with and represses MEF2A transcriptional activity. J Biol Chem. 2000;275(20):15594-9.
367. Dressel U, Bailey PJ, Wang SC, Downes M, Evans RM, Muscat GE. A dynamic role for HDAC7 in MEF2-mediated muscle differentiation. J Biol Chem. 2001;276(20):17007-13.
368. Fischle W, Dequiedt F, Hendzel MJ, Guenther MG, Lazar MA, Voelter W, et al. Enzymatic Activity Associated with Class IIHDACs Is Dependent on a Multiprotein ComplexContaining HDAC3 and SMRT/N-CoR. Molecular Cell. 2002;9:45-7.
369. Parra M. Class IIa HDACs - new insights into their functions in physiology and pathology. FEBS J. 2015;282(9):1736-44.
370. Jeong JW, Bae MK, Ahn MY, Kim SH, Sohn TK, Bae MH, et al. Regulation and destabilization of HIF-1a by ARD1-mediated acetylation. Cell. 2002;111(5):709-20.
371. Lim JH, Lee YM, Chun YS, Chen J, Kim JE, Park JW. Sirtuin 1 modulates cellular responses to hypoxia by deacetylating hypoxia-inducible factor 1alpha. Mol Cell. 2010;38(6):864-78.
372. Geng H, Harvey CT, Pittsenbarger J, Liu Q, Beer TM, Xue C, et al. HDAC4 protein regulates HIF1alpha protein lysine acetylation and cancer cell response to hypoxia. J Biol Chem. 2011;286(44):38095-102.
373. Zeng L, Yang X, Wen Y, Mai S, Wang M, Zhang M, et al. Overexpressed HDAC4 is associated with poor survival and promotes tumor progression in esophageal carcinoma. Aging. 2016;8(6):1236-49.
374. OuYang C, Shu G, Liu J, Deng S, Lu P, Li Y, et al. HDAC5, Negatively Regulated by miR-148a-3p, Promotes Colon Cancer Cell Migration. Cancer Sci. 2022;(published online ahead of print).
375. Mottet D, Bellahcene A, Pirotte S, Waltregny D, Deroanne C, Lamour V, et al. Histone deacetylase 7 silencing alters endothelial cell migration, a key step in angiogenesis. Circ Res. 2007;101(12):1237-46.
376. Aldana-Masangkay GI, Sakamoto KM. The role of HDAC6 in cancer. J Biomed Biotechnol. 2011;2011:875824.
377. Gao L, Cueto MA, Asselbergs F, Atadja P. Cloning and functional characterization of HDAC11, a novel member of the human histone deacetylase family. J Biol Chem. 2002;277(28):25748-55.
378. Choudhary C, Kumar C, Gnad F, Nielsen ML, Rehman M, Walther TC, et al. Lysine acetylation targets protein complexes and co-regulates major cellular functions. Science. 2009;325(5942):834-40.
379. Kim G-W, Yang X-J. Comprehensive lysine acetylomes emerging from bacteria to humans. Trends in biochemical sciences. 2011;36(4):211-20.
380. Kim SC, Sprung R, Chen Y, Xu Y, Ball H, Pei J, et al. Substrate and functional diversity of lysine acetylation revealed by a proteomics survey. Molecular cell. 2006;23(4):607-18.
381. Palazzo A, Ackerman B, Gundersen GG. Tubulin acetylation and cell motility. Nature. 2003;421(6920):230-.
382. Hubbert C, Guardiola A, Shao R, Kawaguchi Y, Ito A, Nixon A, et al. HDAC6 is a microtubule-associated deacetylase. Nature. 2002;417(6887):455-8.
383. Chang J, Baloh RH, Milbrandt J. The NIMA-family kinase Nek3 regulates microtubule acetylation in neurons. Journal of cell science. 2009;122(13):2274-82.

384. Kovacs JJ, Murphy PJ, Gaillard S, Zhao X, Wu JT, Nicchitta CV, et al. HDAC6 regulates Hsp90 acetylation and chaperone-dependent activation of glucocorticoid receptor. Mol Cell. 2005;18(5):601-7.
385. Li Z, Zhu WG. Targeting histone deacetylases for cancer therapy: from molecular mechanisms to clinical implications. Int J Biol Sci. 2014;10(7):757-70.
386. Thurn KT, Thomas S, Raha P, Qureshi I, Munster PN. Histone deacetylase regulation of ATM-mediated DNA damage signaling. Mol Cancer Ther. 2013;12(10):2078-87.
387. Miller KM, Tjeertes JV, Coates J, Legube G, Polo SE, Britton S, et al. Human HDAC1 and HDAC2 function in the DNA-damage response to promote DNA nonhomologous end-joining. Nat Struct Mol Biol. 2010;17(9):1144-51.
388. Bhaskara S, Knutson SK, Jiang G, Chandrasekharan MB, Wilson AJ, Zheng S, et al. Hdac3 is essential for the maintenance of chromatin structure and genome stability. Cancer Cell. 2010;18(5):436-47.
389. Bhaskara S, Chyla BJ, Amann JM, Knutson SK, Cortez D, Sun Z-W, et al. Deletion of Histone Deacetylase 3 reveals critical roles in S-phase progression and DNA damage control. Mol Cell. 2008;30(1):61-72.
390. Kao GD, McKenna WG, Guenther MG, Muschel RJ, Lazar MA, Yen TJ. Histone deacetylase 4 interacts with 53BP1 to mediate the DNA damage response. J Cell Biol. 2003;160(7):1017-27.
391. Zhang M, Hu C, Moses N, Haakenson J, Xiang S, Quan D, et al. HDAC6 regulates DNA damage response via deacetylating MLH1. J Biol Chem. 2019;294(15):5813-26.
392. Zhang M, Xiang S, Joo HY, Wang L, Williams KA, Liu W, et al. HDAC6 deacetylates and ubiquitinates MSH2 to maintain proper levels of MutSalpha. Mol Cell. 2014;55(1):31-46.
393. Kotian S, Liyanarachchi S, Zelent A, Parvin JD. Histone deacetylases 9 and 10 are required for homologous recombination. J Biol Chem. 2011;286(10):7722-6.
394. Enzenhofer E, Kadletz L, Stanisz I, Kotowski U, Seemann R, Schmid R, et al. Effect of the histone deacetylase inhibitor resminostat on head and neck squamous cell carcinoma cell lines. Head Neck. 2017;39(5):900-7.
395. Chen X, Wong P, Radany E, Wong JYC. HDAC Inhibitor, Valproic Acid, Induces p53-Dependent Radiosensitization of Colon Cancer Cells. Cancer Biotherapy. 2009;24(6):689-99.
396. Perona M, Thomasz L, Rossich L, Rodriguez C, Pisarev MA, Rosemblit C, et al. Radiosensitivity enhancement of human thyroid carcinoma cells by the inhibitors of histone deacetylase sodium butyrate and valproic acid. Mol Cell Endocrinol. 2018;478:141-50.
397. Shoji M, Ninomiya I, Makino I, Kinoshita J, Nakamura K, Oyama K, et al. Valproic acid, a histone deacetylase inhibitor, enhances radiosensitivity in esophageal squamous cell carcinoma. Int J Oncol. 2012;40(6):2140-6.
398. Yu JI, Choi C, Shin SW, Son A, Lee GH, Kim SY, et al. Valproic Acid Sensitizes Hepatocellular Carcinoma Cells to Proton Therapy by Suppressing NRF2 Activation. Sci Rep. 2017;7(1):14986.
399. Baschnagel A, Russo A, Burgan WE, Carter D, Beam K, Palmieri D, et al. Vorinostat enhances the radiosensitivity of a breast cancer brain metastatic cell line grown in vitro and as intracranial xenografts. Mol Cancer Ther. 2009;8(6):1589-95.
400. Munshi A, Tanaka T, Hobbs ML, Tucker SL, Richon VM, Meyn RE. Vorinostat, a histone deacetylase inhibitor, enhances the response of human tumor cells to ionizing radiation through prolongation of gamma-H2AX foci. Mol Cancer Ther. 2006;5(8):1967-74.
401. Saelen MG, Ree AH, Kristian A, Fleten KG, Furee T, Hektoen HH, et al. Radiosensitization by the histone deacetylase inhibitor vorinostat under hypoxia and with capecitabine in experimental colorectal carcinoma. Radiation Oncology. 2012;7(165).
402. Moertl S, Payer S, Kell R, Winkler K, Anastasov N, Atkinson MJ. Comparison of Radiosensitization by HDAC Inhibitors CUDC-101 and SAHA in Pancreatic Cancer Cells. Int J Mol Sci. 2019;20(13).
403. Schlaff CD, Arscott WT, Gordon I, Tandle A, Tofilon P, Camphausen K. Radiosensitization Effects of Novel Triple-Inhibitor CUDC-101 in Glioblastoma Multiforme and Breast Cancer Cells In Vitro. International Journal of Radiation Oncology*Biology*Physics. 2013;87(2).
404. Choi C, Lee GH, Son A, Yoo GS, Yu JI, Park HC. Downregulation of Mcl-1 by Panobinostat Potentiates Proton Beam Therapy in Hepatocellular Carcinoma Cells. Cells. 2021;10(3).
405. Groselj B, Ruan JL, Scott H, Gorrill J, Nicholson J, Kelly J, et al. Radiosensitization In Vivo by Histone Deacetylase Inhibition with No Increase in Early Normal Tissue Radiation Toxicity. Mol Cancer Ther. 2018;17(2):381-92.

406. Xiao W, Graham PH, Hao J, Chang L, Ni J, Power CA, et al. Combination therapy with the histone deacetylase inhibitor LBH589 and radiation is an effective regimen for prostate cancer cells. PLoS One. 2013;8(8):e74253.
407. Paillas S, Then CK, Kilgas S, Ruan JL, Thompson J, Elliott A, et al. The Histone Deacetylase Inhibitor Romidepsin Spares Normal Tissues While Acting as an Effective Radiosensitizer in Bladder Tumors in Vivo. Int J Radiat Oncol Biol Phys. 2020;107(1):212-21.
408. Rossetti A, Petragnano F, Milazzo L, Vulcano F, Macioce G, Codenotti S, et al. Romidepsin (FK228) fails in counteracting the transformed phenotype of rhabdomyosarcoma cells but efficiently radiosensitizes, in vitro and in vivo, the alveolar phenotype subtype. Int J Radiat Biol. 2021;97(7):943-57.
409. Kawano T, Akiyama M, Agawa-Ohta M, Mikami-Terao Y, Iwase S, Yanagisawa T, et al. Histone deacetylase inhibitors valproic acid and depsipeptide sensitize retinoblastoma cells to radiotherapy by increasing H2AX phosphorylation and p53 acetylation-phosphorylation. Int J Oncol. 2010;37(4):787-95.
410. Marampon F, Di Nisio V, Pietrantoni I, Petragnano F, Fasciani I, Scicchitano BM, et al. Pro-differentiating and radiosensitizing effects of inhibiting HDACs by PXD-101 (Belinostat) in in vitro and in vivo models of human rhabdomyosarcoma cell lines. Cancer Lett. 2019;461:90-101.
411. Banuelos CA, Banath JP, MacPhail SH, Zhao J, Reitsema T, Olive PL. Radiosensitization by the histone deacetylase inhibitor PCI-24781. Clin Cancer Res. 2007;13(22 Pt 1):6816-26.
412. Rivera S, Leteur C, Mégnin F, Law F, Martins I, Kloos I, et al. Time dependent modulation of tumor radiosensitivity by a pan HDAC inhibitor: abexinostat. Oncotarget. 2017;8(34):56210-27.
413. Zhou C, Fabbrizi MR, Hughes JR, Grundy GJ, Parsons JL. Effectiveness of PARP inhibition in enhancing the radiosensitivity of 3D spheroids of head and neck squamous cell carcinoma. Front Oncol. 2022;12:940377.
414. Carter RJ, Nickson CM, Thompson JM, Kacperek A, Hill MA, Parsons JL. Complex DNA Damage Induced by High Linear Energy Transfer Alpha-Particles and Protons Triggers a Specific Cellular DNA Damage Response. Int J Radiat Oncol Biol Phys. 2018;100(3):776-84.
415. Nickson CM, Parsons JL. Monitoring regulation of DNA repair activities of cultured cells in-gel using the comet assay. Front Genet. 2014;5:232.
416. O'Steen S, Green DJ, Gopal AK, Orozco JJ, Kenoyer AL, Lin Y, et al. Venetoclax Synergizes with Radiotherapy for Treatment of B-cell Lymphomas. Cancer Res. 2017;77(14):3885-93.
417. Zerp SF, Stoter TR, Hoebers FJ, van den Brekel MW, Dubbelman R, Kuipers GK, et al. Targeting anti-apoptotic Bcl-2 by AT-101 to increase radiation efficacy: data from in vitro and clinical pharmacokinetic studies in head and neck cancer. Radiat Oncol. 2015;10:158.
418. Jung M, Dritschilo A. A NF-kB signaling pathway as a target for human tumor radiosensitization. Semin Radiat Oncol. 2001;11:346-51.
419. Wang R, Peng S, Zhang X, Wu Z, Duan H, Yuan Y, et al. Inhibition of NF-kappaB improves sensitivity to irradiation and EGFR-TKIs and decreases irradiation-induced lung toxicity. Int J Cancer. 2019;144(1):200-9.
420. Liu X, Tu Y, Wang Y, Zhou D, Chong Y, Shi L, et al. Reversible inhibitor of CRM1 sensitizes glioblastoma cells to radiation by blocking the NF-kappaB signaling pathway. Cancer Cell Int. 2020;20:97.
421. Harada T, Harada K, Ueyama Y. The enhancement of tumor radioresponse by combined treatment with cepharanthine is accompanied by the inhibition of DNA damage repair and the induction of apoptosis in oral squamous cell carcinoma. Int J Oncol. 2012;41(2):565-72.
422. Chiu SJ, Hsaio CH, Tseng HH, Su YH, Shih WL, Lee JW, et al. Rosiglitazone enhances the radiosensitivity of p53-mutant HT-29 human colorectal cancer cells. Biochem Biophys Res Commun. 2010;394(3):774-9.
423. Affolter A, Samosny G, Heimes AS, Schneider J, Weichert W, Stenzinger A, et al. Multikinase inhibitors sorafenib and sunitinib as radiosensitizers in head and neck cancer cell lines. Head Neck. 2017;39(4):623-32.
424. Tai TS, Lin PM, Wu CF, Hung SK, Huang CI, Wang CC, et al. CDK4/6 Inhibitor LEE011 Is a Potential Radiation-sensitizer in Head and Neck Squamous Cell Carcinoma: An In Vitro Study. Anticancer Res. 2019;39(2):713-20.
425. Xu WH, Han M, Dong Q, Fu ZX, Diao YY, Liu H, et al. Doxorubicin-mediated radiosensitivity in multicellular spheroids from a lung cancer cell line is enhanced by composite micelle encapsulation. Int J Nanomedicine. 2012;7:2661-71.
426. Minehan KJ, Bonner JA. The interaction of etoposide with radiation: variation in cytotoxicity with the sequence of treatment. Life Sciences. 1993;53(15):PL237-PL42.

427. Agoni L, Basu I, Gupta S, Alfieri A, Gambino A, Goldberg GL, et al. Rigosertib is a more effective radiosensitizer than cisplatin in concurrent chemoradiation treatment of cervical carcinoma, in vitro and in vivo. Int J Radiat Oncol Biol Phys. 2014;88(5):1180-7.
428. Liu N, Wang YA, Sun Y, Ecsedy J, Sun J, Li X, et al. Inhibition of Aurora A enhances radiosensitivity in selected lung cancer cell lines. Respir Res. 2019;20(1):230.
429. Niermann KJ, Moretti L, Giacalone NJ, Sun Y, Schleicher SM, Kopsombut P, et al. Enhanced radiosensitivity of androgen-resistant prostate cancer: AZD1152-mediated Aurora kinase B inhibition. Radiat Res. 2011;175(4):444-51.
430. Macha MA, Rachagani S, Qazi AK, Jahan R, Gupta S, Patel A, et al. Afatinib radiosensitizes head and neck squamous cell carcinoma cells by targeting cancer stem cells. Oncotarget. 2017;8(13):20961-73.
431. Guo Q, He J, Shen F, Zhang W, Yang X, Zhang C, et al. TCN, an AKT inhibitor, exhibits potent antitumor activity and enhances radiosensitivity in hypoxic esophageal squamous cell carcinoma in vitro and in vivo. Oncol Lett. 2017;13(2):949-54.
432. Estrada-Bernal A, Chatterjee M, Haque SJ, Yang L, Morgan MA, Kotian S, et al. MEK inhibitor GSK1120212-mediated radiosensitization of pancreatic cancer cells involves inhibition of DNA double-strand break repair pathways. Cell Cycle. 2015;14(23):3713-24.
433. Chung EJ, Brown AP, Asano H, Mandler M, Burgan WE, Carter D, et al. In vitro and in vivo radiosensitization with AZD6244 (ARRY-142886), an inhibitor of mitogen-activated protein kinase/extracellular signal-regulated kinase 1/2 kinase. Clin Cancer Res. 2009;15(9):3050-7.
434. Lin YC, Hung MS, Lin CK, Li JM, Lee KD, Li YC, et al. CK2 inhibitors enhance the radiosensitivity of human non-small cell lung cancer cells through inhibition of stat3 activation. Cancer Biother Radiopharm. 2011;26(3):381-8.
435. Bridges KA, Toniatti C, Buser CA, Liu H, Buchholz TA, Meyn RE. Niraparib (MK-4827), a novel poly(ADP-ribose) polymerase inhibitor, radiosensitizes human lung and breast cancer cells. . Oncotarget. 2014;5(13):076–5086
436. Tang M, Liu Q, Zhou L, Chen L, Yang X, Yu J, et al. The poly (ADP-ribose) polymerase inhibitor rucaparib suppresses proliferation and serves as an effective radiosensitizer in cervical cancer. Invest New Drugs. 2019;37(1):65-75.
437. Enzenhofer E, Kadletz L, Stanisz I, Kotowski U, Seemann R, Schmid R, et al. Effect of the histone deacetylase inhibitor resminostat on head and neck squamous cell carcinoma cell lines. Oncotarget. 2017;39(5):900-7.
438. Friedrich J, Seidel C, Ebner R, Kunz-Schughart LA. Spheroid-based drug screen: considerations and practical approach. Nat Protoc. 2009;4(3):309-24.
439. Zhang YQ, Zhang JJ, Song HJ, Li DW. Expression and prognostic influence of NF-kappaB and EGFR in esophageal cancer. Genet Mol Res. 2015;14(4):16819-26.
440. Deng XZ, Geng SS, Luo M, Chai JJ, Xu Y, Chen CL, et al. Curcumin potentiates laryngeal squamous carcinoma radiosensitivity via NF-KappaB inhibition by suppressing IKKgamma expression. J Recept Signal Transduct Res. 2020;40(6):541-9.
441. Huang WL, Wu SF, Xu ST, Ma YC, Wang R, Jin S, et al. Allicin enhances the radiosensitivity of colorectal cancer cells via inhibition of NF-kappaB signaling pathway. J Food Sci. 2020;85(6):1924-31.
442. Qian J, Luo Y, Gu X, Wang X. Inhibition of SENP6-induced radiosensitization of human hepatocellular carcinoma cells by blocking radiation-induced NF-kappaB activation. Cancer Biother Radiopharm. 2013;28(3):196-200.
443. Pan PH, Lin SY, Ou YC, Chen WY, Chuang YH, Yen YJ, et al. Stearic acid attenuates cholestasis-induced liver injury. Biochem Biophys Res Commun. 2010;391(3):1537-42.
444. Mitchel J, Bajaj P, Patil K, Gunnarson A, Pourchet E, Kim YN, et al. Computational Identification of Stearic Acid as a Potential PDK1 Inhibitor and In Vitro Validation of Stearic Acid as Colon Cancer Therapeutic in Combination with 5-Fluorouracil. Cancer Inform. 2021;13(20):1769351211065979.
445. Habib NA, Wood CB, Apostolov K, Barker W, Hershmann MJ, Heinemann D, et al. Stearic acid and carcinogenesis. Br J Cancer. 1987;56(4):455-8.
446. Williams LT. Signal transduction by the platelet-derived growth factor receptor. Science. 1989;243(4898):1564-70.
447. Montmayeur JP, Valius M, Vandenheede J, Kazlauskas A. The platelet-derived growth factor beta receptor triggers multiple cytoplasmic signaling cascades that arrive at the nucleus as distinguishable inputs. J Biol Chem. 1997;272(51):32670-8.

448. Carvalho I, Milanezi F, Martins A, Reis RM, Schmitt F. Overexpression of platelet-derived growth factor receptor alpha in breast cancer is associated with tumour progression. Breast Cancer Res. 2005;7(5):R788-95.
449. Lin LH, Lin JS, Yang CC, Cheng HW, Chang KW, Liu CJ. Overexpression of Platelet-Derived Growth Factor and Its Receptor Are Correlated with Oral Tumorigenesis and Poor Prognosis in Oral Squamous Cell Carcinoma. Int J Mol Sci. 2020;21(7).
450. Manzat Saplacan RM, Balacescu L, Gherman C, Chira RI, Craiu A, Mircea PA, et al. The Role of PDGFs and PDGFRs in Colorectal Cancer. Mediators Inflamm. 2017;2017:4708076.
451. Higuchi A, Oshima T, Yoshihara K, Sakamaki K, Aoyama T, Suganuma N, et al. Clinical significance of platelet-derived growth factor receptor-beta gene expression in stage II/III gastric cancer with S-1 adjuvant chemotherapy. Oncol Lett. 2017;13(2):905-11.
452. Lin CL, Tsai ML, Chen YH, Liu WN, Lin CY, Hsu KW, et al. Platelet-Derived Growth Factor Receptor-alpha Subunit Targeting Suppresses Metastasis in Advanced Thyroid Cancer In Vitro and In Vivo. Biomol Ther (Seoul). 2021;29(5):551-61.
453. Hong JD, Wang X, Peng YP, Peng JH, Wang J, Dong YP, et al. Silencing platelet-derived growth factor receptor-beta enhances the radiosensitivity of C6 glioma cells in vitro and in vivo. Oncol Lett. 2017;14(1):329-36.
454. Carapancea M, Cosaceanu D, Budiu R, Kwiecinska A, Tataranu L, Ciubotaru V, et al. Dual targeting of IGF-1R and PDGFR inhibits proliferation in high-grade gliomas cells and induces radiosensitivity in JNK-1 expressing cells. J Neurooncol. 2007;85(3):245-54.
455. Ranza E, Bertolotti A, Facoetti A, Mariotti L, Pasi F, Ottolenghi A, et al. Influence of Imatinib Mesylate on Radiosensitivity of Astrocytoma Cells. Anticancer Research. 2009;29(11):4575-8.
456. Timke C, Zieher H, Roth A, Hauser K, Lipson KE, Weber KJ, et al. Combination of vascular endothelial growth factor receptor/platelet-derived growth factor receptor inhibition markedly improves radiation tumor therapy. Clin Cancer Res. 2008;14(7):2210-9.
457. Abdollahi A, Lipson KE, Han X, Krempien R, Trinh T, Weber KJ, et al. SU5416 and SU6668 attenuate the angiogenic effects of radiation-induced tumor cell growth factor production and amplify the direct anti-endothelial action of radiation in vitro. Cancer Res. 2003;63(13):3755-63.
458. Lu B, Geng L, Musiek A, Tan J, Cao C, Donnelly E, et al. Broad spectrum receptor tyrosine kinase inhibitor, SU6668, sensitizes radiation via targeting survival pathway of vascular endothelium. Int J Radiat Oncol Biol Phys. 2004;58(3):844-50.
459. Ning S, Laird D, Cherrington JM, Knox SJ. The Antiangiogenic Agents SU5416 and SU6668 Increase the Antitumor Effects of Fractionated Irradiation. Radiation Research. 2002;157(1):45-51.
460. Balkwill F. TNF-alpha in promotion and progression of cancer. Cancer Metastasis Rev. 2006;25(3):409-16.
461. Miles DW, Happerfield LC, Naylor MS, Bobrow LG, Rubens RD, Balkwill FR. Expression of tumour necrosis factor (TNF alpha) and its receptors in benign and malignant breast tissue. Int J Cancer. 1994;56(6):777-82.
462. Ma Y, Ren Y, Dai ZJ, Wu CJ, Ji YH, Xu J. IL-6, IL-8 and TNF-alpha levels correlate with disease stage in breast cancer patients. Adv Clin Exp Med. 2017;26(3):421-6.
463. Eggermont AMM, de Wilt JHW, ten Hagen TLM. Current uses of isolated limb perfusion in the clinic and a model system for new strategies. The Lancet Oncology. 2003;4(7):429-37.
464. Curnis F, Sacchi A, Corti A. Improving chemotherapeutic drug penetration in tumors by vascular targeting and barrier alteration. Journal of Clinical Investigation. 2002;110(4):475-82.
465. Balkwill F. Tumor necrosis factor or tumor promoting factor? Cytokine Growth Factor Rev. 2002;13:135-41.
466. Nishi K, Luo H, Ishikura S, Doi K, Iwaihara Y, Wills L, et al. Apremilast Induces Apoptosis of Human Colorectal Cancer Cells with Mutant KRAS. Anticancer Res. 2017;37(7):3833-9.
467. Mauceri HJ, Beckett MA, Liang H, Sutton HG, Pitroda S, Galka E, et al. Translational strategies exploiting TNF-alpha that sensitize tumors to radiation therapy. Cancer Gene Ther. 2009;16(4):373-81.
468. Wang B, Ge Y, Gu X. Analysis of esophageal cancer cell lines exposed to X-ray based on radiosensitivity influence by tumor necrosis factor-alpha. J Xray Sci Technol. 2016;24(5):761-9.
469. Xia H, Yu C, Zhang Y, Yu J, Li J, Zhang W, et al. Tumor necrosis factor-α enhances radiosensitivity of A549 cells. Nan Fang Yi Ke Da Xue Xue Bao (Journal of Southern Medical University). 2012;32(4):565-8.
470. Oda K, Matsuoka Y, Funahashi A, Kitano H. A comprehensive pathway map of epidermal growth factor receptor signaling. Mol Syst Biol. 2005;1:2005 0010.

471. Grandis JR, Melhem MF, Gooding WE, Day R, Holst VA, Wagener MM, et al. Levels of TGF-alpha and EGFR protein in head and nek squamous cell carcinoma and patient survival. J Natl Cancer Inst. 1998;90(11):824-32.
472. Zhu X, Zhang F, Zhang W, He J, Zhao Y, Chen X. Prognostic role of epidermal growth factor receptor in head and neck cancer: a meta-analysis. J Surg Oncol. 2013;108(6):387-97.
473. Zhang S, Fu Y, Wang D, Wang J. Icotinib enhances lung cancer cell radiosensitivity in vitro and in vivo by inhibiting MAPK/ERK and AKT activation. Clin Exp Pharmacol Physiol. 2018.
474. Huang F, Liang X, Min X, Zhang Y, Wang G, Peng Z, et al. Simultaneous Inhibition of EGFR and HER2 via Afatinib Augments the Radiosensitivity of Nasopharyngeal Carcinoma Cells. J Cancer. 2019;10(9):2063-73.
475. Akimoto T, Nonaka T, Ishikawa H, Sakurai H, Saitoh J, Takahashi T, et al. Genistein, a tyrosine kinase inhibitor, enhanced radiosensitivity in human esophageal cancer cell lines in vitro: Possible involvement of inhibition of survival signal transduction pathways. Int J Radiat Oncol Biol Phys. 2001;50(1):195-201.
476. Champoux JJ. DNA topoisomerases: structure, function, and mechanism. Annu Rev Biochem. 2001;70:369-413.
477. Delgado JL, Hsieh CM, Chan NL, Hiasa H. Topoisomerases as anticancer targets. Biochem J. 2018;475(2):373-98.
478. Gruca A, Krawczyk Z, Szeja W, Grynkiewicz G, Rusin A. Synthetic genistein glycosides inhibiting EGFR phosphorylation enhance the effect of radiation in HCT 116 colon cancer cells. Molecules. 2014;19(11):18558-73.
479. Liu X, Sun C, Jin X, Li P, Ye F, Zhao T, et al. Genistein enhances the radiosensitivity of breast cancer cells via G(2)/M cell cycle arrest and apoptosis. Molecules. 2013;18(11):13200-17.
480. Liu XX, Sun C, Jin XD, Li P, Zheng XG, Zhao T, et al. Genistein sensitizes sarcoma cells in vitro and in vivo by enhancing apoptosis and by inhibiting DSB repair pathways. J Radiat Res. 2016;57(3):227-37.
481. Tang Q, Ma J, Sun J, Yang L, Yang F, Zhang W, et al. Genistein and AG1024 synergistically increase the radiosensitivity of prostate cancer cells. Oncol Rep. 2018;40(2):579-88.
482. Yan H, Jiang J, Du A, Gao J, Zhang D, Song L. Genistein Enhances Radiosensitivity of Human Hepatocellular Carcinoma Cells by Inducing G2/M Arrest and Apoptosis. Radiat Res. 2020;193(3):286-300.
483. Zhang Z, Jin F, Lian X, Li M, Wang G, Lan B, et al. Genistein promotes ionizing radiation-induced cell death by reducing cytoplasmic Bcl-xL levels in non-small cell lung cancer. Sci Rep. 2018;8(1):328.
484. Alhasan SA, Aranha O, Sarkar FH. Genistein elicits pleiotropic molecular effects on head and neck cancer cells. Clin Cancer Res. 2001;7(12):4174-81.
485. Alhasan SA, Pietrasczkiwicz H, Alonso MD, Ensley J, Sarkar FH. Genistein-induced cell cycle arrest and apoptosis in a head and neck squamous cell carcinoma cell line. Nutr Cancer. 1999;34(1):12-9.
486. Ardito F, Di Gioia G, Pellegrino MR, Lo Muzio L. Genistein as a Potential Anticancer Agent Against Head and Neck Squamous Cell Carcinoma. Curr Top Med Chem. 2018;18(3):174-81.
487. Gao Y, Shang Q, Li W, Guo W, Stojadinovic A, Mannion C, et al. Antibiotics for cancer treatment: A double-edged sword. J Cancer. 2020;11(17):5135-49.
488. Reva ON, Rademan S, Visagie MH, Lebelo MT, Gwangwa MV, Klochko VV, et al. Comparison of structures and cytotoxicity of mupirocin and batumin against melanoma and several other cancer cell lines. Future Med Chem. 2019;11(7):677-91.
489. Novotny-Diermayr V, Sangthongpitag K, Hu CY, Wu X, Sausgruber N, Yeo P, et al. SB939, a novel potent and orally active histone deacetylase inhibitor with high tumor exposure and efficacy in mouse models of colorectal cancer. Mol Cancer Ther. 2010;9(3):642-52.
490. Wang H, Yu N, Chen D, Lee KC, Lye PL, Chang JW, et al. Discovery of (2E)-3-{2-butyl-1-[2-(diethylamino)ethyl]-1H-benzimidazol-5-yl}-N-hydroxyacrylami de (SB939), an orally active histone deacetylase inhibitor with a superior preclinical profile. J Med Chem. 2011;54(13):4694-720.
491. Razak AR, Hotte SJ, Siu LL, Chen EX, Hirte HW, Powers J, et al. Phase I clinical, pharmacokinetic and pharmacodynamic study of SB939, an oral histone deacetylase (HDAC) inhibitor, in patients with advanced solid tumours. Br J Cancer. 2011;104(5):756-62.
492. Yong WP, Goh BC, Soo RA, Toh HC, Ethirajulu K, Wood J, et al. Phase I and pharmacodynamic study of an orally administered novel inhibitor of histone deacetylases, SB939, in patients with refractory solid malignancies. Ann Oncol. 2011;22(11):2516-22.

493. Okabe S, Tauchi T, Tanaka Y, Kimura S, Maekawa T, Ohyashiki K. Activity of histone deacetylase inhibitors and an Aurora kinase inhibitor in BCR-ABL-expressing leukemia cells: Combination of HDAC and Aurora inhibitors in BCR-ABL-expressing cells. Cancer Cell Int. 2013;13(1):32.
494. Rauzan M, Chuah CT, Ko TK, Ong ST. The HDAC inhibitor SB939 overcomes resistance to BCR-ABL kinase Inhibitors conferred by the BIM deletion polymorphism in chronic myeloid leukemia. PLoS One. 2017;12(3):e0174107.
495. Abaza YM, Kadia TM, Jabbour EJ, Konopleva MY, Borthakur G, Ferrajoli A, et al. Phase 1 dose escalation multicenter trial of pracinostat alone and in combination with azacitidine in patients with advanced hematologic malignancies. Cancer. 2017;123(24):4851-9.
496. Garcia-Manero G, Abaza Y, Takahashi K, Medeiros BC, Arellano M, Khaled SK, et al. Pracinostat plus azacitidine in older patients with newly diagnosed acute myeloid leukemia: results of a phase 2 study. Blood Adv. 2019;3(4):508-18.
497. Novotny-Diermayr V, Hart S, Goh KC, Cheong A, Ong LC, Hentze H, et al. The oral HDAC inhibitor pracinostat (SB939) is efficacious and synergistic with the JAK2 inhibitor pacritinib (SB1518) in preclinical models of AML. Blood Cancer J. 2012;2(5):e69.
498. Chen J, Li N, Liu B, Ling J, Yang W, Pang X, et al. Pracinostat (SB939), a histone deacetylase inhibitor, suppresses breast cancer metastasis and growth by inactivating the IL-6/STAT3 signalling pathways. Life Sci. 2020;248:117469.
499. Chen M, Zhang L, Zhan R, Zheng X. The novel histone deacetylase inhibitor pracinostat suppresses the malignant phenotype in human glioma. Mol Biol Rep. 2022.
500. Lai CJ, Bao R, Tao X, Wang J, Atoyan R, Qu H, et al. CUDC-101, a multitargeted inhibitor of histone deacetylase, epidermal growth factor receptor, and human epidermal growth factor receptor 2, exerts potent anticancer activity. Cancer Res. 2010;70(9):3647-56.
501. Wang J, Pursell NW, Samson ME, Atoyan R, Ma AW, Selmi A, et al. Potential advantages of CUDC-101, a multitargeted HDAC, EGFR, and HER2 inhibitor, in treating drug resistance and preventing cancer cell migration and invasion. Mol Cancer Ther. 2013;12(6):925-36.
502. Zhang L, Zhang Y, Mehta A, Boufraquech M, Davis S, Wang J, et al. Dual inhibition of HDAC and EGFR signaling with CUDC-101 induces potent suppression of tumor growth and metastasis in anaplastic thyroid cancer. Oncotarget. 2015;6(11):9073-85.
503. Shimizu T, LoRusso PM, Papadopoulos KP, Patnaik A, Beeram M, Smith LS, et al. Phase I first-in-human study of CUDC-101, a multitargeted inhibitor of HDACs, EGFR, and HER2 in patients with advanced solid tumors. Clin Cancer Res. 2014;20(19):5032-40.
504. Nickson CM, Moori P, Carter RJ, Rubbi CP, Parsons JL. Misregulation of DNA damage repair pathways in HPV-positive head and neck squamous cell carcinoma contributes to cellular radiosensitivity. Oncotarget. 2017;8(18):29963-75.
505. Carter RJ, Nickson CM, Thompson JM, Kacperek A, Hill MA, Parsons JL. Characterisation of Deubiquitylating Enzymes in the Cellular Response to High-LET Ionizing Radiation and Complex DNA Damage. Int J Radiat Oncol Biol Phys. 2019;104(3):656-65.
506. Ferreira SC, Jr., Martins ML, Vilela MJ. Morphology transitions induced by chemotherapy in carcinomas in situ. Phys Rev E Stat Nonlin Soft Matter Phys. 2003;67(5 Pt 1):051914.
507. Uzunparmak B, Gao M, Lindemann A, Erikson K, Wang L, Lin E, et al. Caspase-8 loss radiosensitizes head and neck squamous cell carcinoma to SMAC mimetic-induced necroptosis. JCI Insight. 2020;5(23).
508. Yamakawa N, Takahashi A, Mori E, Imai Y, Furusawa Y, Ohnishi K, et al. High LET radiation enhances apoptosis in mutated p53 cancer cells through Caspase-9 activation. Cancer Sci. 2008;99(7):1455-60.
509. Cerna D, Lim B, Adelabu Y, Yoo S, Carter D, Fahim A, et al. SMAC Mimetic/IAP Inhibitor Birinapant Enhances Radiosensitivity of Glioblastoma Multiforme. Radiat Res. 2021;195(6):549-60.
510. Toni T, Viswanathan R, Robbins Y, Gunti S, Yang X, Huynh A, et al. Combined Inhibition of IAPs and WEE1 Enhances TNFalpha- and Radiation-Induced Cell Death in Head and Neck Squamous Carcinoma. Cancers (Basel). 2023;15(4).
511. Li G, Wang Z, Chong T, Yang J, Li H, Chen H. Curcumin enhances the radiosensitivity of renal cancer cells by suppressing NF-kappaB signaling pathway. Biomed Pharmacother. 2017;94:974-81.
512. Ren K, Li Z, Li Y, Zhang W, Han X. Sulforaphene enhances radiosensitivity of hepatocellular carcinoma through suppression of the NF-kappaB pathway. J Biochem Mol Toxicol. 2017;31(8).

513. Wang Z, Shen W, Li X, Feng Y, Qian K, Wang G, et al. The PPARgamma Agonist Rosiglitazone Enhances the Radiosensitivity of Human Pancreatic Cancer Cells. Drug Des Devel Ther. 2020;14:3099-110.
514. Mehta M, Griffith J, Panneerselvam J, Babu A, Mani J, Herman T, et al. Regorafenib sensitizes human breast cancer cells to radiation by inhibiting multiple kinases and inducing DNA damage. Int J Radiat Biol. 2021;97(8):1109-20.
515. Mu X, Ma J, Zhang Z, Zhou H, Xu S, Qin Y, et al. Famitinib enhances nasopharyngeal cancer cell radiosensitivity by attenuating radiation-induced phosphorylation of platelet-derived growth factor receptor and c-kit and inhibiting microvessel formation. Int J Radiat Biol. 2015;91(9):771-6.
516. Meng Y, Beckett MA, Liang H, Mauceri HJ, van Rooijen N, Cohen KS, et al. Blockade of tumor necrosis factor alpha signaling in tumor-associated macrophages as a radiosensitizing strategy. Cancer Res. 2010;70(4):1534-43.
517. Kodym E, Kodym R, Reis AE, Habib AA, Story MD, Saha D. The small-molecule CDK inhibitor, SNS-032, enhances cellular radiosensitivity in quiescent and hypoxic non-small cell lung cancer cells. Lung Cancer. 2009;66(1):37-47.
518. Qin W, Su Y, Ding X, Zhao R, Zhao Z, Wang Y. CDK4/6 inhibitor enhances the radiosensitization of esophageal
squamous cell carcinoma (ESCC) by activating autophagy signaling via the suppression of mTOR. Am J Transl Res. 2022;14(3):1616-27.
519. Zhang W, Li L, Guo E, Zhou H, Ming J, Sun L, et al. Inhibition of PDK1 enhances radiosensitivity and reverses epithelial-mesenchymal transition in nasopharyngeal carcinoma. Head Neck. 2022;44(7):1576-87.
520. Xiao S, Yang Z, Lv R, Zhao J, Wu M, Liao Y, et al. miR-135b contributes to the radioresistance by targeting GSK3beta in human glioblastoma multiforme cells. PLoS One. 2014;9(9):e108810.
521. Guo W, Ahmed KM, Hui Y, Guo G, Li JJ. siRNA-mediated MDM2 inhibition sensitizes human lung cancer A549 cells to radiation. Int J Oncol. 2007;30:1447-52.
522. He T, Guo J, Song H, Zhu H, Di X, Min H, et al. Nutlin-3, an Antagonist of MDM2, Enhances the Radiosensitivity of Esophageal Squamous Cancer with Wild-Type p53. Pathol Oncol Res. 2018;24(1):75-81.
523. Hagege A, Ambrosetti D, Boyer J, Bozec A, Doyen J, Chamorey E, et al. The Polo-like kinase 1 inhibitor onvansertib represents a relevant treatment for head and neck squamous cell carcinoma resistant to cisplatin and radiotherapy. Theranostics. 2021;11(19):9571-86.
524. Harris PS, Venkataraman S, Alimova I, Birks DK, Donson A, Knipstein J, et al. Polo-like kinase 1 (PLK1) inhibition suppresses
cell growth and enhances radiation sensitivity in
medulloblastoma cells. BMC Cancer. 2012;12(80).
525. Wang B, Huang X, Liang H, Yang H, Guo Z, Ai M, et al. PLK1 Inhibition Sensitizes Breast Cancer Cells to Radiation via Suppressing Autophagy. Int J Radiat Oncol Biol Phys. 2021;110(4):1234-47.
526. Wang D, Veo B, Pierce A, Fosmire S, Madhavan K, Balakrishnan I, et al. A novel PLK1 inhibitor onvansertib effectively sensitizes MYC-driven medulloblastoma to radiotherapy. Neuro Oncol. 2022;24(3):414-26.
527. Li M, Liu H, Zhao Q, Han S, Zhou L, Liu W, et al. Targeting Aurora B kinase with Tanshinone IIA suppresses tumor growth and overcomes radioresistance. Cell Death Dis. 2021;12(2):152.
528. Lin ZZ, Chou CH, Cheng AL, Liu WL, Chia-Hsien Cheng J. Radiosensitization by combining an aurora kinase inhibitor with radiotherapy in hepatocellular carcinoma through cell cycle interruption. Int J Cancer. 2014;135(2):492-501.
529. Liu F, Zhang Y, Dong Y, Ning P, Zhang Y, Sun H, et al. Knockdown of AURKA sensitizes the efficacy of radiation in human colorectal cancer. Life Sci. 2021;271:119148.
530. Moretti L, Niermann K, Schleicher S, Giacalone NJ, Varki V, Kim KW, et al. MLN8054, a small molecule inhibitor of aurora kinase a, sensitizes androgen-resistant prostate cancer to radiation. Int J Radiat Oncol Biol Phys. 2011;80(4):1189-97.
531. Wang J, Hu T, Wang Q, Chen R, Xie Y, Chang H, et al. Repression of the AURKA-CXCL5 axis induces autophagic cell death and promotes radiosensitivity in non-small-cell lung cancer. Cancer Lett. 2021;509:89-104.
532. Chen Q, Zheng W, Zhu L, Yao D, Wang C, Song Y, et al. ANXA6 Contributes to Radioresistance by Promoting Autophagy via Inhibiting the PI3K/AKT/mTOR Signaling Pathway in Nasopharyngeal Carcinoma. Front Cell Dev Biol. 2020;8:232.

533. Horn D, Hess J, Freier K, Hoffmann J, Freudlsperger C. Targeting EGFR-PI3K-AKT-mTOR signaling enhances radiosensitivity in head and neck squamous cell carcinoma. Expert Opin Ther Targets. 2015;19(6):795-805.
534. Li HF, Kim JS, Waldman T. Radiation-induced Akt activation modulates radioresistance in human glioblastoma cells. Radiat Oncol. 2009;4:43.
535. Liu T, Sun Q, Li Q, Yang H, Zhang Y, Wang R, et al. Dual PI3K/mTOR inhibitors, GSK2126458 and PKI-587, suppress tumor progression and increase radiosensitivity in nasopharyngeal carcinoma. Mol Cancer Ther. 2015;14(2):429-39.
536. Yang L, Yang G, Ding Y, Dai Y, Xu S, Guo Q, et al. Inhibition of PI3K/AKT Signaling Pathway Radiosensitizes Pancreatic Cancer Cells with ARID1A Deficiency in Vitro. J Cancer. 2018;9(5):890-900.
537. Wanigasooriya K, Barros-Silva JD, Tee L, El-Asrag ME, Stodolna A, Pickles OJ, et al. Patient Derived Organoids Confirm That PI3K/AKT Signalling Is an Escape Pathway for Radioresistance and a Target for Therapy in Rectal Cancer. Front Oncol. 2022;12:920444.
538. Kim KH, Kim HS, Kim SC, Kim D, Kim YB, Chung HC, et al. Gene Expression Profiling Identifies Akt as a Target for Radiosensitization in Gastric Cancer Cells. Front Oncol. 2020;10:562284.
539. Lang L, Lam T, Chen A, Jensen C, Duncan L, Kong FC, et al. Circumventing AKT-Associated Radioresistance in Oral Cancer by Novel Nanoparticle-Encapsulated Capivasertib. Cells. 2020;9(3).
540. Ciccarelli C, Di Rocco A, Gravina GL, Mauro A, Festuccia C, Del Fattore A, et al. Disruption of MEK/ERK/c-Myc signaling radiosensitizes prostate cancer cells in vitro and in vivo. J Cancer Res Clin Oncol. 2018;144(9):1685-99.
541. Hensch NR, Bondra K, Wang L, Sreenivas P, Zhao XR, Modi P, et al. Sensitization to Ionizing Radiation by MEK Inhibition Is Dependent on SNAI2 in Fusion-Negative Rhabdomyosarcoma. Mol Cancer Ther. 2023;22(1):123-34.
542. Kim SY, Jeong E, Lee T, Kim H, Kim CH. The Combination of Trametinib, a MEK Inhibitor, and Temsirolimus, an mTOR Inhibitor, Radiosensitizes Lung Cancer Cells. Anticancer Res. 2021;41(6):2885-94.
543. Li Q, Li K, Yang T, Zhang S, Zhou Y, Li Z, et al. Association of protein kinase CK2 inhibition with cellular radiosensitivity of non-small cell lung cancer. Sci Rep. 2017;7(1):16134.
544. Pompsch M, Vogel J, Classen F, Kranz P, Iliakis G, Riffkin H, et al. The presumed MTH1-inhibitor TH588 sensitizes colorectal carcinoma cells to ionizing radiation in hypoxia. BMC Cancer. 2018;18(1):1190.
545. Saleh EM. Inhibition of topoisomerase IIalpha sensitizes FaDu cells to ionizing radiation by diminishing DNA repair. Tumour Biol. 2015;36(11):8985-92.
546. Stathopoulos GP, Kapranos N, Manolopoulos L, Papadimitriou C, Adamopoulos G. Topoisomerase II alpha expression in squamous cell carcinomas of the head and neck. Anticancer Res. 2000;20(1A):177-82.
547. Wee CW, Kim JH, Kim HJ, Kang HC, Suh SY, Shin BS, et al. Radiosensitization of Glioblastoma Cells by a Novel DNA Methyltransferase-inhibiting Phthalimido-Alkanamide Derivative. Anticancer Res. 2019;39(2):759-69.
548. Kang HC, Chie EK, Kim HJ, Kim JH, Kim IH, Kim K, et al. A phthalimidoalkanamide derived novel DNMT inhibitor enhanced radiosensitivity of A549 cells by inhibition of homologous recombination of DNA damage. Invest New Drugs. 2019;37(6):1158-65.
549. Wilson GD, Saunders MI, Dische S, Richman PI, Daley FM, Bentzen SM. Bcl-2 expression in head and neck cancer: an enigmatic prognostic marker. 2001. 2001;49(49):435-41.
550. Rahmanian N, Hosseinimehr SJ, Khalaj A. The paradox role of caspase cascade in ionizing radiation therapy. J Biomed Sci. 2016;23(1):88.
551. Pickering CR, Zhang J, Yoo SY, Bengtsson L, Moorthy S, Neskey DM, et al. Integrative genomic characterization of oral squamous cell carcinoma identifies frequent somatic drivers. Cancer Discov. 2013;3(7):770-81.
552. Wagner N, Wagner KD. The Role of PPARs in Disease. Cells. 2020;9(11).
553. Theocharis S, Klijanienko J, Giaginis C, Rodriguez J, Jouffroy T, Girod A, et al. Peroxisome proliferator-activated receptor-gamma in mobile tongue squamous cell carcinoma: associations with clinicopathological parameters and patients survival. J Cancer Res Clin Oncol. 2011;137(2):251-9.
554. Wang J, Cui R, Clement CG, Nawgiri R, Powell DW, Pinchuk IV, et al. Activation PDGFR-alpha/AKT Mediated Signaling Pathways in Oral Squamous Cell Carcinoma by Mesenchymal Stem/Stromal Cells Promotes Anti-apoptosis and Decreased Sensitivity to Cisplatin. Front Oncol. 2020;10:552.

555. Ugolkov AV, Matsangou M, Taxter TJ, O'Halloran TV, Cryns VL, Giles FJ, et al. Aberrant expression of glycogen synthase kinase-3beta in human breast and head and neck cancer. Oncol Lett. 2018;16(5):6437-44.
556. Yang X, Chen X, Zeng L, Deng J, Ma L, Jin C, et al. Rab1A promotes cancer metastasis and radioresistance through activating GSK-3β/Wnt/β-catenin signaling in nasopharyngeal carcinoma. Aging. 2020;12(20):20380-95.
557. Cahilly-Snyder L, Yang-Feng T, Francke U, George DL. Molecular analysis and chromosomal mapping of amplified genes isolated from a transformed mouse 3T3 cell line. Somatic Cell and Molecular Genetics. 1987;13(3):235-44.
558. Cai Y, Dodhia S, Su GH. Dysregulations in the PI3K pathway and targeted therapies for head and neck squamous cell carcinoma. Oncotarget. 2017;8(13):22203-17.
559. Marquard FE, Jucker M. PI3K/AKT/mTOR signaling as a molecular target in head and neck cancer. Biochem Pharmacol. 2020;172:113729.
560. Cheng Y, Chen J, Shi Y, Fang X, Tang Z. MAPK Signaling Pathway in Oral Squamous Cell Carcinoma: Biological Function and Targeted Therapy. Cancers (Basel). 2022;14(19).
561. Litchfield DW. Protein kinase CK2: structure, regulation and role in cellular decisions of life and death. Biochem J. 2003;369:1-15.
562. Faust RA, Gapany M, Tristani P, Davis A, Adams GL, Ahmed K. Elevated protein kinase CK2 activity in chromatin of head and neck tumors: associationwith malignant transformation. Cancer Lett. 1996:31-5.
563. Gapany M, Faust RA, Tawfic S, Davis A, Adams GL, Ahmed K. Association of Elevated Protein Kinase CK2 Activity with Aggressive Behavior
of Squamous Cell Carcinoma of the Head and Neck. Molecular Medicine. 1995;1(6):1076-551.
564. Trembley JH, Wang G, Unger G, Slaton J, Ahmed K. Protein kinase CK2 in health and disease: CK2: a key player in cancer biology. Cell Mol Life Sci. 2009;66(11-12):1858-67.
565. Liu L, Zou JJ, Luo HS, Wu DH. Effect of protein kinase CK2 gene silencing on radiosensitization in human nasopharyngeal carcinoma cells. Nan Fang Yi Ke Da Xue Xue Bao. 2009;29(8):1551-3.
566. Rudling A, Gustafsson R, Almlöf I, Homan E, Scobie M, Warpman Berglund U, et al. Fragment-Based Discovery and Optimization of Enzyme Inhibitors by Docking of Commercial Chemical Space. J Med Chem. 2017;60(19):8160-9.
567. Yin Y, Chen F. Targeting human MutT homolog 1 (MTH1) for cancer eradication: current progress and perspectives. Acta Pharm Sin B. 2020;10(12):2259-71.
568. Abbas HHK, Alhamoudi KMH, Evans MD, Jones GDD, Foster SS. MTH1 deficiency selectively increases non-cytotoxic oxidative DNA damage in lung cancer cells: more bad news than good? BMC Cancer. 2018;18(1):423.
569. Giribaldi MG, Munoz A, Halvorsen K, Patel A, Rai P. MTH1 expression is required for effective transformation by oncogenic HRAS. Oncotarget. 2015;6(13):11519-29.
570. McPherson LA, Troccoli CI, Ji D, Bowles AE, Gardiner ML, Mohsen MG, et al. Increased MTH1-specific 8-oxodGTPase activity is a hallmark of cancer in colon, lung and pancreatic tissue. DNA Repair (Amst). 2019;83:102644.
571. Okamoto K, Toyokuni S, Kim WJ, Ogawa O, Kakehi Y, Arao S, et al. Overexpression of human mutT homologue gene messenger RNA in renal-cell carcinoma: evidence of persistent oxidative stress in cancer. Int J Cancer. 1996;65(4):437-41.
572. Song WJ, Jiang P, Cai JP, Zheng ZQ. Expression of Cytoplasmic 8-oxo-Gsn and MTH1 Correlates with Pathological Grading in Human Gastric Cancer. Asian Pac J Cancer Prev. 2015;16(15):6335-8.
573. Skidmore CJ, Davies MI, Goodwin PM, Halldorsson H, Lewis PJ, Shall S, et al. The involvement of poly(ADP-ribose) polymerase in the degradation of NAD caused by gamma-radiation and N-methyl-N-nitrosourea. Eur J Biochem. 1979;101(1):135-42.
574. Hayashi S, Hatashita M, Matsumoto H, Shioura H, Kitai R, Kano E. Enhancement of radiosensitivity by topoisomerase II inhibitor, amrubicin and amrubicinol, in human lung adenocarcinoma A549 cells and kinetics of apoptosis and necrosis induction. Int J Mol Med. 2006;18(5):909-15.
575. Kulis M, Esteller M. DNA methylation and cancer. Adv Genet. 2010;70:27-56.
576. Varela-Rey M, Woodhoo A, Martinez-Chantar ML, Mato JM, Lu SC. Alcohol, DNA methylation, and cancer. Alcohol Res. 2013;35(1):25-35.

577. Zhu X, Wang Y, Tan L, Fu X. The pivotal role of DNA methylation in the radio-sensitivity of tumor radiotherapy. Cancer Med. 2018;7(8):3812-9.
578. Zhou Y, Shao C. Histone methylation can either promote or reduce cellular radiosensitivity by regulating DNA repair pathways. Mutat Res Rev Mutat Res. 2021;787:108362.
579. Wei W, Dong Z, Gao H, Zhang YY, Shao LH, Jin LL, et al. MicroRNA-9 enhanced radiosensitivity and its mechanism of DNA methylation in non-small cell lung cancer. Gene. 2019;710:178-85.
580. Chi HC, Tsai CY, Tsai MM, Lin KH. Impact of DNA and RNA Methylation on Radiobiology and Cancer Progression. Int J Mol Sci. 2018;19(2).
581. Kim JS, Kim SY, Lee M, Kim SH, Kim SM, Kim EJ. Radioresistance in a human laryngeal squamous cell carcinoma cell line is associated with DNA methylation changes and topoisomerase II α. Cancer Biol Ther. 2015;16(4):558-66.
582. Yu Y, Guan H, Jiang L, Li X, Xing L, Sun X. Nimotuzumab, an EGFR-targeted antibody, promotes radiosensitivity of recurrent esophageal squamous cell carcinoma. Int J Oncol. 2020;56(4):945-56.
583. Mehanna H, Robinson M, Hartley A, Kong A, Foran B, Fulton-Lieuw T, et al. Radiotherapy plus cisplatin or cetuximab in low-risk human papillomavirus-positive oropharyngeal cancer (De-ESCALaTE HPV): an open-label randomised controlled phase 3 trial. Lancet. 2019;393(10166):51-60.
584. Gillison ML, Trotti AM, Harris J, Eisbruch A, Harari PM, Adelstein DJ, et al. Radiotherapy plus cetuximab or cisplatin in human papillomavirus-positive oropharyngeal cancer (NRG Oncology RTOG 1016): a randomised, multicentre, non-inferiority trial. Lancet. 2019;393(10166):40-50.
585. Kiweler N, Wunsch D, Wirth M, Mahendrarajah N, Schneider G, Stauber RH, et al. Histone deacetylase inhibitors dysregulate DNA repair proteins and antagonize metastasis-associated processes. J Cancer Res Clin Oncol. 2020;146(2):343-56.
586. Kachhap SK, Rosmus N, Collis SJ, Kortenhorst MS, Wissing MD, Hedayati M, et al. Downregulation of homologous recombination DNA repair genes by HDAC inhibition in prostate cancer is mediated through the E2F1 transcription factor. PLoS One. 2010;5(6):e11208.
587. Lee JH, Choy ML, Ngo L, Foster SS, Marks PA. Histone deacetylase inhibitor induces DNA damage, which normal but not transformed cells can repair. Proc Natl Acad Sci U S A. 2010;107(33):14639-44.
588. Park PJ. ChIP–seq: advantages and challenges of a maturing technology. Nature Reviews Genetics. 2009;10(10):669-80.
589. Buenrostro JD, Wu B, Chang HY, Greenleaf WJ. ATAC-seq: A Method for Assaying Chromatin Accessibility Genome-Wide. Curr Protoc Mol Biol. 2015;109:21.9.1-.9.9.
590. Woudstra EC. Chromatin structure and cellular radiosensitivity: a comparison of two human tumour cell lines. Int J Radiation Biology. 2009;70(6):693-703.
591. Gordon DJ, Milner AE, Beaney RP, Grdina DJ, Vaughn ATM. Cellular radiosensitivity in V79 cells is linked to alterations in chromatin structure. Int J Radiat Oncol Biol Phys. 1990;19(5):1199-201.
592. Oleinick NL, Chiu SM. Nuclear and Chromatin Structures and Their Influence on the Radiosensitivity of DNA. Radiation Protection Dosimetry. 1994;52(1-4):353-8.
593. Roos WP, Binder A, Bohm L. The influence of chromatin structure on initial DNA damage and radiosensitivity in CHO-K1 and xrs1 cells at low doses of irradiation 1-10 Gy. Radiat Environ Biophys. 2002;41(3):199-206.
594. Painter RB. Structural changes in chromatin as the basis for radiosensitivity in ataxia telangiectasia. Cytogenet Cell Genet. 1982;33(1-2):139-44.
595. Tanaka N, Osman AA, Takahashi Y, Lindemann A, Patel AA, Zhao M, et al. Head and neck cancer organoids established by modification of the CTOS method can be used to predict in vivo drug sensitivity. Oral Oncol. 2018;87:49-57.
596. Fabbrizi MR, Parsons JL. Radiotherapy and the cellular DNA damage response: current and future perspectives on head and neck cancer treatment. Cancer Drug Resistance. 2020.
597. Hill MA. Radiation Track Structure: How the Spatial Distribution of Energy Deposition Drives Biological Response. Clin Oncol (R Coll Radiol). 2020;32(2):75-83.
598. Goodhead DT. Energy deposition stochastics and track structure: what about the target? Radiat Prot Dosimetry. 2006;122(1-4):3-15.
599. Fabbrizi MR, Parsons JL. Radiotherapy and the cellular DNA damage response: current and future perspectives on head and neck cancer treatment. Cancer Drug Resist. 2020;3(4):775-90.

600. Wilkinson B, Hill MA, Parsons JL. The Cellular Response to Complex DNA Damage Induced by Ionising Radiation. Int J Mol Sci. 2023;24(5).
601. Hughes JR, Parsons JL. FLASH Radiotherapy: Current Knowledge and Future Insights Using Proton-Beam Therapy. Int J Mol Sci. 2020;21(18).
602. Vozenin MC, De Fornel P, Petersson K, Favaudon V, Jaccard M, Germond JF, et al. The Advantage of FLASH Radiotherapy Confirmed in Mini-pig and Cat-cancer Patients. Clin Cancer Res. 2019;25(1):35-42.
603. Favaudon V, Caplier L, Monceau V, Pouzoulet F, Sayarath M, Fouillade C, et al. Ultrahigh dose-rate FLASH irradiation increases the differential response between normal
and tumor tissue in mice. Sci Trans Med. 2014;6:245ra93.
604. Wilson JD, Hammond EM, Higgins GS, Petersson K. Ultra-High Dose Rate (FLASH) Radiotherapy: Silver Bullet or Fool's Gold? Frontiers in Oncology. 2020;9.
605. Spitz DR, Buettner GR, Petronek MS, St-Aubin JJ, Flynn RT, Waldron TJ, et al. An integrated physico-chemical approach for explaining the differential impact of FLASH versus conventional dose rate irradiation on cancer and normal tissue responses. Radiother Oncol. 2019;139:23-7.
606. Grimes DR, Partridge M. A mechanistic investigation of the oxygen fixation hypothesis and oxygen enhancement ratio. Biomedical physics & engineering express. 2015;1(4):045209.
607. Pratx G, Kapp DS. A computational model of radiolytic oxygen depletion during FLASH irradiation and its effect on the oxygen enhancement ratio. Physics in Medicine & Biology. 2019;64(18):185005.
608. Buonanno M, Grilj V, Brenner DJ. Biological effects in normal cells exposed to FLASH dose rate protons. Radiotherapy and Oncology. 2019;139:51-5.
609. Petersson K, Adrian G, Butterworth K, McMahon SJ. A quantitative analysis of the role of oxygen tension in FLASH radiation therapy. International Journal of Radiation Oncology* Biology* Physics. 2020;107(3):539-47.
610. Arina A, Beckett M, Fernandez C, Zheng W, Pitroda S, Chmura SJ, et al. Tumor-reprogrammed resident T cells resist radiation to control tumors. Nature communications. 2019;10(1):3959.
611. Holmgaard RB, Schaer DA, Li Y, Castaneda SP, Murphy MY, Xu X, et al. Targeting the TGFβ pathway with galunisertib, a TGFβRI small molecule inhibitor, promotes anti-tumor immunity leading to durable, complete responses, as monotherapy and in combination with checkpoint blockade. Journal for immunotherapy of cancer. 2018;6:1-15.

CHAPTER 10: SUPPLEMENTARY DATA

10.1. Validation screen statistical analysis

Statistical analysis was performed on three independent experiments using a two-tailed *t-test*. P-values for each drug are displayed in the tables below, with statistically significant values **highlighted**.

Table 10.1: Stearic Acid

Day	5	8	10	12	15
0.03 µM	0.869068585	0.42593498	0.961771415	0.79900158	0.767865666
0.03 µM + 1 Gy	0.47162588	0.22307478	0.38603808	0.91983136	0.82980938
1 µM	0.32440362	**0.02535171**	**0.01174329**	0.1874652	0.13846981
1 µM + 1 Gy	0.05877205	0.17378424	**0.0460478**	0.05634426	0.20723958
5 µM	0.1113435	0.0883221	0.7225418	0.1305668	0.5850047
5 µM + 1 Gy	0.1420734	0.3106291	0.7829946	0.1526922	0.0749842
5 µM + 2 Gy	0.7282571	0.2636631	0.4087946	0.5483649	**0.023555**
10 µM	0.2532577	0.1419449	0.5781187	0.5852537	**0.0489348**
10 µM + 1 Gy	0.0802221	0.4590108	0.1647714	0.0834042	0.0710191
10 µM + 2 Gy	0.6234922	0.1996604	0.8808159	0.9344179	**0.0489348**

Table 10.2: Orantinib

Day	5	8	10	12	15
0.03 µM	0.679788875	0.145063902	0.993659529	0.610117027	0.798284237
0.03 µM + 1 Gy	0.40680739	0.23968579	0.58135948	0.72336734	0.76592271
1 µM	0.0758672	**0.00704198**	**0.02152624**	0.06311611	0.11175854
1 µM + 1 Gy	0.18407474	0.29461927	0.19177688	0.12760955	0.2427853
5 µM	0.07844784	0.05078516	**0.00215467**	**0.0184097**	**0.0174771**
5 µM + 1 Gy	0.81162773	0.18931032	**0.02825051**	0.05559315	**0.04686633**
5 µM + 2 Gy	0.1998743	0.09283748	**0.02753744**	**0.04122783**	0.05535132
10 µM	0.9895645	0.81410708	0.19098046	0.83393619	0.77827266
10 µM + 1 Gy	0.38281368	0.40010378	0.30413023	0.05533107	**0.01703837**
10 µM + 2 Gy	0.46191332	0.23912447	0.82447575	0.81045805	0.77827266

Table 10.3: Apremilast

Day	5	8	10	12	15
0.03 µM	0.59709196	0.842218489	0.936284142	0.340741614	0.702230528
0.03 µM + 1 Gy	0.05176635	0.13308291	0.73404068	0.87610488	0.93962271
1 µM	0.94186176	0.34612366	0.3020403	0.83391424	0.2007717
1 µM + 1 Gy	0.38845061	0.47641458	0.88733178	0.90920453	0.76283255
5 µM	0.60894111	0.12801892	0.18732065	0.09153893	0.89457189
5 µM + 1 Gy	0.33963028	0.84837121	0.60735419	0.42826373	0.79592363
5 µM + 2 Gy	0.21897117	0.17208721	0.18262735	0.47235291	0.38126055
10 µM	0.3653701	0.31047819	0.44369988	0.10452098	0.92084186
10 µM + 1 Gy	0.78967346	0.44435298	0.10955082	0.07814959	0.27496267
10 µM + 2 Gy	0.86752525	0.93361513	0.99842298	0.76966589	0.92084186

Table 10.4: CUDC-101

Day	5	8	10	12	15
0.03 μM	0.717155061	0.829326995	0.760758998	0.154804725	0.061504604
0.03 μM + 1 Gy	0.31915767	0.22430068	0.78784973	0.6722695	0.35331863
1 μM	0.15169598	**0.03628025**	0.07542215	0.72767839	0.41980309
1 μM + 1 Gy	0.13670468	0.5632376	0.36909183	0.68904007	0.83520883
5 μM	**0.00586599**	**0.00150166**	**0.00054233**	**0.00010794**	**0.01071439**
5 μM + 1 Gy	**0.01599115**	**0.02364585**	**0.01230643**	**0.0275451**	0.07505204
5 μM + 2 Gy	0.18227549	**0.02241285**	**0.04210721**	0.0622708	0.05221772
10 μM	0.26354678	**0.00066792**	**5.7037E-06**	**1.9629E-05**	**0.01985212**
10 μM + 1 Gy	**0.00795797**	**0.00941584**	**0.00797746**	**0.01634174**	**0.04127623**
10 μM + 2 Gy	**0.04500215**	**0.00618875**	**0.01649757**	**0.03406131**	**0.01985212**

Table 10.5: Mocetinostat

Day	5	8	10	12	15
0.03 μM	0.19168111	0.580277293	0.938822392	0.228500679	0.646367745
0.03 μM + 1 Gy	0.30031205	0.19493013	0.69526791	0.70310449	0.30685036
1 μM	0.90517212	**0.00034319**	**0.00088001**	**0.00155016**	**0.00260339**
1 μM + 1 Gy	0.34393526	0.30739676	0.07127442	0.10975227	0.06943291
5 μM	0.41868971	0.2022418	0.75522013	**0.00723922**	0.36058318
5 μM + 1 Gy	0.60558174	0.81594664	0.19378617	0.38191027	0.42554279
5 μM + 2 Gy	0.98915764	0.98440913	0.30523616	0.97065562	0.52147923
10 μM	0.05890764	0.14086028	0.82064582	0.40924429	0.47337129
10 μM + 1 Gy	0.50384861	0.88280285	0.35404846	0.41232969	0.81140733
10 μM + 2 Gy	0.47006263	0.61574542	0.80785469	0.99203502	0.47337129

Table 10.6: Pracinostat

Day	5	8	10	12	15
0.03 μM	0.884916502	0.722176005	0.430629814	0.217728652	0.059909318
0.03 μM + 1 Gy	0.35283744	0.24590626	0.39408425	0.23659893	0.39899224
1 μM	0.05935883	**0.01965221**	**0.01460409**	0.18799874	0.52211657
1 μM + 1 Gy	0.56912662	0.17081703	0.38744829	0.18029841	0.84175416
5 μM	0.16458001	**0.00199349**	**3.4049E-05**	**0.00052889**	**0.0213011**
5 μM + 1 Gy	**0.04665844**	**0.02709826**	**0.01306457**	**0.03448191**	**0.01225889**
5 μM + 2 Gy	0.18446269	**0.02312514**	**0.03421619**	**0.00925416**	**0.02179595**
10 μM	0.91767168	0.10934211	0.71372429	0.69383547	0.50777078
10 μM + 1 Gy	0.9320723	0.59480982	0.25331151	0.2921685	0.59536801
10 μM + 2 Gy	0.66525843	0.18046933	0.67563717	0.07763506	0.50777078

Table 10.7: Resminostat

Day	5	8	10	12	15
0.03 μM	0.745502318	0.243300824	0.646232849	0.411703656	0.664119464
0.03 μM + 1 Gy	0.82071464	0.25440043	0.26013319	0.74776235	0.82998593
1 μM	0.31103111	**0.02500091**	**0.03122686**	0.28382217	0.22601472
1 μM + 1 Gy	0.06417847	0.65017612	0.13500471	0.2162467	0.35127285
5 μM	**0.03862241**	0.50621991	0.0825941	0.28335989	0.15124777
5 μM + 1 Gy	0.63525636	0.21058868	0.06612058	**0.03153221**	0.10558422
5 μM + 2 Gy	0.68943448	0.48852843	0.06394746	0.22428291	**0.04114646**
10 μM	0.11101405	0.97376757	0.17699578	0.73069015	**0.02498701**
10 μM + 1 Gy	0.49522878	0.45566318	0.93227892	0.11405977	0.10656341
10 μM + 2 Gy	0.6623229	0.2350171	0.08809798	0.09684896	**0.02098187**

Table 10.8: Icotinib

Day	5	8	10	12	15
0.03 µM	0.125683359	0.389430412	0.749802776	0.756335038	0.695836594
0.03 µM + 1 Gy	0.33441003	0.22299738	0.64716301	0.47093845	0.50105195
1 µM	0.99784915	0.14359161	0.22199342	0.6638152	0.50164305
1 µM + 1 Gy	0.26635311	0.74641405	0.71309027	0.38936066	0.80326788
5 µM	0.31646629	0.33333586	0.80798288	0.11685324	0.68527962
5 µM + 1 Gy	0.37530064	0.81627052	0.7637716	0.98132965	0.96510395
5 µM + 2 Gy	0.4089506	0.75805244	0.44289272	0.95512384	0.90268519
10 µM	0.92069586	0.2241405	0.30900133	0.73149233	0.42857896
10 µM + 1 Gy	0.33305204	0.06354717	0.40285649	0.34524501	0.71234859
10 µM + 2 Gy	0.23750119	0.39438067	0.14884705	0.71858753	0.42857896

Table 10.9: Rociletinib

Day	5	8	10	12	15
0.03 µM	0.204562792	0.132018955	0.516385449	0.874524204	0.994334812
0.03 µM + 1 Gy	0.39299973	0.25130793	0.73113806	0.33398732	0.48991855
1 µM	**0.0159314**	0.08492461	0.12761216	0.23133046	0.06219199
1 µM + 1 Gy	0.23516645	0.58756035	0.80305431	0.7860582	0.76445267
5 µM	0.3856645	0.2145613	0.0728635	0.7011189	0.1642757
5 µM + 1 Gy	0.9790477	0.503114	0.0721695	0.0692051	0.0607501
5 µM + 2 Gy	0.163599	0.122448	0.1067678	0.15007	0.1396449
10 µM	0.3443519	0.58989	0.0879845	0.6577108	**0.0046169**
10 µM + 1 Gy	0.9167383	0.6986342	0.0910446	**0.0205159**	0.1005725
10 µM + 2 Gy	0.1172226	0.0589182	**0.0100831**	**0.0441895**	**0.0046169**

Table 10.10: Lidocaine HCl

Day	5	8	10	12	15
0.03 µM	0.192757046	0.915992973	0.906573056	0.574265448	0.884946614
0.03 µM + 1 Gy	0.54960465	0.25124795	0.56003228	0.76223939	0.70860667
1 µM	**0.01326276**	**0.00310119**	**0.00194322**	**0.01397275**	**0.00238619**
1 µM + 1 Gy	0.06866937	0.2609029	0.11527928	0.12832289	0.29034351
5 µM	0.3427304	0.630182	**0.0438548**	0.7054476	0.1272723
5 µM + 1 Gy	0.4790256	0.229396	0.1115552	**0.0473709**	0.1018078
5 µM + 2 Gy	0.5009077	0.4814635	**0.0491461**	0.1875482	0.07422
10 µM	**0.0023537**	0.1340693	**0.0356791**	0.456842	**0.0068983**
10 µM + 1 Gy	0.3622161	0.0603121	0.061077	0.0767258	0.1201946
10 µM + 2 Gy	**0.0268349**	**0.017791**	**0.0067247**	**0.0185028**	**0.0068983**

Table 10.11: Afatinib

Day	5	8	10	12	15
0.03 µM	0.741624566	0.603226911	0.871263549	0.678708059	0.729387642
0.03 µM + 1 Gy	0.22533275	0.22087587	0.89896473	0.87450644	0.73240046
1 µM	**0.00528982**	**0.00149891**	**0.00158099**	**0.01658008**	**0.00701846**
1 µM + 1 Gy	0.07387304	0.12270577	**0.03217719**	0.07245792	0.21167253
5 µM	0.08078079	0.05946831	0.07263139	0.09484175	**0.01959006**
5 µM + 1 Gy	0.53912329	0.77106702	0.9606423	0.50229721	0.52035762
5 µM + 2 Gy	0.52559701	0.23710876	0.66346117	0.83446296	0.55540286
10 µM	0.13217265	**0.02486138**	**0.00932653**	**0.0033821**	0.83588274
10 µM + 1 Gy	0.29135076	**0.02512479**	0.06052232	0.91471605	0.6610442
10 µM + 2 Gy	0.90403865	0.55988466	0.90069487	0.6138535	0.83588274

Table 10.12: Genistein

Day	5	8	10	12	15
0.03 µM	0.19057389	0.446681843	0.289880704	**0.030022302**	0.05519134
0.03 µM + 1 Gy	0.27954339	0.16298557	0.20978986	0.65216475	0.54585349
1 µM	0.06371076	0.06365934	0.05214467	0.10102562	0.1783287
1 µM + 1 Gy	0.27942912	0.79356065	0.09746788	0.21930916	0.57773405
5 µM	0.6366155	0.525491	0.1709202	0.5805211	0.322862
5 µM + 1 Gy	0.6491608	0.1837904	0.0662892	**0.0459113**	0.0744657
5 µM + 2 Gy	0.3005236	**0.0442919**	**0.0200957**	0.1314902	0.0560279
10 µM	0.0758455	0.3628533	0.697595	0.2309061	0.0989375
10 µM + 1 Gy	0.6821156	0.9663203	0.9940496	0.0940113	0.1460341
10 µM + 2 Gy	0.4764567	0.3633363	0.0933513	0.221912	0.0989375

Table 10.13: Dexrazoxane HCl

Day	5	8	10	12	15
0.03 µM	0.658704223	0.739779023	0.758358115	0.595371009	0.888039148
0.03 µM + 1 Gy	0.33994679	0.19153679	0.33937269	0.39062608	0.24538158
1 µM	0.65222761	0.07230254	0.15546165	0.25202698	0.34811808
1 µM + 1 Gy	0.74010134	0.2265484	0.47878215	0.4384984	0.2186797
5 µM	0.21940548	0.60560923	0.0795479	0.06384014	0.09156486
5 µM + 1 Gy	0.80659672	0.44623881	0.19966832	0.3219796	0.09062806
5 µM + 2 Gy	0.0625083	0.10507364	**0.04367515**	0.14254856	**0.04712934**
10 µM	0.81471848	0.77019039	0.79605788	0.65133984	0.33292732
10 µM + 1 Gy	0.36103906	0.16381792	0.26759688	0.20742321	0.2277727
10 µM + 2 Gy	0.4688151	0.38953402	0.38822385	0.92138735	0.33292732

Table 10.14: Novobiocin Sodium

Day	5	8	10	12	15
0.03 µM	0.408934727	0.558455503	0.987059966	0.282254821	0.623242404
0.03 µM + 1 Gy	0.62394217	0.1790186	0.95979446	0.59925301	0.38184396
1 µM	0.85626558	0.14487986	0.40376547	0.90599359	0.93187059
1 µM + 1 Gy	0.51905716	0.31479152	0.71746055	0.8331599	0.76267723
5 µM	0.76472794	0.22750698	**0.00165713**	0.54366719	0.22008294
5 µM + 1 Gy	0.41024524	0.36875047	0.53726066	0.45699018	0.6931965
5 µM + 2 Gy	0.49936619	0.18230859	0.11051275	0.48996721	0.09534479
10 µM	0.27970712	0.94208869	0.83873832	0.58714821	0.11258549
10 µM + 1 Gy	0.70633395	0.3848775	0.47980967	**0.04727221**	0.05667627
10 µM + 2 Gy	0.69788938	0.36937313	0.12004549	0.46834763	0.11258549

Table 10.15: Enoxacin

Day	5	8	10	12	15
0.03 µM	0.414573736	0.567910608	0.958073227	0.365644396	0.846951151
0.03 µM + 1 Gy	0.49178285	0.21836025	0.43572965	0.24892771	0.19773134
1 µM	0.96426867	**0.02265345**	0.13919514	0.22277799	0.15623799
1 µM + 1 Gy	0.65687825	0.38779436	0.6803282	0.79975655	0.92045854
5 µM	0.6135752	0.2202	0.2476182	0.4548481	0.7146758
5 µM + 1 Gy	0.4785445	0.547819	0.6043829	0.8100522	0.9591176
5 µM + 2 Gy	0.4554216	0.7328783	0.2543391	0.8393757	0.4594255
10 µM	0.7290987	0.6789527	0.4154612	0.6296395	**0.0299739**
10 µM + 1 Gy	0.3341821	0.2887452	0.146972	0.1340475	0.0852249
10 µM + 2 Gy	0.0692271	**0.0179104**	**0.0221754**	0.2002852	**0.0299739**

Table 10.16: Fidaxomicin

Day	5	8	10	12	15
0.03 µM	0.403043572	0.82797784	0.280013317	0.201492257	0.18884375
0.03 µM + 1 Gy	0.14697125	0.16185827	0.95994911	0.62337314	0.2815301
1 µM	0.45925944	0.13373865	**0.04941407**	0.24123171	0.10245529
1 µM + 1 Gy	0.06528279	0.65815294	0.27885234	0.3670519	0.63388336
5 µM	0.59448026	0.8108174	**0.00189633**	0.22052819	0.09744302
5 µM + 1 Gy	0.50650155	0.86983488	0.96392268	0.51119896	0.55595389
5 µM + 2 Gy	0.58539041	0.9815267	0.22866421	0.76896305	0.32294661
10 µM	0.42766256	0.71571106	**0.04397072**	0.88436173	**0.00688249**
10 µM + 1 Gy	0.59274591	0.90163065	**0.0214468**	0.08727358	**0.03384106**
10 µM + 2 Gy	0.27441876	**0.01816732**	**0.01910918**	**0.02911735**	**0.00688249**

Table 10.17: Mupirocin

Day	5	8	10	12	15
0.03 µM	0.221147684	0.393815234	0.455748791	0.896664243	0.676817424
0.03 µM + 1 Gy	0.2817653	0.19299278	0.88268693	0.72694715	0.84836682
1 µM	0.13632727	0.08063807	0.08295081	0.4899615	0.38284003
1 µM + 1 Gy	0.56156101	0.49489094	0.40401077	0.45172962	0.54758354
5 µM	0.57978965	0.24781225	0.19682725	0.78479456	0.6570467
5 µM + 1 Gy	0.66674813	0.6461824	0.80322765	0.384769	0.38665262
5 µM + 2 Gy	0.3641803	0.2950914	0.12678019	0.30267169	0.23101489
10 µM	0.8723086	0.76513273	**0.03193313**	0.14603922	0.14037381
10 µM + 1 Gy	0.79161284	0.22458439	0.06172174	0.06012126	0.24105379
10 µM + 2 Gy	0.49626198	0.19581805	0.06503543	0.17810914	0.14037381

CHAPTER 11: APPENDIX I

11.1.1. Cell Growth and Survival Candidates

In the initial drug screen, the NF-κB inhibitor stearic acid appeared to radiosensitise FaDu spheroids at 1 μM, with a relative percentage growth of 40 % in comparison to X-ray controls. However, this effect was not seen in the initial validation experiments (figure 11.1a). 0.03 μM stearic acid treatment resulted in a growth rate comparable to DMSO controls at both 0 Gy and 1 Gy while 1 μM alone only slightly reduced overall growth, but to a statistically significant degree in both unirradiated and irradiated conditions ($p < 0.05$; *t-test*, see supplementary table 10.1). Interestingly, the higher concentrations of stearic acid appeared to markedly enhance growth at all radiation doses (figure 11.1b). Both 5 μM and 10 μM plus 2 Gy x-rays were significantly higher than DMSO controls on day 15 ($p < 0.05$; *t-test*, supplementary table 10.1). Overall, there is no strong evidence from this data that stearic acid is radiosensitising FaDu spheroids.

Orantinib appeared to radiosensitise spheroids at the low concentration of 0.03 μM in the initial drug screen. In the initial validation experiments (figure 11.2a), 0.03 μM treatment resulted in spheroids with comparable growth levels to the relevant controls at both 0 Gy and 1 Gy, while 1 μM orantinib was slightly impairing spheroid growth – this difference was statistically significant on days 8 and 10 post-seeding ($p < 0.05$, respectively; *t-test*, supplementary table 10.2). As with stearic acid treatment, the high concentrations of 5 μM and 10 μM orantinib unexpectedly seemed to be promoting growth more than the low concentrations (figure 11.2b). 5 μM significantly promoted growth at both doses of IR ($p < 0.05$; *t-test*, supplementary table 10.2). 10 μM had a similar effect, but only at a radiation

dose of 1 Gy ($p < 0.05$; *t-test,* supplementary table 10.2). Overall, I cannot conclude from this data that orantinib can radiosensitise FaDu spheroids.

Similar to orantinib, apremilast appeared to radiosensitise spheroids in the initial drug screen at the low concentration of 0.03 μM, however, the inhibitor did not have this effect in the initial validation experiments, where neither concentration of apremilast did not cause a statistically significant difference in growth at any time point (figure 11.3a; *t-test,* supplementary table 10.3).5 μM apremilast enhanced spheroid growth compared to controls at all radiation doses, while 10 μM decreased growth at both x-ray doses – but enhanced growth as a single agent (figure 11.3b). None of these differences were statistically significant, and I can conclude from this data that apremilast does not radiosensitise FaDu spheroids.

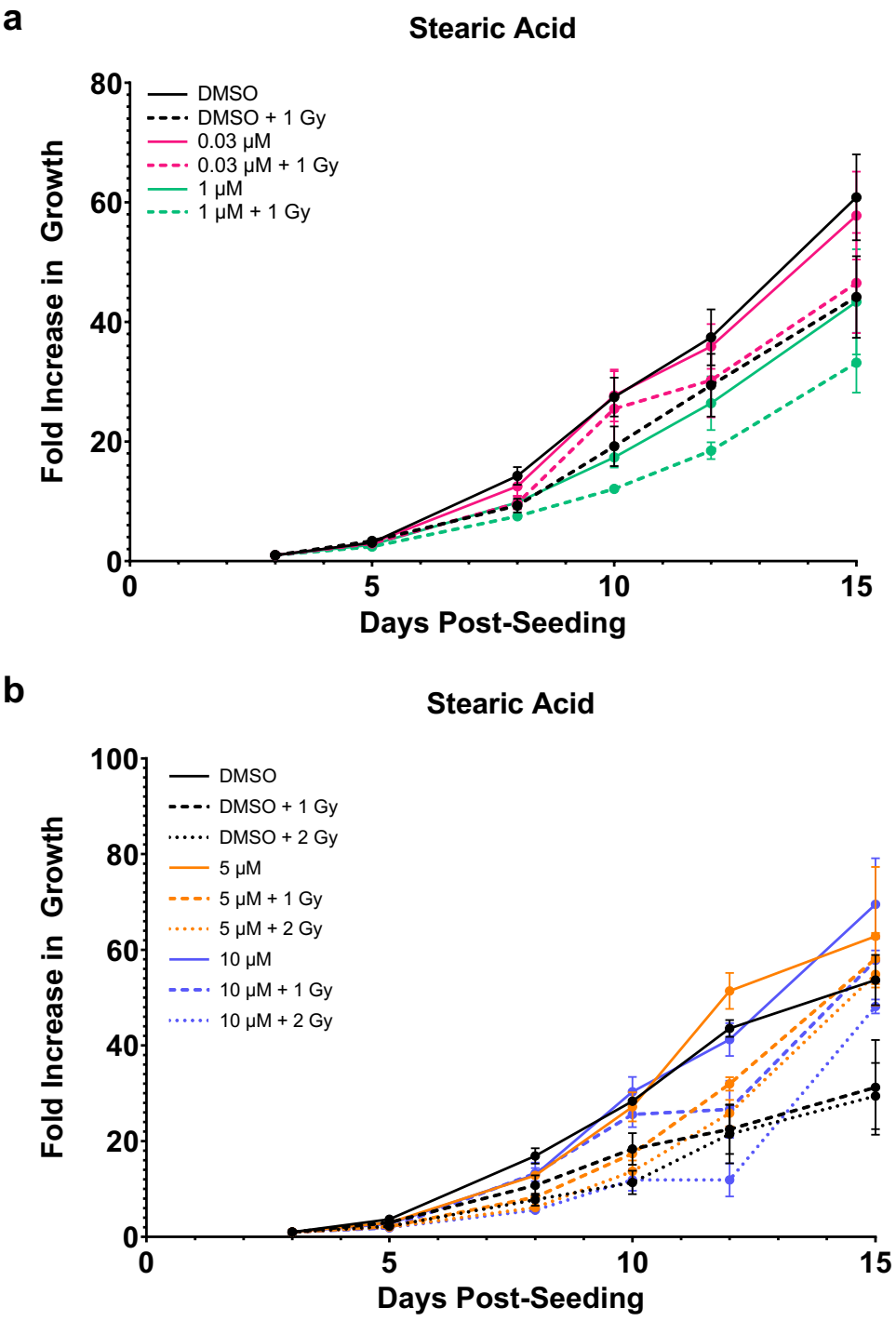

Figure 11.1: Spheroid growth following stearic acid treatment

FaDu cells were seeded into ULA plates and incubated for 24 hours to allow spheroid formation. Stearic acid was then added at two concentrations, either (a) 0.03 µM and 1 µM or (b) 5 µM and 10 µM. 24 hours after inhibitor treatment, spheroids were irradiated with either (a) 1 Gy or (b) 1 Gy and 2 Gy X-rays. Images of the spheroids were captured on days 3, 5, 8, 10, 12 and 15 post-seeding, which were used to measure the fold increase in growth over time. The data are presented as mean ± SEM of triplicate wells and are representative of three independent experiments.

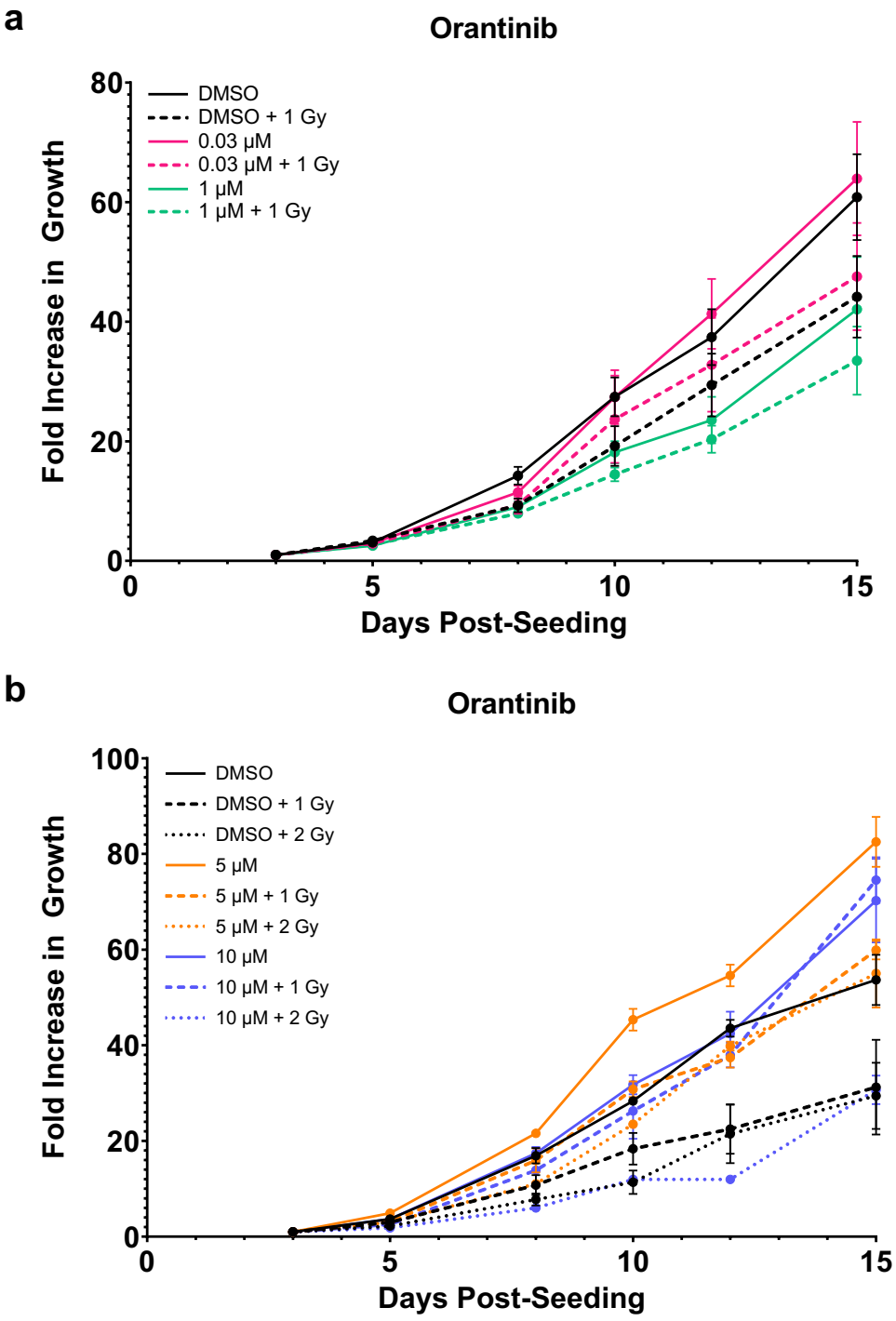

Figure 11.2: Spheroid growth following orantinib treatment

FaDu cells were seeded into ULA plates and incubated for 24 hours to allow spheroid formation. Orantinib was then added at either (a) 0.03 µM and 1 µM or (b) 5 µM and 10 µM. Following 24 hours of inhibitor treatment, spheroids were irradiated with either (a) 1 Gy or (b) 1 Gy and 2 Gy X-rays. Images of the spheroids were captured on days 3, 5, 8, 10, 12 and 15 post-seeding, which were used to measure the fold increase in growth over time. The data are presented as mean ± SEM of triplicate wells and are representative of three independent experiments.

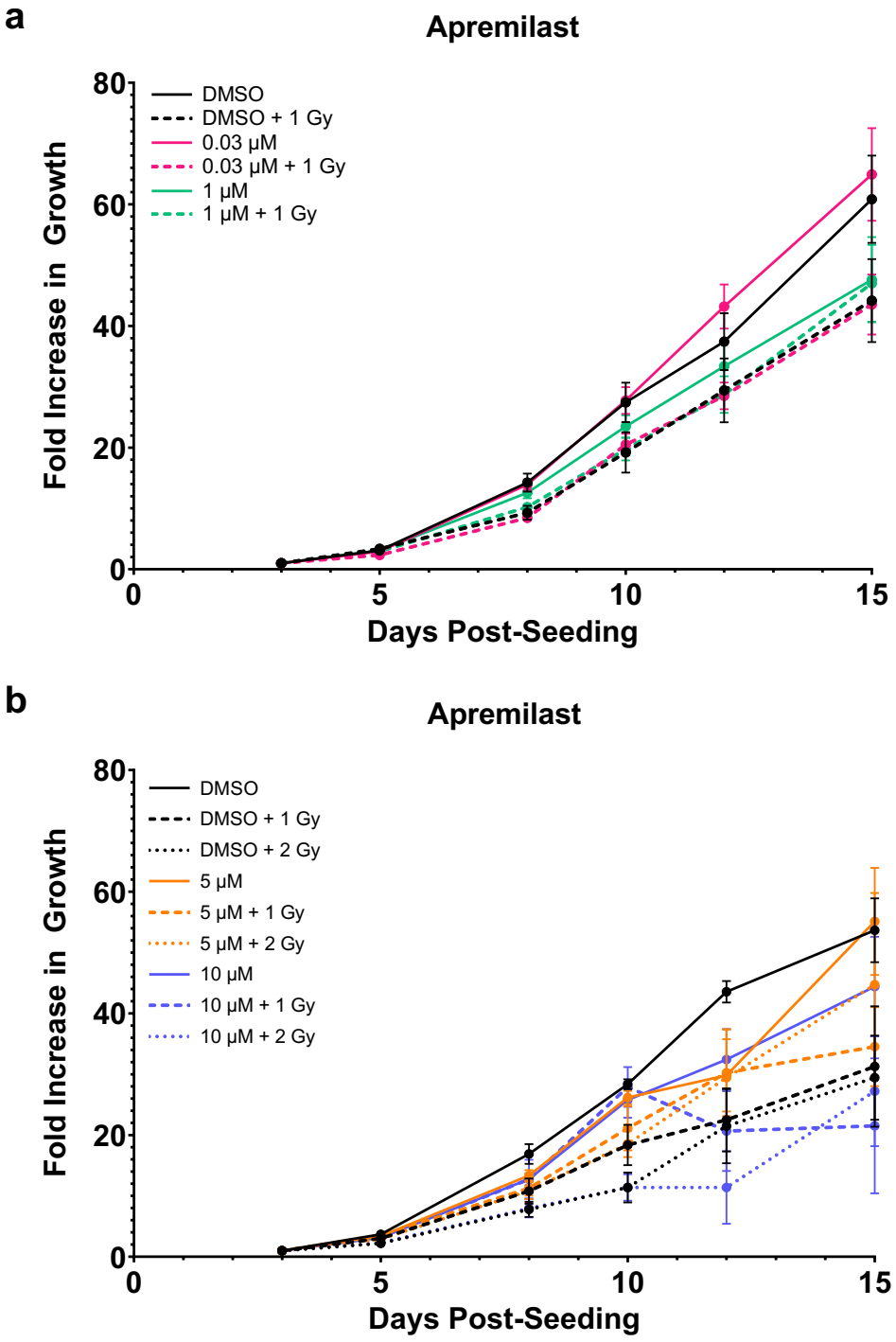

Figure 11.3: Spheroid growth following apremilast treatment

FaDu cells were seeded into ULA plates and incubated for 24 hours to allow spheroid formation. Afatinib was then added at two concentrations: either (a) 0.03 µM and 1 µM or (b) 5 µM and 10 µM. Following 24 hours of inhibitor treatment, spheroids were irradiated with either (a) 1 Gy or (b) 1 Gy and 2 Gy X-rays. Images of the spheroids were captured on days 3, 5, 8, 10, 12 and 15 post-seeding, which were used to measure the fold increase in growth over time. The data are presented as mean ± SEM of triplicate wells and are representative of three independent experiments.

11.1.2. Chromatin Organisation Candidates

Mocetinostat appeared to be radiosensitising spheroids at 1 μM in the initial drug screen. In the first set of validation experiments (figure 11.4a), 0.03 μM mocetinostat increased spheroid growth when combined with IR, while 1 μM mocetinostat plus X-rays reduced growth, although not to a statistically significant level. When using higher concentrations, both concentrations of mocetinostat when combined with X-rays observably enhanced spheroid growth in comparison to irradiated controls (figure 11.4b), and overall, there is no significant data to suggest this inhibitor can act as a radiosensitiser.

Resminostat appeared to be radiosensitising spheroids in the initial screen at the low concentration of 0.03 μM, however, in the first validation experiments, neither concentration of resminostat caused a dramatic reduction of growth when combined with 1 Gy X-rays (figure 11.5a). When the more intense treatments of 5 μM and 10 μM inhibitor were used, resminostat enhanced spheroid growth regardless of treatment condition (figure 11.5b). Based on these data, it appears that resminostat cannot radiosensitise FaDu spheroids.

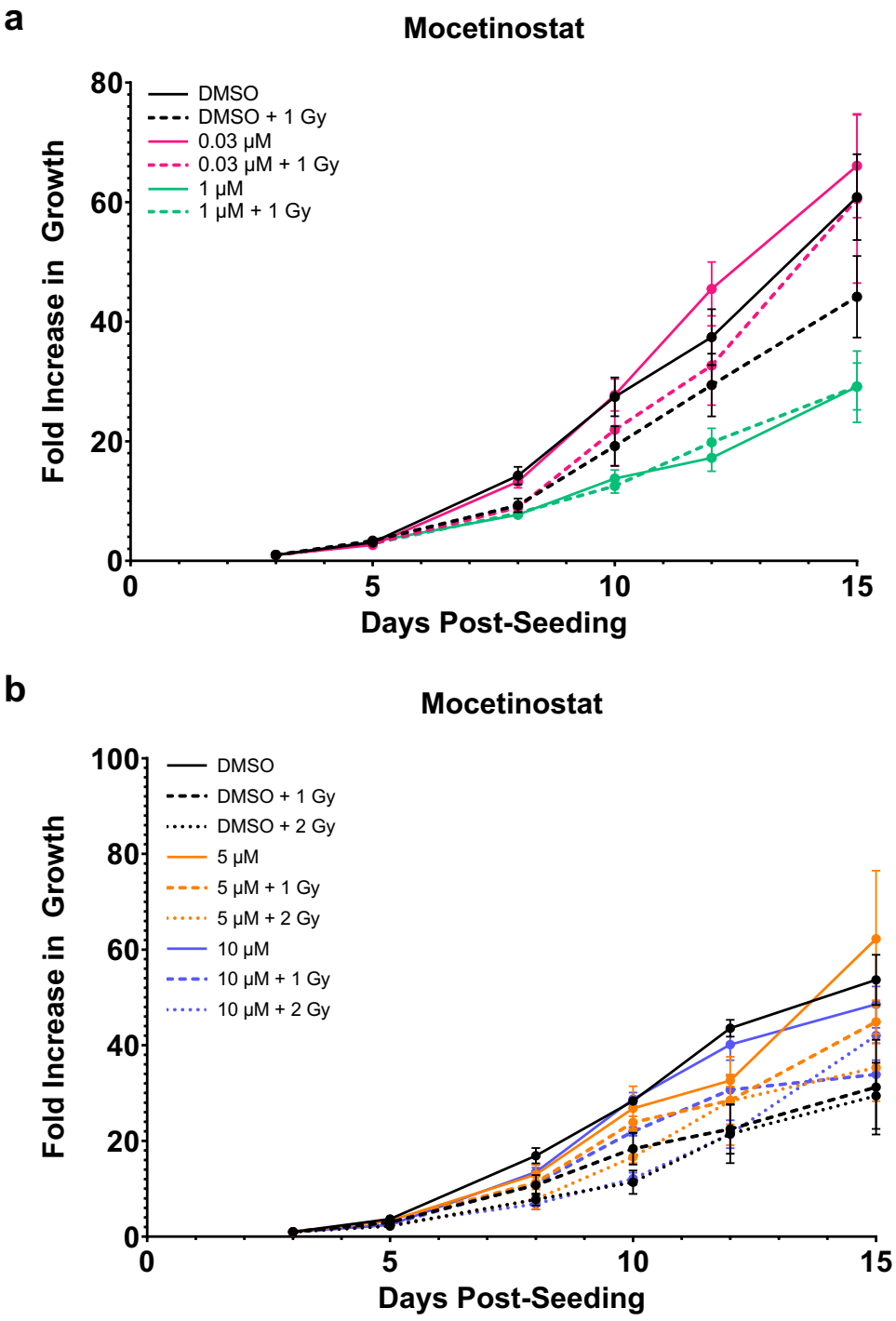

Figure 11.4: Spheroid growth following mocetinostat treatment

FaDu cells were seeded into ULA plates and incubated for 24 hours to allow spheroid formation. Following this, mocetinostat was added at either (a) 0.03 μM and 1 μM or (b) 5 μM and 10 μM. Following 24 hours of inhibitor treatment, spheroids were irradiated with either (a) 1 Gy or (b) 1 Gy and 2 Gy X-rays. Images of the spheroids were captured on days 3, 5, 8, 10, 12 and 15 post-seeding, which were used to measure the fold increase in growth over time. The data are presented as mean ± SEM of triplicate wells and are representative of three independent experiments.

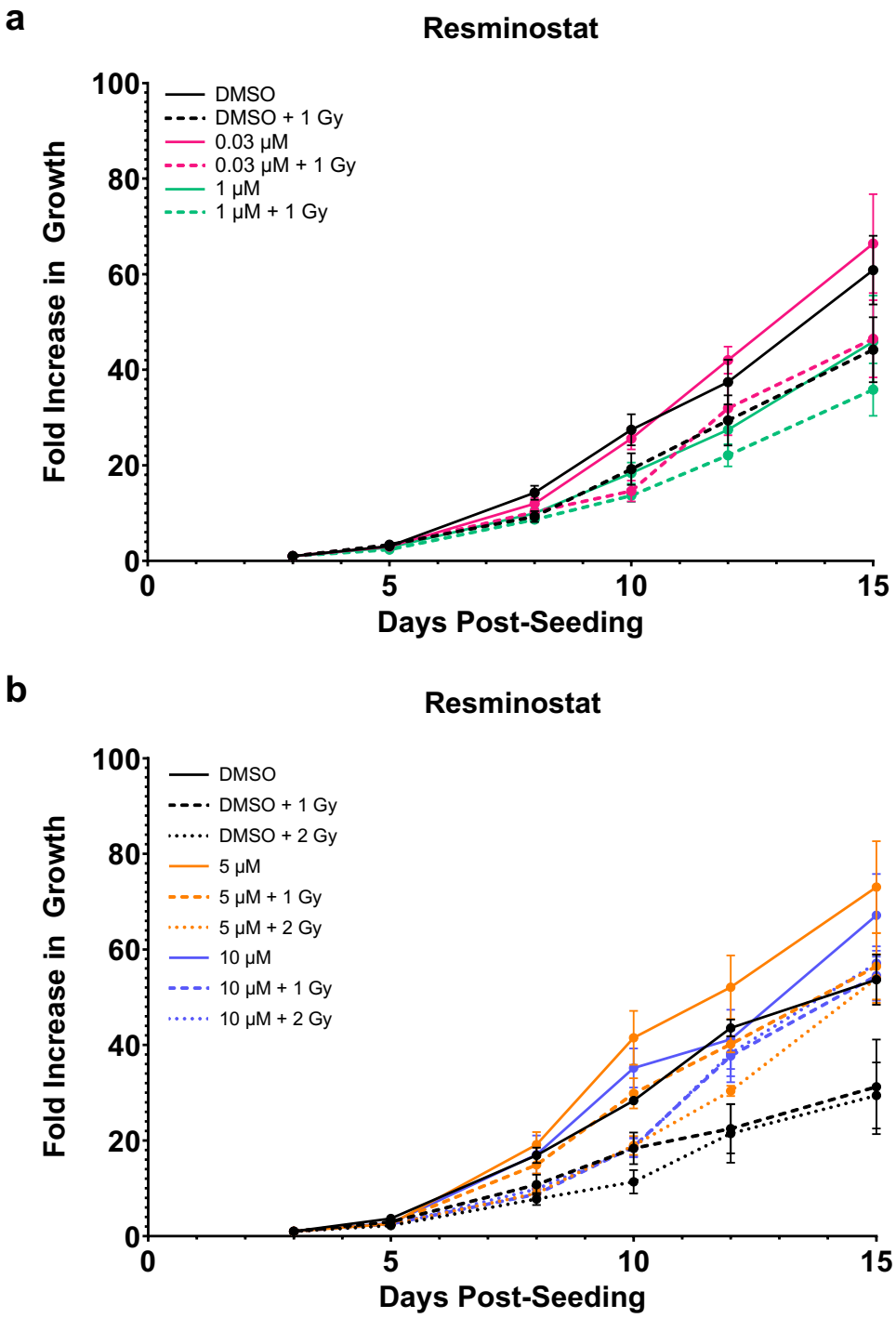

Figure 11.5: Spheroid growth following resminostat treatment

FaDu cells were seeded into ULA plates and incubated for 24 hours to allow spheroid formation. Following this, resminostat was added at either (a) 0.03 µM and 1 µM or (b) 5 µM and 10 µM. Following 24 hours of inhibitor treatment, spheroids were irradiated with either (a) 1 Gy or (b) 1 Gy and 2 Gy X-rays. Images of the spheroids were captured on days 3, 5, 8, 10, 12 and 15 post-seeding, which were used to measure the fold increase in growth over time. The data are presented as mean ± SEM of triplicate wells and are representative of three independent experiments.

11.1.3. Cell Signalling Candidates

In the initial drug screen, the EGFR inhibitor icotinib appeared to be radiosensitising spheroids at a concentration of 0.03 μM, while in the first set of validation experiments, neither concentration had a marked impact on growth (figure 11.6a). 5 μM icotinib plus X-rays – both 1 Gy and 2 Gy – had almost no effect on spheroid growth, while 10 μM treatment markedly increased spheroid growth at both doses of X-rays (figure 11.6b). None of these differences were statistically significant (*t-test*, supplementary table 10.8), and from this data, I cannot draw a conclusion that icotinib can radiosensitise FaDu spheroids.

Rociletinib seemed to have radiosensitising ability at a concentration of 1 μM in the initial drug screen, however this was not replicated in the initial validation experiments, where both concentrations of rociletinib enhanced spheroid growth when combined with X-rays (figure 11.7a). Similarly, the higher concentrations of 5 μM and 10 μM were also found to markedly enhanced spheroid growth compared to the DMSO controls (figure 11.7b). This enhancement was statistically significant following 5 μM plus 1 Gy X-rays and 10 μM plus 2 Gy X-rays ($p < 0.05$; *t-test*, supplementary table 10.9). From this data, I can conclude that rociletinib does not radiosensitise FaDu spheroids, and in fact may be promoting spheroid radioresistance.

Lidocaine HCl appeared to be having a striking radiosensitisation effect in the initial drug screen, as at a low concentration of 0.03 μM the spheroid growth was reduced to 17 % relative to controls following exposure to IR. In contrast, no radiosensitisation was observed in the first set of validation experiments (figure 11.8a). 0.03 μM lidocaine HCl plus 1 Gy X-rays enhanced spheroid growth compared to controls, while 1 μM caused a slight reduction. In the

second set of validation experiments (figure 11.8b), neither 5 μM nor 10 μM caused a reduction in spheroid growth. Quite the opposite, both treatments caused a striking and statistically significant increase in spheroid growth by the end of the experiment – except 10 μM plus 1 Gy X-rays, which did not show statistical significance ($p < 0.05$; *t-test*, supplementary table 10.10). From this data, I can conclude that while lidocaine HCl combined with IR is a more effective treatment than IR alone when used at a concentration of 1 μM, there is no observed radiosensitisation following use of this inhibitor.

In the initial drug screen, afatinib appeared to be radiosensitising FaDu spheroids at the low concentration of 0.03 μM, however, in the first set of validation experiments, 0.03 μM afatinib plus 1 Gy X-rays was comparable to the irradiated controls at all time points (figure 11.9a). The addition of 1 Gy X-rays to 1 μM afatinib only slightly reduced overall growth, however this was statistically significant ($p < 0.05$; *t-test*, supplementary table 10.11). In the second set of validation experiments (figure 11.9b), 5 μM afatinib plus 1 Gy X-rays seemed to enhance growth in comparison to DMSO plus 1 Gy, while in contrast, 10 μM afatinib reduced spheroid growth when combined with 1 Gy X-rays, but only to a minor degree, although this was statistically significant ($p < 0.05$; *t-test*, supplementary table 10.11). When combined with 2 Gy, both concentrations of afatinib caused a higher overall growth relative to controls by the end of the experiment. At this point, there is insufficient evidence to support the hypothesis that afatinib can radiosensitise FaDu spheroids.

In the initial drug screen, genistein appeared to be radiosensitising spheroids at a concentration of 1 μM. In the first set of validation experiments, both 0.03 μM and 1 μM reduced overall spheroid growth when combined with X-rays, but not to a marked or statistically significant degree (figure 11.10a). In the second set of validation experiments (figure 11.10b), spheroids treated with 5

μM genistein plus both 1 Gy and 2 Gy X-rays grew at a consistently higher rate than controls, and the enhancement of growth was statistically significant ($p < 0.05$; *t-test*, supplementary table 10.12). 10 μM genistein in combination with 1 Gy X-rays also enhanced growth when combined with either dose of X-rays, although there was a lack of statistical significance. From these experiments, it appears clear that genistein does not radiosensitise FaDu spheroids.

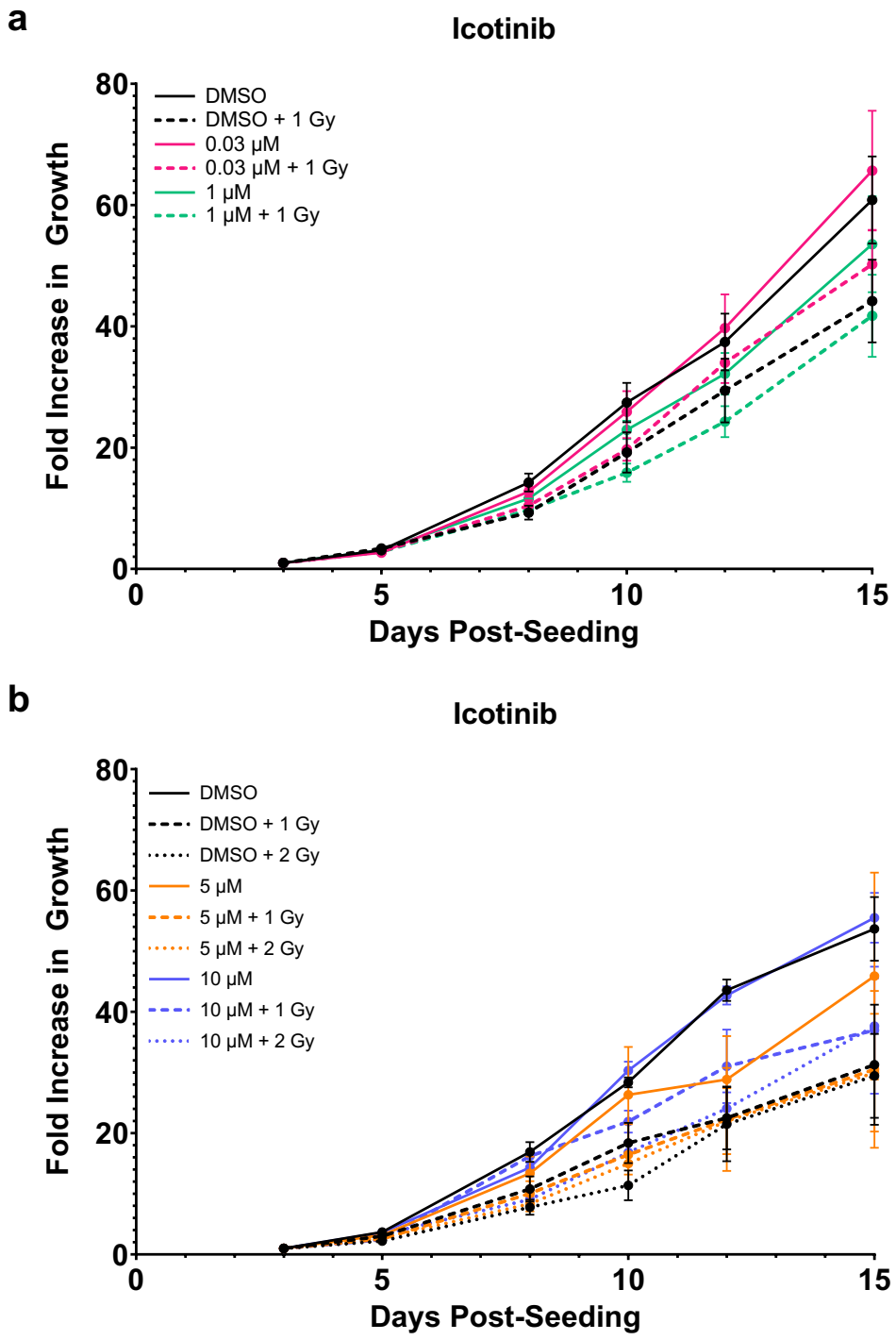

Figure 11.6: Spheroid growth following icotinib treatment

FaDu cells were seeded into ULA plates and incubated for 24 hours to allow spheroid formation, after which icotinib was added at either (a) 0.03 µM and 1 µM or (b) 5 µM and 10 µM. Following 24 hours of inhibitor treatment, spheroids were irradiated with either (a) 1 Gy or (b) 1 Gy and 2 Gy X-rays. Images of the spheroids were captured on days 3, 5, 8, 10, 12 and 15 post-seeding, which were used to measure the fold increase in growth over time. The data are presented as mean ± SEM of triplicate wells and are representative of three independent experiments.

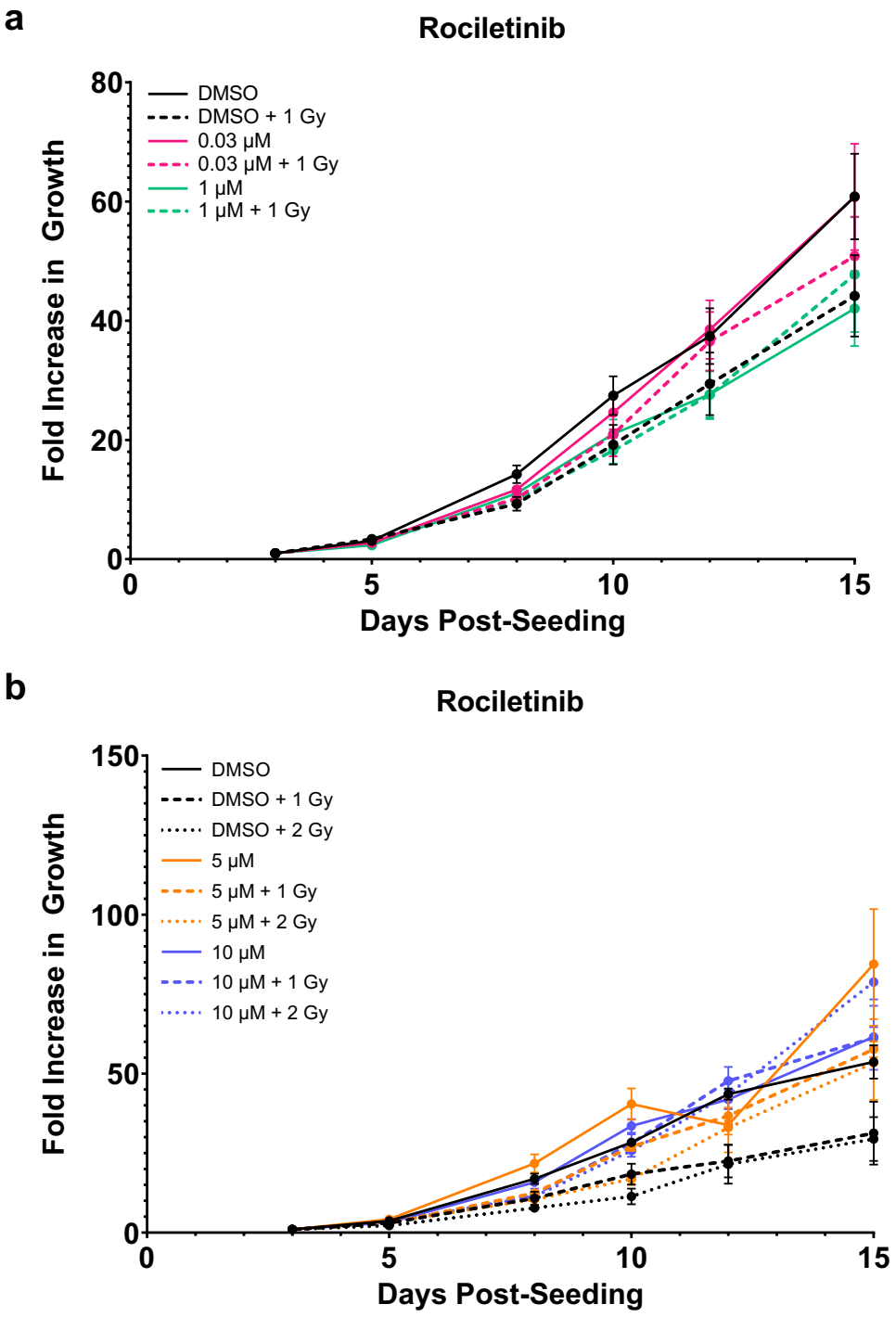

Figure 11.7: Spheroid growth following rociletinib treatment

FaDu cells were seeded into ULA plates and incubated for 24 hours to allow spheroid formation. After this time, rociletinib was added at either (a) 0.03 μM and 1 μM or (b) 5 μM and 10 μM. Following 24 hours of inhibitor treatment, spheroids were irradiated with either (a) 1 Gy or (b) 1 Gy and 2 Gy X-rays. Images of the spheroids were captured on days 3, 5, 8, 10, 12 and 15 post-seeding, which were used to measure the fold increase in growth over time. The data are presented as mean ± SEM of triplicate wells and are representative of three independent experiments.

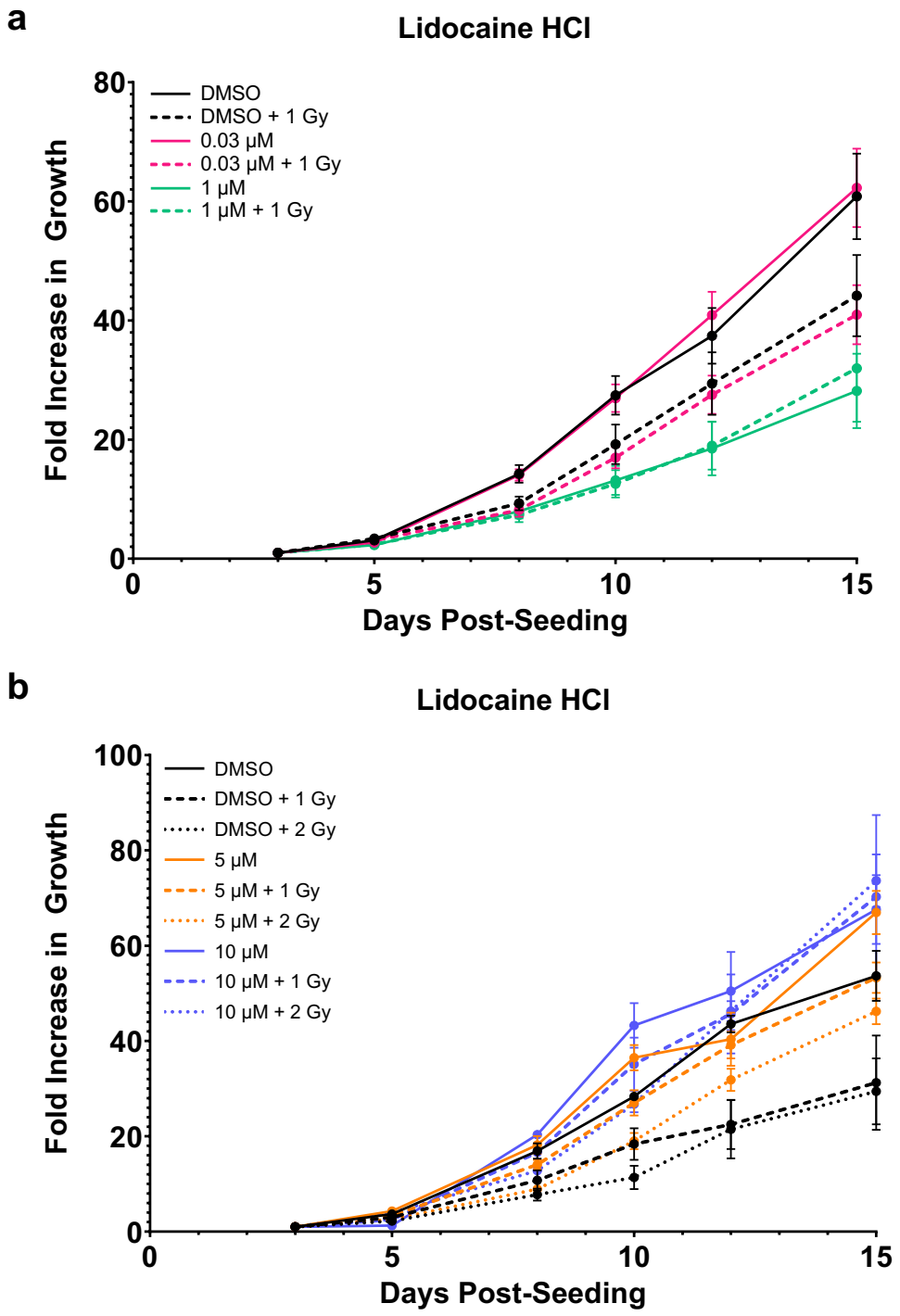

Figure 11.8: Spheroid growth following lidocaine HCl treatment

FaDu cells were seeded into ULA plates and incubated for 24 hours to allow spheroid formation. After this time, lidocaine HCl was added at either (a) 0.03 µM and 1 µM or (b) 5 µM and 10 µM. Following 24 hours of inhibitor treatment, spheroids were irradiated with either (a) 1 Gy or (b) 1 Gy and 2 Gy X-rays. Images of the spheroids were captured on days 3, 5, 8, 10, 12 and 15 post-seeding, which were used to measure the fold increase in growth over time. The data are presented as mean ± SEM of triplicate wells and are representative of three independent experiments.

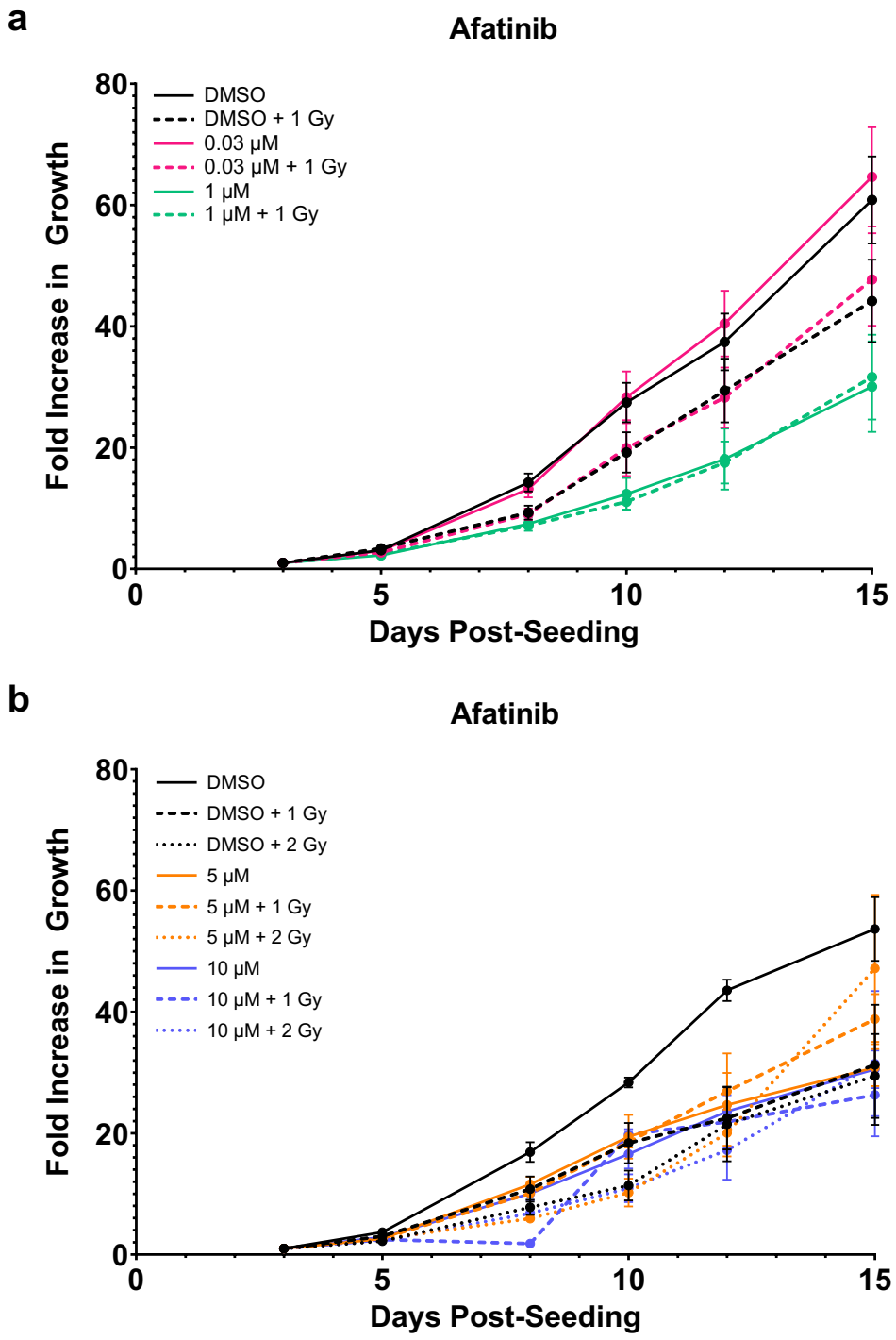

Figure 11.9: Spheroid growth following afatinib treatment

FaDu cells were seeded into ULA plates and incubated for 24 hours to allow spheroid formation. Afatinib was subsequently added at either (a) 0.03 µM and 1 µM or (b) 5 µM and 10 µM. Following 24 hours of inhibitor treatment, spheroids were irradiated with either (a) 1 Gy or (b) 1 Gy and 2 Gy X-rays. Images of the spheroids were captured on days 3, 5, 8, 10, 12 and 15 post-seeding, which were used to measure the fold increase in growth over time. The data are presented as mean ± SEM of triplicate wells and are representative of three independent experiments.

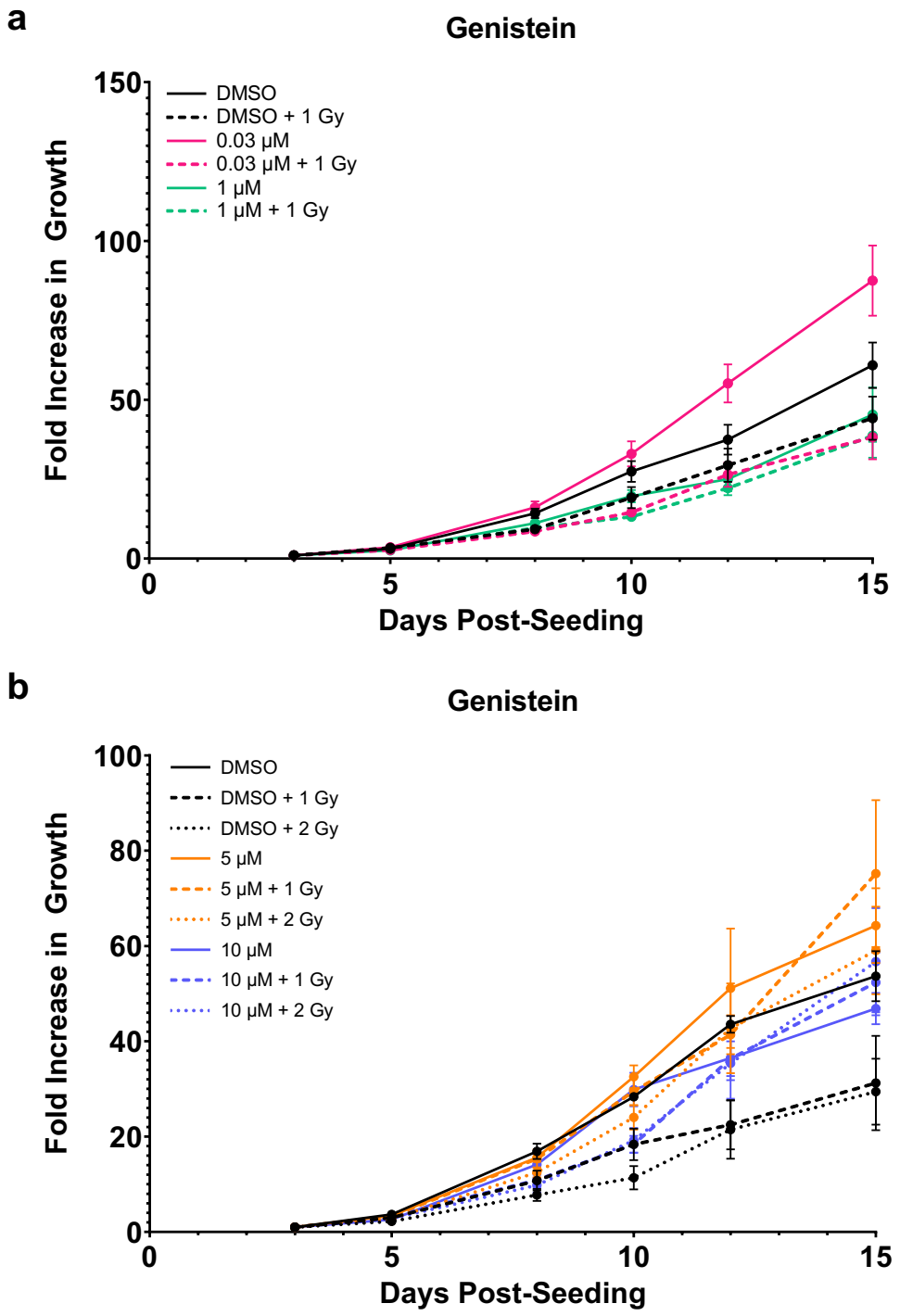

Figure 11.10: Spheroid growth following genistein treatment

FaDu cells were seeded into ULA plates and incubated for 24 hours to allow spheroid formation. Genistein was subsequently added at either (a) 0.03 µM and 1 µM or (b) 5 µM and 10 µM. Following 24 hours of inhibitor treatment, spheroids were irradiated with either (a) 1 Gy or (b) 1 Gy and 2 Gy X-rays. Images of the spheroids were captured on days 3, 5, 8, 10, 12 and 15 post-seeding, which were used to measure the fold increase in growth over time. The data are presented as mean ± SEM of triplicate wells and are representative of three independent experiments.

11.1.4. Cell Cycle Regulation Candidates

The topoisomerase inhibitor dexrazoxane HCl appeared to radiosensitise FaDu spheroids in the initial drug screen at the low concentration of 0.03 μM, but in contrast to this, in the first set of validation experiments both 0.03 μM and 1 μM plus 1 Gy X-rays markedly enhanced growth compared to controls (figure 11.11a). However, this enhancement was not statistically significant (*t-test*, supplementary table 10.13). When using higher concentrations of 5 μM and 10 μM, all the irradiated spheroids had a similar growth up to 8 days post-seeding, regardless of inhibitor concentration or radiation dose, and by the end of the experiment, all spheroids had a higher overall growth than their respective controls (figure 11.11b). Overall, this data suggests that dexrazoxane HCl increases radioresistance in FaDu spheroids.

Novobiocin sodium also seemed to be radiosensitising spheroids at 0.03 μM in the initial drug screen, reducing overall growth to 45 % relative to the irradiated controls. However, in the first set of validation experiments, all treatment conditions enhanced spheroid growth compared to the controls (figure 11.12a). In the second set of validation experiments (figure 11.12b), 5 μM plus 1 Gy X-rays reduced overall spheroid growth, however, the variation within these experiments meant there was a lack of statistical significance for this treatment condition (*t-test*, supplementary table 10.14). 10 μM plus 1 Gy caused a dramatic and statistically significant enhancement of spheroid growth compared to the 1 Gy controls ($p < 0.05$; *t-test*, supplementary table 10.14). Both concentrations of novobiocin sodium caused a remarkably similar enhancement of spheroid growth when combined with 2 Gy. Overall, this is not sufficient evidence to draw any conclusions from regarding novobiocin sodium and its role as a radiosensitiser. Although the results are largely

suggesting novobiocin promotes radioresistance, the large error bars in this dataset mean further evidence would be required.

Enoxacin, similar to the other topoisomerase inhibitors, appeared to be radiosensitising at 0.03 μM in the initial drug screen. In contrast, 0.03 μM actually enhanced spheroid growth in the first set of validation experiments (figure 11.13a). In the second set of validation experiments (figure 11.13b) 5 μM enoxacin plus 1 Gy X-rays caused an observable, but not significant, decrease in spheroid growth, while 10 μM enoxacin plus 1 Gy X-rays resulted in spheroid growth that was dramatically higher than DMSO controls – although again, not statistically significant (*t-test*, supplementary table 10.15). Both concentrations of enoxacin plus 2 Gy X-rays enhanced growth compared to the irradiated controls, and therefore from this data, there is insufficient evidence to claim that enoxacin can radiosensitise FaDu spheroids.

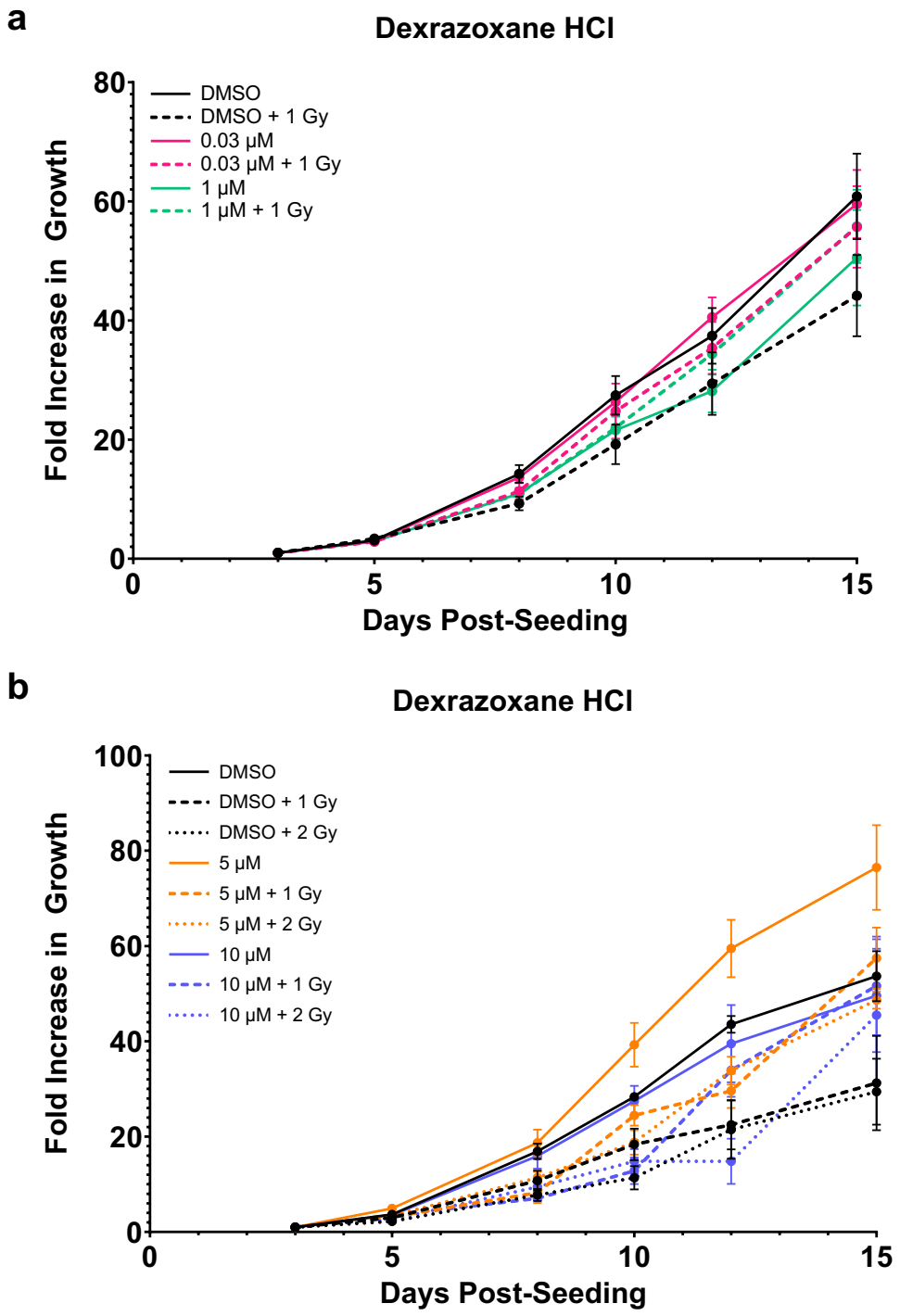

Figure 11.11: Spheroid growth following dexrazoxane HCl treatment

FaDu cells were seeded into ULA plates and incubated for 24 hours to allow spheroid formation. Following this, dexrazoxane HCl was added at two concentrations: either (a) 0.03 µM and 1 µM or (b) 5 µM and 10 µM. Following 24 hours of inhibitor treatment, spheroids were irradiated with either (a) 1 Gy or (b) 1 Gy and 2 Gy X-rays. Images of the spheroids were captured on days 3, 5, 8, 10, 12 and 15 post-seeding, which were used to measure the fold increase in growth over time. The data are presented as mean ± SEM of triplicate wells and are representative of three independent experiments.

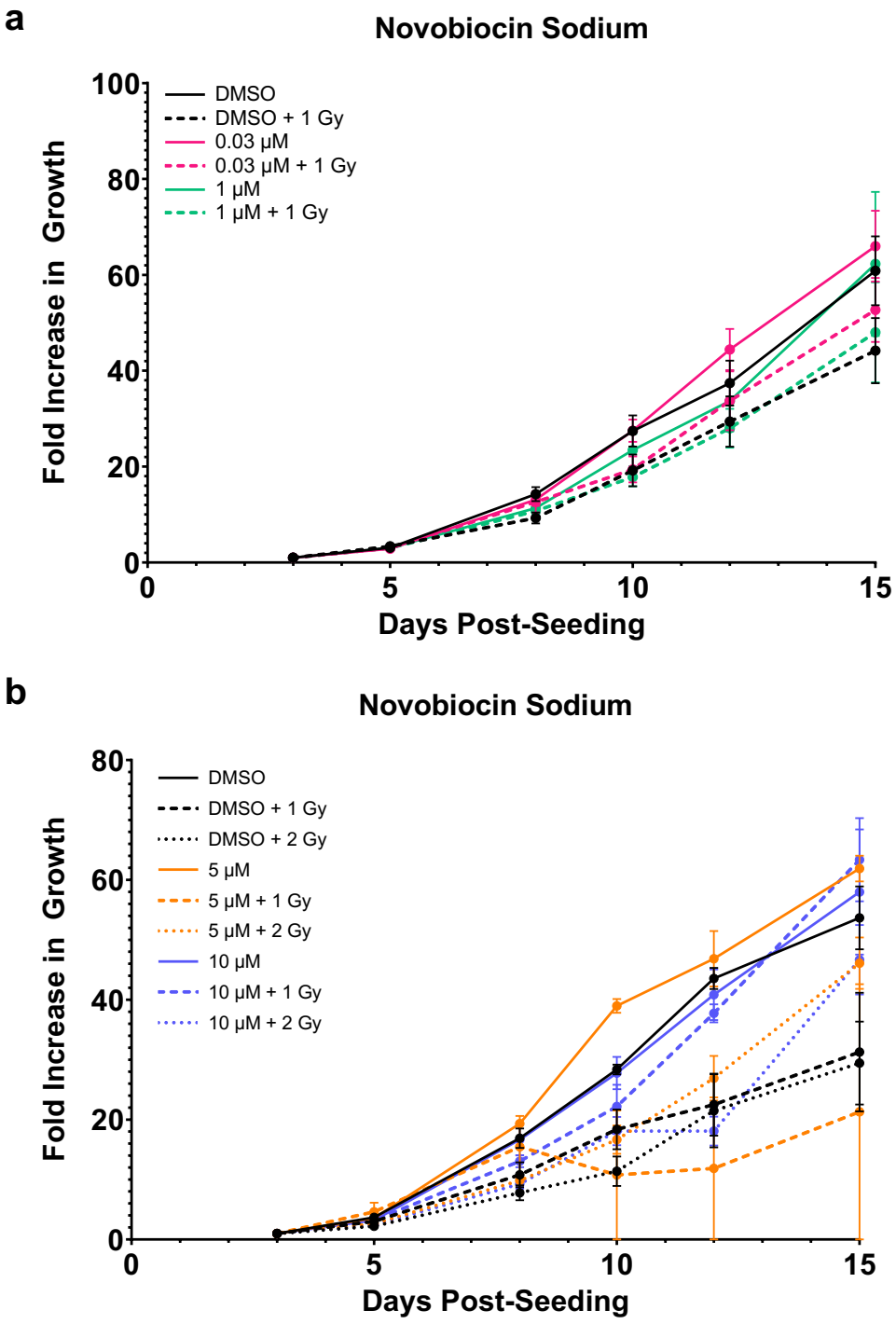

Figure 11.12: Spheroid growth following novobiocin sodium treatment

FaDu cells were seeded into ULA plates and incubated for 24 hours to allow spheroid formation. Novobiocin sodium was subsequently added at two concentrations: either (a) 0.03 µM and 1 µM or (b) 5 µM and 10 µM. Following 24 hours of inhibitor treatment, spheroids were irradiated with either (a) 1 Gy or (b) 1 Gy and 2 Gy X-rays. Images of the spheroids were captured on days 3, 5, 8, 10, 12 and 15 post-seeding, which were used to measure the fold increase in growth over time. The data are presented as mean ± SEM of triplicate wells and are representative of three independent experiments.

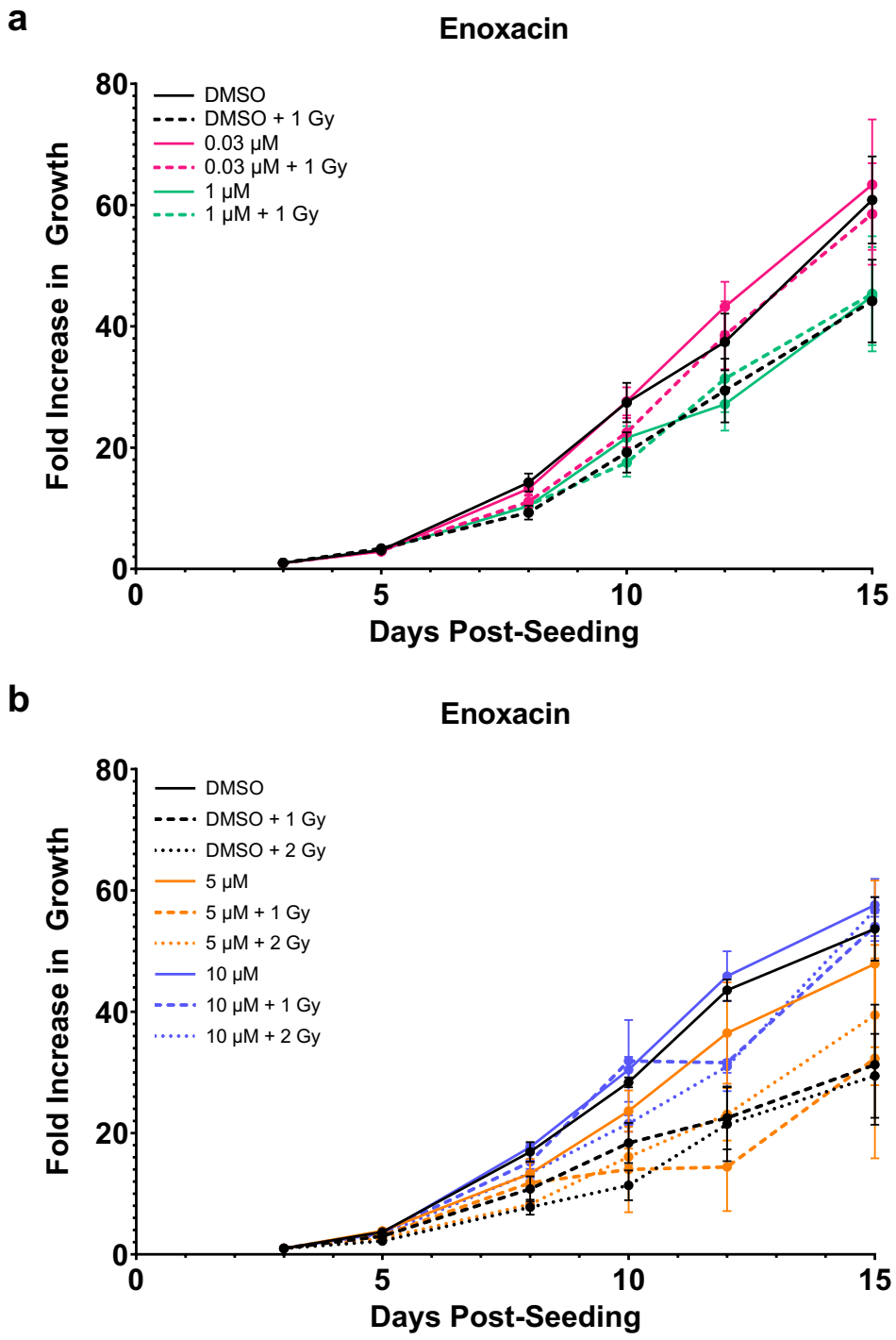

Figure 11.13: Spheroid growth following enoxacin treatment

FaDu cells were seeded into ULA plates and incubated for 24 hours to allow spheroid formation. Enoxacin was then added at either (a) 0.03 µM and 1 µM or (b) 5 µM and 10 µM. Following 24 hours of inhibitor treatment, spheroids were irradiated with either (a) 1 Gy or (b) 1 Gy and 2 Gy X-rays. Images of the spheroids were captured on days 3, 5, 8, 10, 12 and 15 post-seeding, which were used to measure the fold increase in growth over time. The data are presented as mean ± SEM of triplicate wells and are representative of three independent experiments.

11.1.5. DNA/RNA synthesis Candidates

Fidaxomicin, an inhibitor of DNA/RNA synthesis, appeared to be radiosensitising FaDu spheroids at a concentration of 1 μM in the initial drug screen. However, this observation was not replicated in validation experiments (figure 11.14a). 0.03 μM fidaxomicin enhanced growth when combined with X-rays, and while it did reduce growth at 1 μM, it was only slight and not to a statistically significant level (*t-test,* supplementary table 10.16). In the second set of validation experiments (figure 11.14b), When combined with 1 Gy X-rays, 5 μM slightly enhanced growth compared to the controls, while 10 μM plus 1 Gy X-rays caused a marked and statistically significant increase in spheroid growth ($p < 0.05$; *t-test,* supplementary table 10.16). 5 μM fidaxomicin plus 2 Gy X-rays resulted in slightly higher growth, and once again 10 μM fidaxomicin plus 2 Gy X-rays caused a dramatic and significant enhancement of growth compared to the irradiated controls ($p < 0.05$; *t-test,* supplementary table 10.16). Based on this data, I can conclude that fidaxomicin can increase resistance of FaDu spheroids to X-rays.

Mupirocin, an RNA synthetase inhibitor, appeared to be radiosensitising FaDu spheroids when used at the low concentration of 0.03 μM in the initial drug screen. In the first set of validation experiments (figure 11.15a), growth following 0.03 μM mupirocin plus 1 Gy X-rays was comparable – even slightly higher – to the irradiated controls. 1 μM mupirocin did reduce growth in combination with IR, but only very slightly. In the second set of validation experiments (figure 11.15b), both 5 μM and 10 μM mupirocin combined with both 1 Gy and 2 Gy X-rays enhanced spheroid growth, although this was only statistically significant following 10 μM plus 2 Gy treatment ($p < 0.05$; *t-test,* supplementary table 10.17). Overall, I can conclude from this data that mupirocin cannot radiosensitise FaDu spheroids.

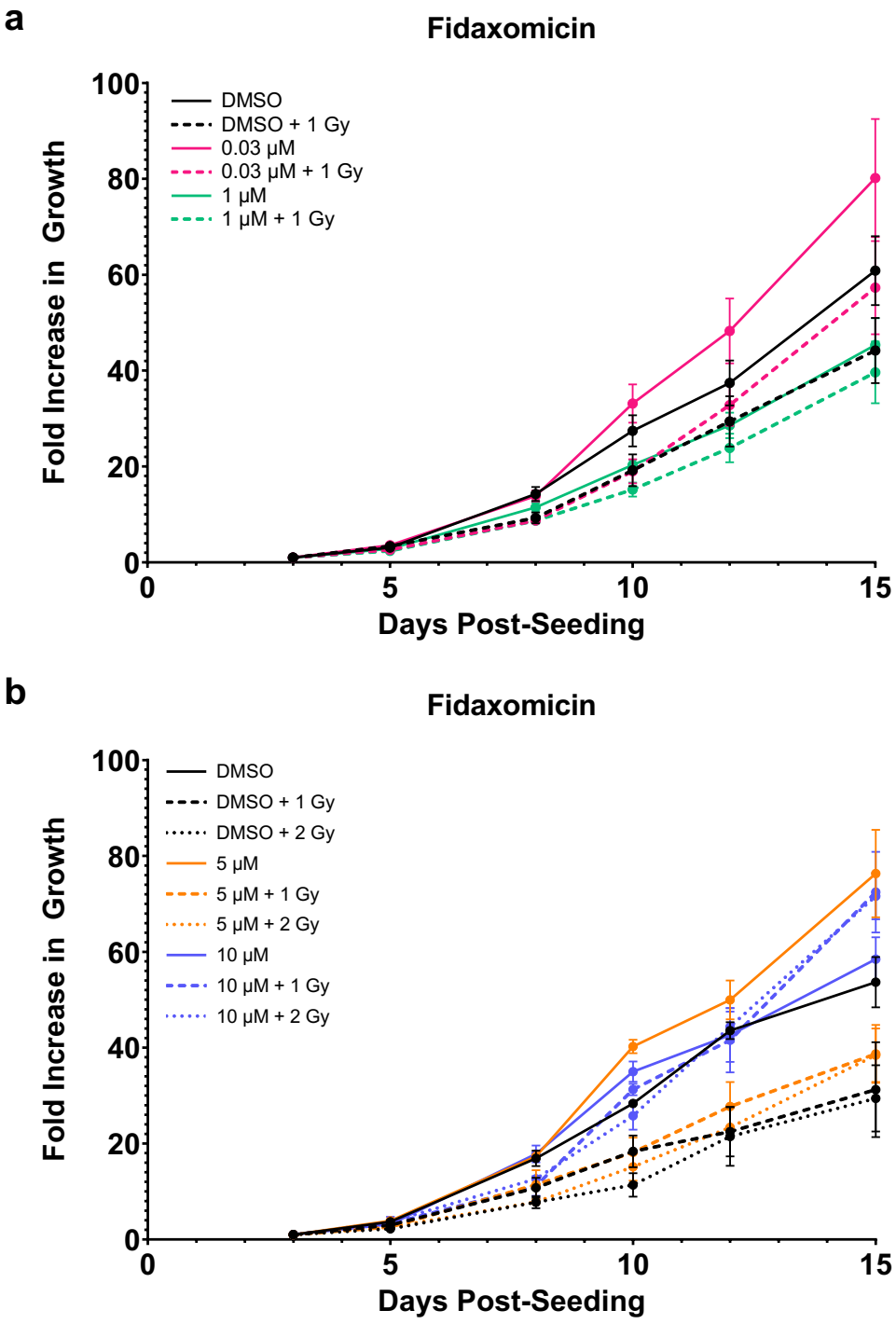

Figure 11.14: Spheroid growth following fidaxomicin treatment

FaDu cells were seeded into ULA plates and incubated for 24 hours to allow spheroid formation, after which fidaxomicin was added at either (a) 0.03 µM and 1 µM or (b) 5 µM and 10 µM. Following 24 hours of inhibitor treatment, spheroids were irradiated with either (a) 1 Gy or (b) 1 Gy and 2 Gy X-rays. Images of the spheroids were captured on days 3, 5, 8, 10, 12 and 15 post-seeding, which were used to measure the fold increase in growth over time. The data are presented as mean ± SEM of triplicate wells and are representative of three independent experiments.

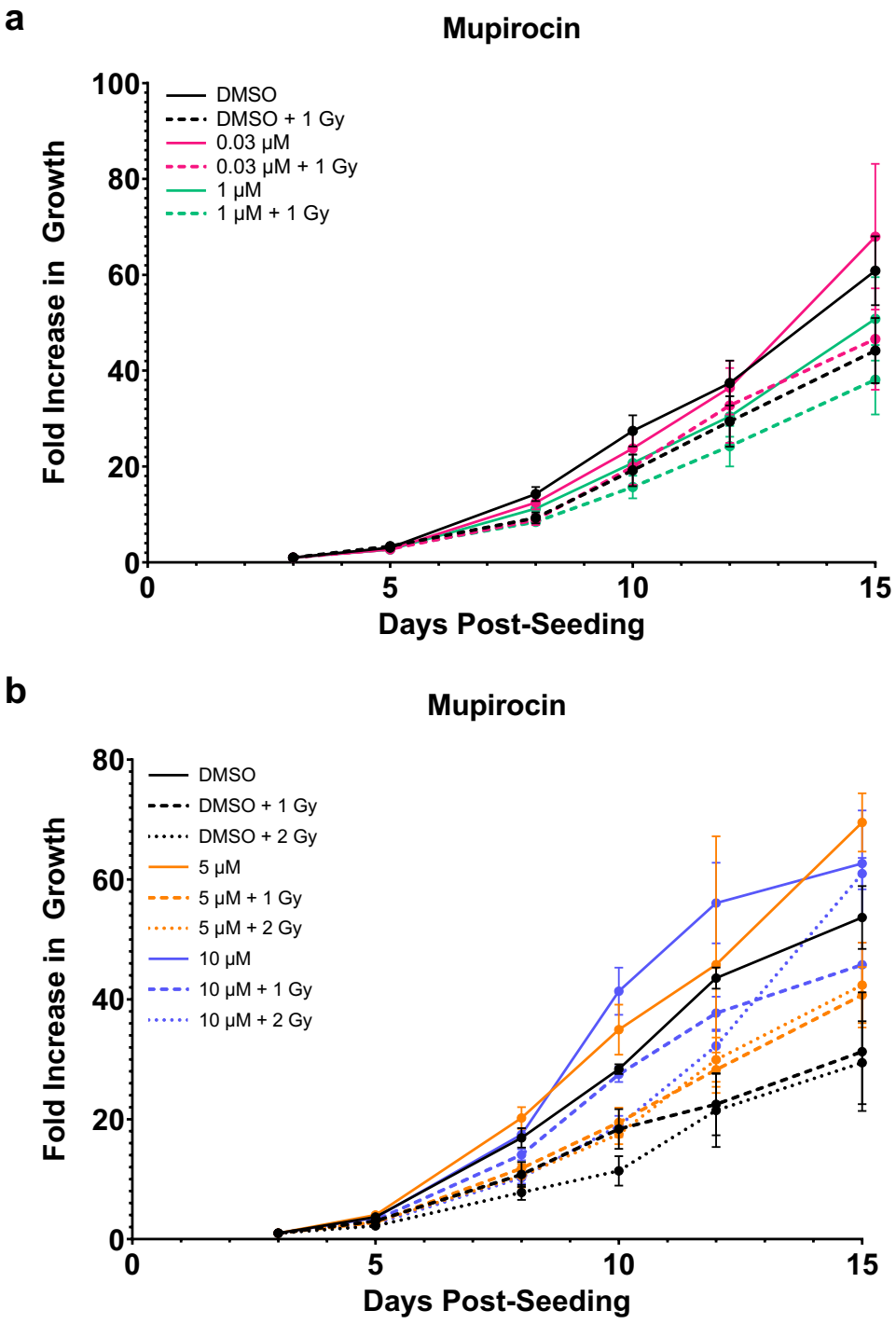

Figure 11.15: Spheroid growth following mupirocin treatment

FaDu cells were seeded into ULA plates and incubated for 24 hours to allow spheroid formation, and mupirocin was subsequently added at either (a) 0.03 µM and 1 µM or (b) 5 µM and 10 µM. Following 24 hours of inhibitor treatment, spheroids were irradiated with either (a) 1 Gy or (b) 1 Gy and 2 Gy X-rays. Images of the spheroids were captured on days 3, 5, 8, 10, 12 and 15 post-seeding, which were used to measure the fold increase in growth over time. The data are presented as mean ± SEM of triplicate wells and are representative of three independent experiments.